

A Synthesis of Global Coastal Ocean Greenhouse Gas Fluxes

Laure Resplandy¹, Allison Hogikyan¹, Hermann Werner Bange², Daniele Bianchi³, Thomas S Weber⁴, Wei-Jun Cai⁵, Scott C. Doney⁶, Katja Fennel⁷, Marion Gehlen⁸, Judith Hauck⁹, Fabrice Lacroix¹⁰, Peter Landschützer¹⁰, Corinne Le Quéré¹¹, Jens Daniel Müller¹², Raymond Gabriel Najjar¹³, Alizée Roobaert¹⁴, Sarah Berthet¹⁵, Laurent Bopp¹⁶, Trang Thi-Tuyet Chau⁸, Minhan Dai¹⁷, Nicolas Gruber¹², Tatiana Ilyina¹⁸, Annette Kock¹⁹, Manfredi Manizza²⁰, Zouhair Lachkar²¹, Goulven Gildas Laruelle²², Enhui Liao²³, Ivan D. Lima²⁴, Cara Nissen²⁵, Christian Rödenbeck²⁶, Roland Séférian²⁷, Jörg Schwinger²⁸, Katsuya Toyama²⁹, Hiroyuki Tsujino³⁰, and Pierre Regnier²²

¹Princeton University

²GEOMAR Helmholtz Centre for Ocean Research Kiel

³University of California Los Angeles

⁴University of Rochester

⁵University of Delaware

⁶University of Virginia

⁷Dalhousie University

⁸LSCE

⁹Alfred Wegener Institute Helmholtz Centre for Polar and Marine Research

¹⁰Max Planck Institute for Meteorology

¹¹School of Environmental Sciences, University of East Anglia, UK

¹²ETH Zürich

¹³The Pennsylvania State University

¹⁴Université libre de Bruxelles (ULB)

¹⁵Centre National de Recherches Météorologiques

¹⁶LMD/IPSL

¹⁷Xiamen University

¹⁸Max Planck Institute of Meteorology

¹⁹GEOMAR, Helmholtz Centre for Ocean Research

²⁰Scripps Institution of Oceanography

²¹New York University Abu Dhabi

²²Université Libre de Bruxelles

²³Shanghai Jiao Tong University

²⁴Woods Hole Oceanographic Institution

²⁵University of Colorado Boulder

²⁶Max Planck Institute for Biogeochemistry

²⁷CNRM (Météo-France/CNRS)

²⁸NORCE Climate & Environment

²⁹MRI

³⁰Meteorological Research Institute, Japan Meteorological Business Support Center

April 18, 2023

Abstract

The coastal ocean contributes to regulating atmospheric greenhouse gas concentrations by taking up carbon dioxide (CO₂) and releasing nitrous oxide (N₂O) and methane (CH₄). Major advances have improved our understanding of the coastal air-sea exchanges of these three gasses since the first phase of the Regional Carbon Cycle Assessment and Processes (RECCAP in 2013), but a comprehensive view that integrates the three gasses at the global scale is still lacking. In this second phase (RECCAP2), we quantify global coastal ocean fluxes of CO₂, N₂O and CH₄ using an ensemble of global gap-filled observation-based products and ocean biogeochemical models. The global coastal ocean is a net sink of CO₂ in both observational products and models, but the magnitude of the median net global coastal uptake is ~60% larger in models (-0.72 vs. -0.44 PgC/yr, 1998-2018, coastal ocean area of 77 million km²). We attribute most of this model-product difference to the seasonality in sea surface CO₂ partial pressure at mid- and high-latitudes, where models simulate stronger winter CO₂ uptake. The global coastal ocean is a major source of N₂O (+0.70 PgCO₂-e /yr in observational product and +0.54 PgCO₂-e /yr in model median) and of CH₄ (+0.21 PgCO₂-e /yr in observational product), which offsets a substantial proportion of the net radiative effect of coastal CO₂ uptake (35-58% in CO₂-equivalents). Data products and models need improvement to better resolve the spatio-temporal variability and long term trends in CO₂, N₂O and CH₄ in the global coastal ocean.

A Synthesis of Global Coastal Ocean Greenhouse Gas Fluxes

L. Resplandy¹, A. Hogikyan², H. W. Bange³, D. Bianchi⁴, T. Weber⁵, Wei-Jun Cai⁶, S.C. Doney⁷, K. Fennel⁸, M. Gehlen⁹, J. Hauck¹⁰, F. Lacroix¹¹, P. Landschützer^{12,13}, C. Le Quéré¹⁴, J. D. Müller¹⁵, R. G. Najjar¹⁶, A. Roobaert¹⁷, J. Schwinger¹⁸, S. Berthet¹⁹, L. Bopp²⁰, T.T.T. Chau⁹, M. Dai²¹, N. Gruber¹⁵, T. Ilyina¹³, A. Kock^{3*}, M. Manizza²², Z. Lachkar²³, G. G. Laruelle¹⁷, E. Liao^{1†}, I.D. Lima²⁴, C. Nissen^{10,25}, C. Rödenbeck²⁶, R. Séférian¹⁹, K. Toyama²⁷, H. Tsujino²⁷, P. Regnier¹⁷

¹Department of Geosciences and High Meadows Environmental Institute, Princeton University, Princeton, NJ, USA

²Atmospheric and Oceanic Sciences Program, Princeton University, Princeton, NJ, USA

³GEOMAR Helmholtz Centre for Ocean Research Kiel, Kiel, Germany

⁴Department of Atmospheric and Oceanic Sciences, University of California Los Angeles, Los Angeles, CA, USA

⁵Department of Earth and Environmental Science, University of Rochester, NY, USA

⁶School of Marine Science and Policy, University of Delaware, Newark, Delaware, 19716, USA

⁷Department of Environmental Sciences, University of Virginia, Charlottesville, VA, USA

⁸Department of Oceanography, Dalhousie University, Halifax, Canada

⁹Laboratoire des Sciences du Climat et de l'Environnement, LSCE/IPSL, CEA-CNRS-UVSQ, Université Paris-Saclay, F-91191 Gif-sur-Yvette, France

¹⁰Alfred-Wegener-Institut, Helmholtz-Zentrum für Polar- und Meeresforschung, Germany

¹¹Climate and Environmental Physics / Oeschger Centre for Climate Change Research (OCCR), University of Bern, Switzerland

¹²Flanders Marine Institute (VLIZ), Ostend Belgium

¹³Max Planck Institute for Meteorology, Hamburg, Germany

¹⁴School of Environmental Sciences, University of East Anglia, Norwich Research Park, NR4 7TJ, Norwich, UK

¹⁵Environmental Physics, Institute of Biogeochemistry and Pollutant Dynamics, ETH Zurich, Zürich, Switzerland

¹⁶Department of Meteorology and Atmospheric Science, The Pennsylvania State University, University Park, Pennsylvania, USA

¹⁷Dept. Geoscience, Environment and Society - BGEOSSYS, Université Libre de Bruxelles, Brussels, Belgium

¹⁸NORCE Climate & Environment, Bjerknes Centre for Climate Research, Bergen, Norway

¹⁹CNRM, Université de Toulouse, Météo France, CNRS, Toulouse, France

²⁰LMD/IPSL, ENS, Université PSL, École Polytechnique, Institut Polytechnique de Paris, Sorbonne Université, CNRS, Paris, France

²¹State Key Lab of Marine Environmental Science and College of Ocean and Earth Sciences, Xiamen University, Xiamen 361102, China

²²Geosciences Research Division, Scripps Institution of Oceanography, University of California - San Diego, La Jolla, USA

²³Arabian Center for Climate and Environmental Sciences, New York University Abu Dhabi, Abu Dhabi, United Arab Emirates

²⁴Department of Marine Chemistry and Geochemistry, Woods Hole Oceanographic Institution, Woods Hole, MA, USA

²⁵Department of Atmospheric and Oceanic Sciences and Institute of Arctic and Alpine Research, University of Colorado, Boulder, Colorado, USA

²⁶MPI Biogeochemistry, Jena, Germany

²⁷JMA Meteorological Research Institute, Tsukuba, Ibaraki, Japan

*now at State Office for the Environment of the State of Schleswig-Holstein, Flintbek, Germany

†now at School of Oceanography, Shang Jiao Tong University, Shanghai, 200030, China

Corresponding author: Laure Resplandy, laurer@princeton.edu

51

Key Points:

52

- We synthesize air-sea fluxes of CO₂, nitrous oxide and methane in the global coastal ocean using observation-based products and ocean models

53

54

- The coastal ocean CO₂ sink is 60% larger in ocean models than in observation-based products due to systematic differences in seasonality

55

56

- Coastal nitrous oxide and methane emissions offset 30-58% of net CO₂ coastal uptake radiative effect

57

Abstract

The coastal ocean contributes to regulating atmospheric greenhouse gas concentrations by taking up carbon dioxide (CO_2) and releasing nitrous oxide (N_2O) and methane (CH_4). Major advances have improved our understanding of the coastal air-sea exchanges of these three gasses since the first phase of the Regional Carbon Cycle Assessment and Processes (RECCAP in 2013), but a comprehensive view that integrates the three gasses at the global scale is still lacking. In this second phase (RECCAP2), we quantify global coastal ocean fluxes of CO_2 , N_2O and CH_4 using an ensemble of global gap-filled observation-based products and ocean biogeochemical models. The global coastal ocean is a net sink of CO_2 in both observational products and models, but the magnitude of the median net global coastal uptake is $\sim 60\%$ larger in models (-0.72 vs. $-0.44 \text{ PgC yr}^{-1}$, 1998-2018, coastal ocean area of 77 million km^2). We attribute most of this model-product difference to the seasonality in sea surface CO_2 partial pressure at mid- and high-latitudes, where models simulate stronger winter CO_2 uptake. The global coastal ocean is a major source of N_2O ($+0.70 \text{ PgCO}_2\text{-e yr}^{-1}$ in observational product and $+0.54 \text{ PgCO}_2\text{-e yr}^{-1}$ in model median) and of CH_4 ($+0.21 \text{ PgCO}_2\text{-e yr}^{-1}$ in observational product), which offsets a substantial proportion of the net radiative effect of coastal CO_2 uptake (35-58% in CO_2 - equivalents). Data products and models need improvement to better resolve the spatio-temporal variability and long term trends in CO_2 , N_2O and CH_4 in the global coastal ocean.

Plain Language Summary

The coastal ocean regulates greenhouse gases. It acts as a sink of carbon dioxide (CO_2) but also releases nitrous oxide (N_2O) and methane (CH_4) to the atmosphere. This synthesis contributes to the second phase of the Regional Carbon Cycle Assessment and Processes (RECCAP2) and provides a comprehensive view of the coastal air-sea fluxes of these three greenhouse gases at the global scale. We use a multi-faceted approach combining gap-filled observation-based products and ocean biogeochemical models. We show that the global coastal ocean is a net sink of CO_2 in both observational products and models, but the coastal uptake of CO_2 is $\sim 60\%$ larger in models than in observation-based products due to model-product differences in seasonality. We also find that the coastal emissions of N_2O and CH_4 counteract a substantial part of the climate buffering effect of coastal CO_2 uptake (by 35-58% in CO_2 -equivalents). Improvements to resolve long term trends in CO_2 , N_2O and CH_4 in the global coastal ocean are crucially needed.

1 Introduction

Coastal oceans play an important role in the global carbon cycle by serving as a hub of exchange between the land-aquatic continuum, sediments, the atmosphere, and the open ocean (Bauer et al., 2013; Chen & Borges, 2009; F. Mackenzie et al., 1998; Ward et al., 2020). They are often defined as ocean waters over continental shelves shallower than $\sim 200\text{-m}$ water depth, albeit sometimes extending further offshore (typically to 300 km from the coastline and 1000 m isobath, Laruelle et al., 2018). Coastal waters contribute to the global oceanic uptake of anthropogenic carbon by absorbing carbon dioxide (CO_2) directly from the atmosphere and by burying, transforming, or outgassing the carbon delivered by terrestrial ecosystems to the coastal ocean (e.g., Regnier et al., 2022).

A notable milestone in the efforts to quantify the CO_2 exchange between the atmosphere and coastal oceans was reached by Chen et al. (2013) during the first phase of the Regional Carbon Cycle Assessment and Processes (RECCAP), an international effort to establish the mean carbon balance and change over the period 1990–2009 for all subcontinents and ocean basins. These authors expanded on prior work at the scale of continental shelves (W.-J. Cai et al., 2006; Laruelle et al., 2010) and examined the global

atmospheric CO₂ uptake by coastal waters using a compilation of surface ocean partial pressure of CO₂ (pCO₂) data available for 87 shelves. They concluded that most coastal waters act as a sink for atmospheric CO₂, except for tropical coastal systems that were identified as weak CO₂ sources, and found the global coastal CO₂ uptake to be 0.4 PgC yr⁻¹ (for a surface area of coastal waters of 30.3 million km²).

Since the completion of RECCAP, the amount of available pCO₂ measurements in the coastal ocean has increased tremendously, reaching millions shortly after the RECCAP assessment was released (e.g., Surface Ocean CO₂ Atlas database SOCAT Bakker et al., 2014) and ~19 million in the most recent publication (Bakker et al., 2022). In parallel, statistical gap-filling methods, initially developed for the open ocean, have been applied to these fast expanding datasets to resolve the spatio-temporal variability of the air-sea CO₂ flux in the coastal ocean (Laruelle et al., 2014; Roobaert et al., 2019; Landschützer et al., 2020; Chau et al., 2022). These global gap-filled observation-based coastal products led to a downward revision of the global coastal ocean CO₂ uptake to about half of the RECCAP value (0.15-0.20 PgC yr⁻¹, Roobaert et al., 2019; Chau et al., 2022). This downward revision was corroborated by a recent synthesis of 214 regionally aggregated CO₂ flux estimates, leading to a net uptake of 0.25 PgC yr⁻¹ (Dai et al., 2022), although these assessments covered slightly different periods and coastal areas (1985-2019 and ~22 million km² in Chau et al., 2022; 1998-2015 and 28 million km² in Roobaert et al., 2019; 1998-present and ~30 million km² in Dai et al., 2022).

While coastal waters are a sink of CO₂, they are also the main oceanic source of two other important greenhouse gases: nitrous oxide (N₂O) and methane (CH₄) (e.g., Weber et al., 2019; Yang et al., 2020; Saunio et al., 2020; Wan et al., 2022). RECCAP did not consider N₂O and CH₄, but recent studies have compiled oceanic N₂O and CH₄ measurements (Kock & Bange, 2015) and applied statistical gap-filling techniques similar to those employed for CO₂ to assess the global ocean air-sea N₂O and CH₄ fluxes (Weber et al., 2019; Yang et al., 2020). These studies have greatly improved the quantification of N₂O and CH₄ air-sea fluxes at the global scale, but coastal ocean N₂O and CH₄ emissions remain highly uncertain and the extent to which these emissions offset the present-day coastal CO₂ uptake is unknown.

Coastal air-sea fluxes of CO₂, N₂O and CH₄ have strong spatial and seasonal variability. Regional-scale observational and modeling studies have greatly improved the quantification of the mean and temporal variability of air-sea fluxes of greenhouse gases in individual regions across the globe (e.g., Anderson et al., 2009; Güllow et al., 2013; Turi et al., 2014; Arévalo-Martínez et al., 2015; Pipko et al., 2017; Mayer et al., 2018; Fennel et al., 2019; Gomez et al., 2020; Hauri et al., 2021; Louchard et al., 2021). However, the limited spatial coverage of these studies largely inhibits a global-scale perspective. Global gap-filled observational products and global ocean biogeochemical models now run at a reasonably high horizontal resolution (0.5° or higher) to simulate coastal CO₂ (Bourgeois et al., 2016; Lacroix et al., 2020, 2021; Roobaert et al., 2022) and N₂O (Ganesan et al., 2020; Stell et al., 2022; Berthet et al., 2022) fluxes, recently complemented these regional-scale studies.

As a result of observational and modeling advances since RECCAP, a global view of the coastal ocean's spatial and seasonal patterns in air-sea greenhouse gas fluxes has started to emerge, at least for CO₂ fluxes. Polar and subpolar coastal oceans, such as the northwest North Atlantic along the Canadian and US coast (Thomas et al., 2004; Fennel & Wilkin, 2009; Previdi et al., 2009; Signorini et al., 2013; Lachkar & Gruber, 2013; Laruelle et al., 2015; Cahill et al., 2016; Gustafsson et al., 2019), the European shelves (Thomas et al., 2004; Cossarini et al., 2015; Neumann et al., 2022; Gustafsson et al., 2019) and Arctic and Antarctic shelf (Arrigo et al., 2008; Pipko et al., 2017, 2021; Ouyang, Sciusco, et al., 2022) generally are strong sinks of CO₂ characterized by large seasonal variations, and likely account for about 90% of the annual global coastal CO₂ uptake (while representing ~45% of the global coastal surface area, see Laruelle et al., 2014; Roobaert et

al., 2019; Dai et al., 2022). There are exceptions with subpolar and polar shelves where outgassing has been identified, such as the Scotian Shelf (Rutherford et al., 2021; Rutherford & Fennel, 2022) or the Laptev Sea in the Arctic (Anderson et al., 2009). Coastal upwelling regions, such as the nearshore California Current, are sources of CO₂ to the atmosphere with a marked seasonality that follows the upwelling dynamics (Lachkar & Gruber, 2013; Dai et al., 2013; Turi et al., 2014; Fiechter et al., 2014; Damien et al., 2023). Tropical systems, such as the Gulf of Mexico (Xue et al., 2016; Laurent et al., 2017) and the South China Sea (Wan et al., 2022), are mostly identified as weak CO₂ sources with weak seasonal variability (Laruelle et al., 2014, 2015; Roobaert et al., 2019; Dai et al., 2022). Our knowledge of N₂O and CH₄ variability in the global coastal ocean is more limited, but gap-filled products and global models suggest that N₂O and CH₄ annual emissions strongly vary between coastal regions (e.g., Weber et al., 2019; Yang et al., 2020; Ganesan et al., 2020; Stell et al., 2022). These products and models offer a remarkable opportunity to establish a greenhouse gas budget for the global coastal ocean, and improve our understanding of its spatial and seasonal variability.

Rising atmospheric CO₂ levels influence coastal CO₂ uptake on multi-decadal time-scales. Prior syntheses at the global scale including RECCAP (W.-J. Cai et al., 2006; Laruelle et al., 2010; Chen et al., 2013; Bauer et al., 2013; Regnier et al., 2013) and at the regional scale (Liu et al., 2018; Fennel & Testa, 2019; Legge et al., 2020) clearly support the view that the coastal ocean is currently a sink of atmospheric CO₂, but the extent to which it has changed on longer time-scales remains controversial (see Dai et al., 2022, for a review). F. T. Mackenzie et al. (2005) from a modeling perspective and later W. Cai et al. (2021) from observations first hypothesized that the potential of the coastal ocean to act as a sink for CO₂ might be increasing with time. This view is increasingly supported by time series analyses that suggest that trends in sea surface pCO₂ are overall weaker than the atmospheric pCO₂ trend in most coastal regions. This finding further implies an intensified CO₂ uptake or decreased outgassing, although potential trends in winds and sea ice may also play a role (Bauer et al., 2013; Wang et al., 2017; Laruelle et al., 2018; Dai et al., 2022). However, exceptions have been identified in regions where coastal ocean pCO₂ increases at a similar rate (i.e., near-zero changes in the flux) or even at higher rates (i.e., reduced CO₂ uptake or intensified outgassing) than atmospheric pCO₂ (e.g., California Current, South and Mid Atlantic Bight, Baltic Sea Reimer et al., 2017; Laruelle et al., 2018; Schneider & Müller, 2018; Dai et al., 2022). The quantification of coastal CO₂ flux trends from observations is, however, still strongly restricted by the limited spatial coverage and/or the relatively short duration of time series.

Global ocean biogeochemical models offer an attractive means of assessing long term trends in air-sea CO₂ flux densities in the coastal ocean and how they differ from those of the open ocean (Regnier et al., 2022). Two such models, with reasonable agreement in regions where time series are available (0.2-0.5° resolution in Bourgeois et al., 2016; 0.4° resolution in Lacroix et al., 2021), suggest that the global coastal CO₂ sink density has increased at a slightly slower rate than the open ocean CO₂ sink since the preindustrial era, even when accounting for increasing global nutrient sources via river and atmospheric transports (Lacroix et al., 2020). Both models, however, have important limitations and potential biases related to their representation of fine-scale hydrodynamics of shelf circulation and biophysical processes that impact biogeochemical cycling in the shallow ocean (Mathis et al., 2022; Rutherford & Fennel, 2018).

In this second phase of the Regional Carbon Cycle Assessment and Processes (RECCAP2), we aim to address gaps in our understanding of air-sea greenhouse gas fluxes for the global coastal ocean using a multi-methodological approach that relies on an ensemble of global gap-filled observation-based products and ocean biogeochemical models. Our objectives are threefold. First, we revisit the estimate of the net coastal ocean CO₂ flux, and combine it with CH₄ and N₂O emissions to derive a global climatological coastal ocean budget of greenhouse gas fluxes (section 3.1). Second, we analyze the spatial and sea-

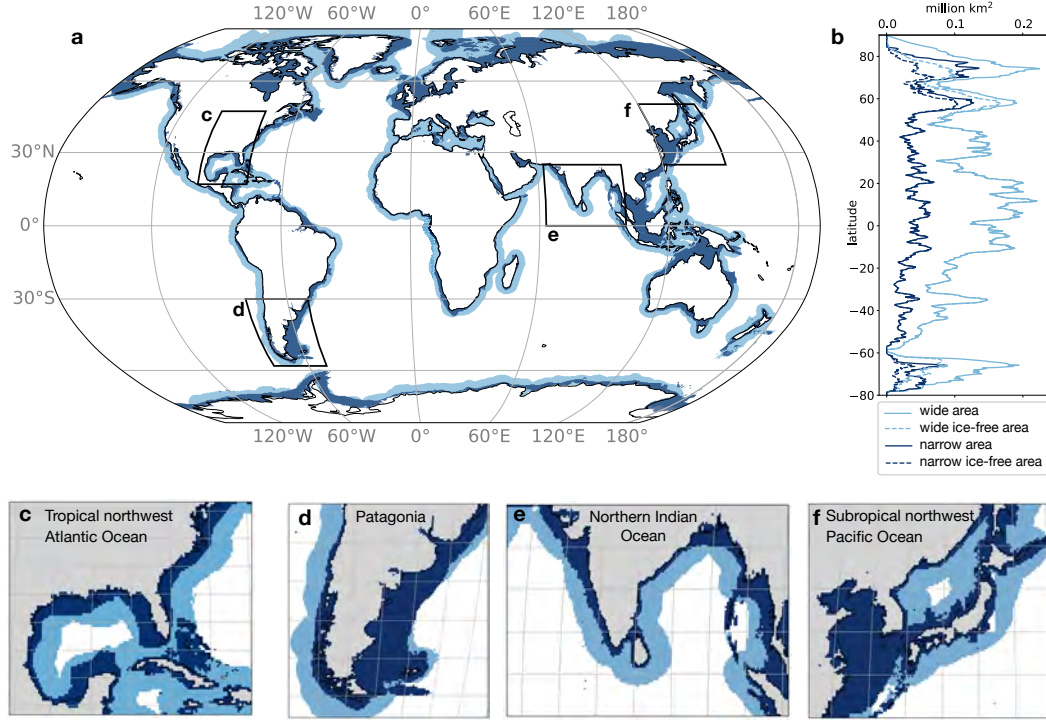


Figure 1. a) Coastal masks used in this study for the wide (dark + light blue) and narrow (dark blue) coastal oceans, b) Surface area (in km^2) at each latitude in the wide (light blue) and narrow (dark blue) coastal ocean masks (solid lines) and the 1998-2018 averaged sea-ice free surface area (dashed lines). c-f) Insets showing the extent of the narrow and wide coastal oceans in four coastal regions. Sea ice coverage used in b is from NOAA OISST. See Methods for details.

sonal variability in the CO_2 flux density and how it might differ from that of the open ocean, and examine spatial patterns in coastal CH_4 and N_2O fluxes (sections 3.2 and 3.3). Third, we investigate trends in the coastal CO_2 flux over the last four decades (section 3.3). This synthesis does not cover the seasonal and interannual variability in N_2O and CH_4 fluxes, as these temporal scales are either unresolved (CH_4) or have not yet been analyzed (N_2O) in the coastal ocean. We consider the net contemporary air-sea fluxes (natural + anthropogenic) of CO_2 , N_2O and CH_4 using the 1998-2018 period (except if specified otherwise). Our approach combines observation-based and model-based estimates with different strengths and limitations discussed in Section 4.

2 Methods

2.1 Coastal ocean definition and analysis period

Different definitions of coastal oceans are used in the literature (Chen et al., 2013; Laruelle et al., 2017). We primarily use a “wide” coastal ocean definition following Laruelle et al. (2017), where the seaward boundary is 300 km from shore or the 1000-m isobath, whichever is further from shore, amounting to a total coastal ocean area of 77.2 million km^2 (Fig 1). This wide coastal ocean definition allows us to examine coastally influenced regions of the ocean, i.e., that part of the ocean that is impacted by the presence of the coastal boundary, while also maximizing the number of observation-based and model-based estimates we can use in this study (i.e., a narrower definition would exclude prod-

ucts of lower horizontal resolution). This wide coastal ocean area is, however, more than twice the surface area commonly used to examine coastal ocean biogeochemical dynamics (e.g. Chen et al., 2013). We therefore further use a “narrow” coastal ocean definition, which is delimited by the shelf break (defined as the isobath with maximum slope increase in the 0-1000 m interval) and amounting to a total area of 28 million km² (see details in Laruelle et al., 2013, 2014). See Figure 1 for maps and area latitudinal distribution of the narrow and wide coastal waters. The landward boundary in the masks used to define the narrow and wide coastal oceans excludes estuaries and coastal vegetation, which are described in (Rosentreter et al., 2023).

The analysis is done over the 1998-2018 period to maximize the number of models and observation-based products available (see Tables 1-3 for periods covered by models and observation-based products). Note that this period differs from the one used in the open-ocean RECCAP2 studies that analyze oceanic CO₂ fluxes since 1985. All trends are calculated as linear trends over the 1998-2018 period.

2.2 Datasets

We use observation-based and model-based estimates with different strengths and limitations. Notably, gap-filled global observational-based products rely on observations that are often too sparse to capture the full range of spatio-temporal variability in coastal regions (except in densely sampled regions such as major parts of the North American and European ocean margins) and are highly sensitive to the wind product and the choice of the gas exchange coefficient formulation (e.g., Roobaert et al., 2018). In contrast, ocean biogeochemical models can be associated with systematic biases. For instance, only some of the models used here include land-sea riverine carbon inputs which sustain an oceanic CO₂ outgassing flux, and land-sea nutrient inputs which would yield an opposing biologically-driven oceanic CO₂ uptake in coastal waters (Resplandy et al., 2018; Hauck et al., 2020; Regnier et al., 2022; Gao et al., 2023, see Tables 1-3).

2.2.1 Observation-based pCO₂-products

We use 4 global pCO₂-products that provide global monthly gridded surface ocean pCO₂ (noted pCO₂ here) and air-sea CO₂ flux fields based on observations from the SOCAT database which compiles surface ocean pCO₂ observations and provides a subset after quality control (Bakker et al., 2016, 2022). Three of them use neural network-based interpolation methods: Coastal-SOM-FFN (Laruelle et al., 2017; Roobaert et al., 2019, 2022), merged-SOM-FFN (Landschützer et al., 2020) and CMEMS-LSCE-FFNN (which we refer as CMEMS, Chau et al., 2022), while the fourth product, Carboscope-1, uses a simple statistical representation of mixed-layer biogeochemistry fitted to the pCO₂ data (Rödenbeck et al., 2022). All these products are using SOCAT pCO₂ observations and are therefore not independent (see SI for details on SOCAT versions and Fig. S1 for SOCAT data coverage). In particular, the Merged-SOM-FFN product merged the Coastal-SOM-FFN (Laruelle et al., 2017) with an open ocean SOM-FFN product (Landschützer et al., 2014) to produce a global ocean product; the Coastal-SOM-FFN and Merged-SOM-FFN are therefore identical in the nearshore coastal region and only differ in the more offshore band of the wide coastal domain (see details in Landschützer et al., 2020). Coastal-SOM-FFN (and therefore also the near-shore product in Merged-SOM-FFN) was designed for the coastal ocean and uses coastal SOCAT data for their neural network training. In the three other products that use both open ocean and coastal ocean data (i.e. CMEMS, Carboscope-1 and offshore portion of Merged-SOM-FFN), the coastal estimate may be strongly influenced by open-ocean information extrapolated towards the coast. See Tables 1-3 and Supplementary Information S1 for details on pCO₂-products (e.g., period, wind speed product, gas exchange formulation).

Carboscope-1 and CMEMS products resolve interannual variability over the whole 1998-2018 period and may be used to estimate decadal trends, while Coastal-SOM-FFN and Merged-SOM-FFN provide a 1998-2015 monthly climatology and do not resolve interannual variability. $p\text{CO}_2$ -products often have unrealistic $p\text{CO}_2$ values under sea-ice (Laruelle et al., 2017). We therefore used the sea-ice fraction from the NOAA-OISST product (Reynolds et al., 2007) to mask $p\text{CO}_2$ and CO_2 flux values under sea-ice in the four products. We mask both to keep consistency but this method should not impact the flux dramatically since it is often inhibited by sea-ice in flux formulations. In this study, we also filled the missing values north of 75N in CMEMS using the Coastal-SOM-FFN climatology. This approach only marginally impacts the results (adds $-0.03 \text{ PgC yr}^{-1}$ to the wide coastal ocean net CO_2 flux) because the surface area north of 75N contributes 5 million km^2 to the wide coastal ocean (6% of the total wide area) but only 1.4 million km^2 is ice-free on average for the entire study period. This filled-in version of CMEMS is referred to as CMEMS* and we report no long-term trend in the Arctic for this product.

We also illustrate the sensitivity of the flux in $p\text{CO}_2$ -products to the choice of the wind speed product and gas transfer coefficient (k_w) formulation (e.g., Roobaert et al., 2018) by presenting a second version of the Coastal-SOM-FFN flux product but with a different wind product and k_w (labeled Coastal-SOM-FFN- k_w) in which the CO_2 flux is calculated as $F = k_w \text{ Ko } (p\text{CO}_{2a} - p\text{CO}_2)$ where Ko is the gas solubility and $p\text{CO}_{2a}$ the atmospheric $p\text{CO}_2$. The default version of Coastal-SOM-FFN uses the ERA5 wind speeds and the k_w formulation from (Ho et al., 2011), whereas Coastal-SOM-FFN- k_w uses JRA55v1.3 winds and the Wanninkhof (1992) k_w formulation (i.e., wind and formulation used in some ocean biogeochemical models, see Tables 1-3 for details on k_w parametrization and wind products used in models and products). The four $p\text{CO}_2$ -products are used for the analysis of the wide and narrow coastal oceans, and the three $p\text{CO}_2$ -products that extend outside of the coastal domain are used for the open ocean (CMEMS*, Merged-SOM-FFN, and Carboscope-1). Coastal-SOM-FFN- k_w is only shown in the wide coastal ocean for discussion and is not used to compute the $p\text{CO}_2$ -product median.

2.2.2 Observation-based N_2O and CH_4 flux products

We used two observation-based estimates of the N_2O and CH_4 fluxes. In each case, we use an estimate based on a simple extrapolation of the MEMENTO (Marine Methane and Nitrous Oxide) database to the 45 MARGINS and CATchments Segmentation (MARCATS, Figure S2) coastal regions (referred to as MARCATS- N_2O and MARCATS- CH_4 Kock & Bange, 2015), and an estimate that extrapolates MEMENTO and supplementary observations to a global 0.25-degree climatology using supervised machine learning models (Weber et al., 2019; Yang et al., 2020, referred to as Weber- CH_4 and Yang- N_2O). The MARCATS- N_2O and MARCATS- CH_4 products provide an annual mean value based on data from 1980 to 2016, Yang- N_2O provides a monthly climatology for 1988-2017 and Weber- CH_4 an annual mean value for 1999-2016 (Table 1). In Yang- N_2O surface N_2O disequilibrium was extrapolated globally using an ensemble of 100 Random Regression Forest (RRF) models, and in Weber- CH_4 surface CH_4 disequilibrium was extrapolated using 1000 RRF models and 1000 Artificial Neural Network (ANN) models. In both cases, diffusive fluxes were calculated and uncertainty propagated by coupling the mapped disequilibrium to multiple high-resolution wind reanalysis products (two in Yang- N_2O , four in Weber- CH_4), and multiple piston velocity parameterizations (two in Yang- N_2O and four in Weber- CH_4). These estimates for each gas are not independent as they use the same MEMENTO database. The Yang- N_2O and Weber- CH_4 products use interpolation techniques to fill observational gaps, but the lack of observations likely leads to large uncertainties in coastal regions.

For CH_4 emissions, the contribution from gas bubble plumes must be taken into account in addition to the diffusive flux (arising from the air-sea difference in partial pres-

sure and a gas exchange coefficient). The MEMENTO database allows the calculation of the diffusive CH_4 flux only, because CH_4 from bubble plumes are usually not captured by the conventional CH_4 measurements based on discrete samples or continuous underway measurement systems. An estimate of the ebullitive (i.e. bubbling) CH_4 fluxes is, however, included in Weber- CH_4 (but not in MARCATS- CH_4), by combining previous seafloor emissions estimates with models of bubble transfer to the surface (Weber et al., 2019). We evaluated the uncertainty on the net Weber- CH_4 flux in the narrow and wide coastal oceans from the quadrature of uncertainties on diffusive and ebullitive fluxes, using a 50% uncertainty on diffusive flux and a 60% uncertainty on ebullitive flux (Weber et al., 2019). More details on these products can be found in Supplementary Information S1.

2.2.3 Ocean models for CO_2 and N_2O fluxes

For CO_2 , we used 15 ocean general circulation models coupled with biogeochemical modules: 11 are global and 4 are regional models, all covering the study period of 1998-2018 except CCSM-WHOI which ends in 2017 (see details in Tables 2-3). Most global models have native horizontal grid resolutions varying between 0.25° and 1° in the coastal domain, except FESOM-HR which has an unstructured mesh that reaches higher resolution (see Fig S3) and MPIOM-HAMMOC, NEMO-PlankTOM12 and CCSM-WHOI which have a coarser resolution of $\sim 1.5^\circ$, $\sim 2^\circ$ and $\sim 3^\circ$ respectively (Table 2). The regional models covering the Indian Ocean (NYUAD-ROMS-Indian) and Northwest Atlantic Ocean (NW-Atl) have horizontal resolutions of approximately 10 km. The regional models covering the Atlantic (ETHZ-ROMS-Atl) and Pacific Ocean (ETHZ-ROMS-Pac) have resolution varying in space between 4 km and 120 km: the ETHZ-ROMS-Atl telescopes to focus on the Amazon outflow region where the resolution is higher and the ROMS-ETHZ-Pac grid focuses on the California Current region (Table 3). We note that some of these models include land-sea nutrient and carbon inputs by rivers, while others do not. Details on these models can be found in Tables 2-3 and Supplementary information S1.

For N_2O , we use 5 models: three of them are also used for CO_2 (CNRM-HR, CNRM-LR, and NEMO-PlankTOM5) and cover the full study period (1998-2018), while the two other models are from the ECCO family (ECCO-Darwin and ECCO2-Darwin) in which the circulation is optimized to capture the distribution of tracers such as temperature and salinity in the ocean but cover shorter periods (ECCO-Darwin for 1997-2013 and ECCO2-Darwin for 2006-2013). See Table 2 and Supplementary Information S1 for further details and references on each model.

Model-based analyses in this study use all global models available for the wide coastal ocean (i.e. 11 models for CO_2 and 5 for N_2O), but subsets of models with higher native horizontal resolution are used for the narrow coastal ocean (4 models for CO_2 : CNRM-HR, FESOM-HR, MOM6, MRI-ESM2.1, and 3 models for N_2O : CNRM-HR, ECCO-Darwin and ECCO2-Darwin, see Table 2). Global averages and integrated fluxes are based on the global models, while regional models were used in addition to the global models for the analysis at the grid-point scale (e.g. maps).

2.3 Grid harmonization and coastal waters area rescaling

All models and data products were re-gridded from their native grid onto the same $1/4^\circ$ grid for analysis. Yet, due to differences in horizontal resolution and ocean-land mask definition, observational products and ocean biogeochemical models can have different coastal ocean areas, even after they have been re-gridded to the same $1/4^\circ$ grid (for example, wide coastal ocean areas resolved by the models range from 34 to 76 million km^2 vs. 77.2 million km^2 in the mask of Laruelle et al. (2017), see Tables 1-3 and Fig 1). To minimize the effect of this common issue, most results are presented as area-weighted

averages of CO₂, N₂O and CH₄ flux densities (per m²) and surface ocean pCO₂ masked using time varying ice-free surface to account for fractional sea ice coverage (in μ atm). We used the ice fraction from the NOAA-OISST product for pCO₂-products and the ice fraction of each individual model for models. For the globally integrated CO₂ flux (in PgC yr⁻¹), we used the globally averaged CO₂ flux densities found in each pCO₂-product and model for the narrow and wide coastal oceans and multiplied them by the corresponding coastal area of Laruelle et al. (2017, narrow area = 28 million km²; wide area = 77 million km²). We did not apply this area rescaling to the globally integrated fluxes of N₂O and CH₄ given the smaller number of products/models available.

2.4 Calculation of CO₂ equivalents global coastal fluxes and uncertainties

We computed CO₂ equivalent fluxes of N₂O and CH₄ to provide a global greenhouse gas flux integral (i.e., spatially integrated annual net air-sea flux of greenhouse gasses) in gigatonnes of CO₂ equivalent (PgCO₂-e) for the wide coastal ocean. We used the Intergovernmental Panel on Climate Change (IPCC) Assessment Report 6 (Arias et al., 2021) updated 100-year global warming potential for N₂O ($GWP_{N_2O} = 273$, i.e. the 100-year time integrated radiative forcing from the instantaneous release of 1 kg of N₂O is 273 times larger than the forcing of 1 kg of CO₂) and for CH₄ of non-fossil fuel origin ($GWP_{CH_4} = 27.2$). We calculated two budgets for the wide coastal ocean: one using observation-based flux products only and one using mostly models. The observation-based budget uses the global gap-filled observational products, i.e. the 4 pCO₂-product median flux for CO₂ (CMEMS*, Carboscope-1, Coastal-SOM-FFN and Merged-SOM-FFN), the Yang-N₂O flux for N₂O and the Weber-CH₄ flux for CH₄. Uncertainty bars presented for this observation-based budget give the ranges of all products presented in this study, i.e. the 4 pCO₂-product range for CO₂, the 2 observational-product range for N₂O (Yang-N₂O and MARCATS-N₂O) and the 2 observational-product range for CH₄ (i.e. the low bound corresponds to the low uncertainty bound of Weber-CH₄ and the high bound to the value of MARCATS-CH₄). The model-based budget uses the 11 global model median flux for CO₂, the 4 global model median flux for N₂O, and the product-based Weber-CH₄ flux for CH₄ as no model is available. Uncertainty bars presented for this model-based budget are the 11-model range for CO₂, the 4-model range for N₂O, and the 2 observational product range for CH₄ (same as the product-based budget described above).

3 Results

3.1 Global coastal ocean greenhouse gas fluxes

In this section, we present a compilation of observation-based and modeled net air-sea fluxes of CO₂ (4 pCO₂-products and 11 global ocean models), N₂O (2 observation-based products and 4 global ocean models) and CH₄ (2 observation-based products) in the global coastal ocean (Figure 2), and assess the contribution of the coastal ocean to the atmospheric greenhouse gas budget by combining the three gasses using a single CO₂-equivalent flux (Figure 3).

3.1.1 Net coastal CO₂ uptake

The pCO₂-products yield a weaker net CO₂ uptake than the global ocean biogeochemical models in the wide coastal ocean during the 1998-2018 period (Figure 2a). The pCO₂-product estimates (-0.59 to -0.37 PgC yr⁻¹) fall at the upper (less negative) end of the model range (-0.92 to -0.38 PgC yr⁻¹), and in the pCO₂-product flux median (-0.44 PgC yr⁻¹) is about two thirds of the model median (-0.72 PgC yr⁻¹). Most of this model-product mismatch can be attributed to differences in ocean pCO₂ seasonality at mid- and high-latitudes (poleward of 25N and 25S), which tend to reinforce the north-

ern hemisphere winter uptake in models compared to $p\text{CO}_2$ -products (see details in section 3.2.2). These differences in $p\text{CO}_2$ seasonality are likely to be further amplified by differences in wind speed and gas exchange coefficient formulation (see Methods and Table 1-3). For instance, the net CO_2 uptake in the Coastal-SOM-FFN product increases by about 50% and falls closer to the model median when changing the wind speed product (from ERA5 to JRA55) and gas exchange coefficient formulation (from Ho et al., 2011 to Wanninkhof 1992) used to compute the flux (from $-0.44 \text{ PgC yr}^{-1}$ in Coastal-SOM-FFN to $-0.65 \text{ PgC yr}^{-1}$ in Coastal-SOM-FFN- k_w , blue dot vs. blue circle in Figure 2a, see further details in section 3.2.2).

Another factor that can explain part of the model-product discrepancy is the absence of land-sea carbon and nutrient inputs in many of the global ocean biogeochemical models (see Table 2). The missing land-sea carbon inputs and associated CO_2 outgassing would result in a stronger CO_2 uptake at the scale of the global ocean but the proportion of this land-driven CO_2 outgassing occurring in the coastal ocean, and therefore the bias introduced here in our model-based estimates, is very poorly constrained. Open-ocean RECCAP2 chapters used a model-based estimate of the spatial distribution of this land-driven CO_2 outgassing (Lacroix et al., 2020) scaled up to match an independent bottom up constraint on its global magnitude ($0.65 \pm 0.3 \text{ PgC/yr}$ Regnier et al., 2022). This combined estimate suggests that the missing land-driven outgassing could amount to 0.12 PgC yr^{-1} in the wide coastal ocean, potentially explaining part of the gap between $p\text{CO}_2$ -products and model median, despite the large unconstrained uncertainty of this estimate. In contrast, the missing land-sea nutrient inputs could reduce the biologically-driven uptake of CO_2 in coastal waters and potentially offset the bias tied to the lack of land-sea carbon inputs (Gao et al., 2023). However, we find no clear relationship between the strength of the simulated net coastal CO_2 uptake and the presence or absence of land-sea inputs in the global ocean biogeochemical models used here (i.e., models with weaker coastal CO_2 uptake more in line with $p\text{CO}_2$ -products are not systematically the ones with land-sea inputs), suggesting that land-driven inputs are likely not the main factor in this discrepancy. In addition, we note that using the subset of four global models with higher horizontal resolution (CNRM-HR, FESOM-HR, MOM6, MRI-ESM2.1 with nominal resolution of 0.5 degree or higher), which are likely to better capture coastal dynamics, yields a slightly weaker net CO_2 uptake (median of $-0.65 \text{ PgC yr}^{-1}$ for only four models vs. $-0.72 \text{ PgC yr}^{-1}$ for all global models), slightly closer to the $p\text{CO}_2$ -products median ($-0.44 \text{ PgC yr}^{-1}$) and in relatively good agreement with one of the $p\text{CO}_2$ -products ($-0.59 \text{ PgC yr}^{-1}$ in CMEMS*, Figure 2a).

We can compare the net CO_2 flux estimates presented here to prior work using the narrower definition of the coastal ocean ending at the shelf break (28 million km^2), a domain more aligned with the definition used in past studies (Supplementary Table S2). For this comparison we include all $p\text{CO}_2$ -products, but use only the subset of four global models with higher horizontal resolution. We find that the narrow coastal ocean accounts for about half of the wide coastal ocean CO_2 uptake (-0.22 out of $-0.44 \text{ PgC yr}^{-1}$ for the 4- $p\text{CO}_2$ -product median and $-0.34 \text{ PgC yr}^{-1}$ out of the $-0.65 \text{ PgC yr}^{-1}$ for the 4-model median), while only accounting for about a third of the surface area. The $p\text{CO}_2$ -product median in the narrow coastal ocean ($-0.22 \text{ PgC yr}^{-1}$) is consistent with the most recent observation-based estimates (Roobaert et al., 2019; Dai et al., 2022; Regnier et al., 2022), but the four $p\text{CO}_2$ -products span a relatively large range with differences of the order of a factor 2 ($-0.12 \text{ PgC yr}^{-1}$ in Carboscope-1 and $-0.31 \text{ PgC yr}^{-1}$ in CMEMS*, see Table S2 for estimates). The 4-model median simulates a slightly stronger sink ($-0.34 \text{ PgC yr}^{-1}$) than these most recent estimates (although it is similar to the estimate of Regnier et al., 2022) but again differences in $p\text{CO}_2$ seasonality, and potentially in wind speed and gas exchange formulation could explain part of this discrepancy. Similarly to the wide coastal ocean, the net CO_2 sink increases by nearly 50% in the narrow coastal ocean from Coastal-SOM-FFN to Coastal-SOM-FFN- k_w (from -0.21 to $-0.31 \text{ PgC yr}^{-1}$, blue dot vs. circle, Figure 2a).

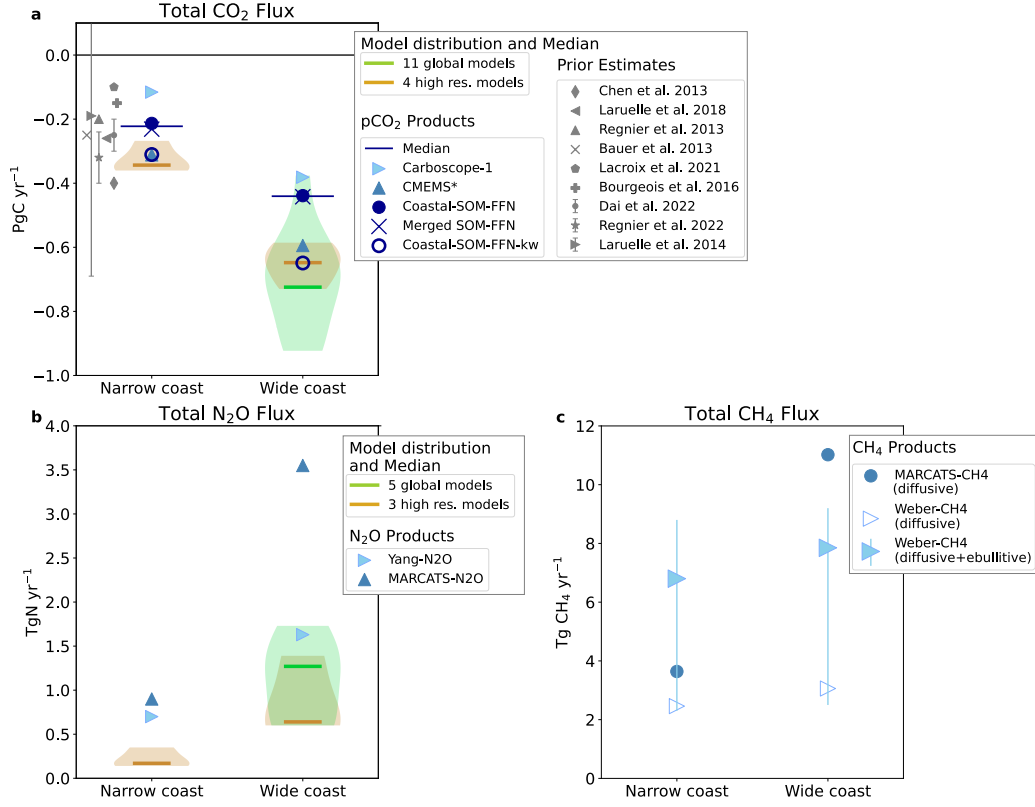


Figure 2. Net globally-integrated coastal fluxes of a) CO₂ [PgC yr⁻¹], b) N₂O [Tg N yr⁻¹] and c) CH₄ [Tg CH₄ yr⁻¹] over the narrow and wide coastal oceans. The model distribution (violin) and median (thick lines) are shown for the full ensemble available in the wide coastal ocean (11 models for CO₂ and 4 for N₂O) and a subset of higher resolution models for the narrow coastal ocean (4 models for CO₂ and 2 for N₂O, see Methods and Table 2 for details). Symbols indicate observation-based products (blue) and previous estimates available for the narrow coastal ocean (grey in panel a, listed in Supplementary Table S2). Coastal-SOM-FFN-k_w, which is a second version of Coastal-SOM-FFN computed using different wind speed and k_w formulation (empty circle, see Methods) is not used in the calculation of the pCO₂-product median. Weber-CH₄ total flux (diffusive+ebullitive) and diffusive contribution (comparable to MARCATS-CH₄ flux) are shown in panel c.

3.1.2 Net N_2O and CH_4 coastal emissions

Estimates of the global coastal emissions of N_2O range from 0.14 to 0.90 Tg N yr⁻¹ in the narrow coastal ocean and from 0.60 to 3.56 Tg N yr⁻¹ in the wide coastal ocean (Figure 2 b). Part of this considerable variability comes from differences between model-based and observation-based estimates, but also from systematic differences between the two observation-based products (MARCATS- N_2O and Yang- N_2O). In the wide coastal ocean, the Yang- N_2O estimate (1.63 Tg N yr⁻¹) falls at the high end of the model estimates (0.60 to 1.73 Tg N yr⁻¹), while MARCATS- N_2O yields N_2O emissions that are more than twice the emissions of Yang- N_2O (3.56 Tg N yr⁻¹, Figure 2 b). This finding implies that global ocean biogeochemical models emission estimates are overall lower than those of the observation-based products. Furthermore, the subset of 3 high-resolution models generally simulate N_2O emissions that are lower than the full set of 5 models and therefore lower than both observation-based estimates (3-model median of 0.64 Tg N yr⁻¹ vs. 5-model median of 1.27 Tg N yr⁻¹ for the wide coastal ocean, Figure 2 b).

In the narrow coastal ocean, the two observation-based estimates are in relatively good agreement (0.90 Tg N yr⁻¹ in MARCATS- N_2O and 0.70 Tg N yr⁻¹ in Yang- N_2O), while the subset of 3 high resolution global ocean models simulate emissions that are again about 2-4 times lower (0.14 to 0.35 Tg N yr⁻¹). The Yang- N_2O product suggests that the narrow coastal ocean accounts for about 50% of the emissions of the wide coastal ocean, while in the subset of 3 global ocean models and MARCATS- N_2O it only accounts for about 25% (Figure 2b). We note, however, that the particularly low model values in both the 5-model ensemble and the 3-model high resolution subset are from ECCO-Darwin and ECCO2-Darwin (0.60-0.64 Tg N yr⁻¹ in the wide and 0.14-0.17 Tg N yr⁻¹ in the narrow coastal ocean) which are based on the same model and are therefore not independent. The fact that global ocean biogeochemical models underestimate coastal N_2O fluxes, in particular nearshore, is likely due to unresolved (e.g. complex microbial production/consumption, sedimentary processes, production in estuarine and coastal vegetation systems transported to the coastal ocean) or spatially under-resolved processes (e.g. high production and remineralization in shallow shelves, and shallow coastal oxygen minimum zones where N_2O emissions take place). Another potential source of bias might be the undersampling of coastal waters in the observations (see Table S1). In particular, observations might be biased high because they are often performed in hotspots of emissions rather than in regions that reflect the mean conditions.

Global CH_4 emissions in Weber- CH_4 include both the diffusive and ebullitive (bubbling) components, and are estimated to be 6.80 [2.30-8.8] Tg CH_4 yr⁻¹ for the narrow coastal ocean and 7.85 [2.50-9.20] Tg CH_4 yr⁻¹ for the wide coastal ocean (Figure 2c). Note that the flux estimates presented here are observation-based only because no model-based estimates are available. The CH_4 flux from Weber- CH_4 is dominated by the ebullitive flux which occurs mostly in shallow waters of the narrow coastal ocean (accounting for 4.33 Tg CH_4 yr⁻¹ in the narrow and 4.79 Tg CH_4 yr⁻¹ in the wide coastal ocean). Subtracting the ebullitive flux from the total Weber- CH_4 fluxes results in a CH_4 diffusive flux of 2.46 [1.23-3.69] Tg CH_4 yr⁻¹ in the narrow coastal ocean, which is in relatively good agreement with the diffusive flux estimated from MARCATS- CH_4 (3.64 Tg CH_4 yr⁻¹). In contrast, the diffusive flux of 3.06 [1.53, 4.59] Tg CH_4 yr⁻¹ obtained in the wide coastal ocean in Weber- CH_4 has a central value ~3.5 times smaller than the diffusive flux of MARCATS- CH_4 (11.02 Tg CH_4 yr⁻¹).

The observation-based estimates of the N_2O emissions and the diffusive flux of CH_4 vary by about 20-30% in the narrow coastal ocean and by about a factor 2 to 3.5 in the wide coastal ocean. The increase in the spread amongst these observational products (which use the same datasets and are therefore not independent) reflects the low number of oceanic N_2O and CH_4 measurements to date, in particular in many coastal regions, as compared to CO_2 . Specifically, the observation density decreases by about a factor 3 from narrow to wide (number of observations per million km² three times lower in the wide coastal

ocean in more than 30 of the 45 regions used for the interpolation, see Table S1). Significant differences between the observation-based estimates (MARCATS-N₂O, MARCATS-CH₄ on the one hand, and Yang-N₂O and Weber-CH₄ on the other hand) can result from (i) applying different approaches for estimating the air-sea gas exchange in combination with using different wind speed products (e.g., Garbe et al., 2014) and (ii) applying different inter- and extrapolation techniques which can introduce significant uncertainties when applied to sparse data. The increase in discrepancy from narrow to wide coastal waters suggests that MARCATS-N₂O and MARCATS-CH₄ may extrapolate local observations over spatial domains where they are not representative anymore. In contrast, the neural networks of Yang-N₂O and Weber-CH₄, albeit also relying on the same MEMENTO dataset, may better capture spatial patterns, such as the overall decrease in CH₄ emissions as the shelf water depth increases.

3.1.3 Combined coastal greenhouse gas emissions

We combined CO₂, N₂O and CH₄ fluxes from observation-based and model-based estimates for the wide coastal ocean using CO₂-equivalent (Figure 3). We find that from a net radiative perspective, N₂O and CH₄ coastal emissions offset much of the coastal CO₂ sink, by ~58% in the product-based budget and ~30% in the model-based budget. As a result, the net greenhouse gas flux into the coastal ocean is -0.66 PgCO₂-e yr⁻¹ in the product-based budget (-1.58 PgCO₂-e yr⁻¹ CO₂ flux offset by +0.70 and +0.21 PgCO₂-e yr⁻¹ of N₂O and CH₄) and -1.81 PgCO₂-e yr⁻¹ in the model-based budget (-2.57 PgCO₂-e yr⁻¹ CO₂ flux offset by +0.54 and +0.21 PgCO₂-e yr⁻¹ of N₂O and CH₄, Figure 3). Most of the difference between the product- and model-based budgets presented here come from the stronger CO₂ uptake in the models mentioned above. There are, however, very few global coastal N₂O and CH₄ estimates and the spread amongst the products and models is large (1 to 2 PgCO₂-e yr⁻¹), indicating that the compensation of the coastal carbon sink could be substantially different from the 30-58% found here.

3.2 Coastal CO₂ dynamics

3.2.1 Contrast between coastal ocean and open ocean

When averaged globally, models and pCO₂-products show lower mean surface ocean pCO₂ and lower CO₂ flux densities (i.e. more uptake) in narrow and wide coastal oceans than in the open ocean (Figure 4). As shown previously for the coastal-SOM-FFN product (Roobaert et al., 2019), this coastal to open ocean difference is however attributable to the increasing contribution of polar waters, characterized by lower flux densities and stronger sinks, to the total surface area from open ocean to narrow coastal domains (polar coastal waters account for 29% of the narrow coastal ocean, 17% of the wide coastal ocean and 2% of open ocean waters, contributions calculated as the percentage of ice-free surface area located poleward of 50 degrees based on NOAA's OISST ice product, Figure 1). This apparent gradient is found in the median of the four pCO₂ products, which shows an increase in global mean sea surface pCO₂ from the narrow coastal ocean to the wide coastal ocean (+ 15 μ atm from 350 to 365 μ atm) and from wide coastal ocean to the open ocean (+7 μ atm from 365 to 372 μ atm for the 1998-2018 period, Figure 4a). The only pCO₂-product among the four that does not capture this coastal to open-ocean difference is Carboscope-1, likely because of potential biases in the Arctic Ocean (pCO₂ values generally higher in Carboscope-1 than in other pCO₂-products and models). The 11-model median simulates slightly higher ocean pCO₂ than the product median but also captures an increase in global mean pCO₂ from wide coastal ocean to open ocean (+6 μ atm from 369 to 375 μ atm) similar to the pCO₂-products. Using the subset of four higher resolution models in the narrow coastal ocean corroborates the presence of this difference in simulated ocean pCO₂. The 4-model median shows a consistently lower mean pCO₂ in the narrow coastal ocean (363 μ atm), compared to the wide coastal ocean (370 μ atm) and to the open ocean (373 μ atm). Thus, although observation-based and mod-

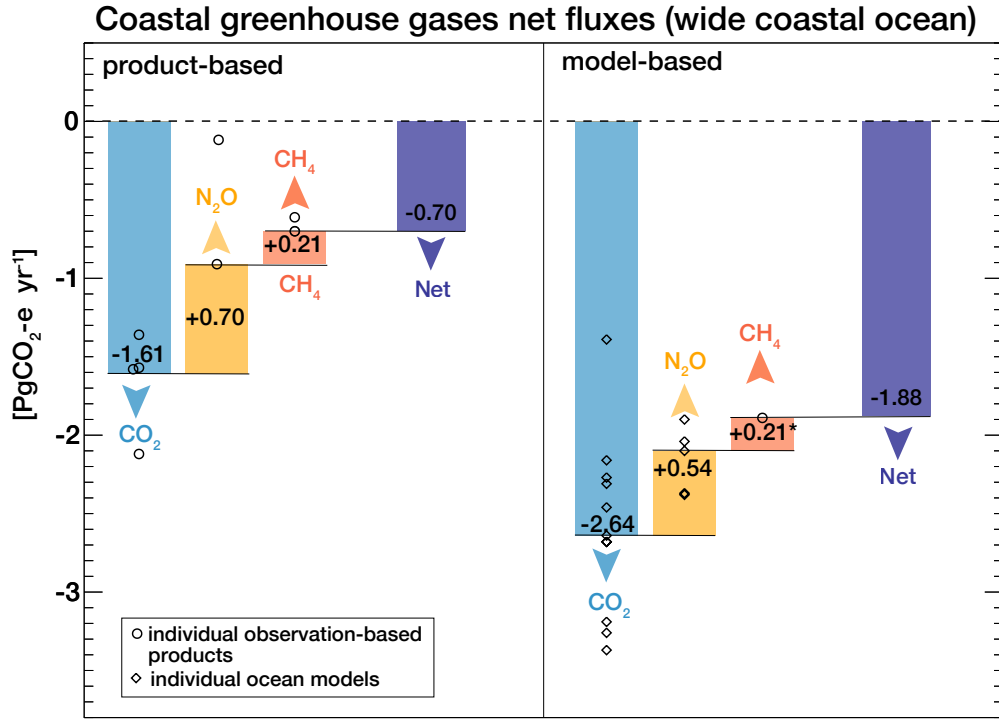


Figure 3. Greenhouse gas air-sea flux in the wide coastal ocean and influence on net atmospheric radiative balance (using $\text{PgCO}_2\text{-e yr}^{-1}$) based on observational products and models of CO_2 , N_2O and CH_4 fluxes. Observations-based central values are from 4 pCO_2 -products, Yang- N_2O and Weber- CH_4 . Model-based central values are from the 11 global models for CO_2 , 4 global models for N_2O , but the Weber- CH_4 product is used for CH_4 as indicated by the asterisk (no model available for CH_4 , hence minimizing the difference between the two assessments). Individual models and observation-based product estimates are shown by symbols. The net GHG flux in $\text{PgCO}_2\text{-e yr}^{-1}$ corresponds to the sum of the three gasses' contributions.

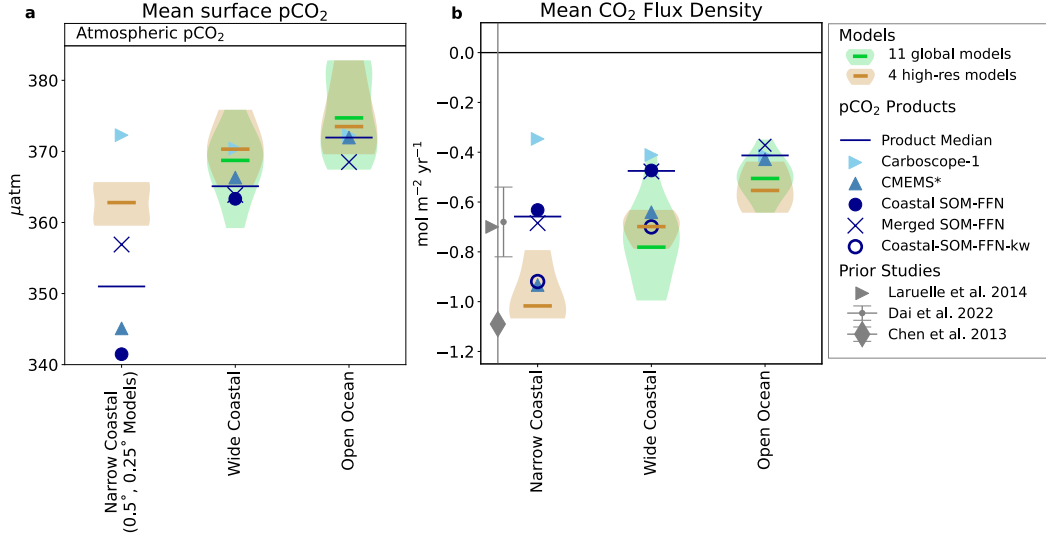


Figure 4. Comparison of globally-averaged coastal ocean and open ocean: a) sea surface pCO₂ [μatm] and b) flux density [mol C m² yr⁻¹] averaged over narrow coastal ocean, wide coastal ocean and open ocean waters in pCO₂-products and ocean models. The model distribution (violin) and median (thick lines) are shown for the full ensemble available in the wide coastal ocean (11 global models in green) and a subset of higher resolution models for the narrow coastal ocean (4 global models in tan, see Methods and Table 2 for details). Symbols indicate global pCO₂-based products (blue), previous estimates (in grey, see Supplementary Table S2 for details). Coastal-SOM-FFN-*k_w*, which is a second version of Coastal-SOM-FFN computed using different wind speed and *k_w* formulation (empty circle, see Methods) is not used in the pCO₂-product median.

eled pCO₂ values show discrepancies in the mean within each domain, the narrow coastal to open ocean differences derived from observations and models are in remarkable agreement, and amount to about 10-15 μatm. A consequence of these differences in sea surface pCO₂ is that the mean partial pressure difference with the atmosphere (mean pCO_{2a} of 385 μatm for 1998-2018) is higher in the coastal ocean than in the open ocean. As a result, air-sea CO₂ flux densities are lower (stronger uptake) in the narrow coastal ocean (-1.02 and -0.66 mol m² yr⁻¹ for 4-model and 4-product medians) than in open ocean waters (-0.55 and -0.41 mol m² yr⁻¹ for 4-model and 4-product medians, Figure 4b). In between, the wide coastal ocean shares characteristics of narrow coastal ocean and open ocean waters and is characterized by intermediate CO₂ flux densities (-0.70 and -0.48 mol m² yr⁻¹ for 4-model and 4-product medians, Figure 4b).

3.2.2 Spatial and seasonal variability in coastal CO₂ sources and sinks

Coastal air-sea CO₂ flux densities are characterized by latitudinal gradients captured by both pCO₂-products and models (Figure 5). Mid- and high-latitude regions (poleward of 25° of latitude) are characterized by annual mean surface ocean pCO₂ lower than the atmosphere (pCO_{2a}=385 ppm for 1998-2018) and thus by oceanic CO₂ uptake, whereas tropical coastal oceans (equatorward of 25° of latitude) are generally associated with pCO₂ similar or slightly higher than the atmospheric level and weak or near-zero CO₂ outgassing (Figure 5 and S4). When averaged latitudinally over the wide coastal ocean, models and products follow a similar pattern, with most negative flux densities (<-1 mol m² yr⁻¹,

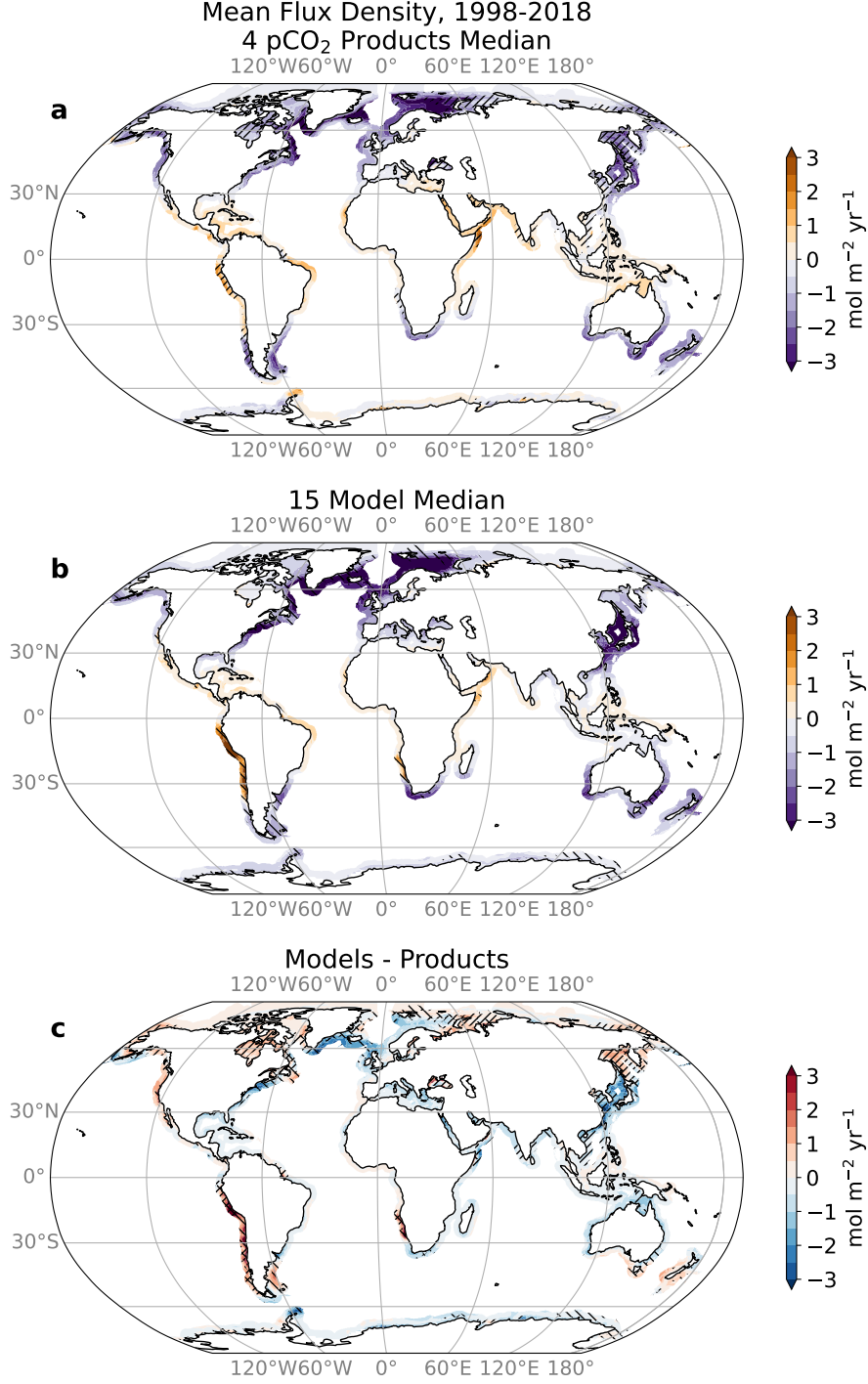


Figure 5. Annual-mean CO₂ flux density [$\text{mol C m}^{-2} \text{ yr}^{-1}$] in the wide coastal ocean for a) the median across the 4 pCO₂-products, b) the median across the 15 models, and c) the difference between model and pCO₂-product medians. The model-median is calculated using the 11 global models and the 4 regional models where available. Hatching indicates the coastal area with root mean square difference (RMSD) greater than 0.60 $\text{mol C m}^{-2} \text{ yr}^{-1}$ across pCO₂ products (panels a and c) or 0.95 $\text{mol C m}^{-2} \text{ yr}^{-1}$ across models (panels b and c) (in both cases the RMSD values correspond to the 20% of coastal area with highest RMSD).

i.e. strongest sinks) at mid-latitudes in both hemispheres (50°S-25°S and 25°N-50°N) and high latitudes in the northern hemisphere (50°N-80°N), and weak sources in the tropical band (typically between 0 and 0.5 mol m² yr⁻¹ in 25°S-25°N, Figure 6a). Largest departures between pCO₂-products and models are found in the northern mid- and high latitudes, where the model median flux densities are often more negative (stronger sink) than the pCO₂-product median (down to -4 mol m² yr⁻¹ in models vs. -2 mol m² yr⁻¹ in pCO₂-products, Figure 6a). These systematically more negative flux densities in the models extend over large coastal areas of the northern hemisphere, including the shelves of western boundary currents (Gulf Stream and Kuroshio), the Norwegian Sea and the southern Greenland basin (blue colors in Figure 5 c), and therefore largely explain the stronger globally integrated coastal sink found in the model median (Fig 2 a). These northern hemisphere regions are relatively well sampled by the SOCAT pCO₂ database (Fig S1), suggesting that the model-product difference might be largely attributable to model biases. Models and pCO₂-products also differ on Antarctic shelves, in particular around the Antarctic Peninsula (around 60°S which is also relatively well sampled compared to the rest of the coastal ocean) where models simulate a weak sink (about -1 mol m² yr⁻¹) but pCO₂-products show a weak source (about +1 mol m² yr⁻¹, Figure 5 and Figure 6a). On the Antarctic shelves, however, the model-product mismatch in CO₂ flux density is confined to a relatively small surface area and the impact on the net global flux is smaller compared to the mismatch found in the northern extratropics. We note that the model median yields less negative or more positive flux densities (i.e. weaker sinks or stronger sources) in some coastal regions, such as the California Current, Peruvian margin, Sea of Okhotsk or Hudson Bay (red colors in Figure 5 c), which offsets part of the stronger sinks simulated in northern and southern extratropical latitudes in the latitudinal mean and global integral.

The global coastal ocean is a sink of CO₂ in all seasons, and pCO₂-products and global ocean biogeochemical models largely agree on the latitudinal patterns in seasonality (Figure 6c-f). Yet, model-product differences emerge in the phasing and amplitude of the seasonality, in particular north of 25°N (Figure 6c-f). In the pCO₂-products, the seasonal amplitude of the air-sea CO₂ flux is similar in both hemispheres and shows a strong latitudinal contrast between: i) the tropics (25°S-25°N), where the seasonal amplitude is small (absolute values <1 mol m² yr⁻¹) and the weak CO₂ source becomes even smaller in winter; ii) the mid-latitudes (50°S-25°S and 25°N-50°N), where the seasonal amplitude is relatively large (absolute values of 1-2.5 mol m² yr⁻¹) and the sink is stronger in winter and spring; and iii) high-latitudes (poleward of 50°N and 50°S), where the seasonal amplitude is also large (similar to mid-latitudes) but the CO₂ sink is stronger in summer (except in the Arctic, north of 80 degree N, where the seasonal amplitude is small, Figure 6b-f). In contrast, the CO₂ sink in the model median is systematically stronger in winter than in summer at all latitudes (except around Antarctica) and does not reproduce the latitudinal change in seasonal phasing obtained in the pCO₂-products (from stronger winter uptake in the tropics to stronger summer uptake at high-latitudes, Figure 6b). In addition, the seasonal amplitude of the CO₂ flux is 50-100% larger in the models at mid-latitudes (despite having a similar phasing, i.e. stronger sink in winter and spring, Figure 6b). As a result of these latitudinal differences in phasing, the products show little seasonality when averaged globally across coastal waters (net median flux of -0.35 PgC yr⁻¹ for DJF vs. -0.32 PgC yr⁻¹ for JJA, Figure 7a). This is largely explained by compensations between mid-latitudes (stronger uptake in winter) and high-latitudes (strong uptake in summer) within each hemisphere (Fig 6), which results in a relatively weak seasonality in both the northern (-0.24 in DJF and -0.22 in JJA) and southern (-0.11 PgC yr⁻¹ in DJF and -0.10 PgC yr⁻¹ in JJA) hemispheres (Figure 7b-c). In the case of the 11-model median, however, this compensation is much weaker and the seasonal cycle is stronger, especially in the northern hemisphere (-0.73 in DJF and 0.00 PgC yr⁻¹ in JJA, Figure 7b-c). As a result, the global coastal ocean in the model median displays a marked seasonality controlled by the seasonality of the northern hemisphere, resulting in a net global coastal sink for DJF (-1.15 PgC yr⁻¹) that is about four times

the sink for JJA ($-0.29 \text{ PgC yr}^{-1}$, Figure 7). This model-product difference in CO_2 flux seasonality and specifically the extremely large boreal winter uptake explains the stronger annual mean global CO_2 sink found in the model median compared to the pCO_2 -products (Figures 2 a, 6 a and 7b).

Model-product differences in CO_2 flux seasonality are largely tied to differences in the surface ocean pCO_2 . The stronger flux seasonality at mid-latitudes in models and the opposed flux seasonality at high latitudes (i.e., stronger uptake in winter in models vs. stronger uptake in summer in products) are both explained by the higher summer ocean pCO_2 (leading to weaker summer uptake) and the lower winter ocean pCO_2 (leading to stronger winter uptake) found in the model median compared to the pCO_2 -product median (Supplementary Figure S5). Differences in ocean pCO_2 can be amplified by the choice of wind speed and gas exchange coefficient formulation. The comparison of the two Coastal-SOM-FFN versions reveals that both the high-latitude summer uptake and the mid-latitude winter uptake are enhanced in Coastal-SOM-FFN- k_w compared to Coastal-SOM-FFN (Figure 7 and S6). This enhancement occurs in both hemispheres but the impact of the northern hemisphere on the global coastal annual mean uptake is larger due to the larger coastal surface area. Despite these systematic differences found between the model median and pCO_2 -product median in the annual mean and seasonal flux, some models reproduce better the latitudinal pattern expected from the pCO_2 -products, in particular the stronger summer uptake at high-latitude in the northern hemisphere (e.g., MOM6-Princeton and MPIOM-HAMOCC, see individual models in Figure S7 and thin green lines overlapping with thin blue lines in Figure 6). We note that this systematic model/product difference in seasonality is also found in the open ocean but that the amplitude of this mismatch is amplified in the coastal ocean (see Figures S7 and S8).

3.2.3 Trends in coastal ocean pCO_2 and air-sea CO_2 flux

For the 1998–2018 period, global coastal pCO_2 trends are slightly weaker than the atmospheric pCO_2 trend ($+20.7 \mu\text{atm/decade}$) in the two time-varying pCO_2 -products (about $+17\text{--}18 \mu\text{atm/decade}$ in the wide coastal ocean) and models ($+17\text{--}20 \mu\text{atm/decade}$ in the wide coastal ocean; see Figure 8a,c). In the narrow coastal ocean, the pCO_2 trends from the pCO_2 -products are lower than in the wide coastal ocean, and fall halfway between the two central values published in previous observation-based estimates ($+16\text{--}17 \mu\text{atm/decade}$ vs. $+19.3 \mu\text{atm/decade}$ in Wang et al., 2017 and $+13 \mu\text{atm/decade}$ in Laruelle et al., 2018). In contrast, the pCO_2 trends found in the subset of four high resolution ocean biogeochemical models are higher in the narrow coastal ocean ($+19.8 \mu\text{atm/decade}$) than in the wide coastal ocean, and in good agreement with the highest of the previous observation-based estimate (Wang et al., 2017).

The trend difference between atmospheric and oceanic pCO_2 leads to an increase in the coastal carbon sink from 1998 to 2018 in pCO_2 -products and models (flux density trends between -0.15 and $-0.04 \text{ mol m}^{-2} \text{ yr}^{-1}$ per decade in the wide coastal ocean, Figure 8b,d). Yet, because the rate of increase in coastal pCO_2 is lower in the pCO_2 -products than in the models, their respective CO_2 uptake trend is larger (Figure 8c). This is consistent with the expectation that a slower increase in sea surface pCO_2 , which does not closely follow the atmospheric pCO_2 trend, should result in a stronger increase of the flux density (e.g., Laruelle et al., 2018). Our results show, however, that pCO_2 trends and flux trends are not directly proportional, suggesting that factors other than pCO_2 variability are at play. These include trends in sea-ice cover (e.g., sea-ice retreat influence on flux trends in the Arctic Ocean) and/or in surface winds (via their effect on the gas exchange transfer velocity). For instance, the Carboscope-1 pCO_2 trends are slightly weaker than the CMEMS* pCO_2 trends in the narrow and wide coastal oceans, and yet the increase in the coastal sink is lower in Carboscope-1 than in CMEMS* (Figure 8c,d). In addition, observation-based CO_2 flux estimation shows that the largest coastal CO_2 sink region in the Arctic Ocean, the Chukchi Sea, is increasing due to increased ice-free

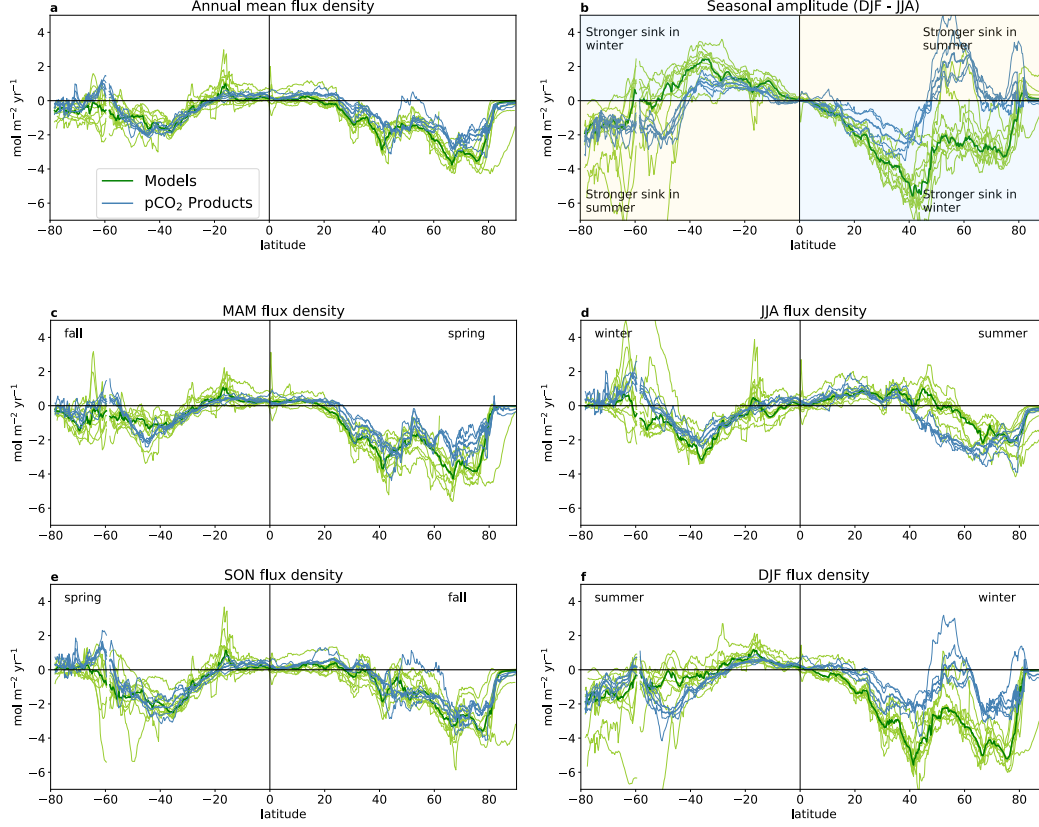


Figure 6. Latitudinal distribution of coastal ocean CO₂ flux and seasonal amplitude (using the wide coastal ocean). Latitudinal distribution of a) annual mean flux density, b) seasonal flux density amplitude, calculated as December-February (DJF) minus June-August (JJA), the blue (orange) quadrants indicate when the ocean uptake is stronger in winter (summer). c-f) seasonal mean flux density for March-May (MAM), JJA, September-November (SON) and DJF. Product and model medians are shown with thick lines and the individual 11 global models and 4 products with thin lines. Units are in mol C m⁻² yr⁻¹ in all panels for consistency, converting from per month to per year also for the 3-month periods.

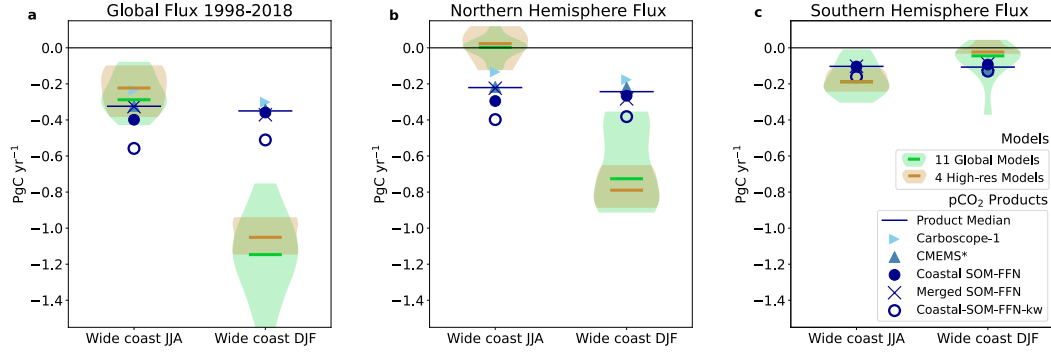


Figure 7. Net air-sea CO_2 flux in June-August (JJA) and December-February (DJF) for a) the global coastal ocean, b-c) the northern and southern hemispheres. The model distribution (violin) and median (thick lines) are shown for the full ensemble available (11 global models in green) and a subset of higher resolution models (4 global models in tan, see Methods and Table 2 for details). Symbols indicate global pCO_2 -based products (blue), prior estimates (grey, see Supplementary Table S2 for details). Coastal-SOM-FFN- k_w , which is a second version of Coastal-SOM-FFN computed using different wind speed and k_w formulation (empty circle, see Methods) is not used in the pCO_2 -product median. Units are in PgC yr^{-1} in all panels for consistency, using a 12-month scale up value for the 3-month periods.

area, longer sea-ice free period, and increased biological production rate (which keeps sea surface pCO_2 increase rate nearly zero) (Ouyang, Collins, et al., 2022). Another example of the decoupling between pCO_2 trends and flux trends is found in the coastal to open ocean difference. The global ocean biogeochemical model ensemble simulates smaller differences between atmospheric and oceanic pCO_2 trends in the coastal ocean than in the open ocean, resulting in a weaker increase in the carbon sink in the coastal ocean (following here the expected link between pCO_2 and flux trends, Figure 8c-d). In contrast to the models, both time-resolving pCO_2 -products reveal higher differences between atmospheric and oceanic pCO_2 trends in the coastal ocean than in the open ocean (Figure 8c), which would suggest a stronger trend in the flux density in the coastal ocean (i.e. a stronger increase in the uptake). However, this expected increase in the uptake is only found in CMEMS* but not in Carbscope-1 (Figure 8d). A precise understanding of the trends in all parameters that control the air-sea fluxes of CO_2 and of the methodological differences in the pCO_2 mapping and flux calculation is crucial to understanding the evolving coastal ocean carbon sink.

Inconsistencies between pCO_2 trends and flux trends arise from the complex and uncertain interplay between the spatio-temporal changes in ocean pCO_2 , wind speed and sea-ice coverage. In particular, trends in ocean pCO_2 and therefore in ΔpCO_2 (difference between coastal ocean surface ocean pCO_2 and atmospheric pCO_2) strongly differ between coastal regions, as well as between the two time-varying pCO_2 -products (Figure S9). CMEMS*, as well as the multi-model median, show more negative ΔpCO_2 trends (potentially stronger uptake or weaker sources with time) in mid-to-high latitudes, but less negative or even positive ΔpCO_2 trends in the tropics and in the Arctic (Figure S10). In contrast, the Carbscope-1 product shows strongly negative ΔpCO_2 trends in the Arctic, and much larger variability in trends at other latitudes. These differences in ΔpCO_2 trends largely translate into consistent flux density trends (negative ΔpCO_2 trends generally yield negative flux trends, i.e., stronger uptake or weaker sources with time, Figures 9 and S10). However we note that in many regions, the ΔpCO_2 trends are amplified or dampened by trends in wind speed and sea-ice coverage, which are also strongly

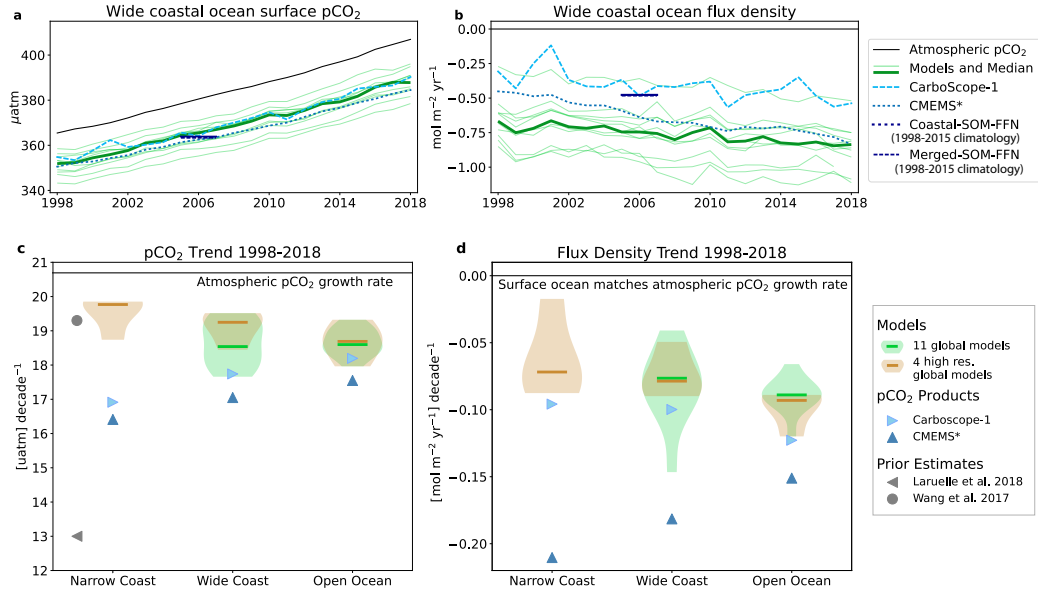


Figure 8. Temporal evolution of the global annual mean a) surface ocean pCO₂ [µatm] and b) net air-sea CO₂ flux density [mol C m⁻² yr⁻¹] in the four pCO₂-products (blue lines) and the 11 global ocean models (thin green lines) and model median (thick green lines) in the wide coastal ocean. Trends in c) ocean surface pCO₂ [µatm decade⁻¹] and d) flux density [mol C m⁻² yr⁻¹] for narrow coastal ocean, wide coastal ocean and open ocean waters. The model distribution (violin) and median (thick lines) are shown for the full model ensemble (11 global models in green) and a subset of higher resolution models (4 global models in tan, see Methods and Table 2 for details). Symbols show the trends for the two time-varying pCO₂-based products (Carboscope-1 and CMEMS* in blue) and prior estimates (in grey, see Table S1 for details).

spatially heterogeneous (see sea-ice trends in Figure S11). This effect is highlighted by the spatial differences and sometimes even a switch in sign between $\Delta p\text{CO}_2$ trends and air-sea CO₂ flux trends in the model median in sea-ice regions (hatching in Figure 9). This is true, for instance, in the Arctic where the ocean models tend to simulate an increase in ocean CO₂ uptake despite a positive trend in $\Delta p\text{CO}_2$ (i.e., ocean pCO₂ increases at a high rate than atmospheric pCO₂ which would reduce ocean uptake with constant sea-ice coverage and winds, Figures 9 and S10). This decoupling between CO₂ flux and $\Delta p\text{CO}_2$ in the Arctic is indeed associated with a decrease in sea ice coverage in most models (Figure S11) and an increase in wind speed in two of the wind products that are widely used in these models (JRA-55 and ERA-5, Figure S12 and Tables 2-3), both effects inducing an increase in the flux with time despite the reduction in $\Delta p\text{CO}_2$. These results clearly indicate that the global coastal sink is increasing. Yet, the magnitude of this increase, its spatial patterns and how it compares to the open ocean are still uncertain.

3.3 Coastal nitrous oxide and methane spatial variability

The spatial distribution of the coastal N₂O fluxes computed with the observation-based (i.e., Yang-N₂O) and a mean of the model-based approaches are shown in Figure 10. Coastal N₂O fluxes are generally positive, indicating that coastal areas are a source of atmospheric N₂O. Flux densities vary considerably, from 0 (= equilibrium with the atmosphere) to about 10 g N m⁻² yr⁻¹. The results from Yang-N₂O reveal hotspots of N₂O emissions in eastern boundary upwelling systems, the upwelling areas of the north-

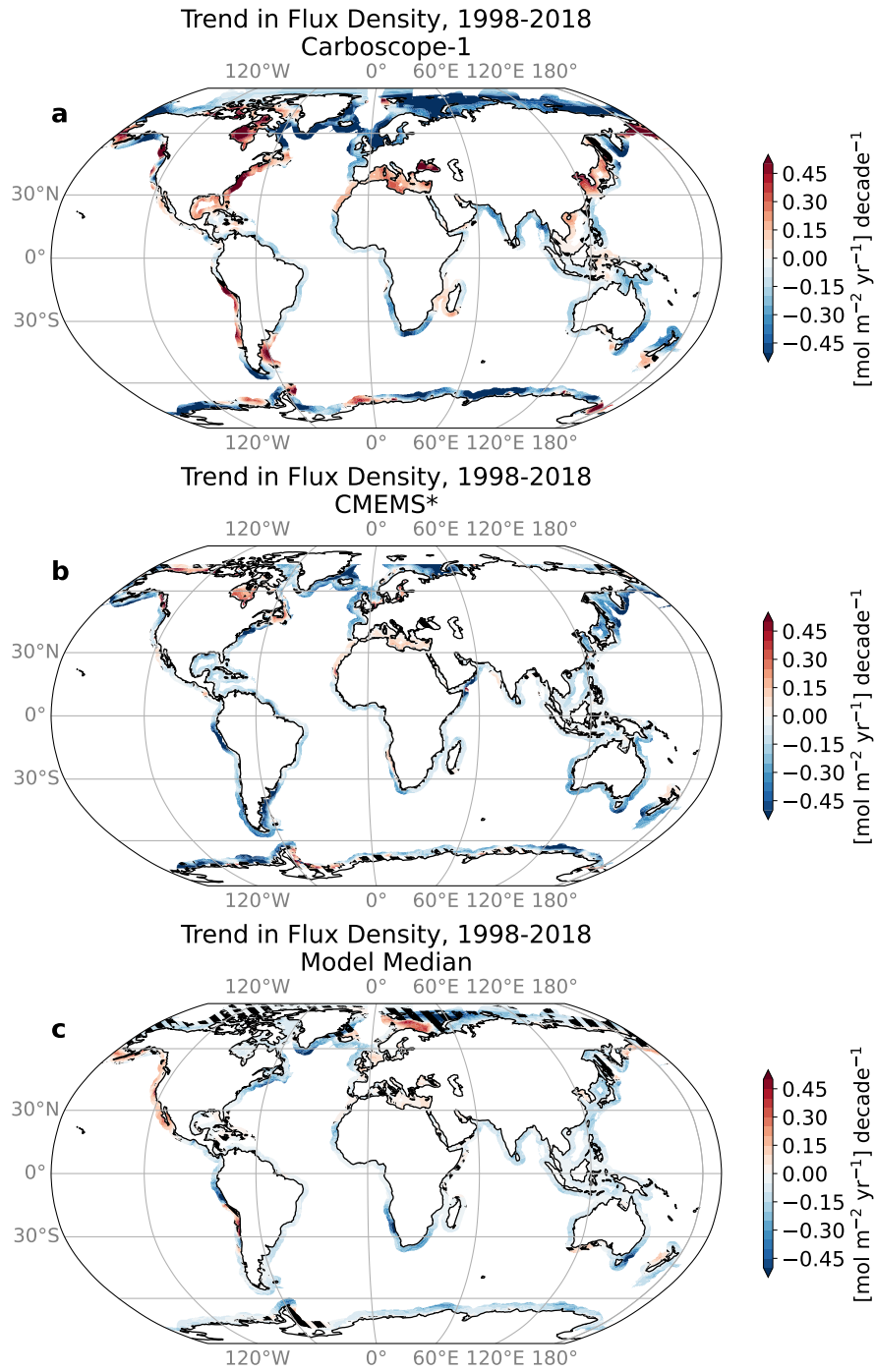


Figure 9. 1998-2018 trend in CO₂ flux [$\text{mol C m}^{-2} \text{ yr}^{-1}$] for a) Carboscope-1; b) CMEMS* (area north of 75° N removed) c) multi-model median (global and regional models). Hatching indicates regions where the flux trend has a different sign than the $\Delta p\text{CO}_2$ trend (shown in Figure S10), highlighting the influence of wind and/or sea-ice trends. Negative values indicate that the ocean uptake increases or the ocean outgassing decreases with time (both leading to more carbon accumulation in the ocean).

western Indian Ocean, the subpolar North Pacific, the Baltic Sea, the Black Sea and the shallow marginal seas of Southeast and East Asia. These are generally characterized by high surface productivity, low subsurface oxygen, and shallow oxyclines. High N_2O emissions from these regions thus likely reflects subsurface water-column production by a combination of nitrification and denitrification pathways, both of which are enhanced in the presence of low O_2 and high remineralization rates, and subsequent transport to the surface by upwelling and mixing processes. Similar hotspot regions are detected in the model-ensemble median, although with somewhat reduced magnitude relative to the observational products, and with the notable exception of marginal seas in Asia and Europe, suggesting that global models might not fully capture the nitrogen cycle in these regions, or the mechanisms transporting N_2O -laden waters to the surface. In addition, the model-ensemble also identifies mid-latitude western boundary systems, including the US East Coast, the North Pacific east of Japan, the southeast coast of Australia, and the southeastern tip of Africa, as additional areas of intense N_2O emissions that are not captured by the Yang- N_2O product. Notably, these regions are not generally characterized by high surface productivity and low subsurface O_2 as coastal upwelling systems, although vigorous mixing along western boundary currents may favor local N_2O outgassing in the models. Most of these regions are also not densely sampled by observations in the MEMENTO database, in particular along the US, South Africa, and Japan eastern coasts, and thus the Yang- N_2O observational extrapolation may be poorly constrained there. The magnitude of the flux in these hotspots often differs among the data products and model-ensemble (Figure 10c). The N_2O flux distributions shown in Figure 10 likely reflect the fact that enhanced coastal N_2O concentrations – and thus enhanced N_2O emissions fluxes – are associated with enhanced land-sea inputs of nitrogen (as nitrate or ammonium) or with upwelling of N_2O -enriched subsurface water masses in upwelling systems.

The spatial distribution of the coastal CH_4 fluxes computed with the observation-based Weber- CH_4 product are shown in Figure 11. Coastal CH_4 fluxes are generally positive and range from 0 to $0.4 \text{ g CH}_4 \text{ m}^{-2} \text{ yr}^{-1}$ indicating that coastal areas are a source of atmospheric CH_4 . Patterns in CH_4 emissions in Weber- CH_4 are largely correlated to water depth with most intense emissions occurring at depth shallower than 50 m (Figure 11). Indeed, coastal emissions of CH_4 are largely fueled by benthic-sourced biogenic methane, which is produced via methanogenesis in anoxic sediments and released diffusively into the overlying water column (Reeburgh, 2007; Arndt et al., 2013; Bourgeois et al., 2016). The benthic CH_4 source is enhanced in coastal waters where the rapid organic matter flux to the seafloor drives sediment anoxia and rapid sediment accumulation inhibits the growth of methane oxidizing microbes (e.g., Egger et al., 2016). Furthermore, aerobic respiration acts as an efficient sink of CH_4 in the water column (Mao et al., 2022), meaning that transfer from the seafloor to the surface must be extremely rapid if CH_4 is to be emitted to the atmosphere. Ebullition (bubbling) from CH_4 -enriched sediments can provide an important alternative pathway for CH_4 to surface (Rehder et al., 1998), but CH_4 is rapidly stripped from rising bubbles (McGinnis et al., 2006) and a small fraction reaches the surface only in shallow water depths. This further strengthens the coastal-offshore gradient in CH_4 emissions, and explains why total emissions differ very little between the narrow and wide coast regions in Weber- CH_4 (Figure 2c). Coastal CH_4 emissions are further enhanced in hotspots under significant influence of freshwater discharge (Rosentreter et al., 2021), which due to their low sulfate concentration, promote the degradation of organic matter through the methanogenesis pathway. In addition to the biogenic CH_4 production pathway, CH_4 emissions can also be driven by geologically sourced methane, originating from shallow seafloor seeps fed by hydrocarbon reservoirs or high-latitude hydrates (Ruppel & Kessler, 2017; Puglini et al., 2020). Overall, the distribution of coastal CH_4 emissions (Figure 11) can largely be understood in terms of water depth, organic matter production and delivery to sediments, and freshwater inputs.

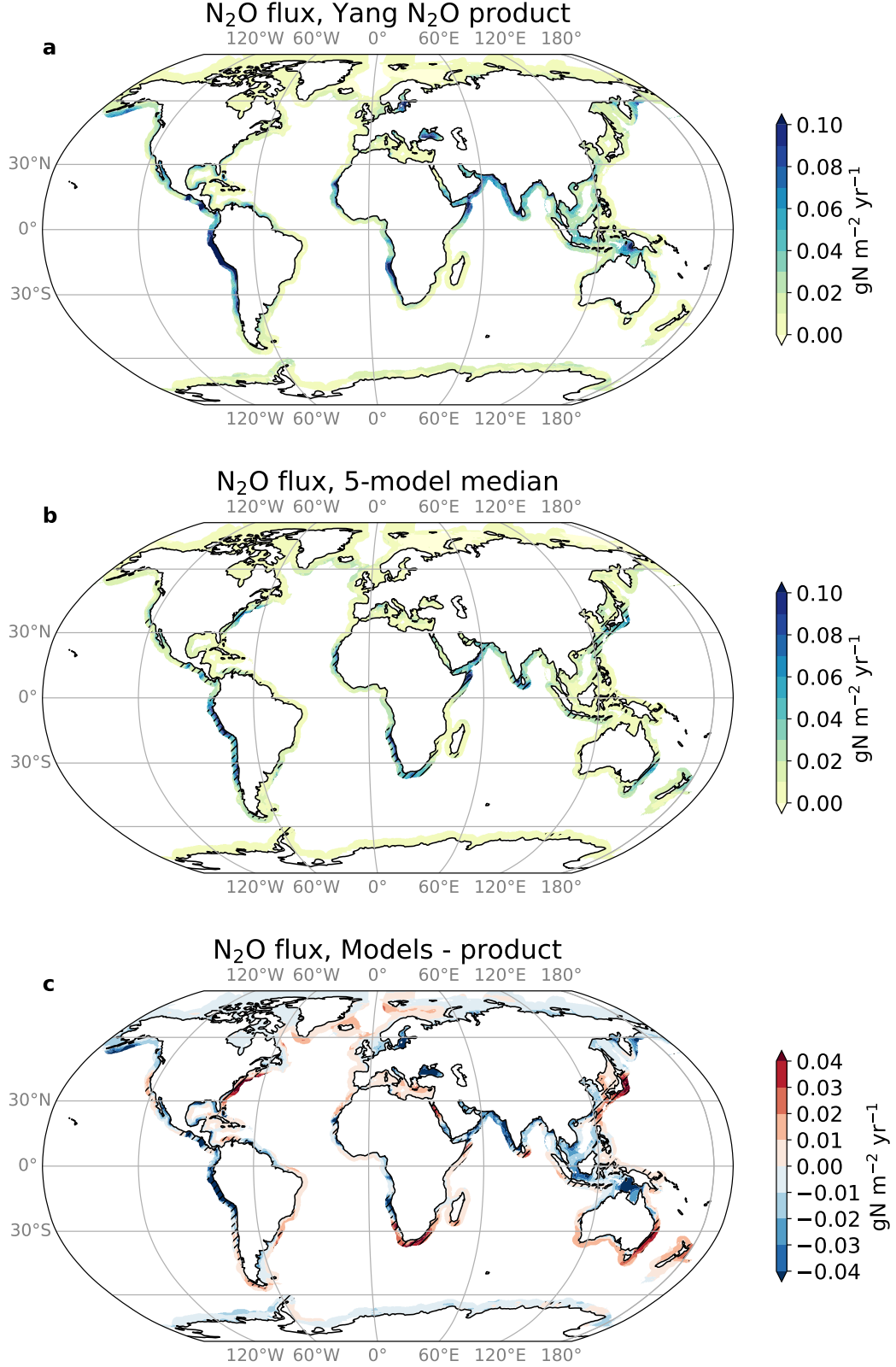


Figure 10. Maps of coastal N_2O flux (in $\text{g N m}^{-2} \text{yr}^{-1}$) from a) Yang-N₂O product and b) the mean of the 5 global ocean models that simulate N_2O (CNRM-LR, CNRM-HR, ECCO-Darwin, ECCO2-Darwin, and NEMO-PlankTOM5). Hatching in panels b-c shows where RMSD among models exceeds $0.016 \text{ g N m}^{-2} \text{yr}^{-1}$ (RMSD threshold corresponds to the 20% of coastal area with highest RMSD).

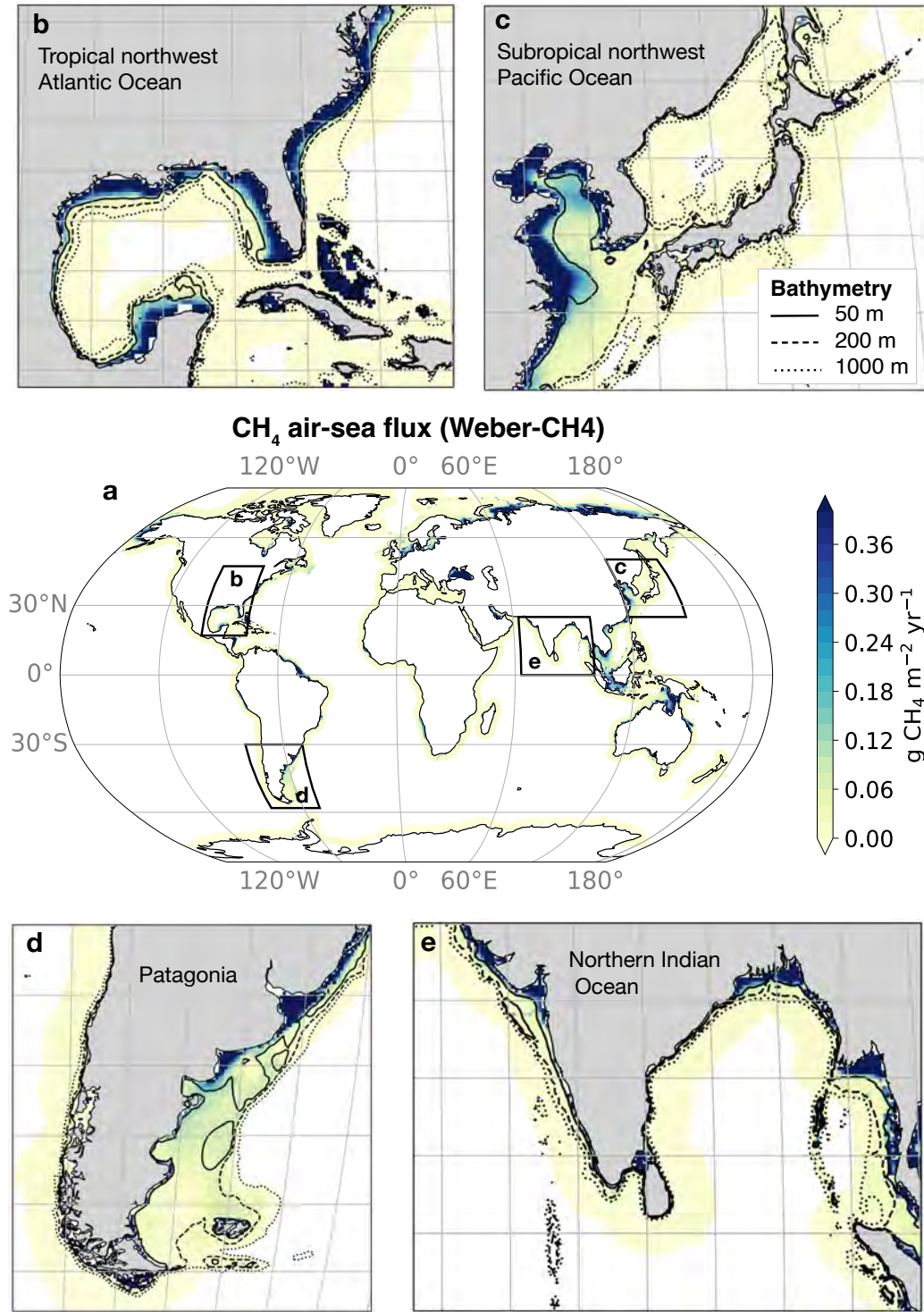


Figure 11. a) Global maps of coastal CH₄ flux from the Weber-CH4 product (includes diffusive and ebullitive flux, in $\text{g CH}_4 \text{ m}^{-2} \text{ yr}^{-1}$); b-e) insets show the CH₄ flux in four coastal regions along with 50, 200 and 1000 m bathymetry contours. CH₄ emissions are most intense in shallow coastal environments.

4 Discussion

4.1 Coastal CO₂ fluxes

This study presents a synthesis of the global coastal ocean air-sea CO₂ fluxes combining observational pCO₂-based products and an ensemble of ocean biogeochemical models. We confirm the hypothesis put forward in prior work (Laruelle et al., 2010, 2014; Roobaert et al., 2019; Dai et al., 2022) that when averaged globally, CO₂ flux densities are more negative (stronger sinks) in the coastal ocean than in the open ocean waters. As put forward by Roobaert et al. (2019), we find that the differences between coastal and open ocean flux densities are largely explained by the disproportionate contribution of high latitude systems (generally strong sinks) to the coastal ocean surface area. Global ocean biogeochemical models and pCO₂-products agree relatively well on the coast-to-open ocean contrast in CO₂ flux densities, but recent syntheses of discrete observations (Cao et al., 2020; Dai et al., 2022) find stronger heterogeneity than the global pCO₂-products and global ocean models presented here, suggesting that gap-filling approaches and global ocean models might smooth some of the coastal ocean spatial variability. Despite the good agreement on the coast-to-open ocean differences, the global ocean biogeochemical models yield a net median CO₂ uptake in the wide coastal ocean that is about 0.28 PgC stronger than the one inferred from pCO₂-products for the 1998-2018 period, equivalent to a ~60% stronger sink (-0.44 PgC yr⁻¹ for products vs. -0.72 PgC yr⁻¹ for models in the wide coastal ocean). This mismatch of model- and product-based work in the net coastal CO₂ sink arises from a combination of factors, including strong differences in the coastal CO₂ flux seasonality (themselves attributed to differences in ocean pCO₂ seasonality and potentially wind speed and gas exchange transfer coefficient formulation) resulting in a stronger wintertime CO₂ uptake in northern subpolar and polar coastal systems in models.

4.1.1 Seasonality

The seasonality in the four pCO₂-products used here falls into three latitudinal regimes. Tropical coastal waters (25°S-25°N) are characterized by small seasonal amplitudes and a stronger sink or weaker source in winter, both attributed to the weak seasonal thermal changes that slightly reduce surface ocean pCO₂ in winter (Laruelle et al., 2014; Roobaert et al., 2019). Mid-latitude coastal waters (50°S-25°S and 25°N-50°N) are characterized by larger seasonal amplitudes and a stronger CO₂ sink in winter and spring, likely due to the combined effect of thermal changes which lowers ocean pCO₂ in winter, biological drawdown of dissolved inorganic carbon (DIC) which further lowers pCO₂ during the spring bloom, and the influence of stronger winds in winter (Laruelle et al., 2014; Roobaert et al., 2022). High latitude coastal waters (poleward of 50°N and 50°S) are characterized by seasonal variations similar in magnitude to mid-latitudes, but where the maximum CO₂ uptake occurs in summer in response to intense biological drawdown. The biologically-driven uptake in high-latitude systems peaks a few months later than in mid-latitude systems because of the poleward propagation of the bloom (Siegel et al., 2002; Roobaert et al., 2019, 2022; Ouyang, Collins, et al., 2022). This marked seasonality in CO₂ fluxes contrasts with the RECCAP synthesis which found very little seasonality in global coastal CO₂ flux densities, although the results were deemed inconclusive because of the sparse data and averaging process required to analyze the data available at the time (Chen et al., 2013). The results found here are, however, consistent with more recent work. In particular, the transition from thermally driven systems in the tropics (stronger winter sinks) to biologically driven systems at high latitudes (stronger summer sinks), and the increase in seasonal amplitude from tropical to high-latitude systems found in the pCO₂-products, are consistent with the global seasonal patterns in the coastal ocean described by (Roobaert et al., 2019), the global open ocean seasonality patterns assessed in the framework of RECCAP2 (Rodgers et al., submitted to the RECCAP2 special is-

sue), and supported by field and remote sensing studies at regional scale (Signorini et al., 2013; Ouyang, Collins, et al., 2022; Tu et al., 2021).

Our synthesis reveals, however, strong differences in seasonality between $p\text{CO}_2$ -products and global ocean biogeochemical models. The model median simulates a weak CO_2 flux seasonality in tropical coastal oceans similarly to the $p\text{CO}_2$ -products, but yields a CO_2 uptake that is stronger in winter at mid- and high-latitudes. This is likely due to a weaker contribution of biologically induced seasonality compared to thermal changes in the models, which would explain the lower surface ocean $p\text{CO}_2$ simulated in winter (due to an underestimated upward transport of remineralized DIC) and the higher $p\text{CO}_2$ simulated in spring/summer (due to a weaker biological drawdown). Part of these systematic differences compensate in the global mean coastal flux (winter vs. summer, northern vs. southern hemisphere), but because the model-product difference is larger in winter in the northern hemisphere, the net CO_2 uptake in the wide coastal ocean is about 60% larger in the model median. The RECCAP2 chapter on open ocean seasonality (Rodgers et al., submitted to the RECCAP2 special issue), finds a similar systematic bias in model winter-to-summer $p\text{CO}_2$, which they attribute to a generally too small surface DIC seasonal cycle in models compared to observation-based reconstructions. This bias is particularly evident in the subpolar North Atlantic and North Pacific Oceans, where it manifests itself not only as a difference in amplitude but also in phasing. In these regions, the simulated too low DIC seasonality results in a thermal control of the $p\text{CO}_2$ seasonality in the global ocean biogeochemical models and thus in a phase shift of the seasonal $p\text{CO}_2$ cycle compared to the observation-based estimate dominated by non-thermal forcing. This suggests that the systematically stronger winter sink and weaker summer sink found in northern coastal waters in the models are at least partly attributable to general biases in the biogeochemical (e.g., bloom dynamics) or physical (e.g., vertical mixing) components of the ocean models, rather than a characteristic of the models that is specific to the coastal ocean. See details in the RECCAP2 studies of (Rodgers et al., submitted to the RECCAP2 special issue). Nevertheless, we find that the amplitude of this systematic model/product difference in seasonality is amplified in the coastal ocean (see Figures S7-S8).

Differences in ocean $p\text{CO}_2$ seasonality between models and $p\text{CO}_2$ products can be amplified by differences in gas exchange coefficient k_w , either through the influence of winds or the gas exchange coefficient formulation (which are different across the different ocean biogeochemical models and $p\text{CO}_2$ -products, Tables 1-3), and maybe to a lesser extent spatio-temporal differences in sea-ice cover (e.g., lower ice cover in some products/models could yield stronger fluxes). In models, the surface $p\text{CO}_2$ and k_w are tightly coupled in the sense that a larger k_w drives down the air-sea $p\text{CO}_2$ disequilibrium and therefore the air-sea CO_2 flux. In contrast, the calculation of the flux in $p\text{CO}_2$ products (except for Carboscope-1 which links fluxes and $p\text{CO}_2$ changes in a mixed-layer carbon budget equation) is done offline without any compensatory effect between k_w and air-sea $p\text{CO}_2$ disequilibrium. Therefore, the observation-based flux assessments are even more sensitive to the choice of the wind and k_w parameterization. For instance, we find that the net global coastal CO_2 uptake in the Coastal-SOM-FFN product is increased by nearly 50% in the wide and the narrow coastal ocean when changing the wind product (from ERA-interim to JRAv1.3) and gas exchange parametrization (from Ho et al., 2011 to Wanninkhof 1992, see Table 1). These results are in line with published literature that assessed the impact of k_w parametrizations on global air-sea CO_2 fluxes (Boutin et al., 2009; Roobaert et al., 2018; Reichl & Deike, 2020), but highlights that its influence is also crucial in the coastal ocean, because of the disproportionate contribution of mid- to high-latitude/high-wind systems in the total coastal area. Furthermore, global wind-based gas exchange parameterization might not capture the complexity of the coastal ocean processes, such as the influence of bubbles entrained by wave breaking (Deike & Melville, 2018; Woolf et al., 2019), the presence of high surfactant concentrations (Pereira et al., 2018), or fine scale water-side convection (Gutiérrez-Loza et al., 2022).

4.1.2 Land-sea fluxes

An additional factor that can explain part of the difference in the net CO_2 uptake between pCO_2 -products and models is the presence of systematic bias in global ocean biogeochemical models, in particular the contribution of carbon and nutrient land-sea riverine inputs or the models' horizontal resolution and ability to resolve coastal dynamics. At pre-industrial times (and assuming steady-state consistent with stable ice-core atmosphere CO_2 values; Elsig et al., 2009), the supply of carbon from land must have been balanced by burial in sediments and an outgassing of CO_2 from the ocean to the atmosphere. This land-driven outgassing flux, recently estimated to be $0.65 \pm 0.3 \text{ PgC yr}^{-1}$ (mean ± 2 -sigma) for the global open ocean (Regnier et al., 2022, note that this outgassing of 0.65 PgC yr^{-1} is quantified for the open ocean outside of the narrow coastal ocean and thus include part of the wide coastal ocean), is still active today and therefore partially offsets the ingassing CO_2 flux that is directly driven by anthropogenic CO_2 emissions to the atmosphere (e.g., Resplandy et al., 2018; Friedlingstein et al., 2022; Regnier et al., 2022). Observation-based pCO_2 -products estimate the net contemporary flux of CO_2 , and therefore implicitly include the fluxes of natural and anthropogenic carbon, as well as the outgassing fluxes of carbon from land origin (e.g., Hauck et al., 2020). Most models, however, do not, or only partially include this land-sea carbon inputs (see Tables 2-3) and are therefore likely to overestimate the net CO_2 ocean uptake, in particular in coastal waters adjacent to the land (Lacroix et al., 2020).

In globally integrated estimates, such as analyzed in the Global Carbon Budget (e.g., Friedlingstein et al., 2022) or the IPCC (Arias et al., 2021), the net air-sea CO_2 flux can in principle be adjusted for the outgassing of carbon from land to isolate the oceanic net sink, or it can be used to shed light on differences between modeled and observation-based flux estimates (e.g., Hauck et al., 2020; Friedlingstein et al., 2022). The RECCAP2 open ocean chapters estimated the spatial distribution of this land-driven CO_2 outgassing by upscaling the spatial distribution from Lacroix et al. (2020) using the global outgassing number of Regnier et al. (2022). This estimate suggests that 0.12 PgC yr^{-1} out of the 0.65 PgC yr^{-1} of land-driven CO_2 outgassing occurs in the wide coastal ocean, which could explain part of the model-product discrepancy. It is important to recognize, however, that the spatial distribution of this land-driven outgassing and contribution to the coastal ocean air-sea flux are very poorly constrained. In particular, we note that the model used to estimate the land-driven outgassing pattern (Lacroix et al., 2020) is lacking some of the processes that control the magnitude (hence the upscaling to match the global number of 0.65 PgC yr^{-1} from Regnier et al. (2022) but also the spatial distribution of this outgassing (e.g., CO_2 uptake by coastal vegetation). Another factor to consider is the land-sea input of nutrients which promotes biological CO_2 uptake in coastal waters downstream of the river mouth (e.g., Louchard et al., 2021; Terhaar et al., 2021; Gao et al., 2023), potentially offsetting the land-driven CO_2 outgassing associated with carbon runoffs, although we do not expect the patterns of the CO_2 outgassing and biological CO_2 uptake to match. In the model ensemble considered here models either include both carbon and nutrient land-sea inputs or neither (Tables 2 and 3). This might explain why models with land-sea carbon inputs did not systematically yield weaker CO_2 uptake in the coastal ocean compared to the one without land-sea inputs. Finally, we find that the subset of global ocean biogeochemical models with highest spatial resolution yields a slightly weaker net CO_2 uptake ($-0.65 \text{ PgC yr}^{-1}$) in better agreement with the pCO_2 -products than the full model ensemble. The small number of models in that subset (4) makes any statistical argument about resolution difficult. Yet, this result suggests that a better representation of fine scale coastal dynamics could improve the representation of the CO_2 flux, likely by improving the representation of the physical and biogeochemical processes controlling CO_2 seasonality in the northern hemisphere (Laurent et al., 2021; Rutherford et al., 2021; Rutherford & Fennel, 2022).

4.1.3 Trends

This synthesis indicates that the coastal ocean CO₂ sink has increased between 1998 and 2018, in line with the expectation from previous work that showed surface pCO₂ in the narrow coastal ocean increasing at a smaller rate than in the atmosphere (Wang et al., 2017; Laruelle et al., 2018). The rate at which the coastal sink has increased is, however, poorly constrained by the models and products presented here (flux density trend varies by a factor 2 between the two time-varying pCO₂-products and by a factor 3 between the 11 models). In addition, it is still unclear if this increase in the global coastal CO₂ sink is comparable, slower or faster than in the open ocean due to the inconsistent responses found in models and the two time-varying pCO₂-products but also in prior modeling and observation-based work (Bourgeois et al., 2016; Wang et al., 2017; Laruelle et al., 2018; Lacroix et al., 2021). The CMEMS* pCO₂-product suggests that the CO₂ uptake increases faster in the coastal ocean than in the open ocean, which is in line with the prior observation-based results of Laruelle et al. (2018). In contrast, the ensemble of 11 global ocean models and the Carboscope-1 pCO₂-product suggest that the coastal ocean sink is increasing at a slightly smaller rate than the open ocean, a result in line with another other prior work based on pCO₂ observations (Wang et al., 2017) and global ocean biogeochemical models (Bourgeois et al., 2016; Lacroix et al., 2021). Bourgeois et al. (2016) explains this weaker increase in the coastal carbon sink by a bottleneck in offshore transport which leads to anthropogenic carbon accumulation and limits the ability of coastal waters to take up anthropogenic carbon. Although we do not quantify surface residence time or off-shelf transport in this study, our finding that the modeled CO₂ sink increases at a lower rate in the coastal region than in the open ocean lends support for this interpretation. Other processes at play could explain this behavior. For instance, relatively shallow waters in coastal oceans might limit the exchanges with deep (free of anthropogenic CO₂) waters, such that the coastal ocean surface layer saturates more quickly with additional CO₂ added to the atmosphere. In models, this slower rate is associated with regions of increased outgassing or reduced uptake, although mid-to-high latitudes can be strongly increasing CO₂ sinks as suggested by observations (Laruelle et al., 2018). However, the regions controlling this slower rate of increase vary across models (e.g., North Pacific, Mediterranean Sea and Parts of the Arctic in the model median in this study vs. tropical ocean and parts of the Arctic in Lacroix et al., 2021), highlighting further the uncertainties that remain in constraining coastal trends.

The slower increasing pCO₂ trend in the coastal ocean was attributed in these model-based studies to an increased outgassing or reduced uptake in tropical and river-dominated Arctic shelves, while mid-to-high latitudes were found to be strongly increasing CO₂ sinks as suggested by observations. Part of the discrepancies between the estimates of the CO₂ flux trends are likely to arise from the sparse temporal pCO₂ observational coverage. For instance the prior studies of Wang et al. (2017) and Laruelle et al. (2018) only covered a small portion of the coastal surface area and might not be representative of the global ocean. This is supported by regional studies that identified coastal ocean pCO₂ trend weaker than the atmospheric pCO₂ trend (i.e. potentially yielding intensified CO₂ uptake or decreased outgassing) such as the northern Gulf Stream margin, the South China Sea, the Sea of Japan, the North Sea and the Antarctic Peninsula (Bauer et al., 2013; Wang et al., 2017; Laruelle et al., 2018; Dai et al., 2022), but also regions where coastal ocean pCO₂ increases at a similar rate (i.e. near-zero changes in the flux) or even higher rates (i.e. reduced CO₂ uptake or intensified outgassing) than atmospheric pCO₂, such as in the Baltic Sea (Schneider & Müller, 2018), the California Current or along the eastern US coast (Reimer et al., 2017; Laruelle et al., 2018; Salisbury & Jönsson, 2018; Xu et al., 2020; Dai et al., 2022). Another source of discrepancy is the decoupling found between global coastal pCO₂ trends and flux trends, suggesting that the CO₂ flux trends are sensitive to trends in winds and sea-ice (via the gas exchange coefficient), and how they combine with the pCO₂ trends. This sensitivity to sea-ice and winds is likely more pronounced in the observation-based estimates, which rely on an “offline” calculation of

the flux (no mechanistic link between $p\text{CO}_2$ disequilibrium, wind and sea-ice, except for CarboScope-1), or even more simply assume that slower trends in coastal ocean $p\text{CO}_2$ translate into faster growing coastal CO_2 flux (e.g., Laruelle et al., 2018), an assumption that is not fulfilled in the 2 $p\text{CO}_2$ -products used in this study (although it does work in the multi-model median).

4.1.4 Conclusions

The systematic differences found between the ensemble median of global ocean models and $p\text{CO}_2$ -products (including the larger net annual mean CO_2 uptake found in global ocean models, the different timing of mid- and high-latitude seasonality and the large range found in flux density trends) should be interpreted with caution. First, some models are capturing better than others the patterns reconstructed by the $p\text{CO}_2$ -products. In particular, some models are able to reproduce the stronger summer sink found at high-latitudes, or simulate a net annual mean CO_2 flux that better matches the product-based estimates. In addition, differences between products and models do not necessarily equate to model bias, as regions of largest product-model mismatch also often correspond to regions where the observational sampling is sparse (68% of the wide coastal ocean surface area was never sampled, and of the sampled area, 33% has data for only one month in a single year, Figure S1) and where the spread across the observation-based products and across the global models is the highest (hatching on Figure 5a,b). In contrast, coastal regions that are relatively well sampled by observations and well constrained by the products generally correspond to regions of agreement between the observation-based and model-based estimates (Roobaert et al., 2022). Thus, while we have overall more confidence in the observation-based estimates of the ocean carbon sink, the uncertainties associated with these reconstructed estimates remain high. This precludes a clear conclusion about whether the observation or model-based estimates are closer to the truth.

4.2 Coastal N_2O and CH_4

The coastal ocean is a substantial source of atmospheric N_2O (Yang et al., 2020) and a minor source of atmospheric CH_4 (Weber et al., 2019; Saunio et al., 2020). The N_2O flux estimates presented here for the narrow coastal ocean (0.14 to 0.75 Tg N yr⁻¹) are at the lower end of previous estimates of the mean global N_2O fluxes from nearshore coastal systems (including shelves, estuaries and upwelling regions) which range from 0.7 to 6.7 Tg N yr⁻¹ (Bange et al., 1996; Seitzinger & Kroeze, 1998). The mean CH_4 flux estimates for the narrow coastal ocean (2.46-3.19 Tg CH_4 yr⁻¹ for the diffusive flux and up to 6.79 Tg CH_4 yr⁻¹ when accounting for the ebullitive flux in the narrow coastal ocean) are in good agreement with a recently published mean CH_4 flux from shelves (0 - 200 m water depth) of 5.7 Tg CH_4 yr⁻¹ (Rosentreter et al., 2021). Nevertheless, quantitative estimates of N_2O and CH_4 emissions remain highly uncertain. Estimates of N_2O emissions in this study vary by a factor of 5-6 in both the narrow and wide coastal ocean, and central values of CH_4 emissions by a factor up to 3.5. The smaller range found here for CH_4 likely reflects the fewer number of estimates available (2 observation-based products only vs. 5 global ocean models and 2 observation-based products for N_2O) rather than stronger constraints on the emissions.

Current observational products only provide a climatological view of N_2O and annual mean view of CH_4 emissions, with limited or missing information on (i) seasonal and inter-annual variability, (ii) fine-scale (i.e., few 10s of km or less) land-ocean gradients, (iii) the effects of mesoscale and submesoscale features such as eddies (Grundle et al., 2017), and (iv) extreme events such as storms and marine heat waves (Borges et al., 2019; Gindorf et al., 2022). Aspects of air-sea gas exchange, such as the effects of surface micro-layers on these gasses (Kock et al., 2012) remain also poorly understood. In parallel, commonly adopted model parameterizations greatly simplify complex source and sink processes that are the focus of ongoing research. For example, there remains

significant uncertainty in the relative importance of the various (micro)biological and photochemical processes driving the production and consumption of N_2O and CH_4 in coastal waters and sediments, and their potential responses to changing oceanic conditions (Bange, 2022). Methane can be produced aerobically in-situ in surface waters, providing the most direct route to the atmosphere. This process has mostly been studied in the open ocean where decomposition of methylphosphonate (MPn, a component of semi-labile dissolved organic matter) appears to be the dominant methanogenesis pathway (Karl et al., 2008; Repeta et al., 2016). Recent evidence suggests the MPn pathway is also active in some coastal waters (Mao et al., 2022), but its importance relative to benthic-sourced CH_4 in coastal waters remains unclear. Additional sources of N_2O and CH_4 remain poorly characterized and are not represented by models, including submarine groundwater discharge (Arévalo-Martínez et al., 2023) and production associated with marine microplastic (Royer et al., 2018; Su et al., 2022), submerged aquatic vegetation (Rosentreter et al., 2021; Hilt et al., 2022; Roth et al., 2023; Rosentreter et al., 2023), and zooplankton (Schmale et al., 2018).

Our study reveals that while coastal N_2O flux emissions from observational products and models generally agree in terms of main patterns and magnitude, emission hotspots in productive, low- O_2 upwelling systems appear to be underestimated by models, suggesting deficiencies in model circulation and parameterization of low- O_2 sources. In contrast, models point to coastal N_2O flux hotspots along mid-latitude western boundaries that are not evident in observational reconstructions. The reason for this mismatch remains unclear, but likely reflects lack of observations from these regions, which could limit the ability of reconstructions to capture coastal hotspots, and potential model biases. The recently proposed Global N_2O Ocean Observation Network (N_2O -ON) (Bange et al., 2019; Bange, 2022) might help to better constrain and understand temporal and spatial variability as well as reduce uncertainties in current global N_2O oceanic emission estimates.

Ongoing environmental changes such as ocean warming, decreasing pH, loss of dissolved oxygen, and eutrophication might significantly alter the production and consumption of both N_2O and CH_4 as well as their distribution patterns in coastal waters and, consequently, their release to the atmosphere (e.g., Rees et al., 2022; Zhou et al., 2023). However, our knowledge of recent trends on which future emissions scenarios of N_2O and CH_4 from the coastal ocean rely upon are still far from complete. In particular, hydrate dissolution due to ocean warming may enhance this flux at the seafloor, but only at the feather-edge of the hydrate stability zone, which occurs in ~ 400 m deep water in mid-latitudes – which could be too deep for the methane to make it to the surface and escape to the atmosphere (Joung et al., 2022). Shallow hydrocarbon-fed seep fields allow for more efficient methane release to atmosphere (Hovland et al., 1993), but their impact appears to be highly localized (Joung et al., 2020), and the global-scale contribution of geological CH_4 to marine emissions remains highly uncertain (Etiope et al., 2019). Understanding CH_4 oxidation dynamics in coastal environments is therefore an important focus area for future research. Although N_2O -ON was originally designed for N_2O only, adding measurements of CH_4 will be facilitated by deploying instruments on the basis of the same technique used for N_2O measurements (i.e. cavity-enhanced absorption spectroscopy), providing new opportunities to establish long-term time-series for these two greenhouse gasses.

4.3 Coastal greenhouse gas atmospheric influence

This synthesis provides an estimate of the coastal contribution to the atmospheric greenhouse gas budget using an ensemble of observation-based products and global ocean biogeochemical models (in CO_2 -equivalent). In both products and models, we find that a significant proportion of the coastal CO_2 uptake (~ 35 - 55%) is offset by N_2O and CH_4 emissions, despite large uncertainties in the magnitude of the mean CO_2 uptake (large

uptake in models) and relatively limited numbers of observation-based products and models available for N_2O and CH_4 fluxes. This offset is significantly larger than in the global ocean, for which a value of about 10% can be calculated based on the CO_2 (Le Quéré et al., 2018), N_2O (Tian et al., 2020), and CH_4 (Saunois et al., 2020) global budgets by the GCP. A smaller offset value on the order of 10-20% has also been reported for estuaries and coastal vegetated ecosystems (Rosentreter et al., 2023), highlighting that the radiative balance on the shelves results from a significant contribution of the 3 greenhouse gasses. Such an offset does not occur in inland waters either (rivers, lakes and reservoirs), as freshwater aquatic systems are a net source of CO_2 , CH_4 and N_2O (Battin et al., 2023)(also Lauerwald et al., in revision for the RECCAP2 special issue), with CO_2 and CH_4 contributing roughly 75% and 25% to the 100-year time-scale global warming potential, respectively, while N_2O is only a marginal contributor. Integrating the three compartments of the land-to-ocean aquatic continuum (LOAC) from streams to the coastal oceans (i.e., inland waters, estuaries and coastal vegetation, and coastal ocean waters (Regnier et al., 2013, 2022), we find that the LOAC is a net source of greenhouse gasses. Indeed, the 8.3 (range of 5.8-12.7) $\text{PgCO}_2\text{-e yr}^{-1}$ emitted by inland waters are only partly compensated by the net uptakes of 0.4 (range 0.2-0.7) $\text{PgCO}_2\text{-e yr}^{-1}$ from estuaries and coastal vegetation and 1.3 (range 0.7-1.8) $\text{PgCO}_2\text{-e yr}^{-1}$ from wide coastal waters. For the 100 year time horizon, the LOAC as a whole thus emits about 6.6 $\text{PgCO}_2\text{-e yr}^{-1}$ globally.

Acknowledgments

The authors have no conflicts of interest. A.K.H. acknowledges support from the National Science Foundation (NSF) Graduate Research Fellowship Program under Grant DGE-2039656. Any opinions, findings, and conclusions or recommendations expressed in this material are those of the author and do not necessarily reflect the views of the NSF. L.R. and E.L. were partly funded by National Oceanic and Atmospheric Administration award NA21OAR4310119. L.R. and M.M. thank NASA for financial support via the grant NASA OCO-2 Science Team Grant 80NSSC18K0893. L.R. additionally thank the Princeton Institute for Computational Science and Engineering (PICSciE) for High Performance Computing (HPC) provision, storage and support. D.B. acknowledges support from NSF grant OCE-1847687, and computational resources from the Expanse system at the San Diego Supercomputer Center through allocation TG-OCE170017 from the Advanced Cyber infrastructure Coordination Ecosystem: Services and Support (ACCESS) program, which is supported by NSF grants 2138259, 2138286, 2138307, 2137603, and 2138296. J.D.M. and N.G. acknowledge support from the European Union’s Horizon 2020 research and innovation programme under grant agreement no. 821003 (project 4C) and no. 820989 (project COMFORT). N.G. additionally thanks for the support of the Swiss National Science Foundation through grant agreement no 175787 (Project X-EBUS). J.S. was supported by the Research Council of Norway (grant no 270061) and acknowledges provision of HPC and storage resources by UNINET/sigma2 (nn/ns9560k). C.L.Q. was funded by the UK Royal Society (grant no. RP\R1\191063). Simulations of the NEMO-PlankTOM model were carried out by D. Willis on the HPC Cluster supported by the Research and Specialist Computing Support service at the University of East Anglia. G.G.L. is a research associate of the FRS-FNRS at the Université Libre de Bruxelles. Finally, we thank the RECCAP2 organisers and scientific steering committee for coordinating and supporting this effort.

Table 1. Description of observation-based products used in this study, including the wind speed product and gas exchange coefficient (k_w) formulation used to compute the fluxes. W92, H11, W14, L13, N00 stands for k_w -formulations from Wanninkhof (1992); Ho et al. (2011); Wanninkhof (2014); Liang et al. (2013); Nightingale et al. (2000) respectively. Mon and Ann stands for monthly and annual mean frequencies. Wide coastal areas are calculated after the products and models have been regridded on the $0.25^\circ \times 0.25^\circ$ grid. Further details and references on observation-based products and models are provided in Supplementary Material.

Product	Gasses	land-sea inputs	Domain	Frequency/period in this study	Horizontal resolution	wide area (million km ²)	wind speed and k_w	Reference
Carboscope-1	CO ₂	N/A	Global	Mon ^a 1998-2018	1°	73.9	JRA55-do v1.5.0 W92 ^b	(Rödenbeck et al., 2022)
CMEMS*	CO ₂	N/A	Global ^c	Mon 1998-2018	1°	55.8	ERA5 W14 ^b	(Chau et al., 2022)
Coastal-SOM-FFN	CO ₂	N/A	Global	Mon 1998-2015	0.25°	77.2	ERA-interim H11	(Roobaert et al., 2019)
Coastal-SOM-FFN- k_w	CO ₂	N/A	Global	Mon 1998-2015	0.25°	77.2	JRAv1.3 W92	
Merged-SOM-FFN	CO ₂	N/A	Global	Mon 1998-2015	0.25°	77.2	ERA-interim H11	(Landschützer et al., 2020)
Yang-N2O	N ₂ O	N/A	Global	Mon 1998-2015	0.25°	73.4	ERA-5 W14 ^b , L13 ^b	(Yang et al., 2020)
Weber-CH4	CH ₄	N/A	Global	Ann 1999-2016	0.25°	73.7	ERA-5 W14 ^b , L13 ^b	(Weber et al., 2019)
MARCATS-N2O & MARCATS-CH4	N ₂ O, CH ₄	N/A	Global	Ann 1980-2016	regional ^d	77.2	NCEP II N00	(Kock & Bange, 2015)

^aFrom originally daily.

^bScaled to global ocean mean value of 16.5 cm/h.

^cMissing Arctic filled with Coastal-SOM-FFN climatology north of 75°N.

^dNo gap filling, one value per MARGins and CATchments Segmentation (MARCATS).

Table 2. Description of global ocean biogeochemical models used in this study, including the wind speed product and gas exchange coefficient (k_w) formulation used to compute the fluxes. W92 and W14 stand for k_w -formulations from Wanninkhof (1992, 2014) respectively. Mon stands for monthly frequency. Wide coastal areas are calculated after the products and models have been regridded on the $0.25^\circ \times 0.25^\circ$ grid. Further details and references on observation-based products and models are provided in Supplementary Material.

Model	Gasses	land-sea inputs	Domain	Frequency/period in this study	Horizontal resolution	wide area (million km ²)	wind speed and k_w	Reference
CCSM-WHOI	CO ₂	No	Global	Mon 1998-2017	3.6°lon 0.8-1.8°lat	34.5	NCEP W92	Doney et al. (2009)
CNRM-LR	CO ₂ , N ₂ O	Yes	Global	Mon 1998-2018	1°lon 0.3-1°lat	64.8	JRA55-do W14	Séférian et al. (2019)
CNRM-HR	CO ₂ , N ₂ O	Yes	Global	Mon 1998-2018	0.25°	71.3	JRA55-do W14	Berthet et al. (2019)
FESOM-LR	CO ₂	No	Global	Mon 1998-2018	unstructured ~1°	75.5	JRA55-do W14	Hauck et al. (2020)
FESOM-HR	CO ₂	No	Global	Mon 1998-2018	unstructured ~0.25°	76.4	JRA55-do W14	Hauck et al. (2020)
IPSL	CO ₂	Yes	Global	Mon 1998-2018	1°lon 0.3-1°lat	65	JRA55-do W14	Bopp et al. (2015)
MOM6-Princeton	CO ₂	Yes ^a	Global	Mon 1998-2018	0.5°lon 0.25-0.5°lat	63.8	JRA55-do v1.3 W92	Liao et al. (2020)
MPIOM-HAMMOC	CO ₂	Yes	Global	Mon 1998-2018	1.5°	44.5	NCEP W14	Ilyina et al. (2013)
MRI-ESM2.1	CO ₂	No	Global	Mon 1998-2018	1°lon 0.3-0.5°lat	66.3	JRA55-do W14	Yukimoto et al. (2019)
NEMO-PlankTOM12	CO ₂	Yes	Global	Mon 1998-2018	2°lon 0.3-1.5°lat	62.8	NCEP W92	Wright et al. (2021)
NEMO-PlankTOM5	N ₂ O	Yes	Global	Mon 1998-2018	2°lon 0.3-1.5°lat	62.8	NCEP W92	Buitenhuis et al. (2018)
NorESM-OC2.0	CO ₂ , N ₂ O	Yes	Global	Mon 1998-2018	nominal 1°	63.9	JRAv1.3 W14	Tjiputra et al. (2020)
ECCO-Darwin	N ₂ O	No	Global	Mon 1997-2014	1/3°lon	66.5	ERA-Interim W92	Carroll et al. (2020)
ECCO2-Darwin	N ₂ O	No	Global	Mon 2006-2013	1/6°lon	90.5	ECMWF & JRA-55 W92	Manizza et al. (2019)

^aCarbon inputs are only partial and calculated to roughly balance burial.

Table 3. Description of regional ocean biogeochemical models used in this study, including the wind speed product and gas exchange coefficient (k_w) formulation used to compute the fluxes. W92, H06 and W14 stand for k_w -formulations from Wanninkhof (1992); Ho et al. (2006); Wanninkhof (2014) respectively. Mon stands for monthly frequency. Further details and references on observation-based products and models are provided in Supplementary Material.

Model	Gasses	land-sea inputs	Domain	Frequency/period in this study	Horizontal resolution	wind speed and k_w	Reference
ETHZ-ROMS-Atl	CO ₂	Yes	regional Atlantic Ocean	Mon 1998-2018	~4-120 km ^a	ERA5 W14	Louchard et al. (2021)
ETHZ-ROMS-Pac	CO ₂	Yes	regional Pacific Ocean	Mon 1998-2018	~4-60 km ^b	ERA5 W14	Desmet et al. (2022)
ACM-NWAtl	CO ₂	Yes	Regional Northwest Atlantic (36.3 to 53.8N; -74.6 to -45.2 E)	Mon 1998-2018	~9.5 km	ERA-interim H06, W14	Rutherford et al. (2021)
NYUAD-ROMS-Indian	CO ₂	nutrients no carbon	regional Indian Ocean (31.5°S to 31°N; 30°E to 120°E)	Mon 1998-2018	1/10°	ERA-interim W14	Lachkar et al. (2021)

^ahighest resolution in Amazon plume and western Africa (2 poles).

^bhighest resolution in California Current (1 pole).

Open Research

All of the RECCAP2 data will be made available in a public repository before publication.

Author contributions

- Conceptualization (Ideas; formulation or evolution of overarching research goals and aims): L.R., P.R.
- Data curation (Management activities to annotate (produce metadata), scrub data and maintain research data (including software code, where it is necessary for interpreting the data itself) for initial use and later re-use): A.K.H., L.B., S.B., S.C.D., K.F., J.H., N.G., C.L.Q., E.L., I.D.L., J.D.M., C.N., L.R., J.S., R.S., K.T., H.T., D.B., T.T.T.C., M.G., A.K., P.L., G.G.L., A.R., C.R., T.W.
- Formal analysis (Application of statistical, mathematical, computational, or other formal techniques to analyse or synthesize study data): A.K.H., L.R.
- Funding acquisition (Acquisition of the financial support for the project leading to this publication): L.R.
- Investigation (Conducting a research and investigation process, specifically performing the experiments, or data/evidence collection): L.B., S.B., S.C.D., K.F., J.H., N.G., C.L.Q., E.L., I.D.L., J.D.M., C.N., L.R., J.S., R.S., K.T., H.T., D.W., D.B., T.T.T.C., M.G., A.K., P.L., G.G.L., A.R., C.R., T.W.
- Methodology (Development or design of methodology; creation of models): A.K.H., L.R., P.R.
- Project administration (Management and coordination responsibility for the research activity planning and execution): N.G., J.H., J.D.M., L.R., P.R.
- Software (Programming, software development; designing computer programs; implementation of the computer code and supporting algorithms; testing of existing code components): A.K.H., L.R.
- Supervision (Oversight and leadership responsibility for the research activity planning and execution, including mentorship external to the core team): L.R., P.R., N.G., J.H., J.D.M.
- Visualization (Preparation, creation and/or presentation of the published work, specifically visualization/data presentation): A.K.H., L.R.
- Writing – original draft (Preparation, creation and/or presentation of the published work, specifically writing the initial draft (including substantive translation)): L.R., P.R., H.W.B., D.B., T.W.
- Writing – review and editing (Preparation, creation and/or presentation of the published work by those from the original research group, specifically critical review, commentary or revision – including pre- or post-publication stages): All co-authors.

References

- Anderson, L. G., Jutterström, S., Hjalmarsson, S., Wählström, I., & Semiletov, I. P. (2009, October). Out-gassing of CO₂ from Siberian Shelf seas by terrestrial organic matter decomposition. *Geophysical Research Letters*, 36(20), L20601. Retrieved 2023-02-14, from <http://doi.wiley.com/10.1029/2009GL040046> doi: 10.1029/2009GL040046
- Arias, P. A., Bellouin, N., Coppola, E., Jones, R. G., Krinner, G., Marotzke, J., ... Zickfeld, K. (2021). Technical Summary. In V. Masson-Delmotte et al. (Eds.), *Climate Change 2021: The Physical Science Basis. Contribution of Working Group I to the Sixth Assessment Report of the Intergovernmental Panel on Climate Change*. Cambridge, UK and New York, NY, USA: Cambridge University Press. Retrieved from <https://www.ipcc.ch/report/ar6/>

- wg1/downloads/report/IPCC_AR6.WGI.TS.pdf (Type: Book Section) doi: 10.1017/9781009157896.002
- Arndt, S., Jørgensen, B., LaRowe, D., Middelburg, J., Pancost, R., & Regnier, P. (2013, August). Quantifying the degradation of organic matter in marine sediments: A review and synthesis. *Earth-Science Reviews*, 123, 53–86. Retrieved 2023-02-27, from <https://linkinghub.elsevier.com/retrieve/pii/S0012825213000512> doi: 10.1016/j.earscirev.2013.02.008
- Arrigo, K. R., van Dijken, G., & Long, M. (2008, November). Coastal Southern Ocean: A strong anthropogenic CO₂ sink. *Geophysical Research Letters*, 35(21), L21602. Retrieved 2023-02-14, from <http://doi.wiley.com/10.1029/2008GL035624> doi: 10.1029/2008GL035624
- Arévalo-Martínez, D. L., Haroon, A., Bange, H. W., Erkul, E., Jegen, M., Moosdorf, N., ... Weymer, B. A. (2023, February). Ideas and perspectives: Land-ocean connectivity through groundwater. *Biogeosciences*, 20(3), 647–662. Retrieved 2023-03-27, from <https://bg.copernicus.org/articles/20/647/2023/> doi: 10.5194/bg-20-647-2023
- Arévalo-Martínez, D. L., Kock, A., Löschner, C. R., Schmitz, R. A., & Bange, H. W. (2015, July). Massive nitrous oxide emissions from the tropical South Pacific Ocean. *Nature Geoscience*, 8(7), 530–533. Retrieved 2023-02-14, from <http://www.nature.com/articles/ngeo2469> doi: 10.1038/ngeo2469
- Bakker, D. C. E., Alin, S. R., Becker, M., Bittig, H. C., Castaño-Primo, R., Feely, R. A., ... Wilson, D. (2022). *Surface Ocean CO₂ Atlas Database Version 2022 (SOCATv2022) (NCEI Accession 0253659)*. NOAA National Centers for Environmental Information. Retrieved 2023-02-14, from <https://www.ncei.noaa.gov/archive/accession/0253659> (Type: dataset) doi: 10.25921/1H9F-NB73
- Bakker, D. C. E., Pfeil, B., Landa, C. S., Metzl, N., O'Brien, K. M., Olsen, A., ... Xu, S. (2016, September). A multi-decade record of high-quality *f*CO₂ data in version 3 of the Surface Ocean CO₂ Atlas (SOCAT). *Earth System Science Data*, 8(2), 383–413. Retrieved from <https://www.earth-syst-sci-data.net/8/383/2016/> doi: <https://doi.org/10.5194/essd-8-383-2016>
- Bakker, D. C. E., Pfeil, B., Smith, K., Hankin, S., Olsen, A., Alin, S. R., ... Watson, A. J. (2014, March). An update to the Surface Ocean CO₂ Atlas (SOCAT version 2). *Earth System Science Data*, 6(1), 69–90. Retrieved 2023-03-23, from <https://essd.copernicus.org/articles/6/69/2014/> doi: 10.5194/essd-6-69-2014
- Bange, H. W. (2022, December). Non-CO₂ greenhouse gases (N₂O, CH₄, CO) and the ocean. *One Earth*, 5(12), 1316–1318. Retrieved 2023-02-14, from <https://linkinghub.elsevier.com/retrieve/pii/S2590332222005875> doi: 10.1016/j.oneear.2022.11.011
- Bange, H. W., Arévalo-Martínez, D. L., de la Paz, M., Farías, L., Kaiser, J., Kock, A., ... Wilson, S. T. (2019, April). A Harmonized Nitrous Oxide (N₂O) Ocean Observation Network for the 21st Century. *Frontiers in Marine Science*, 6, 157. Retrieved 2023-02-14, from <https://www.frontiersin.org/article/10.3389/fmars.2019.00157/full> doi: 10.3389/fmars.2019.00157
- Bange, H. W., Rapsomanikis, S., & Andreae, M. O. (1996). Nitrous oxide in coastal waters. *Global Biogeochemical Cycles*, 10(1), 197–207. Retrieved 2023-02-14, from <https://onlinelibrary.wiley.com/doi/abs/10.1029/95GB03834> (eprint: <https://onlinelibrary.wiley.com/doi/pdf/10.1029/95GB03834>) doi: 10.1029/95GB03834
- Battin, T. J., Lauerwald, R., Bernhardt, E. S., Bertuzzo, E., Gener, L. G., Hall, R. O., ... Regnier, P. (2023, January). River ecosystem metabolism and carbon biogeochemistry in a changing world. *Nature*, 613(7944), 449–459. Retrieved 2023-03-27, from <https://www.nature.com/articles/s41586-022-05500-8> (Number: 7944 Publisher: Nature Publishing Group)

- doi: 10.1038/s41586-022-05500-8
- Bauer, J. E., Cai, W.-J., Raymond, P. A., Bianchi, T. S., Hopkinson, C. S., & Regnier, P. A. G. (2013, December). The changing carbon cycle of the coastal ocean. *Nature*, 504(7478), 61–70. Retrieved 2016-01-12, from <http://www.nature.com/nature/journal/v504/n7478/abs/nature12857.html> doi: 10.1038/nature12857
- Berthet, S., Jouanno, J., Séférian, R., Gehlen, M., & Llovel, W. (2022, August). How does the phytoplankton-light feedback affect marine N₂O inventory? *Earth Syst. Dynam. Discuss.*. Retrieved 2023-03-01, from <https://esd.copernicus.org/preprints/esd-2022-28/> doi: 10.5194/esd-2022-28
- Berthet, S., Séférian, R., Bricaud, C., Chevallier, M., Voldoire, A., & Ethé, C. (2019, June). Evaluation of an Online Grid-Coarsening Algorithm in a Global Eddy-Admitting Ocean Biogeochemical Model. *Journal of Advances in Modeling Earth Systems*, 11(6), 1759–1783. Retrieved 2023-03-01, from <https://onlinelibrary.wiley.com/doi/abs/10.1029/2019MS001644> doi: 10.1029/2019MS001644
- Bopp, L., Lévy, M., Resplandy, L., & Sallée, J. B. (2015, August). Pathways of anthropogenic carbon subduction in the global ocean. *Geophysical Research Letters*, 42(15), 2015GL065073. Retrieved 2015-09-14, from <http://onlinelibrary.wiley.com/doi/10.1002/2015GL065073/abstract> doi: 10.1002/2015GL065073
- Bourgeois, T., Orr, J. C., Resplandy, L., Terhaar, J., Ethé, C., Gehlen, M., & Bopp, L. (2016, July). Coastal-ocean uptake of anthropogenic carbon. *Biogeosciences*, 13(14), 4167–4185. Retrieved 2016-09-23, from <http://www.biogeosciences.net/13/4167/2016/> doi: 10.5194/bg-13-4167-2016
- Boutin, J., Quilfen, Y., Merlivat, L., & Piolle, J. F. (2009, April). Global average of air-sea CO₂ transfer velocity from QuikSCAT scatterometer wind speeds. *Journal of Geophysical Research*, 114(C4), C04007. Retrieved 2023-03-22, from <http://doi.wiley.com/10.1029/2007JC004168> doi: 10.1029/2007JC004168
- Buitenhuis, E. T., Suntharalingam, P., & Le Quéré, C. (2018, April). Constraints on global oceanic emissions of N₂O from observations and models. *Biogeosciences*, 15(7), 2161–2175. Retrieved 2023-02-07, from <https://bg.copernicus.org/articles/15/2161/2018/> (Publisher: Copernicus GmbH) doi: 10.5194/bg-15-2161-2018
- Cahill, B., Wilkin, J., Fennel, K., Vandemark, D., & Friedrichs, M. A. M. (2016, February). Interannual and seasonal variabilities in air-sea CO₂ fluxes along the U.S. eastern continental shelf and their sensitivity to increasing air temperatures and variable winds: U.S. East Coast Shelf Air-Sea CO₂ Fluxes. *Journal of Geophysical Research: Biogeosciences*, 121(2), 295–311. Retrieved 2023-03-23, from <http://doi.wiley.com/10.1002/2015JG002939> doi: 10.1002/2015JG002939
- Cai, W., Yang, K., Wu, L., Huang, G., Santoso, A., Ng, B., ... Yamagata, T. (2021, January). Opposite response of strong and moderate positive Indian Ocean Dipole to global warming. *Nature Climate Change*, 11(1), 27–32. Retrieved 2022-01-28, from <http://www.nature.com/articles/s41558-020-00943-1> doi: 10.1038/s41558-020-00943-1
- Cai, W.-J., Dai, M., & Wang, Y. (2006). Air-sea exchange of carbon dioxide in ocean margins: A province-based synthesis. *Geophysical Research Letters*, 33(12), L12603. Retrieved 2021-09-03, from <http://doi.wiley.com/10.1029/2006GL026219> doi: 10.1029/2006GL026219
- Cao, Z., Yang, W., Zhao, Y., Guo, X., Yin, Z., Du, C., ... Dai, M. (2020, April). Diagnosis of CO₂ dynamics and fluxes in global coastal oceans. *National Science Review*, 7(4), 786–797. Retrieved 2021-09-03, from <https://academic.oup.com/nsr/article/7/4/786/5542784> doi:

- 10.1093/nsr/nwz105
- Carroll, D., Menemenlis, D., Adkins, J. F., Bowman, K. W., Brix, H., Dutkiewicz, S., ... Zhang, H. (2020, October). The ECCO-Darwin Data-Assimilative Global Ocean Biogeochemistry Model: Estimates of Seasonal to Multi-decadal Surface Ocean $p\text{CO}_2$ and Air-Sea CO_2 Flux. *Journal of Advances in Modeling Earth Systems*, 12(10). Retrieved 2023-02-15, from <https://onlinelibrary.wiley.com/doi/10.1029/2019MS001888> doi: 10.1029/2019MS001888
- Chau, T. T. T., Gehlen, M., & Chevallier, F. (2022, February). A seamless ensemble-based reconstruction of surface ocean $p\text{CO}_2$ and air-sea CO_2 fluxes over the global coastal and open oceans. *Biogeosciences*, 19(4), 1087–1109. Retrieved 2023-02-15, from <https://bg.copernicus.org/articles/19/1087/2022/> doi: 10.5194/bg-19-1087-2022
- Chen, C.-T. A., & Borges, A. V. (2009, April). Reconciling opposing views on carbon cycling in the coastal ocean: Continental shelves as sinks and near-shore ecosystems as sources of atmospheric CO_2 . *Deep Sea Research Part II: Topical Studies in Oceanography*, 56(8-10), 578–590. Retrieved 2021-09-03, from <https://linkinghub.elsevier.com/retrieve/pii/S0967064509000162> doi: 10.1016/j.dsr2.2009.01.001
- Chen, C.-T. A., Huang, T.-H., Chen, Y.-C., Bai, Y., He, X., & Kang, Y. (2013, October). Air-sea exchanges of CO_2 in the world's coastal seas. *Biogeosciences*, 10(10), 6509–6544. Retrieved 2021-09-03, from <https://bg.copernicus.org/articles/10/6509/2013/> doi: 10.5194/bg-10-6509-2013
- Cossarini, G., Querin, S., & Solidoro, C. (2015, October). The continental shelf carbon pump in the northern Adriatic Sea (Mediterranean Sea): Influence of wintertime variability. *Ecological Modelling*, 314, 118–134. Retrieved 2023-03-23, from <https://linkinghub.elsevier.com/retrieve/pii/S03044380015003300> doi: 10.1016/j.ecolmodel.2015.07.024
- Dai, M., Cao, Z., Guo, X., Zhai, W., Liu, Z., Yin, Z., ... Du, C. (2013). Why are some marginal seas sources of atmospheric CO_2 ? *Geophysical Research Letters*, 40(10), 2154–2158. Retrieved 2022-04-26, from <https://onlinelibrary.wiley.com/doi/abs/10.1002/grl.50390> (_eprint: <https://onlinelibrary.wiley.com/doi/pdf/10.1002/grl.50390>) doi: 10.1002/grl.50390
- Dai, M., Su, J., Zhao, Y., Hofmann, E. E., Cao, Z., Cai, W.-J., ... Wang, Z. (2022). Carbon Fluxes in the Coastal Ocean: Synthesis, Boundary Processes, and Future Trends. *Annual Review of Earth and Planetary Sciences*, 50(1), 593–626. Retrieved 2022-09-26, from <https://doi.org/10.1146/annurev-earth-032320-090746> (_eprint: <https://doi.org/10.1146/annurev-earth-032320-090746>) doi: 10.1146/annurev-earth-032320-090746
- Damien, P., Bianchi, D., McWilliams, J. C., Kessouri, F., Deutsch, C., Chen, R., & Renault, L. (2023). Enhanced Biogeochemical Cycling Along the U.S. West Coast Shelf. *Global Biogeochemical Cycles*, 37(1), e2022GB007572. Retrieved 2023-02-14, from <https://onlinelibrary.wiley.com/doi/abs/10.1029/2022GB007572> (_eprint: <https://onlinelibrary.wiley.com/doi/pdf/10.1029/2022GB007572>) doi: 10.1029/2022GB007572
- Deike, L., & Melville, W. K. (2018). Gas Transfer by Breaking Waves. *Geophysical Research Letters*, 45(19), 10,482–10,492. Retrieved 2021-11-15, from <https://onlinelibrary.wiley.com/doi/abs/10.1029/2018GL078758> (_eprint: <https://onlinelibrary.wiley.com/doi/pdf/10.1029/2018GL078758>) doi: 10.1029/2018GL078758
- Desmet, F., Gruber, N., Köhn, E. E., Münnich, M., & Vogt, M. (2022, May). Tracking the Space-Time Evolution of Ocean Acidification Extremes in the California Current System and Northeast Pacific. *Journal of Geophysical Research:*

- Oceans, 127(5). Retrieved 2023-03-27, from <https://onlinelibrary.wiley.com/doi/10.1029/2021JC018159> doi: 10.1029/2021JC018159
- Doney, S. C., Lima, I., Feely, R. A., Glover, D. M., Lindsay, K., Mahowald, N., ... Wanninkhof, R. (2009, April). Mechanisms governing interannual variability in upper-ocean inorganic carbon system and air-sea CO₂ fluxes: Physical climate and atmospheric dust. *Deep Sea Research Part II: Topical Studies in Oceanography*, 56(8-10), 640–655. Retrieved 2018-09-13, from <http://linkinghub.elsevier.com/retrieve/pii/S096706450800427X> doi: 10.1016/j.dsr2.2008.12.006
- Egger, M., Lenstra, W., Jong, D., Meysman, F. J. R., Sapart, C. J., van der Veen, C., ... Slomp, C. P. (2016, August). Rapid Sediment Accumulation Results in High Methane Effluxes from Coastal Sediments. *PLoS ONE*, 11(8), e0161609. Retrieved 2023-03-22, from <https://www.ncbi.nlm.nih.gov/pmc/articles/PMC4999275/> doi: 10.1371/journal.pone.0161609
- Elsig, J., Schmitt, J., Leuenberger, D., Schneider, R., Eyer, M., Leuenberger, M., ... Stocker, T. F. (2009, September). Stable isotope constraints on Holocene carbon cycle changes from an Antarctic ice core. *Nature*, 461(7263), 507–510. Retrieved 2023-03-27, from <https://www.nature.com/articles/nature08393> (Number: 7263 Publisher: Nature Publishing Group) doi: 10.1038/nature08393
- Etiope, G., Ciotoli, G., Schwietzke, S., & Schoell, M. (2019, January). Gridded maps of geological methane emissions and their isotopic signature. *Earth System Science Data*, 11(1), 1–22. Retrieved 2023-03-27, from <https://essd.copernicus.org/articles/11/1/2019/> (Publisher: Copernicus GmbH) doi: 10.5194/essd-11-1-2019
- Fennel, K., Alin, S., Barbero, L., Evans, W., Bourgeois, T., Cooley, S., ... Wang, Z. A. (2019, March). Carbon cycling in the North American coastal ocean: a synthesis. *Biogeosciences*, 16(6), 1281–1304. Retrieved 2023-02-14, from <https://bg.copernicus.org/articles/16/1281/2019/> doi: 10.5194/bg-16-1281-2019
- Fennel, K., & Testa, J. M. (2019, January). Biogeochemical Controls on Coastal Hypoxia. *Annual Review of Marine Science*, 11(1), 105–130. Retrieved 2020-09-08, from <http://www.annualreviews.org/doi/10.1146/annurev-marine-010318-095138> (Publisher: Annual Reviews) doi: 10.1146/annurev-marine-010318-095138
- Fennel, K., & Wilkin, J. (2009, September). Quantifying biological carbon export for the northwest North Atlantic continental shelves. *Geophysical Research Letters*, 36(18), L18605. Retrieved 2023-02-15, from <http://doi.wiley.com/10.1029/2009GL039818> doi: 10.1029/2009GL039818
- Fiechter, J., Curchitser, E. N., Edwards, C. A., Chai, F., Goebel, N. L., & Chavez, F. P. (2014). Air-sea CO₂ fluxes in the California Current: Impacts of model resolution and coastal topography. *Global Biogeochemical Cycles*, 28(4), 371–385. Retrieved 2023-02-28, from <https://onlinelibrary.wiley.com/doi/abs/10.1002/2013GB004683> (eprint: <https://onlinelibrary.wiley.com/doi/pdf/10.1002/2013GB004683>) doi: 10.1002/2013GB004683
- Friedlingstein, P., O’Sullivan, M., Jones, M. W., Andrew, R. M., Gregor, L., Hauck, J., ... Zheng, B. (2022). Global Carbon Budget 2022. *Earth System Science Data*, 14(11), 4811–4900. Retrieved from <https://essd.copernicus.org/articles/14/4811/2022/> doi: 10.5194/essd-14-4811-2022
- Ganesan, A. L., Manizza, M., Morgan, E. J., Harth, C. M., Kozlova, E., Lueker, T., ... Rigby, M. (2020, July). Marine Nitrous Oxide Emissions From Three Eastern Boundary Upwelling Systems Inferred From Atmospheric Observations. *Geophysical Research Letters*, 47(14). Retrieved 2023-02-15, from <https://onlinelibrary.wiley.com/doi/10.1029/2020GL087822> doi:

- 10.1029/2020GL087822
- Gao, S., Schwinger, J., Tjiputra, J., Bethke, I., Hartmann, J., Mayorga, E., & Heinze, C. (2023, January). Riverine impact on future projections of marine primary production and carbon uptake. *Biogeosciences*, 20(1), 93–119. Retrieved 2023-02-23, from <https://bg.copernicus.org/articles/20/93/2023/> (Publisher: Copernicus GmbH) doi: 10.5194/bg-20-93-2023
- Garbe, C. S., Rutgersson, A., Boutin, J., de Leeuw, G., Delille, B., Fairall, C. W., ... Zappa, C. J. (2014). Transfer Across the Air-Sea Interface. In P. S. Liss & M. T. Johnson (Eds.), *Ocean-Atmosphere Interactions of Gases and Particles* (pp. 55–112). Berlin, Heidelberg: Springer. Retrieved 2023-02-14, from https://doi.org/10.1007/978-3-642-25643-1_2 doi: 10.1007/978-3-642-25643-1_2
- Gomez, F. A., Wanninkhof, R., Barbero, L., Lee, S.-K., & Hernandez Jr., F. J. (2020, March). Seasonal patterns of surface inorganic carbon system variables in the Gulf of Mexico inferred from a regional high-resolution ocean biogeochemical model. *Biogeosciences*, 17(6), 1685–1700. Retrieved 2023-02-14, from <https://bg.copernicus.org/articles/17/1685/2020/> doi: 10.5194/bg-17-1685-2020
- Grundle, D. S., Löscher, C. R., Krahmann, G., Altabet, M. A., Bange, H. W., Karstensen, J., ... Fiedler, B. (2017, July). Low oxygen eddies in the eastern tropical North Atlantic: Implications for N₂O cycling. *Scientific Reports*, 7(1), 4806. Retrieved 2023-02-14, from <https://www.nature.com/articles/s41598-017-04745-y> doi: 10.1038/s41598-017-04745-y
- Gustafsson, E., Hagens, M., Sun, X., Reed, D. C., Humborg, C., Slomp, C. P., & Gustafsson, B. G. (2019, January). Sedimentary alkalinity generation and long-term alkalinity development in the Baltic Sea. *Biogeosciences*, 16(2), 437–456. Retrieved 2023-02-14, from <https://bg.copernicus.org/articles/16/437/2019/> doi: 10.5194/bg-16-437-2019
- Gutiérrez-Loza, L., Nilsson, E., Wallin, M. B., Sahlée, E., & Rutgersson, A. (2022, December). On physical mechanisms enhancing air-sea CO₂ exchange. *Biogeosciences*, 19(24), 5645–5665. Retrieved 2023-03-22, from <https://bg.copernicus.org/articles/19/5645/2022/> doi: 10.5194/bg-19-5645-2022
- Gülzow, W., Rehder, G., Schneider v. Deimling, J., Seifert, T., & Tóth, Z. (2013, January). One year of continuous measurements constraining methane emissions from the Baltic Sea to the atmosphere using a ship of opportunity. *Biogeosciences*, 10(1), 81–99. Retrieved 2023-02-14, from <https://bg.copernicus.org/articles/10/81/2013/> doi: 10.5194/bg-10-81-2013
- Hauck, J., Zeising, M., Le Quéré, C., Gruber, N., Bakker, D. C. E., Bopp, L., ... Séférián, R. (2020). Consistency and Challenges in the Ocean Carbon Sink Estimate for the Global Carbon Budget. *Frontiers in Marine Science*, 7. Retrieved 2020-12-18, from <https://www.frontiersin.org/articles/10.3389/fmars.2020.571720/full> (Publisher: Frontiers) doi: 10.3389/fmars.2020.571720
- Hauri, C., Pagès, R., McDonnell, A. M. P., Stuecker, M. F., Danielson, S. L., Hedstrom, K., ... Doney, S. C. (2021, September). Modulation of ocean acidification by decadal climate variability in the Gulf of Alaska. *Communications Earth & Environment*, 2(1), 191. Retrieved 2023-02-14, from <https://www.nature.com/articles/s43247-021-00254-z> doi: 10.1038/s43247-021-00254-z
- Hilt, S., Grossart, H., McGinnis, D. F., & Keppler, F. (2022, November). Potential role of submerged macrophytes for oxic methane production in aquatic ecosystems. *Limnology and Oceanography*, 67(S2). Retrieved 2023-02-20, from <https://onlinelibrary.wiley.com/doi/10.1002/lno.12095> doi: 10.1002/lno.12095

- Ho, D. T., Law, C. S., Smith, M. J., Schlosser, P., Harvey, M., & Hill, P. (2006). Measurements of air-sea gas exchange at high wind speeds in the Southern Ocean: Implications for global parameterizations. *Geophysical Research Letters*, *33*(16). Retrieved 2019-06-25, from <https://agupubs.onlinelibrary.wiley.com/doi/abs/10.1029/2006GL026817> doi: 10.1029/2006GL026817
- Ho, D. T., Wanninkhof, R., Schlosser, P., Ullman, D. S., Hebert, D., & Sullivan, K. F. (2011, July). Toward a universal relationship between wind speed and gas exchange: Gas transfer velocities measured with $^3\text{He}/\text{SF}_6$ during the Southern Ocean Gas Exchange Experiment. *Journal of Geophysical Research*, *116*, C00F04. Retrieved 2023-02-15, from <http://doi.wiley.com/10.1029/2010JC006854> doi: 10.1029/2010JC006854
- Hovland, M., Judd, A., & Burke, R. (1993, January). The global flux of methane from shallow submarine sediments. *Chemosphere*, *26*(1-4), 559–578. Retrieved 2023-02-23, from <https://linkinghub.elsevier.com/retrieve/pii/0045653593904428> doi: 10.1016/0045-6535(93)90442-8
- Ilyina, T., Six, K. D., Segschneider, J., Maier-Reimer, E., Li, H., & Núñez-Riboni, I. (2013, June). Global ocean biogeochemistry model HAMOCC: Model architecture and performance as component of the MPI-Earth system model in different CMIP5 experimental realizations. *Journal of Advances in Modeling Earth Systems*, *5*(2), 287–315. Retrieved 2023-02-15, from <https://onlinelibrary.wiley.com/doi/10.1029/2012MS000178> doi: 10.1029/2012MS000178
- Joung, D., Leonte, M., Valentine, D. L., Sparrow, K. J., Weber, T., & Kessler, J. D. (2020, October). Radiocarbon in Marine Methane Reveals Patchy Impact of Seeps on Surface Waters. *Geophysical Research Letters*, *47*(20). Retrieved 2023-03-27, from <https://onlinelibrary.wiley.com/doi/10.1029/2020GL089516> doi: 10.1029/2020GL089516
- Joung, D., Ruppel, C., Southon, J., Weber, T. S., & Kessler, J. D. (2022, November). Negligible atmospheric release of methane from decomposing hydrates in mid-latitude oceans. *Nature Geoscience*, *15*(11), 885–891. Retrieved 2023-03-27, from <https://www.nature.com/articles/s41561-022-01044-8> doi: 10.1038/s41561-022-01044-8
- Karl, D. M., Beversdorf, L., Björkman, K. M., Church, M. J., Martinez, A., & Delong, E. F. (2008, July). Aerobic production of methane in the sea. *Nature Geoscience*, *1*(7), 473–478. Retrieved 2023-03-27, from <https://www.nature.com/articles/ngeo234> (Number: 7 Publisher: Nature Publishing Group) doi: 10.1038/ngeo234
- Kock, A., & Bange, H. (2015, February). Counting the Ocean’s Greenhouse Gas Emissions. *Eos*, *96*. Retrieved 2023-02-14, from <https://eos.org/project-updates/counting-oceans-greenhouse-gas-emissions> doi: 10.1029/2015EO023665
- Kock, A., Schafstall, J., Dengler, M., Brandt, P., & Bange, H. W. (2012, March). Sea-to-air and diapycnal nitrous oxide fluxes in the eastern tropical North Atlantic Ocean. *Biogeosciences*, *9*(3), 957–964. Retrieved 2023-02-14, from <https://bg.copernicus.org/articles/9/957/2012/> (Publisher: Copernicus GmbH) doi: 10.5194/bg-9-957-2012
- Lachkar, Z., & Gruber, N. (2013, January). Response of biological production and air-sea CO₂ fluxes to upwelling intensification in the California and Canary Current Systems. *Journal of Marine Systems*, *109–110*, 149–160. Retrieved 2023-02-15, from <https://www.sciencedirect.com/science/article/pii/S092479631200108X> doi: 10.1016/j.jmarsys.2012.04.003
- Lachkar, Z., Mehari, M., Al Azhar, M., Lévy, M., & Smith, S. (2021, October). Fast local warming is the main driver of recent deoxygenation in the northern Arabian Sea. *Biogeosciences*, *18*(20), 5831–5849. Retrieved 2023-02-15, from <https://bg.copernicus.org/articles/18/5831/2021/> doi:

- 10.5194/bg-18-5831-2021
- Lacroix, F., Ilyina, T., & Hartmann, J. (2020, January). Oceanic CO₂ outgassing and biological production hotspots induced by pre-industrial river loads of nutrients and carbon in a global modeling approach. *Biogeosciences*, 17(1), 55–88. Retrieved 2020-05-05, from <https://www.biogeosciences.net/17/55/2020/> doi: <https://doi.org/10.5194/bg-17-55-2020>
- Lacroix, F., Ilyina, T., Laruelle, G. G., & Regnier, P. (2021). Reconstructing the Preindustrial Coastal Carbon Cycle Through a Global Ocean Circulation Model: Was the Global Continental Shelf Already Both Autotrophic and a CO₂ Sink? *Global Biogeochemical Cycles*, 35(2), e2020GB006603. Retrieved 2021-09-03, from <https://agupubs.onlinelibrary.wiley.com/doi/abs/10.1029/2020GB006603> doi: 10.1029/2020GB006603
- Landschützer, P., Gruber, N., Bakker, D. C. E., & Schuster, U. (2014, September). Recent variability of the global ocean carbon sink. *Global Biogeochemical Cycles*, 28(9), 927–949. Retrieved 2015-08-11, from <http://onlinelibrary.wiley.com/doi/10.1002/2014GB004853/abstract> doi: 10.1002/2014GB004853
- Landschützer, P., Laruelle, G. G., Roobaert, A., & Regnier, P. (2020, October). A uniform pCO₂ climatology combining open and coastal oceans. *Earth System Science Data*, 12(4), 2537–2553. Retrieved 2023-02-14, from <https://essd.copernicus.org/articles/12/2537/2020/> doi: 10.5194/essd-12-2537-2020
- Laruelle, G. G., Cai, W.-J., Hu, X., Gruber, N., Mackenzie, F. T., & Regnier, P. (2018, January). Continental shelves as a variable but increasing global sink for atmospheric carbon dioxide. *Nature Communications*, 9, 454. Retrieved 2021-09-03, from <https://www.ncbi.nlm.nih.gov/pmc/articles/PMC5792465/> doi: 10.1038/s41467-017-02738-z
- Laruelle, G. G., Dürr, H. H., Lauerwald, R., Hartmann, J., Slomp, C. P., Goossens, N., & Regnier, P. A. G. (2013, May). Global multi-scale segmentation of continental and coastal waters from the watersheds to the continental margins. *Hydrology and Earth System Sciences*, 17(5), 2029–2051. Retrieved 2020-03-27, from <https://www.hydrol-earth-syst-sci.net/17/2029/2013/> doi: 10.5194/hess-17-2029-2013
- Laruelle, G. G., Dürr, H. H., Slomp, C. P., & Borges, A. V. (2010). Evaluation of sinks and sources of CO₂ in the global coastal ocean using a spatially-explicit typology of estuaries and continental shelves. *Geophysical Research Letters*, 37(15). Retrieved 2021-09-03, from <https://agupubs.onlinelibrary.wiley.com/doi/abs/10.1029/2010GL043691> (eprint: <https://agupubs.onlinelibrary.wiley.com/doi/pdf/10.1029/2010GL043691>) doi: 10.1029/2010GL043691
- Laruelle, G. G., Landschützer, P., Gruber, N., Tison, J.-L., Delille, B., & Regnier, P. (2017, October). Global high-resolution monthly pCO₂ climatology for the coastal ocean derived from neural network interpolation. *Biogeosciences*, 14(19), 4545–4561. Retrieved 2019-08-29, from <https://www.biogeosciences.net/14/4545/2017/> doi: 10.5194/bg-14-4545-2017
- Laruelle, G. G., Lauerwald, R., Pfeil, B., & Regnier, P. (2014). Regionalized global budget of the CO₂ exchange at the air–water interface in continental shelf seas. *Global Biogeochemical Cycles*, 28(11), 1199–1214. Retrieved 2021-09-03, from <https://agupubs.onlinelibrary.wiley.com/doi/abs/10.1002/2014GB004832> doi: 10.1002/2014GB004832
- Laruelle, G. G., Lauerwald, R., Rotschi, J., Raymond, P. A., Hartmann, J., & Regnier, P. (2015, March). Seasonal response of air–water CO₂ exchange along the land–ocean aquatic continuum of the northeast North American coast. *Biogeosciences*, 12(5), 1447–1458. Retrieved 2023-02-14, from <https://bg.copernicus.org/articles/12/1447/>

- 2015/ doi: 10.5194/bg-12-1447-2015
- Laurent, A., Fennel, K., Cai, W., Huang, W., Barbero, L., & Wanninkhof, R. (2017, January). Eutrophication-induced acidification of coastal waters in the northern Gulf of Mexico: Insights into origin and processes from a coupled physical-biogeochemical model. *Geophysical Research Letters*, 44(2), 946–956. Retrieved 2023-02-15, from <https://onlinelibrary.wiley.com/doi/abs/10.1002/2016GL071881> doi: 10.1002/2016GL071881
- Laurent, A., Fennel, K., & Kuhn, A. (2021, March). An observation-based evaluation and ranking of historical Earth system model simulations in the northwest North Atlantic Ocean. *Biogeosciences*, 18(5), 1803–1822. Retrieved 2023-02-15, from <https://bg.copernicus.org/articles/18/1803/2021/> doi: 10.5194/bg-18-1803-2021
- Legge, O., Johnson, M., Hicks, N., Jickells, T., Diesing, M., Aldridge, J., ... Williamson, P. (2020, March). Carbon on the Northwest European Shelf: Contemporary Budget and Future Influences. *Frontiers in Marine Science*, 7, 143. Retrieved 2023-02-14, from <https://www.frontiersin.org/article/10.3389/fmars.2020.00143/full> doi: 10.3389/fmars.2020.00143
- Le Quéré, C. L., Andrew, R. M., Friedlingstein, P., Sitch, S., Pongratz, J., Manning, A. C., ... Zhu, D. (2018, March). Global Carbon Budget 2017. *Earth System Science Data*, 10(1), 405–448. Retrieved 2018-03-21, from <https://www.earth-syst-sci-data.net/10/405/2018/> doi: <https://doi.org/10.5194/essd-10-405-2018>
- Liang, J.-H., Deutsch, C., McWilliams, J. C., Baschek, B., Sullivan, P. P., & Chiba, D. (2013). Parameterizing bubble-mediated air-sea gas exchange and its effect on ocean ventilation. *Global Biogeochemical Cycles*, 27(3), 894–905. Retrieved 2023-02-14, from <https://onlinelibrary.wiley.com/doi/abs/10.1002/gbc.20080> doi: 10.1002/gbc.20080
- Liao, E., Resplandy, L., Liu, J., & Bowman, K. W. (2020). Amplification of the Ocean Carbon Sink During El Niños: Role of Poleward Ekman Transport and Influence on Atmospheric CO₂. *Global Biogeochemical Cycles*, 34(9), e2020GB006574. Retrieved 2020-10-15, from <http://agupubs.onlinelibrary.wiley.com/doi/abs/10.1029/2020GB006574> doi: 10.1029/2020GB006574
- Liu, Q., Guo, X., Yin, Z., Zhou, K., Roberts, E. G., & Dai, M. (2018, November). Carbon fluxes in the China Seas: An overview and perspective. *Science China Earth Sciences*, 61(11), 1564–1582. Retrieved 2023-02-14, from <http://link.springer.com/10.1007/s11430-017-9267-4> doi: 10.1007/s11430-017-9267-4
- Louchard, D., Gruber, N., & Münnich, M. (2021). The Impact of the Amazon on the Biological Pump and the Air-Sea CO₂ Balance of the Western Tropical Atlantic. *Global Biogeochemical Cycles*, 35(6), e2020GB006818. Retrieved 2021-09-22, from <https://onlinelibrary.wiley.com/doi/abs/10.1029/2020GB006818> doi: 10.1029/2020GB006818
- Mackenzie, F., Lerman, A., & Ver, L. (1998, May). Role of the continental margin in the global carbon balance during the past three centuries. *Geology*, 26. doi: 10.1130/0091-7613(1998)026(0423:ROTCMI)2.3.CO;2
- Mackenzie, F. T., Andersson, A. J., Lerman, A., & Ver, L. M. (2005). Boundary Exchanges in the Global Coastal Margin: Implications for the Organic and Inorganic Carbon Cycles. In *The Sea vol. 13* (pp. 193–225). (Eds Robinson, A. R. & Brink, K. H.) Harvard Univ. Press.
- Manizza, M., Menemenlis, D., Zhang, H., & Miller, C. E. (2019). Modeling the Recent Changes in the Arctic Ocean CO₂ Sink (2006–2013). *Global Biogeochemical Cycles*, 33(3), 420–438. Retrieved 2023-02-15, from <https://onlinelibrary.wiley.com/doi/abs/10.1029/2018GB006070> doi: 10.1029/2018GB006070
- Mao, S.-H., Zhang, H.-H., Zhuang, G.-C., Li, X.-J., Liu, Q., Zhou, Z., ... Yang, G.-

- P. (2022, November). Aerobic oxidation of methane significantly reduces global diffusive methane emissions from shallow marine waters. *Nature Communications*, 13(1), 7309. doi: 10.1038/s41467-022-35082-y
- Mathis, M., Logemann, K., Maerz, J., Lacroix, F., Hagemann, S., Chegini, F., ... Schrum, C. (2022). Seamless integration of the coastal ocean in global marine carbon cycle modeling. *Journal of Advances in Modeling Earth Systems*, n/a(n/a), e2021MS002789. Retrieved 2022-08-22, from <https://onlinelibrary.wiley.com/doi/abs/10.1029/2021MS002789> doi: 10.1029/2021MS002789
- Mayer, B., Rixen, T., & Pohlmann, T. (2018). The Spatial and Temporal Variability of Air-Sea CO₂ Fluxes and the Effect of Net Coral Reef Calcification in the Indonesian Seas: A Numerical Sensitivity Study. *Frontiers in Marine Science*, 5. Retrieved 2023-02-14, from <https://www.frontiersin.org/articles/10.3389/fmars.2018.00116>
- McGinnis, D. F., Greinert, J., Artemov, Y., Beaubien, S. E., & Wüest, A. (2006). Fate of rising methane bubbles in stratified waters: How much methane reaches the atmosphere? *Journal of Geophysical Research*, 111(C9), C09007. Retrieved 2023-02-23, from <http://doi.wiley.com/10.1029/2005JC003183> doi: 10.1029/2005JC003183
- Neumann, T., Radtke, H., Cahill, B., Schmidt, M., & Rehder, G. (2022, November). Non-Redfieldian carbon model for the Baltic Sea (ERGOM version 1.2) – implementation and budget estimates. *Geoscientific Model Development*, 15(22), 8473–8540. Retrieved 2023-02-14, from <https://gmd.copernicus.org/articles/15/8473/2022/> doi: 10.5194/gmd-15-8473-2022
- Nightingale, P. D., Malin, G., Law, C. S., Watson, A. J., Liss, P. S., Liddicoat, M. I., ... Upstill-Goddard, R. C. (2000, March). In situ evaluation of air-sea gas exchange parameterizations using novel conservative and volatile tracers. *Global Biogeochemical Cycles*, 14(1), 373–387. Retrieved 2023-02-15, from <http://doi.wiley.com/10.1029/1999GB900091> doi: 10.1029/1999GB900091
- Ouyang, Z., Collins, A., Li, Y., Qi, D., Arrigo, K. R., Zhuang, Y., ... Cai, W. (2022, August). Seasonal Water Mass Evolution and Non-Redfield Dynamics Enhance CO₂ Uptake in the Chukchi Sea. *Journal of Geophysical Research: Oceans*, 127(8). Retrieved 2023-02-14, from <https://onlinelibrary.wiley.com/doi/10.1029/2021JC018326> doi: 10.1029/2021JC018326
- Ouyang, Z., Sciusco, P., Jiao, T., Feron, S., Lei, C., Li, F., ... Chen, J. (2022, July). Albedo changes caused by future urbanization contribute to global warming. *Nature Communications*, 13(1), 3800. Retrieved 2022-10-27, from <https://www.nature.com/articles/s41467-022-31558-z> (Number: 1 Publisher: Nature Publishing Group) doi: 10.1038/s41467-022-31558-z
- Pereira, R., Ashton, I., Sabbaghzadeh, B., Shutler, J. D., & Upstill-Goddard, R. C. (2018, July). Reduced air–sea CO₂ exchange in the Atlantic Ocean due to biological surfactants. *Nature Geoscience*, 11(7), 492–496. Retrieved 2023-03-22, from <http://www.nature.com/articles/s41561-018-0136-2> doi: 10.1038/s41561-018-0136-2
- Pipko, I. I., Pugach, S. P., Luchin, V. A., Francis, O. P., Savelieva, N. I., Charkin, A. N., ... Semiletov, I. P. (2021, March). Surface CO₂ system dynamics in the Gulf of Anadyr during the open water season. *Continental Shelf Research*, 217, 104371. Retrieved 2023-02-14, from <https://www.sciencedirect.com/science/article/pii/S0278434321000285> doi: 10.1016/j.csr.2021.104371
- Pipko, I. I., Pugach, S. P., Semiletov, I. P., Anderson, L. G., Shakhova, N. E., Gustafsson, , ... Dudarev, O. V. (2017, November). The spatial and interannual dynamics of the surface water carbonate system and air–sea CO₂ fluxes in the outer shelf and slope of the Eurasian Arctic Ocean. *Ocean Science*, 13(6), 997–1016. Retrieved 2023-

- 02-14, from <https://os.copernicus.org/articles/13/997/2017/> doi: 10.5194/os-13-997-2017
- Previdi, M., Fennel, K., Wilkin, J., & Haidvogel, D. (2009, October). Interannual variability in atmospheric CO₂ uptake on the northeast U.S. continental shelf. *Journal of Geophysical Research*, 114(G4), G04003. Retrieved 2023-03-23, from <http://doi.wiley.com/10.1029/2008JG000881> doi: 10.1029/2008JG000881
- Puglini, M., Brovkin, V., Regnier, P., & Arndt, S. (2020, June). Assessing the potential for non-turbulent methane escape from the East Siberian Arctic Shelf. *Biogeosciences*, 17(12), 3247–3275. Retrieved 2023-02-27, from <https://bg.copernicus.org/articles/17/3247/2020/> doi: 10.5194/bg-17-3247-2020
- Reeburgh, W. S. (2007, February). Oceanic Methane Biogeochemistry. *Chemical Reviews*, 107(2), 486–513. Retrieved 2023-03-27, from <https://pubs.acs.org/doi/10.1021/cr050362v> doi: 10.1021/cr050362v
- Rees, A. P., Bange, H. W., Arévalo-Martínez, D. L., Artioli, Y., Ashby, D. M., Brown, I., ... Turley, C. (2022, February). Nitrous oxide and methane in a changing Arctic Ocean. *Ambio*, 51(2), 398–410. Retrieved 2023-03-22, from <https://www.ncbi.nlm.nih.gov/pmc/articles/PMC8692636/> doi: 10.1007/s13280-021-01633-8
- Regnier, P., Friedlingstein, P., Ciais, P., Mackenzie, F. T., Gruber, N., Janssens, I. A., ... Thullner, M. (2013, June). Anthropogenic perturbation of the carbon fluxes from land to ocean. *Nature Geoscience*, 6(8), 597–607. Retrieved 2015-06-25, from <http://www.nature.com/doifinder/10.1038/ngeo1830> doi: 10.1038/ngeo1830
- Regnier, P., Resplandy, L., Najjar, R. G., & Ciais, P. (2022, March). The land-to-ocean loops of the global carbon cycle. *Nature*, 603(7901), 401–410. Retrieved 2022-04-18, from <https://www.nature.com/articles/s41586-021-04339-9> doi: 10.1038/s41586-021-04339-9
- Rehder, G., Keir, R. S., Suess, E., & Pohlmann, T. (1998, September). The Multiple Sources and Patterns of Methane in North Sea Waters. *Aquatic Geochemistry*, 4(3), 403–427. Retrieved 2023-02-14, from <https://doi.org/10.1023/A:1009644600833> doi: 10.1023/A:1009644600833
- Reichl, B. G., & Deike, L. (2020). Contribution of Sea-State Dependent Bubbles to Air-Sea Carbon Dioxide Fluxes. *Geophysical Research Letters*, 47(9), e2020GL087267. Retrieved 2021-10-08, from <https://onlinelibrary.wiley.com/doi/abs/10.1029/2020GL087267> (_eprint: <https://onlinelibrary.wiley.com/doi/pdf/10.1029/2020GL087267>) doi: 10.1029/2020GL087267
- Reimer, J. J., Wang, H., Vargas, R., & Cai, W. (2017, December). Multidecadal f CO₂ Increase Along the United States Southeast Coastal Margin. *Journal of Geophysical Research: Oceans*, 122(12), 10061–10072. Retrieved 2023-03-23, from <https://onlinelibrary.wiley.com/doi/10.1002/2017JC013170> doi: 10.1002/2017JC013170
- Repeta, D. J., Ferrón, S., Sosa, O. A., Johnson, C. G., Repeta, L. D., Acker, M., ... Karl, D. M. (2016, December). Marine methane paradox explained by bacterial degradation of dissolved organic matter. *Nature Geoscience*, 9(12), 884–887. Retrieved 2023-03-27, from <http://www.nature.com/articles/ngeo2837> doi: 10.1038/ngeo2837
- Resplandy, L., Keeling, R. F., Rödenbeck, C., Stephens, B. B., Khatiwala, S., Rodgers, K. B., ... Tans, P. P. (2018). Revision of global carbon fluxes based on a reassessment of oceanic and riverine carbon transport. *Nature Geoscience*, 11, 504–509. Retrieved 2018-06-11, from <https://www.nature.com/articles/s41561-018-0151-3> doi: 10.1038/s41561-018-0151-3
- Reynolds, R. W., Smith, T. M., Liu, C., Chelton, D. B., Casey, K. S., & Schlax,

- M. G. (2007, November). Daily High-Resolution-Blended Analyses for Sea Surface Temperature. *Journal of Climate*, 20(22), 5473–5496. Retrieved 2023-02-15, from <http://journals.ametsoc.org/doi/10.1175/2007JCLI1824.1> doi: 10.1175/2007JCLI1824.1
- Roobaert, A., Laruelle, G. G., Landschützer, P., Gruber, N., Chou, L., & Regnier, P. (2019). The Spatiotemporal Dynamics of the Sources and Sinks of CO₂ in the Global Coastal Ocean. *Global Biogeochemical Cycles*, 33(12), 1693–1714. Retrieved 2020-05-11, from <http://agupubs.onlinelibrary.wiley.com/doi/abs/10.1029/2019GB006239> (eprint: <https://onlinelibrary.wiley.com/doi/pdf/10.1029/2019GB006239>) doi: 10.1029/2019GB006239
- Roobaert, A., Laruelle, G. G., Landschützer, P., & Regnier, P. (2018, March). Uncertainty in the global oceanic CO₂ uptake induced by wind forcing: quantification and spatial analysis. *Biogeosciences*, 15(6), 1701–1720. Retrieved 2023-03-24, from <https://bg.copernicus.org/articles/15/1701/2018/> doi: 10.5194/bg-15-1701-2018
- Roobaert, A., Resplandy, L., Laruelle, G. G., Liao, E., & Regnier, P. (2022, January). A framework to evaluate and elucidate the driving mechanisms of coastal sea surface pCO₂ seasonality using an ocean general circulation model (MOM6-COBALT). *Ocean Science*, 18(1), 67–88. Retrieved 2022-03-17, from <https://os.copernicus.org/articles/18/67/2022/> doi: 10.5194/os-18-67-2022
- Rosentreter, J. A., Borges, A. V., Deemer, B. R., Holgersson, M. A., Liu, S., Song, C., ... Eyre, B. D. (2021, April). Half of global methane emissions come from highly variable aquatic ecosystem sources. *Nature Geoscience*, 14(4), 225–230. Retrieved 2023-02-14, from <http://www.nature.com/articles/s41561-021-00715-2> doi: 10.1038/s41561-021-00715-2
- Rosentreter, J. A., Laruelle, G. G., & et al. (2023). Coastal vegetation and estuaries are collectively a greenhouse gas sink Nature Climate Change, Accepted, 2023. *Accepted in Nature Climate Change*.
- Roth, F., Broman, E., Sun, X., Bonaglia, S., Nascimento, F., Prytherch, J., ... Norkko, A. (2023, January). Methane emissions offset atmospheric carbon dioxide uptake in coastal macroalgae, mixed vegetation and sediment ecosystems. *Nature Communications*, 14(1), 42. Retrieved 2023-02-20, from <https://www.nature.com/articles/s41467-022-35673-9> (Number: 1 Publisher: Nature Publishing Group) doi: 10.1038/s41467-022-35673-9
- Royer, S.-J., Ferrón, S., Wilson, S. T., & Karl, D. M. (2018, August). Production of methane and ethylene from plastic in the environment. *PLOS ONE*, 13(8), e0200574. Retrieved 2023-02-14, from <https://dx.plos.org/10.1371/journal.pone.0200574> doi: 10.1371/journal.pone.0200574
- Ruppel, C. D., & Kessler, J. D. (2017, March). The interaction of climate change and methane hydrates. *Reviews of Geophysics*, 55(1), 126–168. Retrieved 2023-03-27, from <https://onlinelibrary.wiley.com/doi/10.1002/2016RG000534> doi: 10.1002/2016RG000534
- Rutherford, K., & Fennel, K. (2018, October). Diagnosing transit times on the northwestern North Atlantic continental shelf. *Ocean Science*, 14(5), 1207–1221. Retrieved 2023-02-15, from <https://os.copernicus.org/articles/14/1207/2018/> doi: 10.5194/os-14-1207-2018
- Rutherford, K., & Fennel, K. (2022, March). Elucidating Coastal Ocean Carbon Transport Processes: A Novel Approach Applied to the Northwest North Atlantic Shelf. *Geophysical Research Letters*, 49(6). Retrieved 2022-09-13, from <https://onlinelibrary.wiley.com/doi/10.1029/2021GL097614> doi: 10.1029/2021GL097614
- Rutherford, K., Fennel, K., Atamanchuk, D., Wallace, D., & Thomas, H. (2021, December). A modelling study of temporal and spatial pCO₂ variability on the

- biologically active and temperature-dominated Scotian Shelf. *Biogeosciences*, 18(23), 6271–6286. Retrieved 2023-02-15, from <https://bg.copernicus.org/articles/18/6271/2021/> (Publisher: Copernicus GmbH) doi: 10.5194/bg-18-6271-2021
- Rödenbeck, C., DeVries, T., Hauck, J., Le Quéré, C., & Keeling, R. F. (2022, May). Data-based estimates of interannual sea–air CO₂ flux variations 1957–2020 and their relation to environmental drivers. *Biogeosciences*, 19(10), 2627–2652. Retrieved 2023-03-24, from <https://bg.copernicus.org/articles/19/2627/2022/> (Publisher: Copernicus GmbH) doi: 10.5194/bg-19-2627-2022
- Salisbury, J. E., & Jönsson, B. F. (2018, December). Rapid warming and salinity changes in the Gulf of Maine alter surface ocean carbonate parameters and hide ocean acidification. *Biogeochemistry*, 141(3), 401–418. Retrieved 2023-03-27, from <http://link.springer.com/10.1007/s10533-018-0505-3> doi: 10.1007/s10533-018-0505-3
- Saunio, M., Stavert, A. R., Poulter, B., Bousquet, P., Canadell, J. G., Jackson, R. B., ... Zhuang, Q. (2020, July). The Global Methane Budget 2000–2017. *Earth System Science Data*, 12(3), 1561–1623. Retrieved 2023-02-14, from <https://essd.copernicus.org/articles/12/1561/2020/> doi: 10.5194/essd-12-1561-2020
- Schmale, O., Wäge, J., Mohrholz, V., Wasmund, N., Gräwe, U., Rehder, G., ... Loick-Wilde, N. (2018, January). The contribution of zooplankton to methane supersaturation in the oxygenated upper waters of the central Baltic Sea: Methane supersaturation in the Baltic Sea. *Limnology and Oceanography*, 63(1), 412–430. Retrieved 2023-02-20, from <https://onlinelibrary.wiley.com/doi/10.1002/lno.10640> doi: 10.1002/lno.10640
- Schneider, B., & Müller, J. D. (2018). *Biogeochemical Transformations in the Baltic Sea*. Cham: Springer International Publishing. Retrieved 2023-02-14, from <http://link.springer.com/10.1007/978-3-319-61699-5> doi: 10.1007/978-3-319-61699-5
- Seitzinger, S. P., & Kroeze, C. (1998). Global distribution of nitrous oxide production and N inputs in freshwater and coastal marine ecosystems. *Global Biogeochemical Cycles*, 12(1), 93–113. Retrieved 2023-02-14, from <https://onlinelibrary.wiley.com/doi/abs/10.1029/97GB03657> (_eprint: <https://onlinelibrary.wiley.com/doi/pdf/10.1029/97GB03657>) doi: 10.1029/97GB03657
- Siegel, D. A., Doney, S. C., & Yoder, J. A. (2002, April). The North Atlantic Spring Phytoplankton Bloom and Sverdrup’s Critical Depth Hypothesis. *Science*, 296(5568), 730–733. Retrieved 2023-02-14, from <https://www.science.org/doi/10.1126/science.1069174> doi: 10.1126/science.1069174
- Signorini, S. R., Mannino, A., Najjar, R. G., Friedrichs, M. A. M., Cai, W.-J., Salisbury, J., ... Shadwick, E. (2013, October). Surface ocean *p* CO₂ seasonality and sea-air CO₂ flux estimates for the North American east coast: NORTH AMERICAN EAST COAST SEA-AIR CO₂ FLUXES. *Journal of Geophysical Research: Oceans*, 118(10), 5439–5460. Retrieved 2023-02-14, from <http://doi.wiley.com/10.1002/jgrc.20369> doi: 10.1002/jgrc.20369
- Stell, A. C., Bertolacci, M., Zammit-Mangion, A., Rigby, M., Fraser, P. J., Harth, C. M., ... Ganesan, A. L. (2022, October). Modelling the growth of atmospheric nitrous oxide using a global hierarchical inversion. *Atmospheric Chemistry and Physics*, 22(19), 12945–12960. Retrieved 2022-12-02, from <https://acp.copernicus.org/articles/22/12945/2022/> doi: 10.5194/acp-22-12945-2022
- Su, X., Yang, L., Yang, K., Tang, Y., Wen, T., Wang, Y., ... Zhu, Y.-g. (2022, July). Estuarine plastisphere as an overlooked source of N₂O production. *Nature Communications*, 13(1), 3884. Retrieved 2023-02-14, from

- 1889 <https://www.nature.com/articles/s41467-022-31584-x> (Number: 1
 1890 Publisher: Nature Publishing Group) doi: 10.1038/s41467-022-31584-x
- 1891 Séférian, R., Nabat, P., Michou, M., Saint-Martin, D., Voldoire, A., Colin,
 1892 J., ... Madec, G. (2019). Evaluation of CNRM Earth System
 1893 Model, CNRM-ESM2-1: Role of Earth System Processes in Present-
 1894 Day and Future Climate. *Journal of Advances in Modeling Earth*
 1895 *Systems*, 11(12), 4182–4227. Retrieved 2023-03-01, from [https://](https://onlinelibrary.wiley.com/doi/abs/10.1029/2019MS001791)
 1896 onlinelibrary.wiley.com/doi/abs/10.1029/2019MS001791 (eprint:
 1897 <https://onlinelibrary.wiley.com/doi/pdf/10.1029/2019MS001791>) doi:
 1898 10.1029/2019MS001791
- 1899 Terhaar, J., Lauerwald, R., Regnier, P., Gruber, N., & Bopp, L. (2021, January).
 1900 Around one third of current Arctic Ocean primary production sustained
 1901 by rivers and coastal erosion. *Nature Communications*, 12(1), 169. doi:
 1902 10.1038/s41467-020-20470-z
- 1903 Thomas, H., Bozec, Y., Elkalay, K., & de Baar, H. J. W. (2004, May). Enhanced
 1904 open ocean storage of CO₂ from shelf sea pumping. *Science (New York, N.Y.)*,
 1905 304(5673), 1005–1008. doi: 10.1126/science.1095491
- 1906 Tian, H., Xu, R., Canadell, J. G., Thompson, R. L., Winiwarter, W., Sunthar-
 1907 alingam, P., ... Yao, Y. (2020, October). A comprehensive quantification of
 1908 global nitrous oxide sources and sinks. *Nature*, 586(7828), 248–256. Retrieved
 1909 2023-02-14, from <https://www.nature.com/articles/s41586-020-2780-0>
 1910 doi: 10.1038/s41586-020-2780-0
- 1911 Tjiputra, J. F., Schwinger, J., Bentsen, M., Morée, A. L., Gao, S., Bethke, I., ...
 1912 Schulz, M. (2020, May). Ocean biogeochemistry in the Norwegian Earth Sys-
 1913 tem Model version 2 (NorESM2). *Geoscientific Model Development*, 13(5),
 1914 2393–2431. Retrieved 2023-02-15, from [https://gmd.copernicus.org/](https://gmd.copernicus.org/articles/13/2393/2020/)
 1915 [articles/13/2393/2020/](https://gmd.copernicus.org/articles/13/2393/2020/) (Publisher: Copernicus GmbH) doi: 10.5194/
 1916 gmd-13-2393-2020
- 1917 Tu, Z., Le, C., Bai, Y., Jiang, Z., Wu, Y., Ouyang, Z., ... Qi, D. (2021, August).
 1918 Increase in CO₂ Uptake Capacity in the Arctic Chukchi Sea During Sum-
 1919 mer Revealed by Satellite-Based Estimation. *Geophysical Research Letters*,
 1920 48(15). Retrieved 2023-03-27, from [https://onlinelibrary.wiley.com/doi/](https://onlinelibrary.wiley.com/doi/10.1029/2021GL093844)
 1921 [10.1029/2021GL093844](https://onlinelibrary.wiley.com/doi/10.1029/2021GL093844) doi: 10.1029/2021GL093844
- 1922 Turi, G., Lachkar, Z., & Gruber, N. (2014, February). Spatiotemporal variability
 1923 and drivers of pCO₂ and air–sea CO₂ fluxes in the California Current System:
 1924 an eddy-resolving modeling study. *Biogeosciences*, 11(3), 671–690. Retrieved
 1925 2019-04-02, from <https://www.biogeosciences.net/11/671/2014/> doi:
 1926 10.5194/bg-11-671-2014
- 1927 Wan, X. S., Lin, H., Ward, B. B., Kao, S.-J., & Dai, M. (2022). Sig-
 1928 nificant Seasonal N₂O Dynamics Revealed by Multi-Year Observa-
 1929 tions in the Northern South China Sea. *Global Biogeochemical Cy-*
 1930 *cles*, 36(10), e2022GB007333. Retrieved 2023-02-14, from [https://](https://onlinelibrary.wiley.com/doi/abs/10.1029/2022GB007333)
 1931 onlinelibrary.wiley.com/doi/abs/10.1029/2022GB007333 (eprint:
 1932 <https://onlinelibrary.wiley.com/doi/pdf/10.1029/2022GB007333>) doi:
 1933 10.1029/2022GB007333
- 1934 Wang, H., Hu, X., Cai, W.-J., & Sterba-Boatwright, B. (2017). Decadal fCO₂ trends
 1935 in global ocean margins and adjacent boundary current-influenced areas. *Geo-*
 1936 *physical Research Letters*, 44(17), 8962–8970. Retrieved 2022-04-15, from
 1937 <https://onlinelibrary.wiley.com/doi/abs/10.1002/2017GL074724> doi:
 1938 10.1002/2017GL074724
- 1939 Wanninkhof, R. (1992, May). Relationship between wind speed and gas exchange
 1940 over the ocean. *Journal of Geophysical Research: Oceans*, 97(C5), 7373–7382.
 1941 Retrieved 2015-06-22, from [http://onlinelibrary.wiley.com/doi/10.1029/](http://onlinelibrary.wiley.com/doi/10.1029/92JC00188/abstract)
 1942 [92JC00188/abstract](http://onlinelibrary.wiley.com/doi/10.1029/92JC00188/abstract) doi: 10.1029/92JC00188
- 1943 Wanninkhof, R. (2014, June). Relationship between wind speed and gas exchange

- over the ocean revisited. *Limnology and Oceanography: Methods*, 12(6), 351–362. Retrieved 2015-06-22, from <http://onlinelibrary.wiley.com/doi/10.4319/lom.2014.12.351/abstract> doi: 10.4319/lom.2014.12.351
- Ward, N. D., Megonigal, J. P., Bond-Lamberty, B., Bailey, V. L., Butman, D., Canuel, E. A., ... Windham-Myers, L. (2020, May). Representing the function and sensitivity of coastal interfaces in Earth system models. *Nature Communications*, 11(1), 2458. Retrieved 2023-02-14, from <https://www.nature.com/articles/s41467-020-16236-2> (Number: 1 Publisher: Nature Publishing Group) doi: 10.1038/s41467-020-16236-2
- Weber, T., Wiseman, N. A., & Kock, A. (2019, October). Global ocean methane emissions dominated by shallow coastal waters. *Nature Communications*, 10(1), 4584. Retrieved 2020-10-21, from <https://www.nature.com/articles/s41467-019-12541-7> (Number: 1 Publisher: Nature Publishing Group) doi: 10.1038/s41467-019-12541-7
- Woolf, D., Shutler, J., Goddijn-Murphy, L., Watson, A., Chapron, B., Nightingale, P., ... Paul, F. (2019, December). Key Uncertainties in the Recent Air-Sea Flux of CO₂. *Global Biogeochemical Cycles*, 33(12), 1548–1563. Retrieved 2023-04-03, from <https://onlinelibrary.wiley.com/doi/abs/10.1029/2018GB006041> doi: 10.1029/2018GB006041
- Wright, R. M., Le Quéré, C., Buitenhuis, E., Pitois, S., & Gibbons, M. J. (2021, February). Role of jellyfish in the plankton ecosystem revealed using a global ocean biogeochemical model. *Biogeosciences*, 18(4), 1291–1320. Retrieved 2023-03-27, from <https://bg.copernicus.org/articles/18/1291/2021/> (Publisher: Copernicus GmbH) doi: 10.5194/bg-18-1291-2021
- Xu, Y., Cai, W., Wanninkhof, R., Salisbury, J., Reimer, J., & Chen, B. (2020, July). Long-Term Changes of Carbonate Chemistry Variables Along the North American East Coast. *Journal of Geophysical Research: Oceans*, 125(7). Retrieved 2023-02-14, from <https://onlinelibrary.wiley.com/doi/abs/10.1029/2019JC015982> doi: 10.1029/2019JC015982
- Xue, Z., He, R., Fennel, K., Cai, W.-J., Lohrenz, S., Huang, W.-J., ... Zang, Z. (2016, August). Modeling pCO_2 variability in the Gulf of Mexico. *Biogeosciences*, 13(15), 4359–4377. Retrieved 2023-02-14, from <https://bg.copernicus.org/articles/13/4359/2016/> doi: 10.5194/bg-13-4359-2016
- Yang, S., Chang, B. X., Warner, M. J., Weber, T. S., Bourbonnais, A. M., Santoro, A. E., ... Bianchi, D. (2020, June). Global reconstruction reduces the uncertainty of oceanic nitrous oxide emissions and reveals a vigorous seasonal cycle. *Proceedings of the National Academy of Sciences*, 117(22), 11954–11960. Retrieved 2022-05-12, from <https://www.pnas.org/doi/10.1073/pnas.1921914117> (Publisher: Proceedings of the National Academy of Sciences) doi: 10.1073/pnas.1921914117
- Yukimoto, S., Kawai, H., Koshiro, T., Oshima, N., Yoshida, K., Urakawa, S., ... Ishii, M. (2019). The Meteorological Research Institute Earth System Model Version 2.0, MRI-ESM2.0: Description and Basic Evaluation of the Physical Component. *Journal of the Meteorological Society of Japan. Ser. II*, 97(5), 931–965. Retrieved 2023-02-15, from https://www.jstage.jst.go.jp/article/jmsj/97/5/97_2019-051/_article doi: 10.2151/jmsj.2019-051
- Zhou, J., Zheng, Y., Hou, L., An, Z., Chen, F., Liu, B., ... Liu, M. (2023, March). Effects of acidification on nitrification and associated nitrous oxide emission in estuarine and coastal waters. *Nature Communications*, 14(1), 1380. Retrieved 2023-03-22, from <https://www.nature.com/articles/s41467-023-37104-9> doi: 10.1038/s41467-023-37104-9

A Synthesis of Global Coastal Ocean Greenhouse Gas Fluxes

L. Resplandy¹, A. Hogikyan², H. W. Bange³, D. Bianchi⁴, T. Weber⁵, Wei-Jun Cai⁶, S.C. Doney⁷, K. Fennel⁸, M. Gehlen⁹, J. Hauck¹⁰, F. Lacroix¹¹, P. Landschützer^{12,13}, C. Le Quéré¹⁴, J. D. Müller¹⁵, R. G. Najjar¹⁶, A. Roobaert¹⁷, J. Schwinger¹⁸, S. Berthet¹⁹, L. Bopp²⁰, T.T.T. Chau⁹, M. Dai²¹, N. Gruber¹⁵, T. Ilyina¹³, A. Kock^{3*}, M. Manizza²², Z. Lachkar²³, G. G. Laruelle¹⁷, E. Liao^{1†}, I.D. Lima²⁴, C. Nissen^{10,25}, C. Rödenbeck²⁶, R. Séférian¹⁹, K. Toyama²⁷, H. Tsujino²⁷, P. Regnier¹⁷

¹Department of Geosciences and High Meadows Environmental Institute, Princeton University, Princeton, NJ, USA

²Atmospheric and Oceanic Sciences Program, Princeton University, Princeton, NJ, USA

³GEOMAR Helmholtz Centre for Ocean Research Kiel, Kiel, Germany

⁴Department of Atmospheric and Oceanic Sciences, University of California Los Angeles, Los Angeles, CA, USA

⁵Department of Earth and Environmental Science, University of Rochester, NY, USA

⁶School of Marine Science and Policy, University of Delaware, Newark, Delaware, 19716, USA

⁷Department of Environmental Sciences, University of Virginia, Charlottesville, VA, USA

⁸Department of Oceanography, Dalhousie University, Halifax, Canada

⁹Laboratoire des Sciences du Climat et de l'Environnement, LSCE/IPSL, CEA-CNRS-UVSQ, Université Paris-Saclay, F-91191 Gif-sur-Yvette, France

¹⁰Alfred-Wegener-Institut, Helmholtz-Zentrum für Polar- und Meeresforschung, Germany

¹¹Climate and Environmental Physics / Oeschger Centre for Climate Change Research (OCCR), University of Bern, Switzerland

¹²Flanders Marine Institute (VLIZ), Ostend Belgium

¹³Max Planck Institute for Meteorology, Hamburg, Germany

¹⁴School of Environmental Sciences, University of East Anglia, Norwich Research Park, NR4 7TJ, Norwich, UK

¹⁵Environmental Physics, Institute of Biogeochemistry and Pollutant Dynamics, ETH Zurich, Zürich, Switzerland

¹⁶Department of Meteorology and Atmospheric Science, The Pennsylvania State University, University Park, Pennsylvania, USA

¹⁷Dept. Geoscience, Environment and Society - BGEOSSYS, Université Libre de Bruxelles, Brussels, Belgium

¹⁸NORCE Climate & Environment, Bjerknes Centre for Climate Research, Bergen, Norway

¹⁹CNRM, Université de Toulouse, Météo France, CNRS, Toulouse, France

²⁰LMD/IPSL, ENS, Université PSL, École Polytechnique, Institut Polytechnique de Paris, Sorbonne Université, CNRS, Paris, France

²¹State Key Lab of Marine Environmental Science and College of Ocean and Earth Sciences, Xiamen University, Xiamen 361102, China

²²Geosciences Research Division, Scripps Institution of Oceanography, University of California - San Diego, La Jolla, USA

²³Arabian Center for Climate and Environmental Sciences, New York University Abu Dhabi, Abu Dhabi, United Arab Emirates

²⁴Department of Marine Chemistry and Geochemistry, Woods Hole Oceanographic Institution, Woods Hole, MA, USA

²⁵Department of Atmospheric and Oceanic Sciences and Institute of Arctic and Alpine Research, University of Colorado, Boulder, Colorado, USA

²⁶MPI Biogeochemistry, Jena, Germany

²⁷JMA Meteorological Research Institute, Tsukuba, Ibaraki, Japan

*now at State Office for the Environment of the State of Schleswig-Holstein, Flintbek, Germany

†now at School of Oceanography, Shang Jiao Tong University, Shanghai, 200030, China

Corresponding author: Laure Resplandy, laurer@princeton.edu

51

Key Points:

52

- We synthesize air-sea fluxes of CO₂, nitrous oxide and methane in the global coastal ocean using observation-based products and ocean models

53

54

- The coastal ocean CO₂ sink is 60% larger in ocean models than in observation-based products due to systematic differences in seasonality

55

56

- Coastal nitrous oxide and methane emissions offset 30-58% of net CO₂ coastal uptake radiative effect

57

Abstract

The coastal ocean contributes to regulating atmospheric greenhouse gas concentrations by taking up carbon dioxide (CO_2) and releasing nitrous oxide (N_2O) and methane (CH_4). Major advances have improved our understanding of the coastal air-sea exchanges of these three gasses since the first phase of the Regional Carbon Cycle Assessment and Processes (RECCAP in 2013), but a comprehensive view that integrates the three gasses at the global scale is still lacking. In this second phase (RECCAP2), we quantify global coastal ocean fluxes of CO_2 , N_2O and CH_4 using an ensemble of global gap-filled observation-based products and ocean biogeochemical models. The global coastal ocean is a net sink of CO_2 in both observational products and models, but the magnitude of the median net global coastal uptake is $\sim 60\%$ larger in models (-0.72 vs. $-0.44 \text{ PgC yr}^{-1}$, 1998-2018, coastal ocean area of 77 million km^2). We attribute most of this model-product difference to the seasonality in sea surface CO_2 partial pressure at mid- and high-latitudes, where models simulate stronger winter CO_2 uptake. The global coastal ocean is a major source of N_2O ($+0.70 \text{ PgCO}_2\text{-e yr}^{-1}$ in observational product and $+0.54 \text{ PgCO}_2\text{-e yr}^{-1}$ in model median) and of CH_4 ($+0.21 \text{ PgCO}_2\text{-e yr}^{-1}$ in observational product), which offsets a substantial proportion of the net radiative effect of coastal CO_2 uptake (35-58% in CO_2 - equivalents). Data products and models need improvement to better resolve the spatio-temporal variability and long term trends in CO_2 , N_2O and CH_4 in the global coastal ocean.

Plain Language Summary

The coastal ocean regulates greenhouse gases. It acts as a sink of carbon dioxide (CO_2) but also releases nitrous oxide (N_2O) and methane (CH_4) to the atmosphere. This synthesis contributes to the second phase of the Regional Carbon Cycle Assessment and Processes (RECCAP2) and provides a comprehensive view of the coastal air-sea fluxes of these three greenhouse gases at the global scale. We use a multi-faceted approach combining gap-filled observation-based products and ocean biogeochemical models. We show that the global coastal ocean is a net sink of CO_2 in both observational products and models, but the coastal uptake of CO_2 is $\sim 60\%$ larger in models than in observation-based products due to model-product differences in seasonality. We also find that the coastal emissions of N_2O and CH_4 counteract a substantial part of the climate buffering effect of coastal CO_2 uptake (by 35-58% in CO_2 -equivalents). Improvements to resolve long term trends in CO_2 , N_2O and CH_4 in the global coastal ocean are crucially needed.

1 Introduction

Coastal oceans play an important role in the global carbon cycle by serving as a hub of exchange between the land-aquatic continuum, sediments, the atmosphere, and the open ocean (Bauer et al., 2013; Chen & Borges, 2009; F. Mackenzie et al., 1998; Ward et al., 2020). They are often defined as ocean waters over continental shelves shallower than $\sim 200\text{-m}$ water depth, albeit sometimes extending further offshore (typically to 300 km from the coastline and 1000 m isobath, Laruelle et al., 2018). Coastal waters contribute to the global oceanic uptake of anthropogenic carbon by absorbing carbon dioxide (CO_2) directly from the atmosphere and by burying, transforming, or outgassing the carbon delivered by terrestrial ecosystems to the coastal ocean (e.g., Regnier et al., 2022).

A notable milestone in the efforts to quantify the CO_2 exchange between the atmosphere and coastal oceans was reached by Chen et al. (2013) during the first phase of the Regional Carbon Cycle Assessment and Processes (RECCAP), an international effort to establish the mean carbon balance and change over the period 1990–2009 for all subcontinents and ocean basins. These authors expanded on prior work at the scale of continental shelves (W.-J. Cai et al., 2006; Laruelle et al., 2010) and examined the global

atmospheric CO₂ uptake by coastal waters using a compilation of surface ocean partial pressure of CO₂ (pCO₂) data available for 87 shelves. They concluded that most coastal waters act as a sink for atmospheric CO₂, except for tropical coastal systems that were identified as weak CO₂ sources, and found the global coastal CO₂ uptake to be 0.4 PgC yr⁻¹ (for a surface area of coastal waters of 30.3 million km²).

Since the completion of RECCAP, the amount of available pCO₂ measurements in the coastal ocean has increased tremendously, reaching millions shortly after the RECCAP assessment was released (e.g., Surface Ocean CO₂ Atlas database SOCAT Bakker et al., 2014) and ~19 million in the most recent publication (Bakker et al., 2022). In parallel, statistical gap-filling methods, initially developed for the open ocean, have been applied to these fast expanding datasets to resolve the spatio-temporal variability of the air-sea CO₂ flux in the coastal ocean (Laruelle et al., 2014; Roobaert et al., 2019; Landschützer et al., 2020; Chau et al., 2022). These global gap-filled observation-based coastal products led to a downward revision of the global coastal ocean CO₂ uptake to about half of the RECCAP value (0.15-0.20 PgC yr⁻¹, Roobaert et al., 2019; Chau et al., 2022). This downward revision was corroborated by a recent synthesis of 214 regionally aggregated CO₂ flux estimates, leading to a net uptake of 0.25 PgC yr⁻¹ (Dai et al., 2022), although these assessments covered slightly different periods and coastal areas (1985-2019 and ~22 million km² in Chau et al., 2022; 1998-2015 and 28 million km² in Roobaert et al., 2019; 1998-present and ~30 million km² in Dai et al., 2022).

While coastal waters are a sink of CO₂, they are also the main oceanic source of two other important greenhouse gases: nitrous oxide (N₂O) and methane (CH₄) (e.g., Weber et al., 2019; Yang et al., 2020; Saunio et al., 2020; Wan et al., 2022). RECCAP did not consider N₂O and CH₄, but recent studies have compiled oceanic N₂O and CH₄ measurements (Kock & Bange, 2015) and applied statistical gap-filling techniques similar to those employed for CO₂ to assess the global ocean air-sea N₂O and CH₄ fluxes (Weber et al., 2019; Yang et al., 2020). These studies have greatly improved the quantification of N₂O and CH₄ air-sea fluxes at the global scale, but coastal ocean N₂O and CH₄ emissions remain highly uncertain and the extent to which these emissions offset the present-day coastal CO₂ uptake is unknown.

Coastal air-sea fluxes of CO₂, N₂O and CH₄ have strong spatial and seasonal variability. Regional-scale observational and modeling studies have greatly improved the quantification of the mean and temporal variability of air-sea fluxes of greenhouse gases in individual regions across the globe (e.g., Anderson et al., 2009; Güllow et al., 2013; Turi et al., 2014; Arévalo-Martínez et al., 2015; Pipko et al., 2017; Mayer et al., 2018; Fennel et al., 2019; Gomez et al., 2020; Hauri et al., 2021; Louchard et al., 2021). However, the limited spatial coverage of these studies largely inhibits a global-scale perspective. Global gap-filled observational products and global ocean biogeochemical models now run at a reasonably high horizontal resolution (0.5° or higher) to simulate coastal CO₂ (Bourgeois et al., 2016; Lacroix et al., 2020, 2021; Roobaert et al., 2022) and N₂O (Ganesan et al., 2020; Stell et al., 2022; Berthet et al., 2022) fluxes, recently complemented these regional-scale studies.

As a result of observational and modeling advances since RECCAP, a global view of the coastal ocean's spatial and seasonal patterns in air-sea greenhouse gas fluxes has started to emerge, at least for CO₂ fluxes. Polar and subpolar coastal oceans, such as the northwest North Atlantic along the Canadian and US coast (Thomas et al., 2004; Fennel & Wilkin, 2009; Previdi et al., 2009; Signorini et al., 2013; Lachkar & Gruber, 2013; Laruelle et al., 2015; Cahill et al., 2016; Gustafsson et al., 2019), the European shelves (Thomas et al., 2004; Cossarini et al., 2015; Neumann et al., 2022; Gustafsson et al., 2019) and Arctic and Antarctic shelf (Arrigo et al., 2008; Pipko et al., 2017, 2021; Ouyang, Sciusco, et al., 2022) generally are strong sinks of CO₂ characterized by large seasonal variations, and likely account for about 90% of the annual global coastal CO₂ uptake (while representing ~45% of the global coastal surface area, see Laruelle et al., 2014; Roobaert et

al., 2019; Dai et al., 2022). There are exceptions with subpolar and polar shelves where outgassing has been identified, such as the Scotian Shelf (Rutherford et al., 2021; Rutherford & Fennel, 2022) or the Laptev Sea in the Arctic (Anderson et al., 2009). Coastal upwelling regions, such as the nearshore California Current, are sources of CO₂ to the atmosphere with a marked seasonality that follows the upwelling dynamics (Lachkar & Gruber, 2013; Dai et al., 2013; Turi et al., 2014; Fiechter et al., 2014; Damien et al., 2023). Tropical systems, such as the Gulf of Mexico (Xue et al., 2016; Laurent et al., 2017) and the South China Sea (Wan et al., 2022), are mostly identified as weak CO₂ sources with weak seasonal variability (Laruelle et al., 2014, 2015; Roobaert et al., 2019; Dai et al., 2022). Our knowledge of N₂O and CH₄ variability in the global coastal ocean is more limited, but gap-filled products and global models suggest that N₂O and CH₄ annual emissions strongly vary between coastal regions (e.g., Weber et al., 2019; Yang et al., 2020; Ganesan et al., 2020; Stell et al., 2022). These products and models offer a remarkable opportunity to establish a greenhouse gas budget for the global coastal ocean, and improve our understanding of its spatial and seasonal variability.

Rising atmospheric CO₂ levels influence coastal CO₂ uptake on multi-decadal time-scales. Prior syntheses at the global scale including RECCAP (W.-J. Cai et al., 2006; Laruelle et al., 2010; Chen et al., 2013; Bauer et al., 2013; Regnier et al., 2013) and at the regional scale (Liu et al., 2018; Fennel & Testa, 2019; Legge et al., 2020) clearly support the view that the coastal ocean is currently a sink of atmospheric CO₂, but the extent to which it has changed on longer time-scales remains controversial (see Dai et al., 2022, for a review). F. T. Mackenzie et al. (2005) from a modeling perspective and later W. Cai et al. (2021) from observations first hypothesized that the potential of the coastal ocean to act as a sink for CO₂ might be increasing with time. This view is increasingly supported by time series analyses that suggest that trends in sea surface pCO₂ are overall weaker than the atmospheric pCO₂ trend in most coastal regions. This finding further implies an intensified CO₂ uptake or decreased outgassing, although potential trends in winds and sea ice may also play a role (Bauer et al., 2013; Wang et al., 2017; Laruelle et al., 2018; Dai et al., 2022). However, exceptions have been identified in regions where coastal ocean pCO₂ increases at a similar rate (i.e., near-zero changes in the flux) or even at higher rates (i.e., reduced CO₂ uptake or intensified outgassing) than atmospheric pCO₂ (e.g., California Current, South and Mid Atlantic Bight, Baltic Sea Reimer et al., 2017; Laruelle et al., 2018; Schneider & Müller, 2018; Dai et al., 2022). The quantification of coastal CO₂ flux trends from observations is, however, still strongly restricted by the limited spatial coverage and/or the relatively short duration of time series.

Global ocean biogeochemical models offer an attractive means of assessing long term trends in air-sea CO₂ flux densities in the coastal ocean and how they differ from those of the open ocean (Regnier et al., 2022). Two such models, with reasonable agreement in regions where time series are available (0.2-0.5° resolution in Bourgeois et al., 2016; 0.4° resolution in Lacroix et al., 2021), suggest that the global coastal CO₂ sink density has increased at a slightly slower rate than the open ocean CO₂ sink since the preindustrial era, even when accounting for increasing global nutrient sources via river and atmospheric transports (Lacroix et al., 2020). Both models, however, have important limitations and potential biases related to their representation of fine-scale hydrodynamics of shelf circulation and biophysical processes that impact biogeochemical cycling in the shallow ocean (Mathis et al., 2022; Rutherford & Fennel, 2018).

In this second phase of the Regional Carbon Cycle Assessment and Processes (RECCAP2), we aim to address gaps in our understanding of air-sea greenhouse gas fluxes for the global coastal ocean using a multi-methodological approach that relies on an ensemble of global gap-filled observation-based products and ocean biogeochemical models. Our objectives are threefold. First, we revisit the estimate of the net coastal ocean CO₂ flux, and combine it with CH₄ and N₂O emissions to derive a global climatological coastal ocean budget of greenhouse gas fluxes (section 3.1). Second, we analyze the spatial and sea-

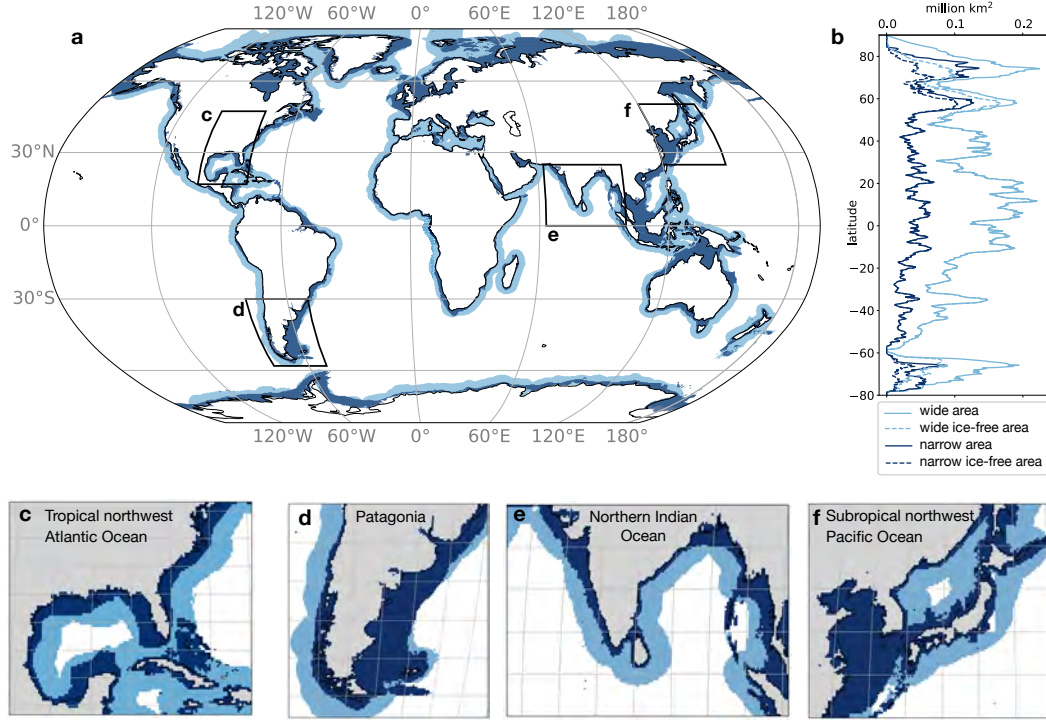


Figure 1. a) Coastal masks used in this study for the wide (dark + light blue) and narrow (dark blue) coastal oceans, b) Surface area (in km^2) at each latitude in the wide (light blue) and narrow (dark blue) coastal ocean masks (solid lines) and the 1998-2018 averaged sea-ice free surface area (dashed lines). c-f) Insets showing the extent of the narrow and wide coastal oceans in four coastal regions. Sea ice coverage used in b is from NOAA OISST. See Methods for details.

sonal variability in the CO_2 flux density and how it might differ from that of the open ocean, and examine spatial patterns in coastal CH_4 and N_2O fluxes (sections 3.2 and 3.3). Third, we investigate trends in the coastal CO_2 flux over the last four decades (section 3.3). This synthesis does not cover the seasonal and interannual variability in N_2O and CH_4 fluxes, as these temporal scales are either unresolved (CH_4) or have not yet been analyzed (N_2O) in the coastal ocean. We consider the net contemporary air-sea fluxes (natural + anthropogenic) of CO_2 , N_2O and CH_4 using the 1998-2018 period (except if specified otherwise). Our approach combines observation-based and model-based estimates with different strengths and limitations discussed in Section 4.

2 Methods

2.1 Coastal ocean definition and analysis period

Different definitions of coastal oceans are used in the literature (Chen et al., 2013; Laruelle et al., 2017). We primarily use a “wide” coastal ocean definition following Laruelle et al. (2017), where the seaward boundary is 300 km from shore or the 1000-m isobath, whichever is further from shore, amounting to a total coastal ocean area of 77.2 million km^2 (Fig 1). This wide coastal ocean definition allows us to examine coastally influenced regions of the ocean, i.e., that part of the ocean that is impacted by the presence of the coastal boundary, while also maximizing the number of observation-based and model-based estimates we can use in this study (i.e., a narrower definition would exclude prod-

ucts of lower horizontal resolution). This wide coastal ocean area is, however, more than twice the surface area commonly used to examine coastal ocean biogeochemical dynamics (e.g. Chen et al., 2013). We therefore further use a “narrow” coastal ocean definition, which is delimited by the shelf break (defined as the isobath with maximum slope increase in the 0-1000 m interval) and amounting to a total area of 28 million km² (see details in Laruelle et al., 2013, 2014). See Figure 1 for maps and area latitudinal distribution of the narrow and wide coastal waters. The landward boundary in the masks used to define the narrow and wide coastal oceans excludes estuaries and coastal vegetation, which are described in (Rosentreter et al., 2023).

The analysis is done over the 1998-2018 period to maximize the number of models and observation-based products available (see Tables 1-3 for periods covered by models and observation-based products). Note that this period differs from the one used in the open-ocean RECCAP2 studies that analyze oceanic CO₂ fluxes since 1985. All trends are calculated as linear trends over the 1998-2018 period.

2.2 Datasets

We use observation-based and model-based estimates with different strengths and limitations. Notably, gap-filled global observational-based products rely on observations that are often too sparse to capture the full range of spatio-temporal variability in coastal regions (except in densely sampled regions such as major parts of the North American and European ocean margins) and are highly sensitive to the wind product and the choice of the gas exchange coefficient formulation (e.g., Roobaert et al., 2018). In contrast, ocean biogeochemical models can be associated with systematic biases. For instance, only some of the models used here include land-sea riverine carbon inputs which sustain an oceanic CO₂ outgassing flux, and land-sea nutrient inputs which would yield an opposing biologically-driven oceanic CO₂ uptake in coastal waters (Resplandy et al., 2018; Hauck et al., 2020; Regnier et al., 2022; Gao et al., 2023, see Tables 1-3).

2.2.1 Observation-based pCO₂-products

We use 4 global pCO₂-products that provide global monthly gridded surface ocean pCO₂ (noted pCO₂ here) and air-sea CO₂ flux fields based on observations from the SOCAT database which compiles surface ocean pCO₂ observations and provides a subset after quality control (Bakker et al., 2016, 2022). Three of them use neural network-based interpolation methods: Coastal-SOM-FFN (Laruelle et al., 2017; Roobaert et al., 2019, 2022), merged-SOM-FFN (Landschützer et al., 2020) and CMEMS-LSCE-FFNN (which we refer as CMEMS, Chau et al., 2022), while the fourth product, Carboscope-1, uses a simple statistical representation of mixed-layer biogeochemistry fitted to the pCO₂ data (Rödenbeck et al., 2022). All these products are using SOCAT pCO₂ observations and are therefore not independent (see SI for details on SOCAT versions and Fig. S1 for SOCAT data coverage). In particular, the Merged-SOM-FFN product merged the Coastal-SOM-FFN (Laruelle et al., 2017) with an open ocean SOM-FFN product (Landschützer et al., 2014) to produce a global ocean product; the Coastal-SOM-FFN and Merged-SOM-FFN are therefore identical in the nearshore coastal region and only differ in the more offshore band of the wide coastal domain (see details in Landschützer et al., 2020). Coastal-SOM-FFN (and therefore also the near-shore product in Merged-SOM-FFN) was designed for the coastal ocean and uses coastal SOCAT data for their neural network training. In the three other products that use both open ocean and coastal ocean data (i.e. CMEMS, Carboscope-1 and offshore portion of Merged-SOM-FFN), the coastal estimate may be strongly influenced by open-ocean information extrapolated towards the coast. See Tables 1-3 and Supplementary Information S1 for details on pCO₂-products (e.g., period, wind speed product, gas exchange formulation).

Carboscope-1 and CMEMS products resolve interannual variability over the whole 1998-2018 period and may be used to estimate decadal trends, while Coastal-SOM-FFN and Merged-SOM-FFN provide a 1998-2015 monthly climatology and do not resolve interannual variability. $p\text{CO}_2$ -products often have unrealistic $p\text{CO}_2$ values under sea-ice (Laruelle et al., 2017). We therefore used the sea-ice fraction from the NOAA-OISST product (Reynolds et al., 2007) to mask $p\text{CO}_2$ and CO_2 flux values under sea-ice in the four products. We mask both to keep consistency but this method should not impact the flux dramatically since it is often inhibited by sea-ice in flux formulations. In this study, we also filled the missing values north of 75N in CMEMS using the Coastal-SOM-FFN climatology. This approach only marginally impacts the results (adds $-0.03 \text{ PgC yr}^{-1}$ to the wide coastal ocean net CO_2 flux) because the surface area north of 75N contributes 5 million km^2 to the wide coastal ocean (6% of the total wide area) but only 1.4 million km^2 is ice-free on average for the entire study period. This filled-in version of CMEMS is referred to as CMEMS* and we report no long-term trend in the Arctic for this product.

We also illustrate the sensitivity of the flux in $p\text{CO}_2$ -products to the choice of the wind speed product and gas transfer coefficient (k_w) formulation (e.g., Roobaert et al., 2018) by presenting a second version of the Coastal-SOM-FFN flux product but with a different wind product and k_w (labeled Coastal-SOM-FFN- k_w) in which the CO_2 flux is calculated as $F = k_w \text{ Ko } (p\text{CO}_{2a} - p\text{CO}_2)$ where Ko is the gas solubility and $p\text{CO}_{2a}$ the atmospheric $p\text{CO}_2$. The default version of Coastal-SOM-FFN uses the ERA5 wind speeds and the k_w formulation from (Ho et al., 2011), whereas Coastal-SOM-FFN- k_w uses JRA55v1.3 winds and the Wanninkhof (1992) k_w formulation (i.e., wind and formulation used in some ocean biogeochemical models, see Tables 1-3 for details on k_w parametrization and wind products used in models and products). The four $p\text{CO}_2$ -products are used for the analysis of the wide and narrow coastal oceans, and the three $p\text{CO}_2$ -products that extend outside of the coastal domain are used for the open ocean (CMEMS*, Merged-SOM-FFN, and Carboscope-1). Coastal-SOM-FFN- k_w is only shown in the wide coastal ocean for discussion and is not used to compute the $p\text{CO}_2$ -product median.

2.2.2 Observation-based N_2O and CH_4 flux products

We used two observation-based estimates of the N_2O and CH_4 fluxes. In each case, we use an estimate based on a simple extrapolation of the MEMENTO (Marine Methane and Nitrous Oxide) database to the 45 MARGins and CATchments Segmentation (MARCATS, Figure S2) coastal regions (referred to as MARCATS- N_2O and MARCATS- CH_4 Kock & Bange, 2015), and an estimate that extrapolates MEMENTO and supplementary observations to a global 0.25-degree climatology using supervised machine learning models (Weber et al., 2019; Yang et al., 2020, referred to as Weber- CH_4 and Yang- N_2O). The MARCATS- N_2O and MARCATS- CH_4 products provide an annual mean value based on data from 1980 to 2016, Yang- N_2O provides a monthly climatology for 1988-2017 and Weber- CH_4 an annual mean value for 1999-2016 (Table 1). In Yang- N_2O surface N_2O disequilibrium was extrapolated globally using an ensemble of 100 Random Regression Forest (RRF) models, and in Weber- CH_4 surface CH_4 disequilibrium was extrapolated using 1000 RRF models and 1000 Artificial Neural Network (ANN) models. In both cases, diffusive fluxes were calculated and uncertainty propagated by coupling the mapped disequilibrium to multiple high-resolution wind reanalysis products (two in Yang- N_2O , four in Weber- CH_4), and multiple piston velocity parameterizations (two in Yang- N_2O and four in Weber- CH_4). These estimates for each gas are not independent as they use the same MEMENTO database. The Yang- N_2O and Weber- CH_4 products use interpolation techniques to fill observational gaps, but the lack of observations likely leads to large uncertainties in coastal regions.

For CH_4 emissions, the contribution from gas bubble plumes must be taken into account in addition to the diffusive flux (arising from the air-sea difference in partial pres-

sure and a gas exchange coefficient). The MEMENTO database allows the calculation of the diffusive CH_4 flux only, because CH_4 from bubble plumes are usually not captured by the conventional CH_4 measurements based on discrete samples or continuous underway measurement systems. An estimate of the ebullitive (i.e. bubbling) CH_4 fluxes is, however, included in Weber- CH_4 (but not in MARCATS- CH_4), by combining previous seafloor emissions estimates with models of bubble transfer to the surface (Weber et al., 2019). We evaluated the uncertainty on the net Weber- CH_4 flux in the narrow and wide coastal oceans from the quadrature of uncertainties on diffusive and ebullitive fluxes, using a 50% uncertainty on diffusive flux and a 60% uncertainty on ebullitive flux (Weber et al., 2019). More details on these products can be found in Supplementary Information S1.

2.2.3 Ocean models for CO_2 and N_2O fluxes

For CO_2 , we used 15 ocean general circulation models coupled with biogeochemical modules: 11 are global and 4 are regional models, all covering the study period of 1998-2018 except CCSM-WHOI which ends in 2017 (see details in Tables 2-3). Most global models have native horizontal grid resolutions varying between 0.25° and 1° in the coastal domain, except FESOM-HR which has an unstructured mesh that reaches higher resolution (see Fig S3) and MPIOM-HAMMOC, NEMO-PlankTOM12 and CCSM-WHOI which have a coarser resolution of $\sim 1.5^\circ$, $\sim 2^\circ$ and $\sim 3^\circ$ respectively (Table 2). The regional models covering the Indian Ocean (NYUAD-ROMS-Indian) and Northwest Atlantic Ocean (NW-Atl) have horizontal resolutions of approximately 10 km. The regional models covering the Atlantic (ETHZ-ROMS-Atl) and Pacific Ocean (ETHZ-ROMS-Pac) have resolution varying in space between 4 km and 120 km: the ETHZ-ROMS-Atl telescopes to focus on the Amazon outflow region where the resolution is higher and the ROMS-ETHZ-Pac grid focuses on the California Current region (Table 3). We note that some of these models include land-sea nutrient and carbon inputs by rivers, while others do not. Details on these models can be found in Tables 2-3 and Supplementary information S1.

For N_2O , we use 5 models: three of them are also used for CO_2 (CNRM-HR, CNRM-LR, and NEMO-PlankTOM5) and cover the full study period (1998-2018), while the two other models are from the ECCO family (ECCO-Darwin and ECCO2-Darwin) in which the circulation is optimized to capture the distribution of tracers such as temperature and salinity in the ocean but cover shorter periods (ECCO-Darwin for 1997-2013 and ECCO2-Darwin for 2006-2013). See Table 2 and Supplementary Information S1 for further details and references on each model.

Model-based analyses in this study use all global models available for the wide coastal ocean (i.e. 11 models for CO_2 and 5 for N_2O), but subsets of models with higher native horizontal resolution are used for the narrow coastal ocean (4 models for CO_2 : CNRM-HR, FESOM-HR, MOM6, MRI-ESM2.1, and 3 models for N_2O : CNRM-HR, ECCO-Darwin and ECCO2-Darwin, see Table 2). Global averages and integrated fluxes are based on the global models, while regional models were used in addition to the global models for the analysis at the grid-point scale (e.g. maps).

2.3 Grid harmonization and coastal waters area rescaling

All models and data products were re-gridded from their native grid onto the same $1/4^\circ$ grid for analysis. Yet, due to differences in horizontal resolution and ocean-land mask definition, observational products and ocean biogeochemical models can have different coastal ocean areas, even after they have been re-gridded to the same $1/4^\circ$ grid (for example, wide coastal ocean areas resolved by the models range from 34 to 76 million km^2 vs. 77.2 million km^2 in the mask of Laruelle et al. (2017), see Tables 1-3 and Fig 1). To minimize the effect of this common issue, most results are presented as area-weighted

averages of CO₂, N₂O and CH₄ flux densities (per m²) and surface ocean pCO₂ masked using time varying ice-free surface to account for fractional sea ice coverage (in μatm). We used the ice fraction from the NOAA-OISST product for pCO₂-products and the ice fraction of each individual model for models. For the globally integrated CO₂ flux (in PgC yr⁻¹), we used the globally averaged CO₂ flux densities found in each pCO₂-product and model for the narrow and wide coastal oceans and multiplied them by the corresponding coastal area of Laruelle et al. (2017, narrow area = 28 million km²; wide area = 77 million km²). We did not apply this area rescaling to the globally integrated fluxes of N₂O and CH₄ given the smaller number of products/models available.

2.4 Calculation of CO₂ equivalents global coastal fluxes and uncertainties

We computed CO₂ equivalent fluxes of N₂O and CH₄ to provide a global greenhouse gas flux integral (i.e., spatially integrated annual net air-sea flux of greenhouse gasses) in gigatonnes of CO₂ equivalent (PgCO₂-e) for the wide coastal ocean. We used the Intergovernmental Panel on Climate Change (IPCC) Assessment Report 6 (Arias et al., 2021) updated 100-year global warming potential for N₂O ($\text{GWP}_{\text{N}_2\text{O}} = 273$, i.e. the 100-year time integrated radiative forcing from the instantaneous release of 1 kg of N₂O is 273 times larger than the forcing of 1 kg of CO₂) and for CH₄ of non-fossil fuel origin ($\text{GWP}_{\text{CH}_4} = 27.2$). We calculated two budgets for the wide coastal ocean: one using observation-based flux products only and one using mostly models. The observation-based budget uses the global gap-filled observational products, i.e. the 4 pCO₂-product median flux for CO₂ (CMEMS*, Carboscope-1, Coastal-SOM-FFN and Merged-SOM-FFN), the Yang-N₂O flux for N₂O and the Weber-CH₄ flux for CH₄. Uncertainty bars presented for this observation-based budget give the ranges of all products presented in this study, i.e. the 4 pCO₂-product range for CO₂, the 2 observational-product range for N₂O (Yang-N₂O and MARCATS-N₂O) and the 2 observational-product range for CH₄ (i.e. the low bound corresponds to the low uncertainty bound of Weber-CH₄ and the high bound to the value of MARCATS-CH₄). The model-based budget uses the 11 global model median flux for CO₂, the 4 global model median flux for N₂O, and the product-based Weber-CH₄ flux for CH₄ as no model is available. Uncertainty bars presented for this model-based budget are the 11-model range for CO₂, the 4-model range for N₂O, and the 2 observational product range for CH₄ (same as the product-based budget described above).

3 Results

3.1 Global coastal ocean greenhouse gas fluxes

In this section, we present a compilation of observation-based and modeled net air-sea fluxes of CO₂ (4 pCO₂-products and 11 global ocean models), N₂O (2 observation-based products and 4 global ocean models) and CH₄ (2 observation-based products) in the global coastal ocean (Figure 2), and assess the contribution of the coastal ocean to the atmospheric greenhouse gas budget by combining the three gasses using a single CO₂-equivalent flux (Figure 3).

3.1.1 Net coastal CO₂ uptake

The pCO₂-products yield a weaker net CO₂ uptake than the global ocean biogeochemical models in the wide coastal ocean during the 1998-2018 period (Figure 2a). The pCO₂-product estimates (-0.59 to -0.37 PgC yr⁻¹) fall at the upper (less negative) end of the model range (-0.92 to -0.38 PgC yr⁻¹), and in the pCO₂-product flux median (-0.44 PgC yr⁻¹) is about two thirds of the model median (-0.72 PgC yr⁻¹). Most of this model-product mismatch can be attributed to differences in ocean pCO₂ seasonality at mid- and high-latitudes (poleward of 25N and 25S), which tend to reinforce the north-

ern hemisphere winter uptake in models compared to $p\text{CO}_2$ -products (see details in section 3.2.2). These differences in $p\text{CO}_2$ seasonality are likely to be further amplified by differences in wind speed and gas exchange coefficient formulation (see Methods and Table 1-3). For instance, the net CO_2 uptake in the Coastal-SOM-FFN product increases by about 50% and falls closer to the model median when changing the wind speed product (from ERA5 to JRA55) and gas exchange coefficient formulation (from Ho et al., 2011 to Wanninkhof 1992) used to compute the flux (from $-0.44 \text{ PgC yr}^{-1}$ in Coastal-SOM-FFN to $-0.65 \text{ PgC yr}^{-1}$ in Coastal-SOM-FFN- k_w , blue dot vs. blue circle in Figure 2a, see further details in section 3.2.2).

Another factor that can explain part of the model-product discrepancy is the absence of land-sea carbon and nutrient inputs in many of the global ocean biogeochemical models (see Table 2). The missing land-sea carbon inputs and associated CO_2 outgassing would result in a stronger CO_2 uptake at the scale of the global ocean but the proportion of this land-driven CO_2 outgassing occurring in the coastal ocean, and therefore the bias introduced here in our model-based estimates, is very poorly constrained. Open-ocean RECCAP2 chapters used a model-based estimate of the spatial distribution of this land-driven CO_2 outgassing (Lacroix et al., 2020) scaled up to match an independent bottom up constraint on its global magnitude ($0.65 \pm 0.3 \text{ PgC/yr}$ Regnier et al., 2022). This combined estimate suggests that the missing land-driven outgassing could amount to 0.12 PgC yr^{-1} in the wide coastal ocean, potentially explaining part of the gap between $p\text{CO}_2$ -products and model median, despite the large unconstrained uncertainty of this estimate. In contrast, the missing land-sea nutrient inputs could reduce the biologically-driven uptake of CO_2 in coastal waters and potentially offset the bias tied to the lack of land-sea carbon inputs (Gao et al., 2023). However, we find no clear relationship between the strength of the simulated net coastal CO_2 uptake and the presence or absence of land-sea inputs in the global ocean biogeochemical models used here (i.e., models with weaker coastal CO_2 uptake more in line with $p\text{CO}_2$ -products are not systematically the ones with land-sea inputs), suggesting that land-driven inputs are likely not the main factor in this discrepancy. In addition, we note that using the subset of four global models with higher horizontal resolution (CNRM-HR, FESOM-HR, MOM6, MRI-ESM2.1 with nominal resolution of 0.5 degree or higher), which are likely to better capture coastal dynamics, yields a slightly weaker net CO_2 uptake (median of $-0.65 \text{ PgC yr}^{-1}$ for only four models vs. $-0.72 \text{ PgC yr}^{-1}$ for all global models), slightly closer to the $p\text{CO}_2$ -products median ($-0.44 \text{ PgC yr}^{-1}$) and in relatively good agreement with one of the $p\text{CO}_2$ -products ($-0.59 \text{ PgC yr}^{-1}$ in CMEMS*, Figure 2a).

We can compare the net CO_2 flux estimates presented here to prior work using the narrower definition of the coastal ocean ending at the shelf break (28 million km^2), a domain more aligned with the definition used in past studies (Supplementary Table S2). For this comparison we include all $p\text{CO}_2$ -products, but use only the subset of four global models with higher horizontal resolution. We find that the narrow coastal ocean accounts for about half of the wide coastal ocean CO_2 uptake (-0.22 out of $-0.44 \text{ PgC yr}^{-1}$ for the 4- $p\text{CO}_2$ -product median and $-0.34 \text{ PgC yr}^{-1}$ out of the $-0.65 \text{ PgC yr}^{-1}$ for the 4-model median), while only accounting for about a third of the surface area. The $p\text{CO}_2$ -product median in the narrow coastal ocean ($-0.22 \text{ PgC yr}^{-1}$) is consistent with the most recent observation-based estimates (Roobaert et al., 2019; Dai et al., 2022; Regnier et al., 2022), but the four $p\text{CO}_2$ -products span a relatively large range with differences of the order of a factor 2 ($-0.12 \text{ PgC yr}^{-1}$ in Carboscope-1 and $-0.31 \text{ PgC yr}^{-1}$ in CMEMS*, see Table S2 for estimates). The 4-model median simulates a slightly stronger sink ($-0.34 \text{ PgC yr}^{-1}$) than these most recent estimates (although it is similar to the estimate of Regnier et al., 2022) but again differences in $p\text{CO}_2$ seasonality, and potentially in wind speed and gas exchange formulation could explain part of this discrepancy. Similarly to the wide coastal ocean, the net CO_2 sink increases by nearly 50% in the narrow coastal ocean from Coastal-SOM-FFN to Coastal-SOM-FFN- k_w (from -0.21 to $-0.31 \text{ PgC yr}^{-1}$, blue dot vs. circle, Figure 2a).

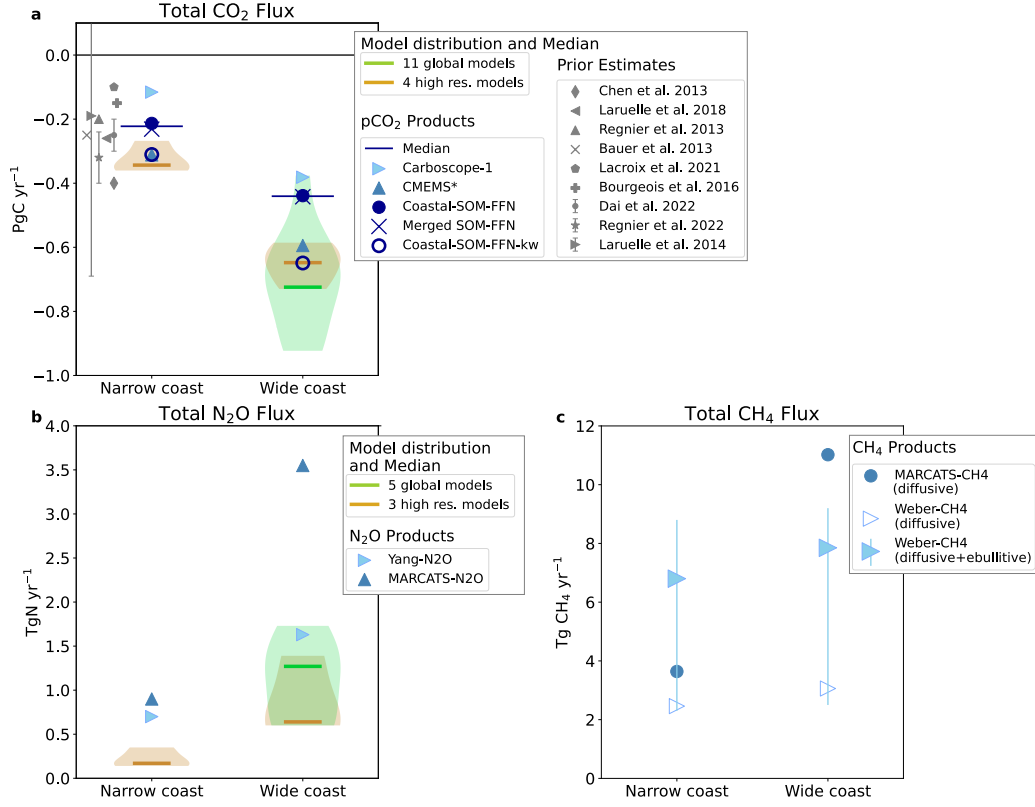


Figure 2. Net globally-integrated coastal fluxes of a) CO₂ [PgC yr⁻¹], b) N₂O [Tg N yr⁻¹] and c) CH₄ [Tg CH₄ yr⁻¹] over the narrow and wide coastal oceans. The model distribution (violin) and median (thick lines) are shown for the full ensemble available in the wide coastal ocean (11 models for CO₂ and 4 for N₂O) and a subset of higher resolution models for the narrow coastal ocean (4 models for CO₂ and 2 for N₂O, see Methods and Table 2 for details). Symbols indicate observation-based products (blue) and previous estimates available for the narrow coastal ocean (grey in panel a, listed in Supplementary Table S2). Coastal-SOM-FFN-k_w, which is a second version of Coastal-SOM-FFN computed using different wind speed and k_w formulation (empty circle, see Methods) is not used in the calculation of the pCO₂-product median. Weber-CH₄ total flux (diffusive+ebullitive) and diffusive contribution (comparable to MARCATS-CH₄ flux) are shown in panel c.

3.1.2 Net N_2O and CH_4 coastal emissions

Estimates of the global coastal emissions of N_2O range from 0.14 to 0.90 Tg N yr⁻¹ in the narrow coastal ocean and from 0.60 to 3.56 Tg N yr⁻¹ in the wide coastal ocean (Figure 2 b). Part of this considerable variability comes from differences between model-based and observation-based estimates, but also from systematic differences between the two observation-based products (MARCATS- N_2O and Yang- N_2O). In the wide coastal ocean, the Yang- N_2O estimate (1.63 Tg N yr⁻¹) falls at the high end of the model estimates (0.60 to 1.73 Tg N yr⁻¹), while MARCATS- N_2O yields N_2O emissions that are more than twice the emissions of Yang- N_2O (3.56 Tg N yr⁻¹, Figure 2 b). This finding implies that global ocean biogeochemical models emission estimates are overall lower than those of the observation-based products. Furthermore, the subset of 3 high-resolution models generally simulate N_2O emissions that are lower than the full set of 5 models and therefore lower than both observation-based estimates (3-model median of 0.64 Tg N yr⁻¹ vs. 5-model median of 1.27 Tg N yr⁻¹ for the wide coastal ocean, Figure 2 b).

In the narrow coastal ocean, the two observation-based estimates are in relatively good agreement (0.90 Tg N yr⁻¹ in MARCATS- N_2O and 0.70 Tg N yr⁻¹ in Yang- N_2O), while the subset of 3 high resolution global ocean models simulate emissions that are again about 2-4 times lower (0.14 to 0.35 Tg N yr⁻¹). The Yang- N_2O product suggests that the narrow coastal ocean accounts for about 50% of the emissions of the wide coastal ocean, while in the subset of 3 global ocean models and MARCATS- N_2O it only accounts for about 25% (Figure 2b). We note, however, that the particularly low model values in both the 5-model ensemble and the 3-model high resolution subset are from ECCO-Darwin and ECCO2-Darwin (0.60-0.64 Tg N yr⁻¹ in the wide and 0.14-0.17 Tg N yr⁻¹ in the narrow coastal ocean) which are based on the same model and are therefore not independent. The fact that global ocean biogeochemical models underestimate coastal N_2O fluxes, in particular nearshore, is likely due to unresolved (e.g. complex microbial production/consumption, sedimentary processes, production in estuarine and coastal vegetation systems transported to the coastal ocean) or spatially under-resolved processes (e.g. high production and remineralization in shallow shelves, and shallow coastal oxygen minimum zones where N_2O emissions take place). Another potential source of bias might be the undersampling of coastal waters in the observations (see Table S1). In particular, observations might be biased high because they are often performed in hotspots of emissions rather than in regions that reflect the mean conditions.

Global CH_4 emissions in Weber- CH_4 include both the diffusive and ebullitive (bubbling) components, and are estimated to be 6.80 [2.30-8.8] Tg CH_4 yr⁻¹ for the narrow coastal ocean and 7.85 [2.50-9.20] Tg CH_4 yr⁻¹ for the wide coastal ocean (Figure 2c). Note that the flux estimates presented here are observation-based only because no model-based estimates are available. The CH_4 flux from Weber- CH_4 is dominated by the ebullitive flux which occurs mostly in shallow waters of the narrow coastal ocean (accounting for 4.33 Tg CH_4 yr⁻¹ in the narrow and 4.79 Tg CH_4 yr⁻¹ in the wide coastal ocean). Subtracting the ebullitive flux from the total Weber- CH_4 fluxes results in a CH_4 diffusive flux of 2.46 [1.23-3.69] Tg CH_4 yr⁻¹ in the narrow coastal ocean, which is in relatively good agreement with the diffusive flux estimated from MARCATS- CH_4 (3.64 Tg CH_4 yr⁻¹). In contrast, the diffusive flux of 3.06 [1.53, 4.59] Tg CH_4 yr⁻¹ obtained in the wide coastal ocean in Weber- CH_4 has a central value ~3.5 times smaller than the diffusive flux of MARCATS- CH_4 (11.02 Tg CH_4 yr⁻¹).

The observation-based estimates of the N_2O emissions and the diffusive flux of CH_4 vary by about 20-30% in the narrow coastal ocean and by about a factor 2 to 3.5 in the wide coastal ocean. The increase in the spread amongst these observational products (which use the same datasets and are therefore not independent) reflects the low number of oceanic N_2O and CH_4 measurements to date, in particular in many coastal regions, as compared to CO_2 . Specifically, the observation density decreases by about a factor 3 from narrow to wide (number of observations per million km² three times lower in the wide coastal

ocean in more than 30 of the 45 regions used for the interpolation, see Table S1). Significant differences between the observation-based estimates (MARCATS-N₂O, MARCATS-CH₄ on the one hand, and Yang-N₂O and Weber-CH₄ on the other hand) can result from (i) applying different approaches for estimating the air-sea gas exchange in combination with using different wind speed products (e.g., Garbe et al., 2014) and (ii) applying different inter- and extrapolation techniques which can introduce significant uncertainties when applied to sparse data. The increase in discrepancy from narrow to wide coastal waters suggests that MARCATS-N₂O and MARCATS-CH₄ may extrapolate local observations over spatial domains where they are not representative anymore. In contrast, the neural networks of Yang-N₂O and Weber-CH₄, albeit also relying on the same MEMENTO dataset, may better capture spatial patterns, such as the overall decrease in CH₄ emissions as the shelf water depth increases.

3.1.3 Combined coastal greenhouse gas emissions

We combined CO₂, N₂O and CH₄ fluxes from observation-based and model-based estimates for the wide coastal ocean using CO₂-equivalent (Figure 3). We find that from a net radiative perspective, N₂O and CH₄ coastal emissions offset much of the coastal CO₂ sink, by ~58% in the product-based budget and ~30% in the model-based budget. As a result, the net greenhouse gas flux into the coastal ocean is -0.66 PgCO₂-e yr⁻¹ in the product-based budget (-1.58 PgCO₂-e yr⁻¹ CO₂ flux offset by +0.70 and +0.21 PgCO₂-e yr⁻¹ of N₂O and CH₄) and -1.81 PgCO₂-e yr⁻¹ in the model-based budget (-2.57 PgCO₂-e yr⁻¹ CO₂ flux offset by +0.54 and +0.21 PgCO₂-e yr⁻¹ of N₂O and CH₄, Figure 3). Most of the difference between the product- and model-based budgets presented here come from the stronger CO₂ uptake in the models mentioned above. There are, however, very few global coastal N₂O and CH₄ estimates and the spread amongst the products and models is large (1 to 2 PgCO₂-e yr⁻¹), indicating that the compensation of the coastal carbon sink could be substantially different from the 30-58% found here.

3.2 Coastal CO₂ dynamics

3.2.1 Contrast between coastal ocean and open ocean

When averaged globally, models and pCO₂-products show lower mean surface ocean pCO₂ and lower CO₂ flux densities (i.e. more uptake) in narrow and wide coastal oceans than in the open ocean (Figure 4). As shown previously for the coastal-SOM-FFN product (Roobaert et al., 2019), this coastal to open ocean difference is however attributable to the increasing contribution of polar waters, characterized by lower flux densities and stronger sinks, to the total surface area from open ocean to narrow coastal domains (polar coastal waters account for 29% of the narrow coastal ocean, 17% of the wide coastal ocean and 2% of open ocean waters, contributions calculated as the percentage of ice-free surface area located poleward of 50 degrees based on NOAA's OISST ice product, Figure 1). This apparent gradient is found in the median of the four pCO₂ products, which shows an increase in global mean sea surface pCO₂ from the narrow coastal ocean to the wide coastal ocean (+ 15 μ atm from 350 to 365 μ atm) and from wide coastal ocean to the open ocean (+7 μ atm from 365 to 372 μ atm for the 1998-2018 period, Figure 4a). The only pCO₂-product among the four that does not capture this coastal to open-ocean difference is Carboscope-1, likely because of potential biases in the Arctic Ocean (pCO₂ values generally higher in Carboscope-1 than in other pCO₂-products and models). The 11-model median simulates slightly higher ocean pCO₂ than the product median but also captures an increase in global mean pCO₂ from wide coastal ocean to open ocean (+6 μ atm from 369 to 375 μ atm) similar to the pCO₂-products. Using the subset of four higher resolution models in the narrow coastal ocean corroborates the presence of this difference in simulated ocean pCO₂. The 4-model median shows a consistently lower mean pCO₂ in the narrow coastal ocean (363 μ atm), compared to the wide coastal ocean (370 μ atm) and to the open ocean (373 μ atm). Thus, although observation-based and mod-

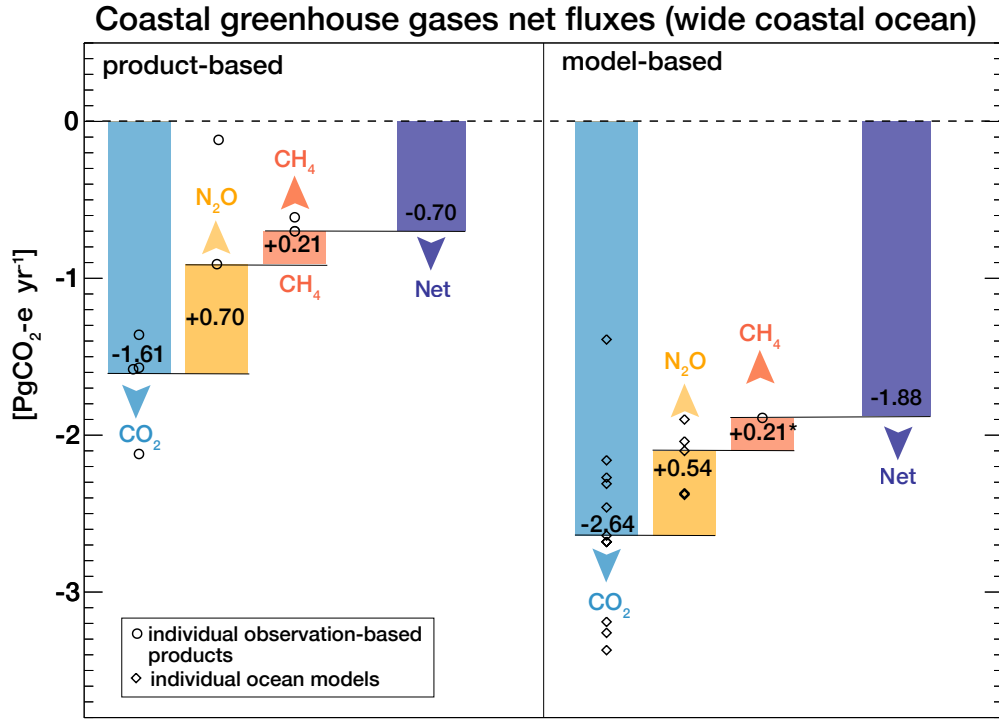


Figure 3. Greenhouse gas air-sea flux in the wide coastal ocean and influence on net atmospheric radiative balance (using $\text{PgCO}_2\text{-e yr}^{-1}$) based on observational products and models of CO_2 , N_2O and CH_4 fluxes. Observations-based central values are from 4 pCO_2 -products, Yang- N_2O and Weber- CH_4 . Model-based central values are from the 11 global models for CO_2 , 4 global models for N_2O , but the Weber- CH_4 product is used for CH_4 as indicated by the asterisk (no model available for CH_4 , hence minimizing the difference between the two assessments). Individual models and observation-based product estimates are shown by symbols. The net GHG flux in $\text{PgCO}_2\text{-e yr}^{-1}$ corresponds to the sum of the three gasses' contributions.

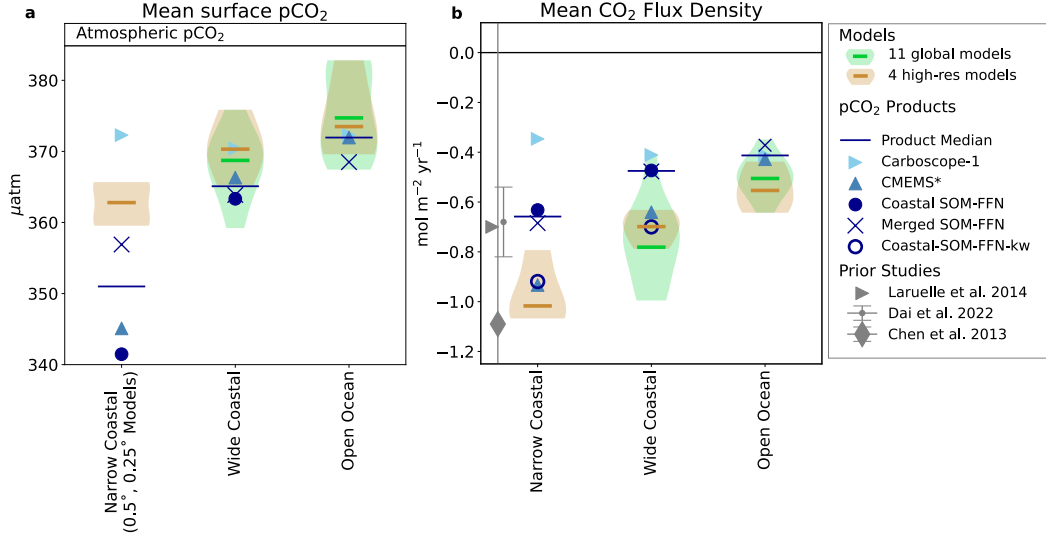


Figure 4. Comparison of globally-averaged coastal ocean and open ocean: a) sea surface pCO₂ [μatm] and b) flux density [mol C m² yr⁻¹] averaged over narrow coastal ocean, wide coastal ocean and open ocean waters in pCO₂-products and ocean models. The model distribution (violin) and median (thick lines) are shown for the full ensemble available in the wide coastal ocean (11 global models in green) and a subset of higher resolution models for the narrow coastal ocean (4 global models in tan, see Methods and Table 2 for details). Symbols indicate global pCO₂-based products (blue), previous estimates (in grey, see Supplementary Table S2 for details). Coastal-SOM-FFN-k_w, which is a second version of Coastal-SOM-FFN computed using different wind speed and k_w formulation (empty circle, see Methods) is not used in the pCO₂-product median.

eled pCO₂ values show discrepancies in the mean within each domain, the narrow coastal to open ocean differences derived from observations and models are in remarkable agreement, and amount to about 10-15 μatm. A consequence of these differences in sea surface pCO₂ is that the mean partial pressure difference with the atmosphere (mean pCO_{2a} of 385 μatm for 1998-2018) is higher in the coastal ocean than in the open ocean. As a result, air-sea CO₂ flux densities are lower (stronger uptake) in the narrow coastal ocean (-1.02 and -0.66 mol m² yr⁻¹ for 4-model and 4-product medians) than in open ocean waters (-0.55 and -0.41 mol m² yr⁻¹ for 4-model and 4-product medians, Figure 4b). In between, the wide coastal ocean shares characteristics of narrow coastal ocean and open ocean waters and is characterized by intermediate CO₂ flux densities (-0.70 and -0.48 mol m² yr⁻¹ for 4-model and 4-product medians, Figure 4b).

3.2.2 Spatial and seasonal variability in coastal CO₂ sources and sinks

Coastal air-sea CO₂ flux densities are characterized by latitudinal gradients captured by both pCO₂-products and models (Figure 5). Mid- and high-latitude regions (poleward of 25° of latitude) are characterized by annual mean surface ocean pCO₂ lower than the atmosphere (pCO_{2a}=385 ppm for 1998-2018) and thus by oceanic CO₂ uptake, whereas tropical coastal oceans (equatorward of 25° of latitude) are generally associated with pCO₂ similar or slightly higher than the atmospheric level and weak or near-zero CO₂ outgassing (Figure 5 and S4). When averaged latitudinally over the wide coastal ocean, models and products follow a similar pattern, with most negative flux densities (<-1 mol m² yr⁻¹,

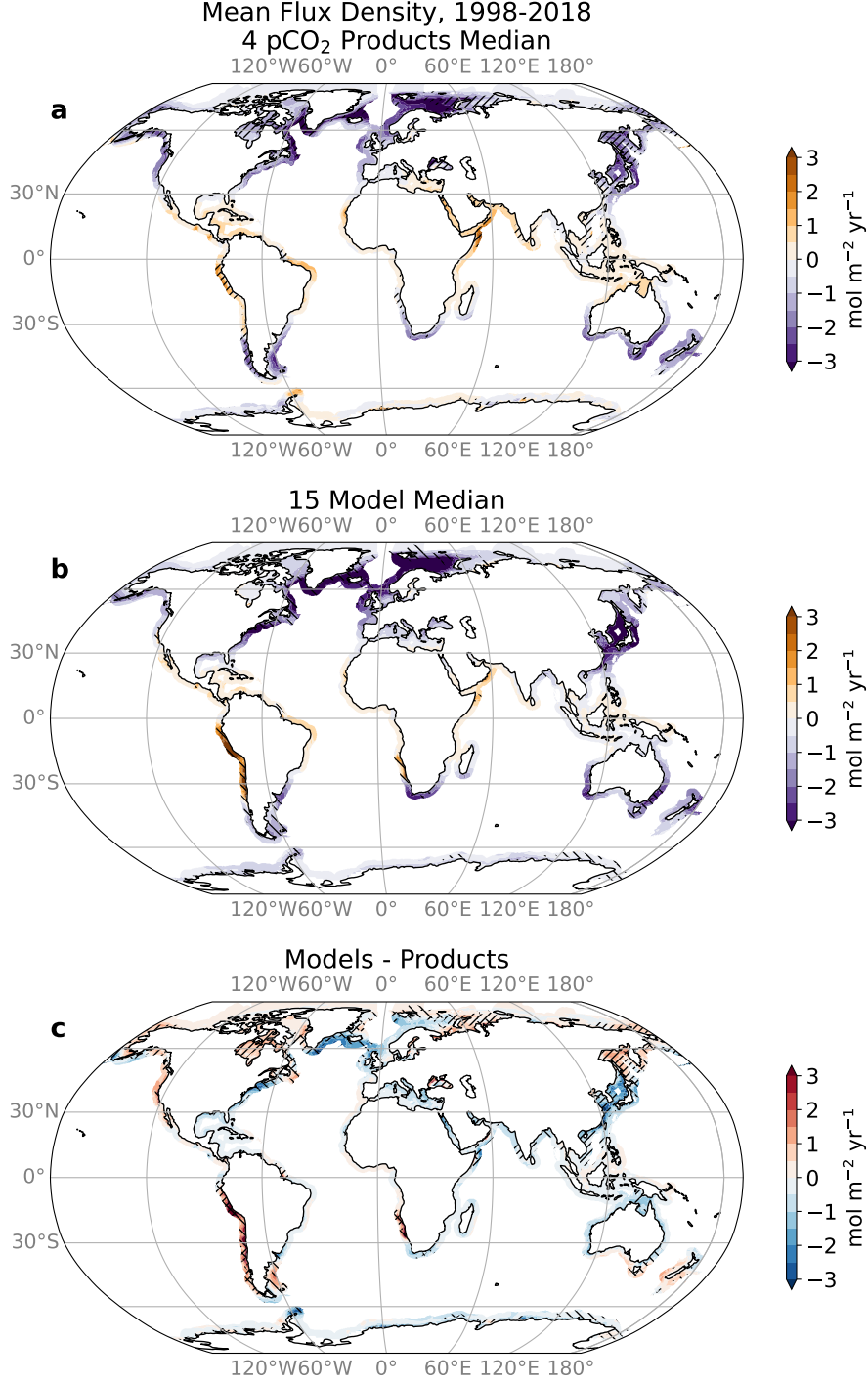


Figure 5. Annual-mean CO₂ flux density [$\text{mol C m}^{-2} \text{ yr}^{-1}$] in the wide coastal ocean for a) the median across the 4 pCO₂-products, b) the median across the 15 models, and c) the difference between model and pCO₂-product medians. The model-median is calculated using the 11 global models and the 4 regional models where available. Hatching indicates the coastal area with root mean square difference (RMSD) greater than 0.60 $\text{mol C m}^{-2} \text{ yr}^{-1}$ across pCO₂ products (panels a and c) or 0.95 $\text{mol C m}^{-2} \text{ yr}^{-1}$ across models (panels b and c) (in both cases the RMSD values correspond to the 20% of coastal area with highest RMSD).

i.e. strongest sinks) at mid-latitudes in both hemispheres (50°S-25°S and 25°N-50°N) and high latitudes in the northern hemisphere (50°N-80°N), and weak sources in the tropical band (typically between 0 and 0.5 mol m² yr⁻¹ in 25°S-25°N, Figure 6a). Largest departures between pCO₂-products and models are found in the northern mid- and high latitudes, where the model median flux densities are often more negative (stronger sink) than the pCO₂-product median (down to -4 mol m² yr⁻¹ in models vs. -2 mol m² yr⁻¹ in pCO₂-products, Figure 6a). These systematically more negative flux densities in the models extend over large coastal areas of the northern hemisphere, including the shelves of western boundary currents (Gulf Stream and Kuroshio), the Norwegian Sea and the southern Greenland basin (blue colors in Figure 5 c), and therefore largely explain the stronger globally integrated coastal sink found in the model median (Fig 2 a). These northern hemisphere regions are relatively well sampled by the SOCAT pCO₂ database (Fig S1), suggesting that the model-product difference might be largely attributable to model biases. Models and pCO₂-products also differ on Antarctic shelves, in particular around the Antarctic Peninsula (around 60°S which is also relatively well sampled compared to the rest of the coastal ocean) where models simulate a weak sink (about -1 mol m² yr⁻¹) but pCO₂-products show a weak source (about +1 mol m² yr⁻¹, Figure 5 and Figure 6a). On the Antarctic shelves, however, the model-product mismatch in CO₂ flux density is confined to a relatively small surface area and the impact on the net global flux is smaller compared to the mismatch found in the northern extratropics. We note that the model median yields less negative or more positive flux densities (i.e. weaker sinks or stronger sources) in some coastal regions, such as the California Current, Peruvian margin, Sea of Okhotsk or Hudson Bay (red colors in Figure 5 c), which offsets part of the stronger sinks simulated in northern and southern extratropical latitudes in the latitudinal mean and global integral.

The global coastal ocean is a sink of CO₂ in all seasons, and pCO₂-products and global ocean biogeochemical models largely agree on the latitudinal patterns in seasonality (Figure 6c-f). Yet, model-product differences emerge in the phasing and amplitude of the seasonality, in particular north of 25°N (Figure 6c-f). In the pCO₂-products, the seasonal amplitude of the air-sea CO₂ flux is similar in both hemispheres and shows a strong latitudinal contrast between: i) the tropics (25°S-25°N), where the seasonal amplitude is small (absolute values <1 mol m² yr⁻¹) and the weak CO₂ source becomes even smaller in winter; ii) the mid-latitudes (50°S-25°S and 25°N-50°N), where the seasonal amplitude is relatively large (absolute values of 1-2.5 mol m² yr⁻¹) and the sink is stronger in winter and spring; and iii) high-latitudes (poleward of 50°N and 50°S), where the seasonal amplitude is also large (similar to mid-latitudes) but the CO₂ sink is stronger in summer (except in the Arctic, north of 80 degree N, where the seasonal amplitude is small, Figure 6b-f). In contrast, the CO₂ sink in the model median is systematically stronger in winter than in summer at all latitudes (except around Antarctica) and does not reproduce the latitudinal change in seasonal phasing obtained in the pCO₂-products (from stronger winter uptake in the tropics to stronger summer uptake at high-latitudes, Figure 6b). In addition, the seasonal amplitude of the CO₂ flux is 50-100% larger in the models at mid-latitudes (despite having a similar phasing, i.e. stronger sink in winter and spring, Figure 6b). As a result of these latitudinal differences in phasing, the products show little seasonality when averaged globally across coastal waters (net median flux of -0.35 PgC yr⁻¹ for DJF vs. -0.32 PgC yr⁻¹ for JJA, Figure 7a). This is largely explained by compensations between mid-latitudes (stronger uptake in winter) and high-latitudes (strong uptake in summer) within each hemisphere (Fig 6), which results in a relatively weak seasonality in both the northern (-0.24 in DJF and -0.22 in JJA) and southern (-0.11 PgC yr⁻¹ in DJF and -0.10 PgC yr⁻¹ in JJA) hemispheres (Figure 7b-c). In the case of the 11-model median, however, this compensation is much weaker and the seasonal cycle is stronger, especially in the northern hemisphere (-0.73 in DJF and 0.00 PgC yr⁻¹ in JJA, Figure 7b-c). As a result, the global coastal ocean in the model median displays a marked seasonality controlled by the seasonality of the northern hemisphere, resulting in a net global coastal sink for DJF (-1.15 PgC yr⁻¹) that is about four times

the sink for JJA ($-0.29 \text{ PgC yr}^{-1}$, Figure 7). This model-product difference in CO_2 flux seasonality and specifically the extremely large boreal winter uptake explains the stronger annual mean global CO_2 sink found in the model median compared to the pCO_2 -products (Figures 2 a, 6 a and 7b).

Model-product differences in CO_2 flux seasonality are largely tied to differences in the surface ocean pCO_2 . The stronger flux seasonality at mid-latitudes in models and the opposed flux seasonality at high latitudes (i.e., stronger uptake in winter in models vs. stronger uptake in summer in products) are both explained by the higher summer ocean pCO_2 (leading to weaker summer uptake) and the lower winter ocean pCO_2 (leading to stronger winter uptake) found in the model median compared to the pCO_2 -product median (Supplementary Figure S5). Differences in ocean pCO_2 can be amplified by the choice of wind speed and gas exchange coefficient formulation. The comparison of the two Coastal-SOM-FFN versions reveals that both the high-latitude summer uptake and the mid-latitude winter uptake are enhanced in Coastal-SOM-FFN- k_w compared to Coastal-SOM-FFN (Figure 7 and S6). This enhancement occurs in both hemispheres but the impact of the northern hemisphere on the global coastal annual mean uptake is larger due to the larger coastal surface area. Despite these systematic differences found between the model median and pCO_2 -product median in the annual mean and seasonal flux, some models reproduce better the latitudinal pattern expected from the pCO_2 -products, in particular the stronger summer uptake at high-latitude in the northern hemisphere (e.g., MOM6-Princeton and MPIOM-HAMOCC, see individual models in Figure S7 and thin green lines overlapping with thin blue lines in Figure 6). We note that this systematic model/product difference in seasonality is also found in the open ocean but that the amplitude of this mismatch is amplified in the coastal ocean (see Figures S7 and S8).

3.2.3 Trends in coastal ocean pCO_2 and air-sea CO_2 flux

For the 1998–2018 period, global coastal pCO_2 trends are slightly weaker than the atmospheric pCO_2 trend ($+20.7 \mu\text{atm/decade}$) in the two time-varying pCO_2 -products (about $+17\text{--}18 \mu\text{atm/decade}$ in the wide coastal ocean) and models ($+17\text{--}20 \mu\text{atm/decade}$ in the wide coastal ocean; see Figure 8a,c). In the narrow coastal ocean, the pCO_2 trends from the pCO_2 -products are lower than in the wide coastal ocean, and fall halfway between the two central values published in previous observation-based estimates ($+16\text{--}17 \mu\text{atm/decade}$ vs. $+19.3 \mu\text{atm/decade}$ in Wang et al., 2017 and $+13 \mu\text{atm/decade}$ in Laruelle et al., 2018). In contrast, the pCO_2 trends found in the subset of four high resolution ocean biogeochemical models are higher in the narrow coastal ocean ($+19.8 \mu\text{atm/decade}$) than in the wide coastal ocean, and in good agreement with the highest of the previous observation-based estimate (Wang et al., 2017).

The trend difference between atmospheric and oceanic pCO_2 leads to an increase in the coastal carbon sink from 1998 to 2018 in pCO_2 -products and models (flux density trends between -0.15 and $-0.04 \text{ mol m}^{-2} \text{ yr}^{-1}$ per decade in the wide coastal ocean, Figure 8b,d). Yet, because the rate of increase in coastal pCO_2 is lower in the pCO_2 -products than in the models, their respective CO_2 uptake trend is larger (Figure 8c). This is consistent with the expectation that a slower increase in sea surface pCO_2 , which does not closely follow the atmospheric pCO_2 trend, should result in a stronger increase of the flux density (e.g., Laruelle et al., 2018). Our results show, however, that pCO_2 trends and flux trends are not directly proportional, suggesting that factors other than pCO_2 variability are at play. These include trends in sea-ice cover (e.g., sea-ice retreat influence on flux trends in the Arctic Ocean) and/or in surface winds (via their effect on the gas exchange transfer velocity). For instance, the Carboscope-1 pCO_2 trends are slightly weaker than the CMEMS* pCO_2 trends in the narrow and wide coastal oceans, and yet the increase in the coastal sink is lower in Carboscope-1 than in CMEMS* (Figure 8c,d). In addition, observation-based CO_2 flux estimation shows that the largest coastal CO_2 sink region in the Arctic Ocean, the Chukchi Sea, is increasing due to increased ice-free

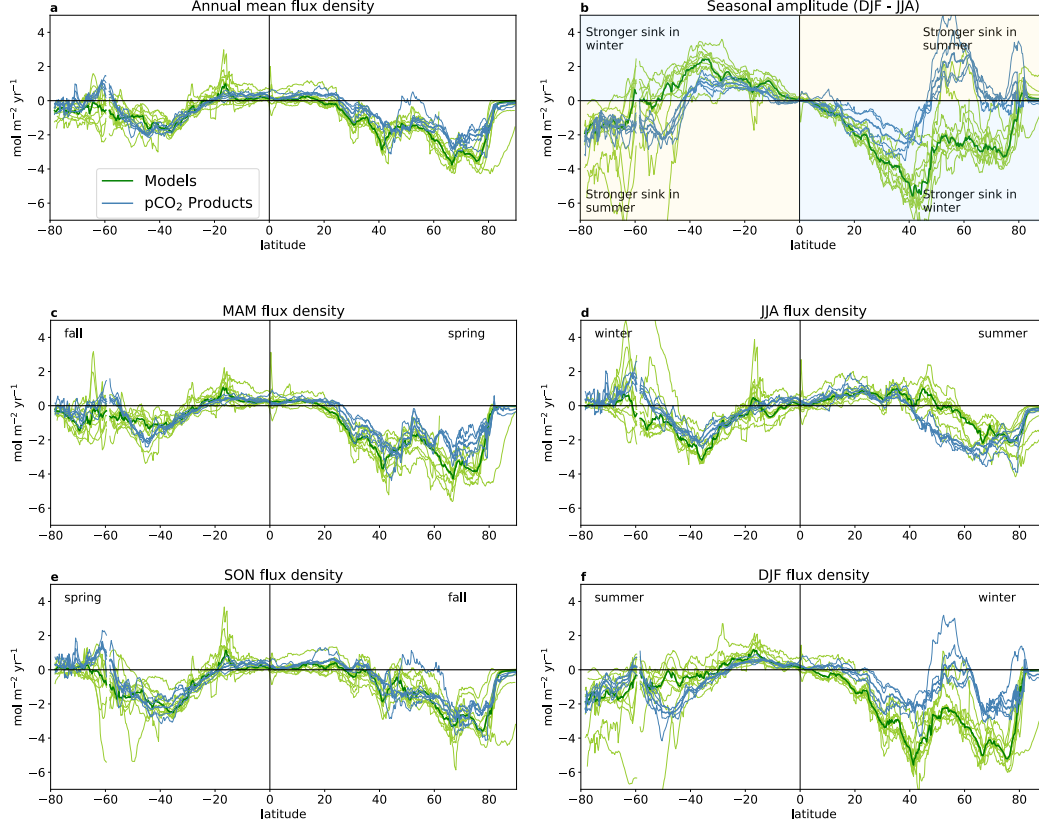


Figure 6. Latitudinal distribution of coastal ocean CO₂ flux and seasonal amplitude (using the wide coastal ocean). Latitudinal distribution of a) annual mean flux density, b) seasonal flux density amplitude, calculated as December-February (DJF) minus June-August (JJA), the blue (orange) quadrants indicate when the ocean uptake is stronger in winter (summer). c-f) seasonal mean flux density for March-May (MAM), JJA, September-November (SON) and DJF. Product and model medians are shown with thick lines and the individual 11 global models and 4 products with thin lines. Units are in mol C m⁻² yr⁻¹ in all panels for consistency, converting from per month to per year also for the 3-month periods.

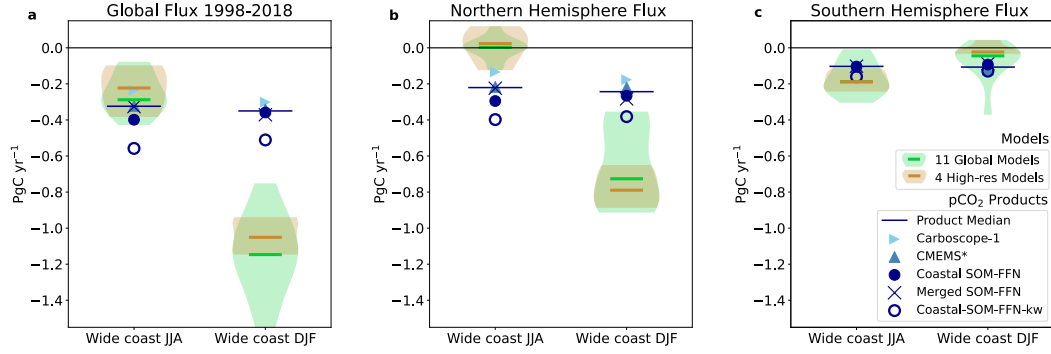


Figure 7. Net air-sea CO_2 flux in June-August (JJA) and December-February (DJF) for a) the global coastal ocean, b-c) the northern and southern hemispheres. The model distribution (violin) and median (thick lines) are shown for the full ensemble available (11 global models in green) and a subset of higher resolution models (4 global models in tan, see Methods and Table 2 for details). Symbols indicate global pCO_2 -based products (blue), prior estimates (grey, see Supplementary Table S2 for details). Coastal-SOM-FFN- k_w , which is a second version of Coastal-SOM-FFN computed using different wind speed and k_w formulation (empty circle, see Methods) is not used in the pCO_2 -product median. Units are in PgC yr^{-1} in all panels for consistency, using a 12-month scale up value for the 3-month periods.

area, longer sea-ice free period, and increased biological production rate (which keeps sea surface pCO_2 increase rate nearly zero) (Ouyang, Collins, et al., 2022). Another example of the decoupling between pCO_2 trends and flux trends is found in the coastal to open ocean difference. The global ocean biogeochemical model ensemble simulates smaller differences between atmospheric and oceanic pCO_2 trends in the coastal ocean than in the open ocean, resulting in a weaker increase in the carbon sink in the coastal ocean (following here the expected link between pCO_2 and flux trends, Figure 8c-d). In contrast to the models, both time-resolving pCO_2 -products reveal higher differences between atmospheric and oceanic pCO_2 trends in the coastal ocean than in the open ocean (Figure 8c), which would suggest a stronger trend in the flux density in the coastal ocean (i.e. a stronger increase in the uptake). However, this expected increase in the uptake is only found in CMEMS* but not in Carbscope-1 (Figure 8d). A precise understanding of the trends in all parameters that control the air-sea fluxes of CO_2 and of the methodological differences in the pCO_2 mapping and flux calculation is crucial to understanding the evolving coastal ocean carbon sink.

Inconsistencies between pCO_2 trends and flux trends arise from the complex and uncertain interplay between the spatio-temporal changes in ocean pCO_2 , wind speed and sea-ice coverage. In particular, trends in ocean pCO_2 and therefore in ΔpCO_2 (difference between coastal ocean surface ocean pCO_2 and atmospheric pCO_2) strongly differ between coastal regions, as well as between the two time-varying pCO_2 -products (Figure S9). CMEMS*, as well as the multi-model median, show more negative ΔpCO_2 trends (potentially stronger uptake or weaker sources with time) in mid-to-high latitudes, but less negative or even positive ΔpCO_2 trends in the tropics and in the Arctic (Figure S10). In contrast, the Carbscope-1 product shows strongly negative ΔpCO_2 trends in the Arctic, and much larger variability in trends at other latitudes. These differences in ΔpCO_2 trends largely translate into consistent flux density trends (negative ΔpCO_2 trends generally yield negative flux trends, i.e., stronger uptake or weaker sources with time, Figures 9 and S10). However we note that in many regions, the ΔpCO_2 trends are amplified or dampened by trends in wind speed and sea-ice coverage, which are also strongly

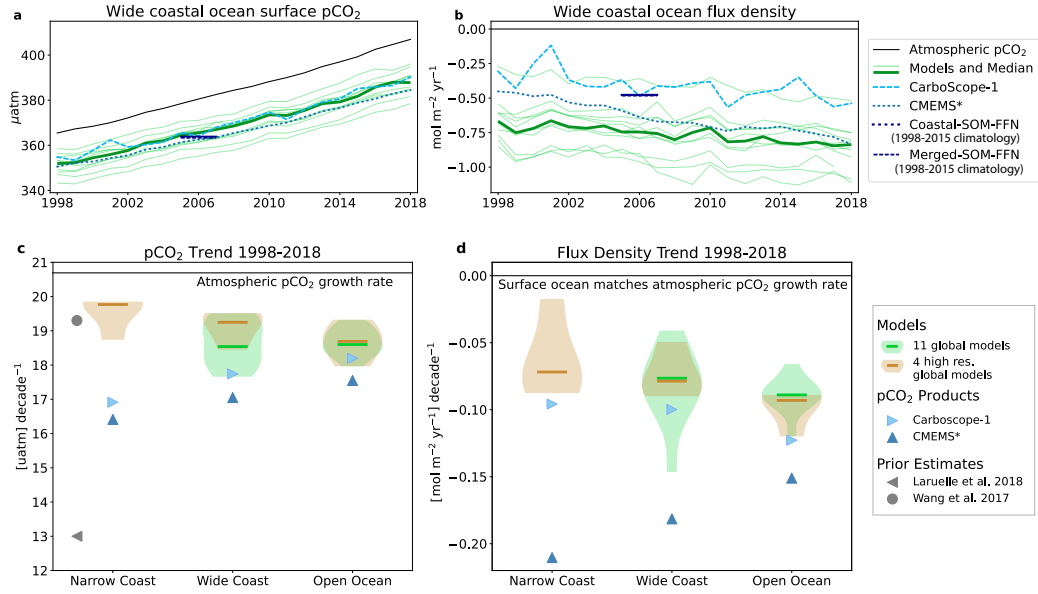


Figure 8. Temporal evolution of the global annual mean a) surface ocean pCO₂ [µatm] and b) net air-sea CO₂ flux density [mol C m⁻² yr⁻¹] in the four pCO₂-products (blue lines) and the 11 global ocean models (thin green lines) and model median (thick green lines) in the wide coastal ocean. Trends in c) ocean surface pCO₂ [µatm decade⁻¹] and d) flux density [mol C m⁻² yr⁻¹] for narrow coastal ocean, wide coastal ocean and open ocean waters. The model distribution (violin) and median (thick lines) are shown for the full model ensemble (11 global models in green) and a subset of higher resolution models (4 global models in tan, see Methods and Table 2 for details). Symbols show the trends for the two time-varying pCO₂-based products (Carboscope-1 and CMEMS* in blue) and prior estimates (in grey, see Table S1 for details).

spatially heterogeneous (see sea-ice trends in Figure S11). This effect is highlighted by the spatial differences and sometimes even a switch in sign between $\Delta p\text{CO}_2$ trends and air-sea CO₂ flux trends in the model median in sea-ice regions (hatching in Figure 9). This is true, for instance, in the Arctic where the ocean models tend to simulate an increase in ocean CO₂ uptake despite a positive trend in $\Delta p\text{CO}_2$ (i.e., ocean pCO₂ increases at a high rate than atmospheric pCO₂ which would reduce ocean uptake with constant sea-ice coverage and winds, Figures 9 and S10). This decoupling between CO₂ flux and $\Delta p\text{CO}_2$ in the Arctic is indeed associated with a decrease in sea ice coverage in most models (Figure S11) and an increase in wind speed in two of the wind products that are widely used in these models (JRA-55 and ERA-5, Figure S12 and Tables 2-3), both effects inducing an increase in the flux with time despite the reduction in $\Delta p\text{CO}_2$. These results clearly indicate that the global coastal sink is increasing. Yet, the magnitude of this increase, its spatial patterns and how it compares to the open ocean are still uncertain.

3.3 Coastal nitrous oxide and methane spatial variability

The spatial distribution of the coastal N₂O fluxes computed with the observation-based (i.e., Yang-N₂O) and a mean of the model-based approaches are shown in Figure 10. Coastal N₂O fluxes are generally positive, indicating that coastal areas are a source of atmospheric N₂O. Flux densities vary considerably, from 0 (= equilibrium with the atmosphere) to about 10 g N m⁻² yr⁻¹. The results from Yang-N₂O reveal hotspots of N₂O emissions in eastern boundary upwelling systems, the upwelling areas of the north-

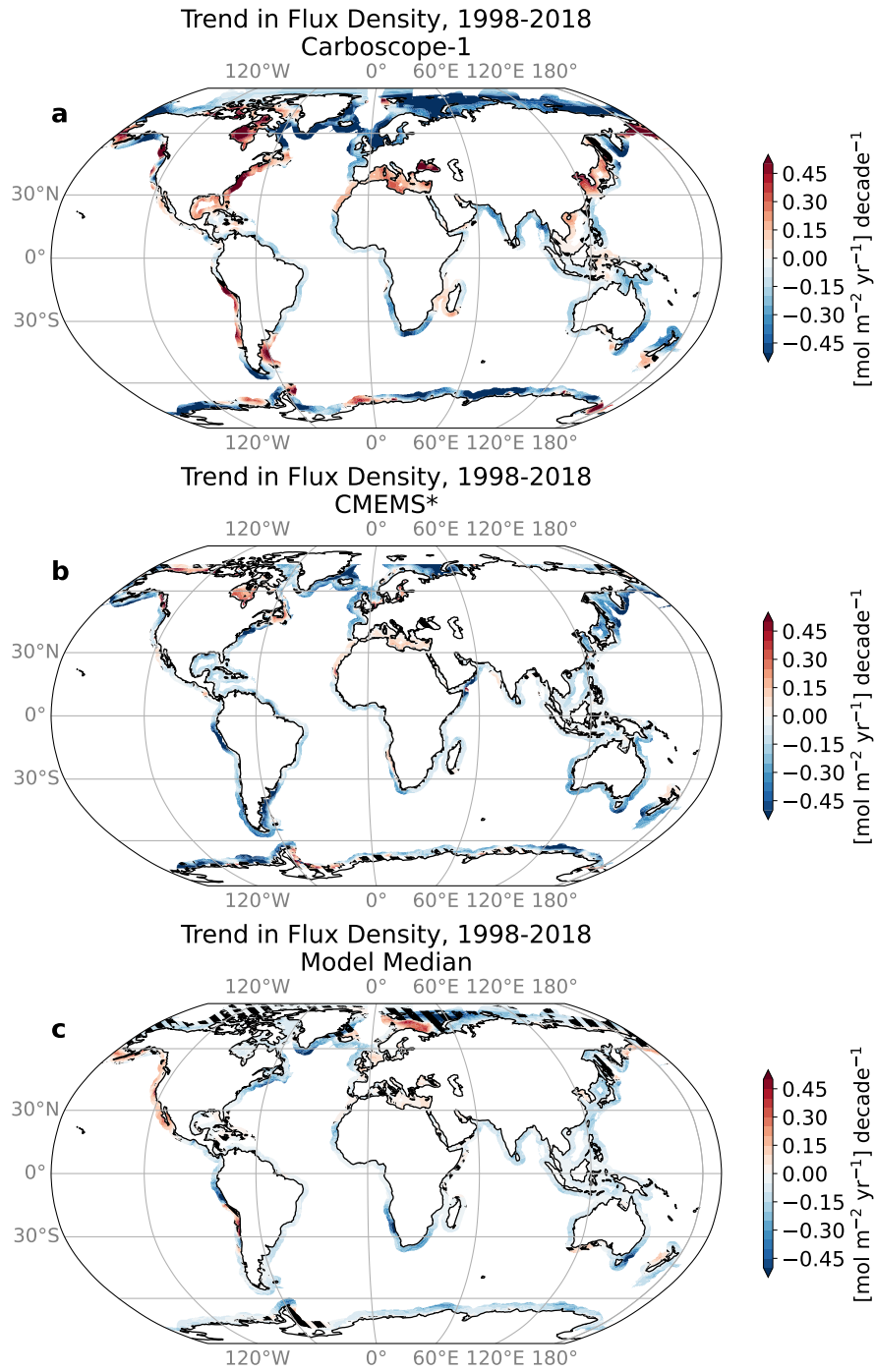


Figure 9. 1998-2018 trend in CO₂ flux [mol C m⁻² yr⁻¹] for a) Carboscope-1; b) CMEMS* (area north of 75° N removed) c) multi-model median (global and regional models). Hatching indicates regions where the flux trend has a different sign than the ΔpCO₂ trend (shown in Figure S10), highlighting the influence of wind and/or sea-ice trends. Negative values indicate that the ocean uptake increases or the ocean outgassing decreases with time (both leading to more carbon accumulation in the ocean).

western Indian Ocean, the subpolar North Pacific, the Baltic Sea, the Black Sea and the shallow marginal seas of Southeast and East Asia. These are generally characterized by high surface productivity, low subsurface oxygen, and shallow oxyclines. High N_2O emissions from these regions thus likely reflect subsurface water-column production by a combination of nitrification and denitrification pathways, both of which are enhanced in the presence of low O_2 and high remineralization rates, and subsequent transport to the surface by upwelling and mixing processes. Similar hotspot regions are detected in the model-ensemble median, although with somewhat reduced magnitude relative to the observational products, and with the notable exception of marginal seas in Asia and Europe, suggesting that global models might not fully capture the nitrogen cycle in these regions, or the mechanisms transporting N_2O -laden waters to the surface. In addition, the model-ensemble also identifies mid-latitude western boundary systems, including the US East Coast, the North Pacific east of Japan, the southeast coast of Australia, and the southeastern tip of Africa, as additional areas of intense N_2O emissions that are not captured by the Yang- N_2O product. Notably, these regions are not generally characterized by high surface productivity and low subsurface O_2 as coastal upwelling systems, although vigorous mixing along western boundary currents may favor local N_2O outgassing in the models. Most of these regions are also not densely sampled by observations in the MEMENTO database, in particular along the US, South Africa, and Japan eastern coasts, and thus the Yang- N_2O observational extrapolation may be poorly constrained there. The magnitude of the flux in these hotspots often differs among the data products and model-ensemble (Figure 10c). The N_2O flux distributions shown in Figure 10 likely reflect the fact that enhanced coastal N_2O concentrations – and thus enhanced N_2O emissions fluxes – are associated with enhanced land-sea inputs of nitrogen (as nitrate or ammonium) or with upwelling of N_2O -enriched subsurface water masses in upwelling systems.

The spatial distribution of the coastal CH_4 fluxes computed with the observation-based Weber- CH_4 product are shown in Figure 11. Coastal CH_4 fluxes are generally positive and range from 0 to $0.4 \text{ g CH}_4 \text{ m}^{-2} \text{ yr}^{-1}$ indicating that coastal areas are a source of atmospheric CH_4 . Patterns in CH_4 emissions in Weber- CH_4 are largely correlated to water depth with most intense emissions occurring at depth shallower than 50 m (Figure 11). Indeed, coastal emissions of CH_4 are largely fueled by benthic-sourced biogenic methane, which is produced via methanogenesis in anoxic sediments and released diffusively into the overlying water column (Reeburgh, 2007; Arndt et al., 2013; Bourgeois et al., 2016). The benthic CH_4 source is enhanced in coastal waters where the rapid organic matter flux to the seafloor drives sediment anoxia and rapid sediment accumulation inhibits the growth of methane oxidizing microbes (e.g., Egger et al., 2016). Furthermore, aerobic respiration acts as an efficient sink of CH_4 in the water column (Mao et al., 2022), meaning that transfer from the seafloor to the surface must be extremely rapid if CH_4 is to be emitted to the atmosphere. Ebullition (bubbling) from CH_4 -enriched sediments can provide an important alternative pathway for CH_4 to surface (Rehder et al., 1998), but CH_4 is rapidly stripped from rising bubbles (McGinnis et al., 2006) and a small fraction reaches the surface only in shallow water depths. This further strengthens the coastal-offshore gradient in CH_4 emissions, and explains why total emissions differ very little between the narrow and wide coast regions in Weber- CH_4 (Figure 2c). Coastal CH_4 emissions are further enhanced in hotspots under significant influence of freshwater discharge (Rosentreter et al., 2021), which due to their low sulfate concentration, promote the degradation of organic matter through the methanogenesis pathway. In addition to the biogenic CH_4 production pathway, CH_4 emissions can also be driven by geologically sourced methane, originating from shallow seafloor seeps fed by hydrocarbon reservoirs or high-latitude hydrates (Ruppel & Kessler, 2017; Puglini et al., 2020). Overall, the distribution of coastal CH_4 emissions (Figure 11) can largely be understood in terms of water depth, organic matter production and delivery to sediments, and freshwater inputs.

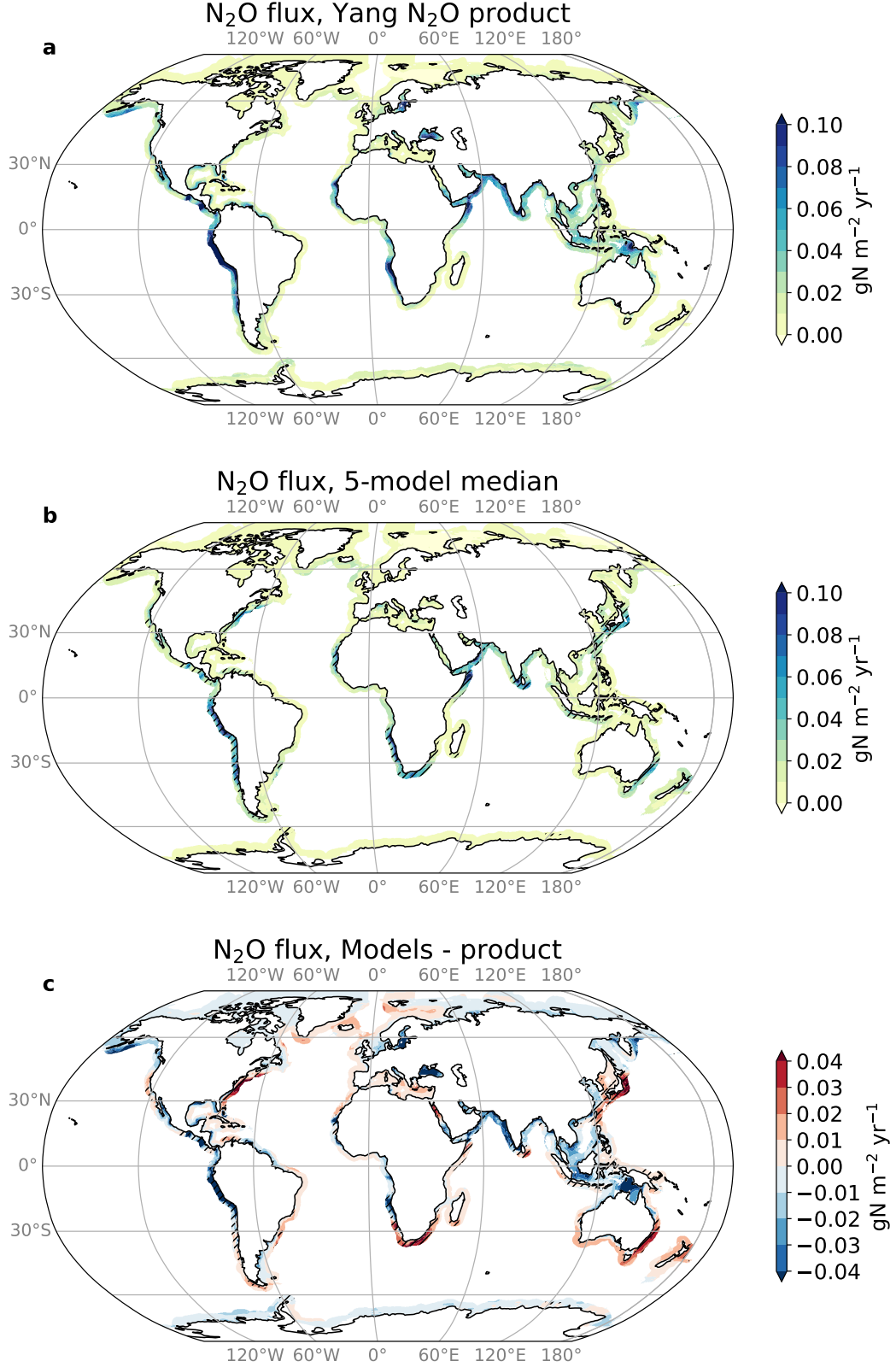


Figure 10. Maps of coastal N₂O flux (in g N m⁻² yr⁻¹) from a) Yang-N₂O product and b) the mean of the 5 global ocean models that simulate N₂O (CNRM-LR, CNRM-HR, ECCO-Darwin, ECCO2-Darwin, and NEMO-PlankTOM5). Hatching in panels b-c shows where RMSD among models exceeds 0.016 g N m⁻² yr⁻¹ (RMSD threshold corresponds to the 20% of coastal area with highest RMSD).

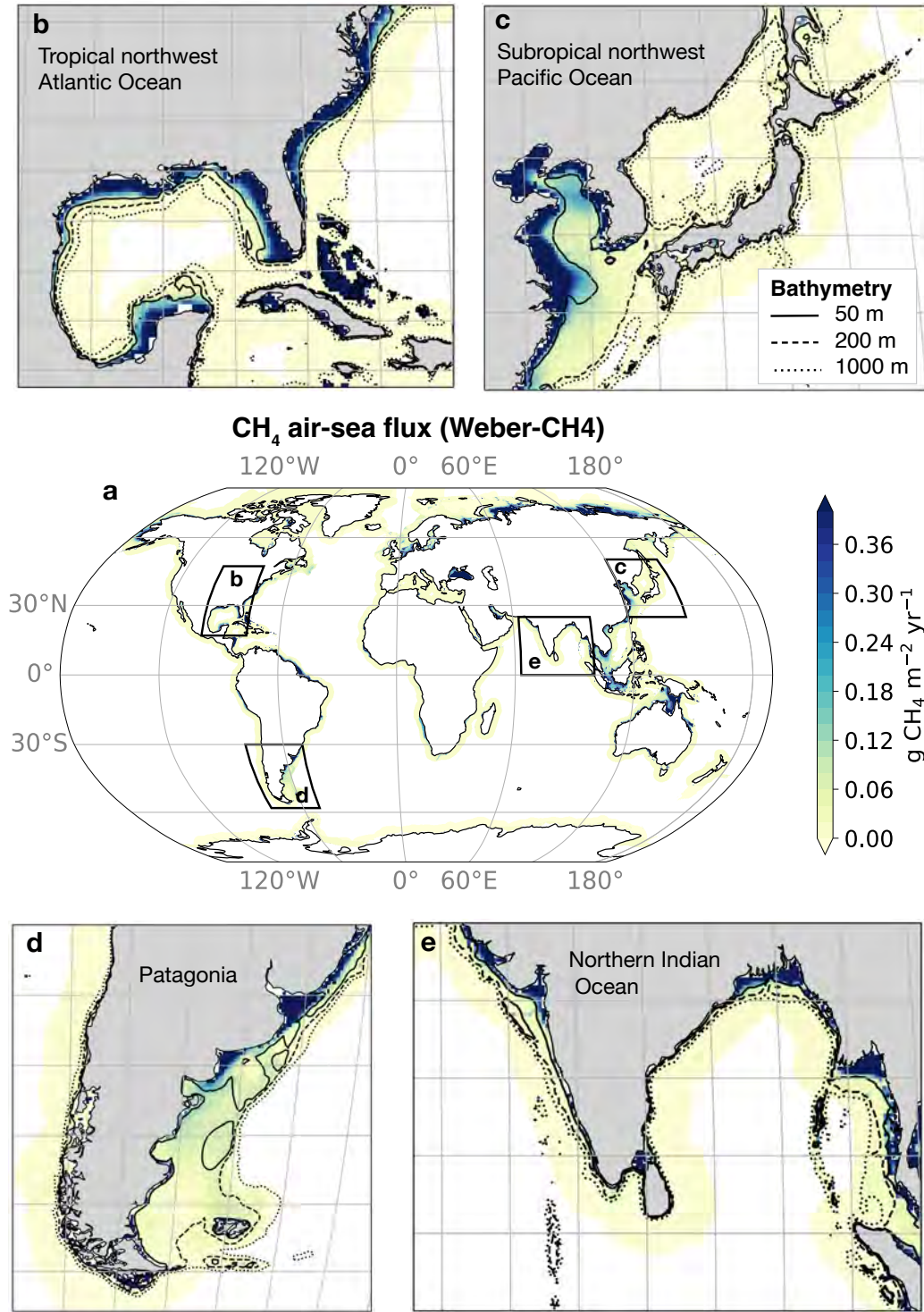


Figure 11. a) Global maps of coastal CH₄ flux from the Weber-CH4 product (includes diffusive and ebullitive flux, in $\text{g CH}_4 \text{ m}^{-2} \text{ yr}^{-1}$); b-e) insets show the CH₄ flux in four coastal regions along with 50, 200 and 1000 m bathymetry contours. CH₄ emissions are most intense in shallow coastal environments.

4 Discussion

4.1 Coastal CO₂ fluxes

This study presents a synthesis of the global coastal ocean air-sea CO₂ fluxes combining observational pCO₂-based products and an ensemble of ocean biogeochemical models. We confirm the hypothesis put forward in prior work (Laruelle et al., 2010, 2014; Roobaert et al., 2019; Dai et al., 2022) that when averaged globally, CO₂ flux densities are more negative (stronger sinks) in the coastal ocean than in the open ocean waters. As put forward by Roobaert et al. (2019), we find that the differences between coastal and open ocean flux densities are largely explained by the disproportionate contribution of high latitude systems (generally strong sinks) to the coastal ocean surface area. Global ocean biogeochemical models and pCO₂-products agree relatively well on the coast-to-open ocean contrast in CO₂ flux densities, but recent syntheses of discrete observations (Cao et al., 2020; Dai et al., 2022) find stronger heterogeneity than the global pCO₂-products and global ocean models presented here, suggesting that gap-filling approaches and global ocean models might smooth some of the coastal ocean spatial variability. Despite the good agreement on the coast-to-open ocean differences, the global ocean biogeochemical models yield a net median CO₂ uptake in the wide coastal ocean that is about 0.28 PgC stronger than the one inferred from pCO₂-products for the 1998-2018 period, equivalent to a ~60% stronger sink (-0.44 PgC yr⁻¹ for products vs. -0.72 PgC yr⁻¹ for models in the wide coastal ocean). This mismatch of model- and product-based work in the net coastal CO₂ sink arises from a combination of factors, including strong differences in the coastal CO₂ flux seasonality (themselves attributed to differences in ocean pCO₂ seasonality and potentially wind speed and gas exchange transfer coefficient formulation) resulting in a stronger wintertime CO₂ uptake in northern subpolar and polar coastal systems in models.

4.1.1 Seasonality

The seasonality in the four pCO₂-products used here falls into three latitudinal regimes. Tropical coastal waters (25°S-25°N) are characterized by small seasonal amplitudes and a stronger sink or weaker source in winter, both attributed to the weak seasonal thermal changes that slightly reduce surface ocean pCO₂ in winter (Laruelle et al., 2014; Roobaert et al., 2019). Mid-latitude coastal waters (50°S-25°S and 25°N-50°N) are characterized by larger seasonal amplitudes and a stronger CO₂ sink in winter and spring, likely due to the combined effect of thermal changes which lowers ocean pCO₂ in winter, biological drawdown of dissolved inorganic carbon (DIC) which further lowers pCO₂ during the spring bloom, and the influence of stronger winds in winter (Laruelle et al., 2014; Roobaert et al., 2022). High latitude coastal waters (poleward of 50°N and 50°S) are characterized by seasonal variations similar in magnitude to mid-latitudes, but where the maximum CO₂ uptake occurs in summer in response to intense biological drawdown. The biologically-driven uptake in high-latitude systems peaks a few months later than in mid-latitude systems because of the poleward propagation of the bloom (Siegel et al., 2002; Roobaert et al., 2019, 2022; Ouyang, Collins, et al., 2022). This marked seasonality in CO₂ fluxes contrasts with the RECCAP synthesis which found very little seasonality in global coastal CO₂ flux densities, although the results were deemed inconclusive because of the sparse data and averaging process required to analyze the data available at the time (Chen et al., 2013). The results found here are, however, consistent with more recent work. In particular, the transition from thermally driven systems in the tropics (stronger winter sinks) to biologically driven systems at high latitudes (stronger summer sinks), and the increase in seasonal amplitude from tropical to high-latitude systems found in the pCO₂-products, are consistent with the global seasonal patterns in the coastal ocean described by (Roobaert et al., 2019), the global open ocean seasonality patterns assessed in the framework of RECCAP2 (Rodgers et al., submitted to the RECCAP2 special is-

sue), and supported by field and remote sensing studies at regional scale (Signorini et al., 2013; Ouyang, Collins, et al., 2022; Tu et al., 2021).

Our synthesis reveals, however, strong differences in seasonality between $p\text{CO}_2$ -products and global ocean biogeochemical models. The model median simulates a weak CO_2 flux seasonality in tropical coastal oceans similarly to the $p\text{CO}_2$ -products, but yields a CO_2 uptake that is stronger in winter at mid- and high-latitudes. This is likely due to a weaker contribution of biologically induced seasonality compared to thermal changes in the models, which would explain the lower surface ocean $p\text{CO}_2$ simulated in winter (due to an underestimated upward transport of remineralized DIC) and the higher $p\text{CO}_2$ simulated in spring/summer (due to a weaker biological drawdown). Part of these systematic differences compensate in the global mean coastal flux (winter vs. summer, northern vs. southern hemisphere), but because the model-product difference is larger in winter in the northern hemisphere, the net CO_2 uptake in the wide coastal ocean is about 60% larger in the model median. The RECCAP2 chapter on open ocean seasonality (Rodgers et al., submitted to the RECCAP2 special issue), finds a similar systematic bias in model winter-to-summer $p\text{CO}_2$, which they attribute to a generally too small surface DIC seasonal cycle in models compared to observation-based reconstructions. This bias is particularly evident in the subpolar North Atlantic and North Pacific Oceans, where it manifests itself not only as a difference in amplitude but also in phasing. In these regions, the simulated too low DIC seasonality results in a thermal control of the $p\text{CO}_2$ seasonality in the global ocean biogeochemical models and thus in a phase shift of the seasonal $p\text{CO}_2$ cycle compared to the observation-based estimate dominated by non-thermal forcing. This suggests that the systematically stronger winter sink and weaker summer sink found in northern coastal waters in the models are at least partly attributable to general biases in the biogeochemical (e.g., bloom dynamics) or physical (e.g., vertical mixing) components of the ocean models, rather than a characteristic of the models that is specific to the coastal ocean. See details in the RECCAP2 studies of (Rodgers et al., submitted to the RECCAP2 special issue). Nevertheless, we find that the amplitude of this systematic model/product difference in seasonality is amplified in the coastal ocean (see Figures S7-S8).

Differences in ocean $p\text{CO}_2$ seasonality between models and $p\text{CO}_2$ products can be amplified by differences in gas exchange coefficient k_w , either through the influence of winds or the gas exchange coefficient formulation (which are different across the different ocean biogeochemical models and $p\text{CO}_2$ -products, Tables 1-3), and maybe to a lesser extent spatio-temporal differences in sea-ice cover (e.g., lower ice cover in some products/models could yield stronger fluxes). In models, the surface $p\text{CO}_2$ and k_w are tightly coupled in the sense that a larger k_w drives down the air-sea $p\text{CO}_2$ disequilibrium and therefore the air-sea CO_2 flux. In contrast, the calculation of the flux in $p\text{CO}_2$ products (except for Carboscope-1 which links fluxes and $p\text{CO}_2$ changes in a mixed-layer carbon budget equation) is done offline without any compensatory effect between k_w and air-sea $p\text{CO}_2$ disequilibrium. Therefore, the observation-based flux assessments are even more sensitive to the choice of the wind and k_w parameterization. For instance, we find that the net global coastal CO_2 uptake in the Coastal-SOM-FFN product is increased by nearly 50% in the wide and the narrow coastal ocean when changing the wind product (from ERA-interim to JRAv1.3) and gas exchange parametrization (from Ho et al., 2011 to Wanninkhof 1992, see Table 1). These results are in line with published literature that assessed the impact of k_w parametrizations on global air-sea CO_2 fluxes (Boutin et al., 2009; Roobaert et al., 2018; Reichl & Deike, 2020), but highlights that its influence is also crucial in the coastal ocean, because of the disproportionate contribution of mid- to high-latitude/high-wind systems in the total coastal area. Furthermore, global wind-based gas exchange parameterization might not capture the complexity of the coastal ocean processes, such as the influence of bubbles entrained by wave breaking (Deike & Melville, 2018; Woolf et al., 2019), the presence of high surfactant concentrations (Pereira et al., 2018), or fine scale water-side convection (Gutiérrez-Loza et al., 2022).

4.1.2 Land-sea fluxes

An additional factor that can explain part of the difference in the net CO_2 uptake between pCO_2 -products and models is the presence of systematic bias in global ocean biogeochemical models, in particular the contribution of carbon and nutrient land-sea riverine inputs or the models' horizontal resolution and ability to resolve coastal dynamics. At pre-industrial times (and assuming steady-state consistent with stable ice-core atmosphere CO_2 values; Elsig et al., 2009), the supply of carbon from land must have been balanced by burial in sediments and an outgassing of CO_2 from the ocean to the atmosphere. This land-driven outgassing flux, recently estimated to be $0.65 \pm 0.3 \text{ PgC yr}^{-1}$ (mean ± 2 -sigma) for the global open ocean (Regnier et al., 2022, note that this outgassing of 0.65 PgC yr^{-1} is quantified for the open ocean outside of the narrow coastal ocean and thus include part of the wide coastal ocean), is still active today and therefore partially offsets the ingassing CO_2 flux that is directly driven by anthropogenic CO_2 emissions to the atmosphere (e.g., Resplandy et al., 2018; Friedlingstein et al., 2022; Regnier et al., 2022). Observation-based pCO_2 -products estimate the net contemporary flux of CO_2 , and therefore implicitly include the fluxes of natural and anthropogenic carbon, as well as the outgassing fluxes of carbon from land origin (e.g., Hauck et al., 2020). Most models, however, do not, or only partially include this land-sea carbon inputs (see Tables 2-3) and are therefore likely to overestimate the net CO_2 ocean uptake, in particular in coastal waters adjacent to the land (Lacroix et al., 2020).

In globally integrated estimates, such as analyzed in the Global Carbon Budget (e.g., Friedlingstein et al., 2022) or the IPCC (Arias et al., 2021), the net air-sea CO_2 flux can in principle be adjusted for the outgassing of carbon from land to isolate the oceanic net sink, or it can be used to shed light on differences between modeled and observation-based flux estimates (e.g., Hauck et al., 2020; Friedlingstein et al., 2022). The RECCAP2 open ocean chapters estimated the spatial distribution of this land-driven CO_2 outgassing by upscaling the spatial distribution from Lacroix et al. (2020) using the global outgassing number of Regnier et al. (2022). This estimate suggests that 0.12 PgC yr^{-1} out of the 0.65 PgC yr^{-1} of land-driven CO_2 outgassing occurs in the wide coastal ocean, which could explain part of the model-product discrepancy. It is important to recognize, however, that the spatial distribution of this land-driven outgassing and contribution to the coastal ocean air-sea flux are very poorly constrained. In particular, we note that the model used to estimate the land-driven outgassing pattern (Lacroix et al., 2020) is lacking some of the processes that control the magnitude (hence the upscaling to match the global number of 0.65 PgC yr^{-1} from Regnier et al. (2022) but also the spatial distribution of this outgassing (e.g., CO_2 uptake by coastal vegetation). Another factor to consider is the land-sea input of nutrients which promotes biological CO_2 uptake in coastal waters downstream of the river mouth (e.g., Louchard et al., 2021; Terhaar et al., 2021; Gao et al., 2023), potentially offsetting the land-driven CO_2 outgassing associated with carbon runoffs, although we do not expect the patterns of the CO_2 outgassing and biological CO_2 uptake to match. In the model ensemble considered here models either include both carbon and nutrient land-sea inputs or neither (Tables 2 and 3). This might explain why models with land-sea carbon inputs did not systematically yield weaker CO_2 uptake in the coastal ocean compared to the one without land-sea inputs. Finally, we find that the subset of global ocean biogeochemical models with highest spatial resolution yields a slightly weaker net CO_2 uptake ($-0.65 \text{ PgC yr}^{-1}$) in better agreement with the pCO_2 -products than the full model ensemble. The small number of models in that subset (4) makes any statistical argument about resolution difficult. Yet, this result suggests that a better representation of fine scale coastal dynamics could improve the representation of the CO_2 flux, likely by improving the representation of the physical and biogeochemical processes controlling CO_2 seasonality in the northern hemisphere (Laurent et al., 2021; Rutherford et al., 2021; Rutherford & Fennel, 2022).

4.1.3 Trends

This synthesis indicates that the coastal ocean CO₂ sink has increased between 1998 and 2018, in line with the expectation from previous work that showed surface pCO₂ in the narrow coastal ocean increasing at a smaller rate than in the atmosphere (Wang et al., 2017; Laruelle et al., 2018). The rate at which the coastal sink has increased is, however, poorly constrained by the models and products presented here (flux density trend varies by a factor 2 between the two time-varying pCO₂-products and by a factor 3 between the 11 models). In addition, it is still unclear if this increase in the global coastal CO₂ sink is comparable, slower or faster than in the open ocean due to the inconsistent responses found in models and the two time-varying pCO₂-products but also in prior modeling and observation-based work (Bourgeois et al., 2016; Wang et al., 2017; Laruelle et al., 2018; Lacroix et al., 2021). The CMEMS* pCO₂-product suggests that the CO₂ uptake increases faster in the coastal ocean than in the open ocean, which is in line with the prior observation-based results of Laruelle et al. (2018). In contrast, the ensemble of 11 global ocean models and the Carboscope-1 pCO₂-product suggest that the coastal ocean sink is increasing at a slightly smaller rate than the open ocean, a result in line with another other prior work based on pCO₂ observations (Wang et al., 2017) and global ocean biogeochemical models (Bourgeois et al., 2016; Lacroix et al., 2021). Bourgeois et al. (2016) explains this weaker increase in the coastal carbon sink by a bottleneck in offshore transport which leads to anthropogenic carbon accumulation and limits the ability of coastal waters to take up anthropogenic carbon. Although we do not quantify surface residence time or off-shelf transport in this study, our finding that the modeled CO₂ sink increases at a lower rate in the coastal region than in the open ocean lends support for this interpretation. Other processes at play could explain this behavior. For instance, relatively shallow waters in coastal oceans might limit the exchanges with deep (free of anthropogenic CO₂) waters, such that the coastal ocean surface layer saturates more quickly with additional CO₂ added to the atmosphere. In models, this slower rate is associated with regions of increased outgassing or reduced uptake, although mid-to-high latitudes can be strongly increasing CO₂ sinks as suggested by observations (Laruelle et al., 2018). However, the regions controlling this slower rate of increase vary across models (e.g., North Pacific, Mediterranean Sea and Parts of the Arctic in the model median in this study vs. tropical ocean and parts of the Arctic in Lacroix et al., 2021), highlighting further the uncertainties that remain in constraining coastal trends.

The slower increasing pCO₂ trend in the coastal ocean was attributed in these model-based studies to an increased outgassing or reduced uptake in tropical and river-dominated Arctic shelves, while mid-to-high latitudes were found to be strongly increasing CO₂ sinks as suggested by observations. Part of the discrepancies between the estimates of the CO₂ flux trends are likely to arise from the sparse temporal pCO₂ observational coverage. For instance the prior studies of Wang et al. (2017) and Laruelle et al. (2018) only covered a small portion of the coastal surface area and might not be representative of the global ocean. This is supported by regional studies that identified coastal ocean pCO₂ trend weaker than the atmospheric pCO₂ trend (i.e. potentially yielding intensified CO₂ uptake or decreased outgassing) such as the northern Gulf Stream margin, the South China Sea, the Sea of Japan, the North Sea and the Antarctic Peninsula (Bauer et al., 2013; Wang et al., 2017; Laruelle et al., 2018; Dai et al., 2022), but also regions where coastal ocean pCO₂ increases at a similar rate (i.e. near-zero changes in the flux) or even higher rates (i.e. reduced CO₂ uptake or intensified outgassing) than atmospheric pCO₂, such as in the Baltic Sea (Schneider & Müller, 2018), the California Current or along the eastern US coast (Reimer et al., 2017; Laruelle et al., 2018; Salisbury & Jönsson, 2018; Xu et al., 2020; Dai et al., 2022). Another source of discrepancy is the decoupling found between global coastal pCO₂ trends and flux trends, suggesting that the CO₂ flux trends are sensitive to trends in winds and sea-ice (via the gas exchange coefficient), and how they combine with the pCO₂ trends. This sensitivity to sea-ice and winds is likely more pronounced in the observation-based estimates, which rely on an “offline” calculation of

the flux (no mechanistic link between $p\text{CO}_2$ disequilibrium, wind and sea-ice, except for CarboScope-1), or even more simply assume that slower trends in coastal ocean $p\text{CO}_2$ translate into faster growing coastal CO_2 flux (e.g., Laruelle et al., 2018), an assumption that is not fulfilled in the 2 $p\text{CO}_2$ -products used in this study (although it does work in the multi-model median).

4.1.4 Conclusions

The systematic differences found between the ensemble median of global ocean models and $p\text{CO}_2$ -products (including the larger net annual mean CO_2 uptake found in global ocean models, the different timing of mid- and high-latitude seasonality and the large range found in flux density trends) should be interpreted with caution. First, some models are capturing better than others the patterns reconstructed by the $p\text{CO}_2$ -products. In particular, some models are able to reproduce the stronger summer sink found at high-latitudes, or simulate a net annual mean CO_2 flux that better matches the product-based estimates. In addition, differences between products and models do not necessarily equate to model bias, as regions of largest product-model mismatch also often correspond to regions where the observational sampling is sparse (68% of the wide coastal ocean surface area was never sampled, and of the sampled area, 33% has data for only one month in a single year, Figure S1) and where the spread across the observation-based products and across the global models is the highest (hatching on Figure 5a,b). In contrast, coastal regions that are relatively well sampled by observations and well constrained by the products generally correspond to regions of agreement between the observation-based and model-based estimates (Roobaert et al., 2022). Thus, while we have overall more confidence in the observation-based estimates of the ocean carbon sink, the uncertainties associated with these reconstructed estimates remain high. This precludes a clear conclusion about whether the observation or model-based estimates are closer to the truth.

4.2 Coastal N_2O and CH_4

The coastal ocean is a substantial source of atmospheric N_2O (Yang et al., 2020) and a minor source of atmospheric CH_4 (Weber et al., 2019; Saunio et al., 2020). The N_2O flux estimates presented here for the narrow coastal ocean (0.14 to 0.75 Tg N yr^{-1}) are at the lower end of previous estimates of the mean global N_2O fluxes from nearshore coastal systems (including shelves, estuaries and upwelling regions) which range from 0.7 to 6.7 Tg N yr^{-1} (Bange et al., 1996; Seitzinger & Kroeze, 1998). The mean CH_4 flux estimates for the narrow coastal ocean (2.46-3.19 Tg CH_4 yr^{-1} for the diffusive flux and up to 6.79 Tg CH_4 yr^{-1} when accounting for the ebullitive flux in the narrow coastal ocean) are in good agreement with a recently published mean CH_4 flux from shelves (0 - 200 m water depth) of 5.7 Tg CH_4 yr^{-1} (Rosentreter et al., 2021). Nevertheless, quantitative estimates of N_2O and CH_4 emissions remain highly uncertain. Estimates of N_2O emissions in this study vary by a factor of 5-6 in both the narrow and wide coastal ocean, and central values of CH_4 emissions by a factor up to 3.5. The smaller range found here for CH_4 likely reflects the fewer number of estimates available (2 observation-based products only vs. 5 global ocean models and 2 observation-based products for N_2O) rather than stronger constraints on the emissions.

Current observational products only provide a climatological view of N_2O and annual mean view of CH_4 emissions, with limited or missing information on (i) seasonal and inter-annual variability, (ii) fine-scale (i.e., few 10s of km or less) land-ocean gradients, (iii) the effects of mesoscale and submesoscale features such as eddies (Grundle et al., 2017), and (iv) extreme events such as storms and marine heat waves (Borges et al., 2019; Gindorf et al., 2022). Aspects of air-sea gas exchange, such as the effects of surface micro-layers on these gasses (Kock et al., 2012) remain also poorly understood. In parallel, commonly adopted model parameterizations greatly simplify complex source and sink processes that are the focus of ongoing research. For example, there remains

significant uncertainty in the relative importance of the various (micro)biological and photochemical processes driving the production and consumption of N_2O and CH_4 in coastal waters and sediments, and their potential responses to changing oceanic conditions (Bange, 2022). Methane can be produced aerobically in-situ in surface waters, providing the most direct route to the atmosphere. This process has mostly been studied in the open ocean where decomposition of methylphosphonate (MPn, a component of semi-labile dissolved organic matter) appears to be the dominant methanogenesis pathway (Karl et al., 2008; Repeta et al., 2016). Recent evidence suggests the MPn pathway is also active in some coastal waters (Mao et al., 2022), but its importance relative to benthic-sourced CH_4 in coastal waters remains unclear. Additional sources of N_2O and CH_4 remain poorly characterized and are not represented by models, including submarine groundwater discharge (Arévalo-Martínez et al., 2023) and production associated with marine microplastic (Royer et al., 2018; Su et al., 2022), submerged aquatic vegetation (Rosentreter et al., 2021; Hilt et al., 2022; Roth et al., 2023; Rosentreter et al., 2023), and zooplankton (Schmale et al., 2018).

Our study reveals that while coastal N_2O flux emissions from observational products and models generally agree in terms of main patterns and magnitude, emission hotspots in productive, low- O_2 upwelling systems appear to be underestimated by models, suggesting deficiencies in model circulation and parameterization of low- O_2 sources. In contrast, models point to coastal N_2O flux hotspots along mid-latitude western boundaries that are not evident in observational reconstructions. The reason for this mismatch remains unclear, but likely reflects lack of observations from these regions, which could limit the ability of reconstructions to capture coastal hotspots, and potential model biases. The recently proposed Global N_2O Ocean Observation Network (N_2O -ON) (Bange et al., 2019; Bange, 2022) might help to better constrain and understand temporal and spatial variability as well as reduce uncertainties in current global N_2O oceanic emission estimates.

Ongoing environmental changes such as ocean warming, decreasing pH, loss of dissolved oxygen, and eutrophication might significantly alter the production and consumption of both N_2O and CH_4 as well as their distribution patterns in coastal waters and, consequently, their release to the atmosphere (e.g., Rees et al., 2022; Zhou et al., 2023). However, our knowledge of recent trends on which future emissions scenarios of N_2O and CH_4 from the coastal ocean rely upon are still far from complete. In particular, hydrate dissolution due to ocean warming may enhance this flux at the seafloor, but only at the feather-edge of the hydrate stability zone, which occurs in ~ 400 m deep water in mid-latitudes – which could be too deep for the methane to make it to the surface and escape to the atmosphere (Joung et al., 2022). Shallow hydrocarbon-fed seep fields allow for more efficient methane release to atmosphere (Hovland et al., 1993), but their impact appears to be highly localized (Joung et al., 2020), and the global-scale contribution of geological CH_4 to marine emissions remains highly uncertain (Etiope et al., 2019). Understanding CH_4 oxidation dynamics in coastal environments is therefore an important focus area for future research. Although N_2O -ON was originally designed for N_2O only, adding measurements of CH_4 will be facilitated by deploying instruments on the basis of the same technique used for N_2O measurements (i.e. cavity-enhanced absorption spectroscopy), providing new opportunities to establish long-term time-series for these two greenhouse gasses.

4.3 Coastal greenhouse gas atmospheric influence

This synthesis provides an estimate of the coastal contribution to the atmospheric greenhouse gas budget using an ensemble of observation-based products and global ocean biogeochemical models (in CO_2 -equivalent). In both products and models, we find that a significant proportion of the coastal CO_2 uptake (~ 35 - 55%) is offset by N_2O and CH_4 emissions, despite large uncertainties in the magnitude of the mean CO_2 uptake (large

uptake in models) and relatively limited numbers of observation-based products and models available for N_2O and CH_4 fluxes. This offset is significantly larger than in the global ocean, for which a value of about 10% can be calculated based on the CO_2 (Le Quéré et al., 2018), N_2O (Tian et al., 2020), and CH_4 (Saunois et al., 2020) global budgets by the GCP. A smaller offset value on the order of 10-20% has also been reported for estuaries and coastal vegetated ecosystems (Rosentreter et al., 2023), highlighting that the radiative balance on the shelves results from a significant contribution of the 3 greenhouse gasses. Such an offset does not occur in inland waters either (rivers, lakes and reservoirs), as freshwater aquatic systems are a net source of CO_2 , CH_4 and N_2O (Battin et al., 2023)(also Lauerwald et al., in revision for the RECCAP2 special issue), with CO_2 and CH_4 contributing roughly 75% and 25% to the 100-year time-scale global warming potential, respectively, while N_2O is only a marginal contributor. Integrating the three compartments of the land-to-ocean aquatic continuum (LOAC) from streams to the coastal oceans (i.e., inland waters, estuaries and coastal vegetation, and coastal ocean waters (Regnier et al., 2013, 2022), we find that the LOAC is a net source of greenhouse gasses. Indeed, the 8.3 (range of 5.8-12.7) $\text{PgCO}_2\text{-e yr}^{-1}$ emitted by inland waters are only partly compensated by the net uptakes of 0.4 (range 0.2-0.7) $\text{PgCO}_2\text{-e yr}^{-1}$ from estuaries and coastal vegetation and 1.3 (range 0.7-1.8) $\text{PgCO}_2\text{-e yr}^{-1}$ from wide coastal waters. For the 100 year time horizon, the LOAC as a whole thus emits about 6.6 $\text{PgCO}_2\text{-e yr}^{-1}$ globally.

Acknowledgments

The authors have no conflicts of interest. A.K.H. acknowledges support from the National Science Foundation (NSF) Graduate Research Fellowship Program under Grant DGE-2039656. Any opinions, findings, and conclusions or recommendations expressed in this material are those of the author and do not necessarily reflect the views of the NSF. L.R. and E.L. were partly funded by National Oceanic and Atmospheric Administration award NA21OAR4310119. L.R. and M.M. thank NASA for financial support via the grant NASA OCO-2 Science Team Grant 80NSSC18K0893. L.R. additionally thank the Princeton Institute for Computational Science and Engineering (PICSciE) for High Performance Computing (HPC) provision, storage and support. D.B. acknowledges support from NSF grant OCE-1847687, and computational resources from the Expanse system at the San Diego Supercomputer Center through allocation TG-OCE170017 from the Advanced Cyber infrastructure Coordination Ecosystem: Services and Support (ACCESS) program, which is supported by NSF grants 2138259, 2138286, 2138307, 2137603, and 2138296. J.D.M. and N.G. acknowledge support from the European Union’s Horizon 2020 research and innovation programme under grant agreement no. 821003 (project 4C) and no. 820989 (project COMFORT). N.G. additionally thanks for the support of the Swiss National Science Foundation through grant agreement no 175787 (Project X-EBUS). J.S. was supported by the Research Council of Norway (grant no 270061) and acknowledges provision of HPC and storage resources by UNINET/sigma2 (nn/ns9560k). C.L.Q. was funded by the UK Royal Society (grant no. RP\R1\191063). Simulations of the NEMO-PlankTOM model were carried out by D. Willis on the HPC Cluster supported by the Research and Specialist Computing Support service at the University of East Anglia. G.G.L. is a research associate of the FRS-FNRS at the Université Libre de Bruxelles. Finally, we thank the RECCAP2 organisers and scientific steering committee for coordinating and supporting this effort.

Table 1. Description of observation-based products used in this study, including the wind speed product and gas exchange coefficient (k_w) formulation used to compute the fluxes. W92, H11, W14, L13, N00 stands for k_w -formulations from Wanninkhof (1992); Ho et al. (2011); Wanninkhof (2014); Liang et al. (2013); Nightingale et al. (2000) respectively. Mon and Ann stands for monthly and annual mean frequencies. Wide coastal areas are calculated after the products and models have been regridded on the $0.25^\circ \times 0.25^\circ$ grid. Further details and references on observation-based products and models are provided in Supplementary Material.

Product	Gasses	land-sea inputs	Domain	Frequency/period in this study	Horizontal resolution	wide area (million km ²)	wind speed and k_w	Reference
Carboscope-1	CO ₂	N/A	Global	Mon ^a 1998-2018	1°	73.9	JRA55-do v1.5.0 W92 ^b	(Rödenbeck et al., 2022)
CMEMS*	CO ₂	N/A	Global ^c	Mon 1998-2018	1°	55.8	ERA5 W14 ^b	(Chau et al., 2022)
Coastal-SOM-FFN	CO ₂	N/A	Global	Mon 1998-2015	0.25°	77.2	ERA-interim H11	(Roobaert et al., 2019)
Coastal-SOM-FFN- k_w	CO ₂	N/A	Global	Mon 1998-2015	0.25°	77.2	JRAv1.3 W92	
Merged-SOM-FFN	CO ₂	N/A	Global	Mon 1998-2015	0.25°	77.2	ERA-interim H11	(Landschützer et al., 2020)
Yang-N2O	N ₂ O	N/A	Global	Mon 1998-2015	0.25°	73.4	ERA-5 W14 ^b , L13 ^b	(Yang et al., 2020)
Weber-CH4	CH ₄	N/A	Global	Ann 1999-2016	0.25°	73.7	ERA-5 W14 ^b , L13 ^b	(Weber et al., 2019)
MARCATS-N2O & MARCATS-CH4	N ₂ O, CH ₄	N/A	Global	Ann 1980-2016	regional ^d	77.2	NCEP II N00	(Kock & Bange, 2015)

^aFrom originally daily.

^bScaled to global ocean mean value of 16.5 cm/h.

^cMissing Arctic filled with Coastal-SOM-FFN climatology north of 75°N.

^dNo gap filling, one value per MARGins and CATCHments Segmentation (MARCATS).

Table 2. Description of global ocean biogeochemical models used in this study, including the wind speed product and gas exchange coefficient (k_w) formulation used to compute the fluxes. W92 and W14 stand for k_w -formulations from Wanninkhof (1992, 2014) respectively. Mon stands for monthly frequency. Wide coastal areas are calculated after the products and models have been regridded on the $0.25^\circ \times 0.25^\circ$ grid. Further details and references on observation-based products and models are provided in Supplementary Material.

Model	Gasses	land-sea inputs	Domain	Frequency/period in this study	Horizontal resolution	wide area (million km ²)	wind speed and k_w	Reference
CCSM-WHOI	CO ₂	No	Global	Mon 1998-2017	3.6°lon 0.8-1.8°lat	34.5	NCEP W92	Doney et al. (2009)
CNRM-LR	CO ₂ , N ₂ O	Yes	Global	Mon 1998-2018	1°lon 0.3-1°lat	64.8	JRA55-do W14	Séférian et al. (2019)
CNRM-HR	CO ₂ , N ₂ O	Yes	Global	Mon 1998-2018	0.25°	71.3	JRA55-do W14	Berthet et al. (2019)
FESOM-LR	CO ₂	No	Global	Mon 1998-2018	unstructured ~1°	75.5	JRA55-do W14	Hauck et al. (2020)
FESOM-HR	CO ₂	No	Global	Mon 1998-2018	unstructured ~0.25°	76.4	JRA55-do W14	Hauck et al. (2020)
IPSL	CO ₂	Yes	Global	Mon 1998-2018	1°lon 0.3-1°lat	65	JRA55-do W14	Bopp et al. (2015)
MOM6-Princeton	CO ₂	Yes ^a	Global	Mon 1998-2018	0.5°lon 0.25-0.5°lat	63.8	JRA55-do v1.3 W92	Liao et al. (2020)
MPIOM-HAMMOC	CO ₂	Yes	Global	Mon 1998-2018	1.5°	44.5	NCEP W14	Ilyina et al. (2013)
MRI-ESM2.1	CO ₂	No	Global	Mon 1998-2018	1°lon 0.3-0.5°lat	66.3	JRA55-do W14	Yukimoto et al. (2019)
NEMO-PlankTOM12	CO ₂	Yes	Global	Mon 1998-2018	2°lon 0.3-1.5°lat	62.8	NCEP W92	Wright et al. (2021)
NEMO-PlankTOM5	N ₂ O	Yes	Global	Mon 1998-2018	2°lon 0.3-1.5°lat	62.8	NCEP W92	Buitenhuis et al. (2018)
NorESM-OC2.0	CO ₂ , N ₂ O	Yes	Global	Mon 1998-2018	nominal 1°	63.9	JRAv1.3 W14	Tjiputra et al. (2020)
ECCO-Darwin	N ₂ O	No	Global	Mon 1997-2014	1/3°lon	66.5	ERA-Interim W92	Carroll et al. (2020)
ECCO2-Darwin	N ₂ O	No	Global	Mon 2006-2013	1/6°lon	90.5	ECMWF & JRA-55 W92	Manizza et al. (2019)

^aCarbon inputs are only partial and calculated to roughly balance burial.

Table 3. Description of regional ocean biogeochemical models used in this study, including the wind speed product and gas exchange coefficient (k_w) formulation used to compute the fluxes. W92, H06 and W14 stand for k_w -formulations from Wanninkhof (1992); Ho et al. (2006); Wanninkhof (2014) respectively. Mon stands for monthly frequency. Further details and references on observation-based products and models are provided in Supplementary Material.

Model	Gasses	land-sea inputs	Domain	Frequency/period in this study	Horizontal resolution	wind speed and k_w	Reference
ETHZ-ROMS-Atl	CO ₂	Yes	regional Atlantic Ocean	Mon 1998-2018	~4-120 km ^a	ERA5 W14	Louchard et al. (2021)
ETHZ-ROMS-Pac	CO ₂	Yes	regional Pacific Ocean	Mon 1998-2018	~4-60 km ^b	ERA5 W14	Desmet et al. (2022)
ACM-NWAtl	CO ₂	Yes	Regional Northwest Atlantic (36.3 to 53.8N; -74.6 to -45.2 E)	Mon 1998-2018	~9.5 km	ERA-interim H06, W14	Rutherford et al. (2021)
NYUAD-ROMS-Indian	CO ₂	nutrients no carbon	regional Indian Ocean (31.5°S to 31°N; 30°E to 120°E)	Mon 1998-2018	1/10°	ERA-interim W14	Lachkar et al. (2021)

^ahighest resolution in Amazon plume and western Africa (2 poles).

^bhighest resolution in California Current (1 pole).

Open Research

All of the RECCAP2 data will be made available in a public repository before publication.

Author contributions

- Conceptualization (Ideas; formulation or evolution of overarching research goals and aims): L.R., P.R.
- Data curation (Management activities to annotate (produce metadata), scrub data and maintain research data (including software code, where it is necessary for interpreting the data itself) for initial use and later re-use): A.K.H., L.B., S.B., S.C.D., K.F., J.H., N.G., C.L.Q., E.L., I.D.L., J.D.M., C.N., L.R., J.S., R.S., K.T., H.T., D.B., T.T.T.C., M.G., A.K., P.L., G.G.L., A.R., C.R., T.W.
- Formal analysis (Application of statistical, mathematical, computational, or other formal techniques to analyse or synthesize study data): A.K.H., L.R.
- Funding acquisition (Acquisition of the financial support for the project leading to this publication): L.R.
- Investigation (Conducting a research and investigation process, specifically performing the experiments, or data/evidence collection): L.B., S.B., S.C.D., K.F., J.H., N.G., C.L.Q., E.L., I.D.L., J.D.M., C.N., L.R., J.S., R.S., K.T., H.T., D.W., D.B., T.T.T.C., M.G., A.K., P.L., G.G.L., A.R., C.R., T.W.
- Methodology (Development or design of methodology; creation of models): A.K.H., L.R., P.R.
- Project administration (Management and coordination responsibility for the research activity planning and execution): N.G., J.H., J.D.M., L.R., P.R.
- Software (Programming, software development; designing computer programs; implementation of the computer code and supporting algorithms; testing of existing code components): A.K.H., L.R.
- Supervision (Oversight and leadership responsibility for the research activity planning and execution, including mentorship external to the core team): L.R., P.R., N.G., J.H., J.D.M.
- Visualization (Preparation, creation and/or presentation of the published work, specifically visualization/data presentation): A.K.H., L.R.
- Writing – original draft (Preparation, creation and/or presentation of the published work, specifically writing the initial draft (including substantive translation)): L.R., P.R., H.W.B., D.B., T.W.
- Writing – review and editing (Preparation, creation and/or presentation of the published work by those from the original research group, specifically critical review, commentary or revision – including pre- or post-publication stages): All co-authors.

References

- Anderson, L. G., Jutterström, S., Hjalmarsson, S., Wählström, I., & Semiletov, I. P. (2009, October). Out-gassing of CO₂ from Siberian Shelf seas by terrestrial organic matter decomposition. *Geophysical Research Letters*, 36(20), L20601. Retrieved 2023-02-14, from <http://doi.wiley.com/10.1029/2009GL040046> doi: 10.1029/2009GL040046
- Arias, P. A., Bellouin, N., Coppola, E., Jones, R. G., Krinner, G., Marotzke, J., ... Zickfeld, K. (2021). Technical Summary. In V. Masson-Delmotte et al. (Eds.), *Climate Change 2021: The Physical Science Basis. Contribution of Working Group I to the Sixth Assessment Report of the Intergovernmental Panel on Climate Change*. Cambridge, UK and New York, NY, USA: Cambridge University Press. Retrieved from <https://www.ipcc.ch/report/ar6/>

- wg1/downloads/report/IPCC_AR6.WGI.TS.pdf (Type: Book Section) doi: 10.1017/9781009157896.002
- Arndt, S., Jørgensen, B., LaRowe, D., Middelburg, J., Pancost, R., & Regnier, P. (2013, August). Quantifying the degradation of organic matter in marine sediments: A review and synthesis. *Earth-Science Reviews*, 123, 53–86. Retrieved 2023-02-27, from <https://linkinghub.elsevier.com/retrieve/pii/S0012825213000512> doi: 10.1016/j.earscirev.2013.02.008
- Arrigo, K. R., van Dijken, G., & Long, M. (2008, November). Coastal Southern Ocean: A strong anthropogenic CO₂ sink. *Geophysical Research Letters*, 35(21), L21602. Retrieved 2023-02-14, from <http://doi.wiley.com/10.1029/2008GL035624> doi: 10.1029/2008GL035624
- Arévalo-Martínez, D. L., Haroon, A., Bange, H. W., Erkul, E., Jegen, M., Moosdorf, N., ... Weymer, B. A. (2023, February). Ideas and perspectives: Land-ocean connectivity through groundwater. *Biogeosciences*, 20(3), 647–662. Retrieved 2023-03-27, from <https://bg.copernicus.org/articles/20/647/2023/> doi: 10.5194/bg-20-647-2023
- Arévalo-Martínez, D. L., Kock, A., Löschner, C. R., Schmitz, R. A., & Bange, H. W. (2015, July). Massive nitrous oxide emissions from the tropical South Pacific Ocean. *Nature Geoscience*, 8(7), 530–533. Retrieved 2023-02-14, from <http://www.nature.com/articles/ngeo2469> doi: 10.1038/ngeo2469
- Bakker, D. C. E., Alin, S. R., Becker, M., Bittig, H. C., Castaño-Primo, R., Feely, R. A., ... Wilson, D. (2022). *Surface Ocean CO₂ Atlas Database Version 2022 (SOCATv2022) (NCEI Accession 0253659)*. NOAA National Centers for Environmental Information. Retrieved 2023-02-14, from <https://www.ncei.noaa.gov/archive/accession/0253659> (Type: dataset) doi: 10.25921/1H9F-NB73
- Bakker, D. C. E., Pfeil, B., Landa, C. S., Metzl, N., O'Brien, K. M., Olsen, A., ... Xu, S. (2016, September). A multi-decade record of high-quality *f*CO₂ data in version 3 of the Surface Ocean CO₂ Atlas (SOCAT). *Earth System Science Data*, 8(2), 383–413. Retrieved from <https://www.earth-syst-sci-data.net/8/383/2016/> doi: <https://doi.org/10.5194/essd-8-383-2016>
- Bakker, D. C. E., Pfeil, B., Smith, K., Hankin, S., Olsen, A., Alin, S. R., ... Watson, A. J. (2014, March). An update to the Surface Ocean CO₂ Atlas (SOCAT version 2). *Earth System Science Data*, 6(1), 69–90. Retrieved 2023-03-23, from <https://essd.copernicus.org/articles/6/69/2014/> doi: 10.5194/essd-6-69-2014
- Bange, H. W. (2022, December). Non-CO₂ greenhouse gases (N₂O, CH₄, CO) and the ocean. *One Earth*, 5(12), 1316–1318. Retrieved 2023-02-14, from <https://linkinghub.elsevier.com/retrieve/pii/S2590332222005875> doi: 10.1016/j.oneear.2022.11.011
- Bange, H. W., Arévalo-Martínez, D. L., de la Paz, M., Farías, L., Kaiser, J., Kock, A., ... Wilson, S. T. (2019, April). A Harmonized Nitrous Oxide (N₂O) Ocean Observation Network for the 21st Century. *Frontiers in Marine Science*, 6, 157. Retrieved 2023-02-14, from <https://www.frontiersin.org/article/10.3389/fmars.2019.00157/full> doi: 10.3389/fmars.2019.00157
- Bange, H. W., Rapsomanikis, S., & Andreae, M. O. (1996). Nitrous oxide in coastal waters. *Global Biogeochemical Cycles*, 10(1), 197–207. Retrieved 2023-02-14, from <https://onlinelibrary.wiley.com/doi/abs/10.1029/95GB03834> (eprint: <https://onlinelibrary.wiley.com/doi/pdf/10.1029/95GB03834>) doi: 10.1029/95GB03834
- Battin, T. J., Lauerwald, R., Bernhardt, E. S., Bertuzzo, E., Gener, L. G., Hall, R. O., ... Regnier, P. (2023, January). River ecosystem metabolism and carbon biogeochemistry in a changing world. *Nature*, 613(7944), 449–459. Retrieved 2023-03-27, from <https://www.nature.com/articles/s41586-022-05500-8> (Number: 7944 Publisher: Nature Publishing Group)

- doi: 10.1038/s41586-022-05500-8
- Bauer, J. E., Cai, W.-J., Raymond, P. A., Bianchi, T. S., Hopkinson, C. S., & Regnier, P. A. G. (2013, December). The changing carbon cycle of the coastal ocean. *Nature*, 504(7478), 61–70. Retrieved 2016-01-12, from <http://www.nature.com/nature/journal/v504/n7478/abs/nature12857.html> doi: 10.1038/nature12857
- Berthet, S., Jouanno, J., Séférian, R., Gehlen, M., & Llovel, W. (2022, August). How does the phytoplankton-light feedback affect marine N₂O inventory? *Earth Syst. Dynam. Discuss.*. Retrieved 2023-03-01, from <https://esd.copernicus.org/preprints/esd-2022-28/> doi: 10.5194/esd-2022-28
- Berthet, S., Séférian, R., Bricaud, C., Chevallier, M., Voldoire, A., & Ethé, C. (2019, June). Evaluation of an Online Grid-Coarsening Algorithm in a Global Eddy-Admitting Ocean Biogeochemical Model. *Journal of Advances in Modeling Earth Systems*, 11(6), 1759–1783. Retrieved 2023-03-01, from <https://onlinelibrary.wiley.com/doi/abs/10.1029/2019MS001644> doi: 10.1029/2019MS001644
- Bopp, L., Lévy, M., Resplandy, L., & Sallée, J. B. (2015, August). Pathways of anthropogenic carbon subduction in the global ocean. *Geophysical Research Letters*, 42(15), 2015GL065073. Retrieved 2015-09-14, from <http://onlinelibrary.wiley.com/doi/10.1002/2015GL065073/abstract> doi: 10.1002/2015GL065073
- Bourgeois, T., Orr, J. C., Resplandy, L., Terhaar, J., Ethé, C., Gehlen, M., & Bopp, L. (2016, July). Coastal-ocean uptake of anthropogenic carbon. *Biogeosciences*, 13(14), 4167–4185. Retrieved 2016-09-23, from <http://www.biogeosciences.net/13/4167/2016/> doi: 10.5194/bg-13-4167-2016
- Boutin, J., Quilfen, Y., Merlivat, L., & Piolle, J. F. (2009, April). Global average of air-sea CO₂ transfer velocity from QuikSCAT scatterometer wind speeds. *Journal of Geophysical Research*, 114(C4), C04007. Retrieved 2023-03-22, from <http://doi.wiley.com/10.1029/2007JC004168> doi: 10.1029/2007JC004168
- Buitenhuis, E. T., Suntharalingam, P., & Le Quéré, C. (2018, April). Constraints on global oceanic emissions of N₂O from observations and models. *Biogeosciences*, 15(7), 2161–2175. Retrieved 2023-02-07, from <https://bg.copernicus.org/articles/15/2161/2018/> (Publisher: Copernicus GmbH) doi: 10.5194/bg-15-2161-2018
- Cahill, B., Wilkin, J., Fennel, K., Vandemark, D., & Friedrichs, M. A. M. (2016, February). Interannual and seasonal variabilities in air-sea CO₂ fluxes along the U.S. eastern continental shelf and their sensitivity to increasing air temperatures and variable winds: U.S. East Coast Shelf Air-Sea CO₂ Fluxes. *Journal of Geophysical Research: Biogeosciences*, 121(2), 295–311. Retrieved 2023-03-23, from <http://doi.wiley.com/10.1002/2015JG002939> doi: 10.1002/2015JG002939
- Cai, W., Yang, K., Wu, L., Huang, G., Santoso, A., Ng, B., ... Yamagata, T. (2021, January). Opposite response of strong and moderate positive Indian Ocean Dipole to global warming. *Nature Climate Change*, 11(1), 27–32. Retrieved 2022-01-28, from <http://www.nature.com/articles/s41558-020-00943-1> doi: 10.1038/s41558-020-00943-1
- Cai, W.-J., Dai, M., & Wang, Y. (2006). Air-sea exchange of carbon dioxide in ocean margins: A province-based synthesis. *Geophysical Research Letters*, 33(12), L12603. Retrieved 2021-09-03, from <http://doi.wiley.com/10.1029/2006GL026219> doi: 10.1029/2006GL026219
- Cao, Z., Yang, W., Zhao, Y., Guo, X., Yin, Z., Du, C., ... Dai, M. (2020, April). Diagnosis of CO₂ dynamics and fluxes in global coastal oceans. *National Science Review*, 7(4), 786–797. Retrieved 2021-09-03, from <https://academic.oup.com/nsr/article/7/4/786/5542784> doi:

- 10.1093/nsr/nwz105
- Carroll, D., Menemenlis, D., Adkins, J. F., Bowman, K. W., Brix, H., Dutkiewicz, S., ... Zhang, H. (2020, October). The ECCO-Darwin Data-Assimilative Global Ocean Biogeochemistry Model: Estimates of Seasonal to Multi-decadal Surface Ocean $p\text{CO}_2$ and Air-Sea CO_2 Flux. *Journal of Advances in Modeling Earth Systems*, 12(10). Retrieved 2023-02-15, from <https://onlinelibrary.wiley.com/doi/10.1029/2019MS001888> doi: 10.1029/2019MS001888
- Chau, T. T. T., Gehlen, M., & Chevallier, F. (2022, February). A seamless ensemble-based reconstruction of surface ocean $p\text{CO}_2$ and air-sea CO_2 fluxes over the global coastal and open oceans. *Biogeosciences*, 19(4), 1087–1109. Retrieved 2023-02-15, from <https://bg.copernicus.org/articles/19/1087/2022/> doi: 10.5194/bg-19-1087-2022
- Chen, C.-T. A., & Borges, A. V. (2009, April). Reconciling opposing views on carbon cycling in the coastal ocean: Continental shelves as sinks and near-shore ecosystems as sources of atmospheric CO_2 . *Deep Sea Research Part II: Topical Studies in Oceanography*, 56(8-10), 578–590. Retrieved 2021-09-03, from <https://linkinghub.elsevier.com/retrieve/pii/S0967064509000162> doi: 10.1016/j.dsr2.2009.01.001
- Chen, C.-T. A., Huang, T.-H., Chen, Y.-C., Bai, Y., He, X., & Kang, Y. (2013, October). Air-sea exchanges of CO_2 in the world's coastal seas. *Biogeosciences*, 10(10), 6509–6544. Retrieved 2021-09-03, from <https://bg.copernicus.org/articles/10/6509/2013/> doi: 10.5194/bg-10-6509-2013
- Cossarini, G., Querin, S., & Solidoro, C. (2015, October). The continental shelf carbon pump in the northern Adriatic Sea (Mediterranean Sea): Influence of wintertime variability. *Ecological Modelling*, 314, 118–134. Retrieved 2023-03-23, from <https://linkinghub.elsevier.com/retrieve/pii/S03044380015003300> doi: 10.1016/j.ecolmodel.2015.07.024
- Dai, M., Cao, Z., Guo, X., Zhai, W., Liu, Z., Yin, Z., ... Du, C. (2013). Why are some marginal seas sources of atmospheric CO_2 ? *Geophysical Research Letters*, 40(10), 2154–2158. Retrieved 2022-04-26, from <https://onlinelibrary.wiley.com/doi/abs/10.1002/grl.50390> (_eprint: <https://onlinelibrary.wiley.com/doi/pdf/10.1002/grl.50390>) doi: 10.1002/grl.50390
- Dai, M., Su, J., Zhao, Y., Hofmann, E. E., Cao, Z., Cai, W.-J., ... Wang, Z. (2022). Carbon Fluxes in the Coastal Ocean: Synthesis, Boundary Processes, and Future Trends. *Annual Review of Earth and Planetary Sciences*, 50(1), 593–626. Retrieved 2022-09-26, from <https://doi.org/10.1146/annurev-earth-032320-090746> (_eprint: <https://doi.org/10.1146/annurev-earth-032320-090746>) doi: 10.1146/annurev-earth-032320-090746
- Damien, P., Bianchi, D., McWilliams, J. C., Kessouri, F., Deutsch, C., Chen, R., & Renault, L. (2023). Enhanced Biogeochemical Cycling Along the U.S. West Coast Shelf. *Global Biogeochemical Cycles*, 37(1), e2022GB007572. Retrieved 2023-02-14, from <https://onlinelibrary.wiley.com/doi/abs/10.1029/2022GB007572> (_eprint: <https://onlinelibrary.wiley.com/doi/pdf/10.1029/2022GB007572>) doi: 10.1029/2022GB007572
- Deike, L., & Melville, W. K. (2018). Gas Transfer by Breaking Waves. *Geophysical Research Letters*, 45(19), 10,482–10,492. Retrieved 2021-11-15, from <https://onlinelibrary.wiley.com/doi/abs/10.1029/2018GL078758> (_eprint: <https://onlinelibrary.wiley.com/doi/pdf/10.1029/2018GL078758>) doi: 10.1029/2018GL078758
- Desmet, F., Gruber, N., Köhn, E. E., Münnich, M., & Vogt, M. (2022, May). Tracking the Space-Time Evolution of Ocean Acidification Extremes in the California Current System and Northeast Pacific. *Journal of Geophysical Research:*

- Oceans, 127(5). Retrieved 2023-03-27, from <https://onlinelibrary.wiley.com/doi/10.1029/2021JC018159> doi: 10.1029/2021JC018159
- Doney, S. C., Lima, I., Feely, R. A., Glover, D. M., Lindsay, K., Mahowald, N., ... Wanninkhof, R. (2009, April). Mechanisms governing interannual variability in upper-ocean inorganic carbon system and air-sea CO₂ fluxes: Physical climate and atmospheric dust. *Deep Sea Research Part II: Topical Studies in Oceanography*, 56(8-10), 640–655. Retrieved 2018-09-13, from <http://linkinghub.elsevier.com/retrieve/pii/S096706450800427X> doi: 10.1016/j.dsr2.2008.12.006
- Egger, M., Lenstra, W., Jong, D., Meysman, F. J. R., Sapart, C. J., van der Veen, C., ... Slomp, C. P. (2016, August). Rapid Sediment Accumulation Results in High Methane Effluxes from Coastal Sediments. *PLoS ONE*, 11(8), e0161609. Retrieved 2023-03-22, from <https://www.ncbi.nlm.nih.gov/pmc/articles/PMC4999275/> doi: 10.1371/journal.pone.0161609
- Elsig, J., Schmitt, J., Leuenberger, D., Schneider, R., Eyer, M., Leuenberger, M., ... Stocker, T. F. (2009, September). Stable isotope constraints on Holocene carbon cycle changes from an Antarctic ice core. *Nature*, 461(7263), 507–510. Retrieved 2023-03-27, from <https://www.nature.com/articles/nature08393> (Number: 7263 Publisher: Nature Publishing Group) doi: 10.1038/nature08393
- Etiope, G., Ciotoli, G., Schwietzke, S., & Schoell, M. (2019, January). Gridded maps of geological methane emissions and their isotopic signature. *Earth System Science Data*, 11(1), 1–22. Retrieved 2023-03-27, from <https://essd.copernicus.org/articles/11/1/2019/> (Publisher: Copernicus GmbH) doi: 10.5194/essd-11-1-2019
- Fennel, K., Alin, S., Barbero, L., Evans, W., Bourgeois, T., Cooley, S., ... Wang, Z. A. (2019, March). Carbon cycling in the North American coastal ocean: a synthesis. *Biogeosciences*, 16(6), 1281–1304. Retrieved 2023-02-14, from <https://bg.copernicus.org/articles/16/1281/2019/> doi: 10.5194/bg-16-1281-2019
- Fennel, K., & Testa, J. M. (2019, January). Biogeochemical Controls on Coastal Hypoxia. *Annual Review of Marine Science*, 11(1), 105–130. Retrieved 2020-09-08, from <http://www.annualreviews.org/doi/10.1146/annurev-marine-010318-095138> (Publisher: Annual Reviews) doi: 10.1146/annurev-marine-010318-095138
- Fennel, K., & Wilkin, J. (2009, September). Quantifying biological carbon export for the northwest North Atlantic continental shelves. *Geophysical Research Letters*, 36(18), L18605. Retrieved 2023-02-15, from <http://doi.wiley.com/10.1029/2009GL039818> doi: 10.1029/2009GL039818
- Fiechter, J., Curchitser, E. N., Edwards, C. A., Chai, F., Goebel, N. L., & Chavez, F. P. (2014). Air-sea CO₂ fluxes in the California Current: Impacts of model resolution and coastal topography. *Global Biogeochemical Cycles*, 28(4), 371–385. Retrieved 2023-02-28, from <https://onlinelibrary.wiley.com/doi/abs/10.1002/2013GB004683> (eprint: <https://onlinelibrary.wiley.com/doi/pdf/10.1002/2013GB004683>) doi: 10.1002/2013GB004683
- Friedlingstein, P., O’Sullivan, M., Jones, M. W., Andrew, R. M., Gregor, L., Hauck, J., ... Zheng, B. (2022). Global Carbon Budget 2022. *Earth System Science Data*, 14(11), 4811–4900. Retrieved from <https://essd.copernicus.org/articles/14/4811/2022/> doi: 10.5194/essd-14-4811-2022
- Ganesan, A. L., Manizza, M., Morgan, E. J., Harth, C. M., Kozlova, E., Lueker, T., ... Rigby, M. (2020, July). Marine Nitrous Oxide Emissions From Three Eastern Boundary Upwelling Systems Inferred From Atmospheric Observations. *Geophysical Research Letters*, 47(14). Retrieved 2023-02-15, from <https://onlinelibrary.wiley.com/doi/10.1029/2020GL087822> doi:

- 10.1029/2020GL087822
- Gao, S., Schwinger, J., Tjiputra, J., Bethke, I., Hartmann, J., Mayorga, E., & Heinze, C. (2023, January). Riverine impact on future projections of marine primary production and carbon uptake. *Biogeosciences*, 20(1), 93–119. Retrieved 2023-02-23, from <https://bg.copernicus.org/articles/20/93/2023/> (Publisher: Copernicus GmbH) doi: 10.5194/bg-20-93-2023
- Garbe, C. S., Rutgersson, A., Boutin, J., de Leeuw, G., Delille, B., Fairall, C. W., ... Zappa, C. J. (2014). Transfer Across the Air-Sea Interface. In P. S. Liss & M. T. Johnson (Eds.), *Ocean-Atmosphere Interactions of Gases and Particles* (pp. 55–112). Berlin, Heidelberg: Springer. Retrieved 2023-02-14, from https://doi.org/10.1007/978-3-642-25643-1_2 doi: 10.1007/978-3-642-25643-1_2
- Gomez, F. A., Wanninkhof, R., Barbero, L., Lee, S.-K., & Hernandez Jr., F. J. (2020, March). Seasonal patterns of surface inorganic carbon system variables in the Gulf of Mexico inferred from a regional high-resolution ocean biogeochemical model. *Biogeosciences*, 17(6), 1685–1700. Retrieved 2023-02-14, from <https://bg.copernicus.org/articles/17/1685/2020/> doi: 10.5194/bg-17-1685-2020
- Grundle, D. S., Löscher, C. R., Krahmann, G., Altabet, M. A., Bange, H. W., Karstensen, J., ... Fiedler, B. (2017, July). Low oxygen eddies in the eastern tropical North Atlantic: Implications for N₂O cycling. *Scientific Reports*, 7(1), 4806. Retrieved 2023-02-14, from <https://www.nature.com/articles/s41598-017-04745-y> doi: 10.1038/s41598-017-04745-y
- Gustafsson, E., Hagens, M., Sun, X., Reed, D. C., Humborg, C., Slomp, C. P., & Gustafsson, B. G. (2019, January). Sedimentary alkalinity generation and long-term alkalinity development in the Baltic Sea. *Biogeosciences*, 16(2), 437–456. Retrieved 2023-02-14, from <https://bg.copernicus.org/articles/16/437/2019/> doi: 10.5194/bg-16-437-2019
- Gutiérrez-Loza, L., Nilsson, E., Wallin, M. B., Sahlée, E., & Rutgersson, A. (2022, December). On physical mechanisms enhancing air-sea CO₂ exchange. *Biogeosciences*, 19(24), 5645–5665. Retrieved 2023-03-22, from <https://bg.copernicus.org/articles/19/5645/2022/> doi: 10.5194/bg-19-5645-2022
- Gülzow, W., Rehder, G., Schneider v. Deimling, J., Seifert, T., & Tóth, Z. (2013, January). One year of continuous measurements constraining methane emissions from the Baltic Sea to the atmosphere using a ship of opportunity. *Biogeosciences*, 10(1), 81–99. Retrieved 2023-02-14, from <https://bg.copernicus.org/articles/10/81/2013/> doi: 10.5194/bg-10-81-2013
- Hauck, J., Zeising, M., Le Quéré, C., Gruber, N., Bakker, D. C. E., Bopp, L., ... Séférián, R. (2020). Consistency and Challenges in the Ocean Carbon Sink Estimate for the Global Carbon Budget. *Frontiers in Marine Science*, 7. Retrieved 2020-12-18, from <https://www.frontiersin.org/articles/10.3389/fmars.2020.571720/full> (Publisher: Frontiers) doi: 10.3389/fmars.2020.571720
- Hauri, C., Pagès, R., McDonnell, A. M. P., Stuecker, M. F., Danielson, S. L., Hedstrom, K., ... Doney, S. C. (2021, September). Modulation of ocean acidification by decadal climate variability in the Gulf of Alaska. *Communications Earth & Environment*, 2(1), 191. Retrieved 2023-02-14, from <https://www.nature.com/articles/s43247-021-00254-z> doi: 10.1038/s43247-021-00254-z
- Hilt, S., Grossart, H., McGinnis, D. F., & Keppler, F. (2022, November). Potential role of submerged macrophytes for oxic methane production in aquatic ecosystems. *Limnology and Oceanography*, 67(S2). Retrieved 2023-02-20, from <https://onlinelibrary.wiley.com/doi/10.1002/lno.12095> doi: 10.1002/lno.12095

- Ho, D. T., Law, C. S., Smith, M. J., Schlosser, P., Harvey, M., & Hill, P. (2006). Measurements of air-sea gas exchange at high wind speeds in the Southern Ocean: Implications for global parameterizations. *Geophysical Research Letters*, *33*(16). Retrieved 2019-06-25, from <https://agupubs.onlinelibrary.wiley.com/doi/abs/10.1029/2006GL026817> doi: 10.1029/2006GL026817
- Ho, D. T., Wanninkhof, R., Schlosser, P., Ullman, D. S., Hebert, D., & Sullivan, K. F. (2011, July). Toward a universal relationship between wind speed and gas exchange: Gas transfer velocities measured with $^3\text{He}/\text{SF}_6$ during the Southern Ocean Gas Exchange Experiment. *Journal of Geophysical Research*, *116*, C00F04. Retrieved 2023-02-15, from <http://doi.wiley.com/10.1029/2010JC006854> doi: 10.1029/2010JC006854
- Hovland, M., Judd, A., & Burke, R. (1993, January). The global flux of methane from shallow submarine sediments. *Chemosphere*, *26*(1-4), 559–578. Retrieved 2023-02-23, from <https://linkinghub.elsevier.com/retrieve/pii/0045653593904428> doi: 10.1016/0045-6535(93)90442-8
- Ilyina, T., Six, K. D., Segschneider, J., Maier-Reimer, E., Li, H., & Núñez-Riboni, I. (2013, June). Global ocean biogeochemistry model HAMOCC: Model architecture and performance as component of the MPI-Earth system model in different CMIP5 experimental realizations. *Journal of Advances in Modeling Earth Systems*, *5*(2), 287–315. Retrieved 2023-02-15, from <https://onlinelibrary.wiley.com/doi/10.1029/2012MS000178> doi: 10.1029/2012MS000178
- Joung, D., Leonte, M., Valentine, D. L., Sparrow, K. J., Weber, T., & Kessler, J. D. (2020, October). Radiocarbon in Marine Methane Reveals Patchy Impact of Seeps on Surface Waters. *Geophysical Research Letters*, *47*(20). Retrieved 2023-03-27, from <https://onlinelibrary.wiley.com/doi/10.1029/2020GL089516> doi: 10.1029/2020GL089516
- Joung, D., Ruppel, C., Southon, J., Weber, T. S., & Kessler, J. D. (2022, November). Negligible atmospheric release of methane from decomposing hydrates in mid-latitude oceans. *Nature Geoscience*, *15*(11), 885–891. Retrieved 2023-03-27, from <https://www.nature.com/articles/s41561-022-01044-8> doi: 10.1038/s41561-022-01044-8
- Karl, D. M., Beversdorf, L., Björkman, K. M., Church, M. J., Martinez, A., & Delong, E. F. (2008, July). Aerobic production of methane in the sea. *Nature Geoscience*, *1*(7), 473–478. Retrieved 2023-03-27, from <https://www.nature.com/articles/ngeo234> (Number: 7 Publisher: Nature Publishing Group) doi: 10.1038/ngeo234
- Kock, A., & Bange, H. (2015, February). Counting the Ocean’s Greenhouse Gas Emissions. *Eos*, *96*. Retrieved 2023-02-14, from <https://eos.org/project-updates/counting-oceans-greenhouse-gas-emissions> doi: 10.1029/2015EO023665
- Kock, A., Schafstall, J., Dengler, M., Brandt, P., & Bange, H. W. (2012, March). Sea-to-air and diapycnal nitrous oxide fluxes in the eastern tropical North Atlantic Ocean. *Biogeosciences*, *9*(3), 957–964. Retrieved 2023-02-14, from <https://bg.copernicus.org/articles/9/957/2012/> (Publisher: Copernicus GmbH) doi: 10.5194/bg-9-957-2012
- Lachkar, Z., & Gruber, N. (2013, January). Response of biological production and air-sea CO₂ fluxes to upwelling intensification in the California and Canary Current Systems. *Journal of Marine Systems*, *109–110*, 149–160. Retrieved 2023-02-15, from <https://www.sciencedirect.com/science/article/pii/S092479631200108X> doi: 10.1016/j.jmarsys.2012.04.003
- Lachkar, Z., Mehari, M., Al Azhar, M., Lévy, M., & Smith, S. (2021, October). Fast local warming is the main driver of recent deoxygenation in the northern Arabian Sea. *Biogeosciences*, *18*(20), 5831–5849. Retrieved 2023-02-15, from <https://bg.copernicus.org/articles/18/5831/2021/> doi:

- 10.5194/bg-18-5831-2021
- Lacroix, F., Ilyina, T., & Hartmann, J. (2020, January). Oceanic CO₂ outgassing and biological production hotspots induced by pre-industrial river loads of nutrients and carbon in a global modeling approach. *Biogeosciences*, 17(1), 55–88. Retrieved 2020-05-05, from <https://www.biogeosciences.net/17/55/2020/> doi: <https://doi.org/10.5194/bg-17-55-2020>
- Lacroix, F., Ilyina, T., Laruelle, G. G., & Regnier, P. (2021). Reconstructing the Preindustrial Coastal Carbon Cycle Through a Global Ocean Circulation Model: Was the Global Continental Shelf Already Both Autotrophic and a CO₂ Sink? *Global Biogeochemical Cycles*, 35(2), e2020GB006603. Retrieved 2021-09-03, from <https://agupubs.onlinelibrary.wiley.com/doi/abs/10.1029/2020GB006603> doi: 10.1029/2020GB006603
- Landschützer, P., Gruber, N., Bakker, D. C. E., & Schuster, U. (2014, September). Recent variability of the global ocean carbon sink. *Global Biogeochemical Cycles*, 28(9), 927–949. Retrieved 2015-08-11, from <http://onlinelibrary.wiley.com/doi/10.1002/2014GB004853/abstract> doi: 10.1002/2014GB004853
- Landschützer, P., Laruelle, G. G., Roobaert, A., & Regnier, P. (2020, October). A uniform pCO₂ climatology combining open and coastal oceans. *Earth System Science Data*, 12(4), 2537–2553. Retrieved 2023-02-14, from <https://essd.copernicus.org/articles/12/2537/2020/> doi: 10.5194/essd-12-2537-2020
- Laruelle, G. G., Cai, W.-J., Hu, X., Gruber, N., Mackenzie, F. T., & Regnier, P. (2018, January). Continental shelves as a variable but increasing global sink for atmospheric carbon dioxide. *Nature Communications*, 9, 454. Retrieved 2021-09-03, from <https://www.ncbi.nlm.nih.gov/pmc/articles/PMC5792465/> doi: 10.1038/s41467-017-02738-z
- Laruelle, G. G., Dürr, H. H., Lauerwald, R., Hartmann, J., Slomp, C. P., Goossens, N., & Regnier, P. A. G. (2013, May). Global multi-scale segmentation of continental and coastal waters from the watersheds to the continental margins. *Hydrology and Earth System Sciences*, 17(5), 2029–2051. Retrieved 2020-03-27, from <https://www.hydrol-earth-syst-sci.net/17/2029/2013/> doi: 10.5194/hess-17-2029-2013
- Laruelle, G. G., Dürr, H. H., Slomp, C. P., & Borges, A. V. (2010). Evaluation of sinks and sources of CO₂ in the global coastal ocean using a spatially-explicit typology of estuaries and continental shelves. *Geophysical Research Letters*, 37(15). Retrieved 2021-09-03, from <https://agupubs.onlinelibrary.wiley.com/doi/abs/10.1029/2010GL043691> (eprint: <https://agupubs.onlinelibrary.wiley.com/doi/pdf/10.1029/2010GL043691>) doi: 10.1029/2010GL043691
- Laruelle, G. G., Landschützer, P., Gruber, N., Tison, J.-L., Delille, B., & Regnier, P. (2017, October). Global high-resolution monthly pCO₂ climatology for the coastal ocean derived from neural network interpolation. *Biogeosciences*, 14(19), 4545–4561. Retrieved 2019-08-29, from <https://www.biogeosciences.net/14/4545/2017/> doi: 10.5194/bg-14-4545-2017
- Laruelle, G. G., Lauerwald, R., Pfeil, B., & Regnier, P. (2014). Regionalized global budget of the CO₂ exchange at the air–water interface in continental shelf seas. *Global Biogeochemical Cycles*, 28(11), 1199–1214. Retrieved 2021-09-03, from <https://agupubs.onlinelibrary.wiley.com/doi/abs/10.1002/2014GB004832> doi: 10.1002/2014GB004832
- Laruelle, G. G., Lauerwald, R., Rotschi, J., Raymond, P. A., Hartmann, J., & Regnier, P. (2015, March). Seasonal response of air–water CO₂ exchange along the land–ocean aquatic continuum of the northeast North American coast. *Biogeosciences*, 12(5), 1447–1458. Retrieved 2023-02-14, from <https://bg.copernicus.org/articles/12/1447/>

- 2015/ doi: 10.5194/bg-12-1447-2015
- Laurent, A., Fennel, K., Cai, W., Huang, W., Barbero, L., & Wanninkhof, R. (2017, January). Eutrophication-induced acidification of coastal waters in the northern Gulf of Mexico: Insights into origin and processes from a coupled physical-biogeochemical model. *Geophysical Research Letters*, 44(2), 946–956. Retrieved 2023-02-15, from <https://onlinelibrary.wiley.com/doi/abs/10.1002/2016GL071881> doi: 10.1002/2016GL071881
- Laurent, A., Fennel, K., & Kuhn, A. (2021, March). An observation-based evaluation and ranking of historical Earth system model simulations in the northwest North Atlantic Ocean. *Biogeosciences*, 18(5), 1803–1822. Retrieved 2023-02-15, from <https://bg.copernicus.org/articles/18/1803/2021/> doi: 10.5194/bg-18-1803-2021
- Legge, O., Johnson, M., Hicks, N., Jickells, T., Diesing, M., Aldridge, J., ... Williamson, P. (2020, March). Carbon on the Northwest European Shelf: Contemporary Budget and Future Influences. *Frontiers in Marine Science*, 7, 143. Retrieved 2023-02-14, from <https://www.frontiersin.org/article/10.3389/fmars.2020.00143/full> doi: 10.3389/fmars.2020.00143
- Le Quéré, C. L., Andrew, R. M., Friedlingstein, P., Sitch, S., Pongratz, J., Manning, A. C., ... Zhu, D. (2018, March). Global Carbon Budget 2017. *Earth System Science Data*, 10(1), 405–448. Retrieved 2018-03-21, from <https://www.earth-syst-sci-data.net/10/405/2018/> doi: <https://doi.org/10.5194/essd-10-405-2018>
- Liang, J.-H., Deutsch, C., McWilliams, J. C., Baschek, B., Sullivan, P. P., & Chiba, D. (2013). Parameterizing bubble-mediated air-sea gas exchange and its effect on ocean ventilation. *Global Biogeochemical Cycles*, 27(3), 894–905. Retrieved 2023-02-14, from <https://onlinelibrary.wiley.com/doi/abs/10.1002/gbc.20080> doi: 10.1002/gbc.20080
- Liao, E., Resplandy, L., Liu, J., & Bowman, K. W. (2020). Amplification of the Ocean Carbon Sink During El Niños: Role of Poleward Ekman Transport and Influence on Atmospheric CO₂. *Global Biogeochemical Cycles*, 34(9), e2020GB006574. Retrieved 2020-10-15, from <http://agupubs.onlinelibrary.wiley.com/doi/abs/10.1029/2020GB006574> doi: 10.1029/2020GB006574
- Liu, Q., Guo, X., Yin, Z., Zhou, K., Roberts, E. G., & Dai, M. (2018, November). Carbon fluxes in the China Seas: An overview and perspective. *Science China Earth Sciences*, 61(11), 1564–1582. Retrieved 2023-02-14, from <http://link.springer.com/10.1007/s11430-017-9267-4> doi: 10.1007/s11430-017-9267-4
- Louchard, D., Gruber, N., & Münnich, M. (2021). The Impact of the Amazon on the Biological Pump and the Air-Sea CO₂ Balance of the Western Tropical Atlantic. *Global Biogeochemical Cycles*, 35(6), e2020GB006818. Retrieved 2021-09-22, from <https://onlinelibrary.wiley.com/doi/abs/10.1029/2020GB006818> doi: 10.1029/2020GB006818
- Mackenzie, F., Lerman, A., & Ver, L. (1998, May). Role of the continental margin in the global carbon balance during the past three centuries. *Geology*, 26. doi: 10.1130/0091-7613(1998)026<0423:ROTCMI>2.3.CO;2
- Mackenzie, F. T., Andersson, A. J., Lerman, A., & Ver, L. M. (2005). Boundary Exchanges in the Global Coastal Margin: Implications for the Organic and Inorganic Carbon Cycles. In *The Sea vol. 13* (pp. 193–225). (Eds Robinson, A. R. & Brink, K. H.) Harvard Univ. Press.
- Manizza, M., Menemenlis, D., Zhang, H., & Miller, C. E. (2019). Modeling the Recent Changes in the Arctic Ocean CO₂ Sink (2006–2013). *Global Biogeochemical Cycles*, 33(3), 420–438. Retrieved 2023-02-15, from <https://onlinelibrary.wiley.com/doi/abs/10.1029/2018GB006070> doi: 10.1029/2018GB006070
- Mao, S.-H., Zhang, H.-H., Zhuang, G.-C., Li, X.-J., Liu, Q., Zhou, Z., ... Yang, G.-

- P. (2022, November). Aerobic oxidation of methane significantly reduces global diffusive methane emissions from shallow marine waters. *Nature Communications*, 13(1), 7309. doi: 10.1038/s41467-022-35082-y
- Mathis, M., Logemann, K., Maerz, J., Lacroix, F., Hagemann, S., Chegini, F., ... Schrum, C. (2022). Seamless integration of the coastal ocean in global marine carbon cycle modeling. *Journal of Advances in Modeling Earth Systems*, n/a(n/a), e2021MS002789. Retrieved 2022-08-22, from <https://onlinelibrary.wiley.com/doi/abs/10.1029/2021MS002789> doi: 10.1029/2021MS002789
- Mayer, B., Rixen, T., & Pohlmann, T. (2018). The Spatial and Temporal Variability of Air-Sea CO₂ Fluxes and the Effect of Net Coral Reef Calcification in the Indonesian Seas: A Numerical Sensitivity Study. *Frontiers in Marine Science*, 5. Retrieved 2023-02-14, from <https://www.frontiersin.org/articles/10.3389/fmars.2018.00116>
- McGinnis, D. F., Greinert, J., Artemov, Y., Beaubien, S. E., & Wüest, A. (2006). Fate of rising methane bubbles in stratified waters: How much methane reaches the atmosphere? *Journal of Geophysical Research*, 111(C9), C09007. Retrieved 2023-02-23, from <http://doi.wiley.com/10.1029/2005JC003183> doi: 10.1029/2005JC003183
- Neumann, T., Radtke, H., Cahill, B., Schmidt, M., & Rehder, G. (2022, November). Non-Redfieldian carbon model for the Baltic Sea (ERGOM version 1.2) – implementation and budget estimates. *Geoscientific Model Development*, 15(22), 8473–8540. Retrieved 2023-02-14, from <https://gmd.copernicus.org/articles/15/8473/2022/> doi: 10.5194/gmd-15-8473-2022
- Nightingale, P. D., Malin, G., Law, C. S., Watson, A. J., Liss, P. S., Liddicoat, M. I., ... Upstill-Goddard, R. C. (2000, March). In situ evaluation of air-sea gas exchange parameterizations using novel conservative and volatile tracers. *Global Biogeochemical Cycles*, 14(1), 373–387. Retrieved 2023-02-15, from <http://doi.wiley.com/10.1029/1999GB900091> doi: 10.1029/1999GB900091
- Ouyang, Z., Collins, A., Li, Y., Qi, D., Arrigo, K. R., Zhuang, Y., ... Cai, W. (2022, August). Seasonal Water Mass Evolution and Non-Redfield Dynamics Enhance CO₂ Uptake in the Chukchi Sea. *Journal of Geophysical Research: Oceans*, 127(8). Retrieved 2023-02-14, from <https://onlinelibrary.wiley.com/doi/10.1029/2021JC018326> doi: 10.1029/2021JC018326
- Ouyang, Z., Sciusco, P., Jiao, T., Feron, S., Lei, C., Li, F., ... Chen, J. (2022, July). Albedo changes caused by future urbanization contribute to global warming. *Nature Communications*, 13(1), 3800. Retrieved 2022-10-27, from <https://www.nature.com/articles/s41467-022-31558-z> (Number: 1 Publisher: Nature Publishing Group) doi: 10.1038/s41467-022-31558-z
- Pereira, R., Ashton, I., Sabbaghzadeh, B., Shutler, J. D., & Upstill-Goddard, R. C. (2018, July). Reduced air–sea CO₂ exchange in the Atlantic Ocean due to biological surfactants. *Nature Geoscience*, 11(7), 492–496. Retrieved 2023-03-22, from <http://www.nature.com/articles/s41561-018-0136-2> doi: 10.1038/s41561-018-0136-2
- Pipko, I. I., Pugach, S. P., Luchin, V. A., Francis, O. P., Savelieva, N. I., Charkin, A. N., ... Semiletov, I. P. (2021, March). Surface CO₂ system dynamics in the Gulf of Anadyr during the open water season. *Continental Shelf Research*, 217, 104371. Retrieved 2023-02-14, from <https://www.sciencedirect.com/science/article/pii/S0278434321000285> doi: 10.1016/j.csr.2021.104371
- Pipko, I. I., Pugach, S. P., Semiletov, I. P., Anderson, L. G., Shakhova, N. E., Gustafsson, , ... Dudarev, O. V. (2017, November). The spatial and interannual dynamics of the surface water carbonate system and air–sea CO₂ fluxes in the outer shelf and slope of the Eurasian Arctic Ocean. *Ocean Science*, 13(6), 997–1016. Retrieved 2023-

- 02-14, from <https://os.copernicus.org/articles/13/997/2017/> doi: 10.5194/os-13-997-2017
- Previdi, M., Fennel, K., Wilkin, J., & Haidvogel, D. (2009, October). Interannual variability in atmospheric CO₂ uptake on the northeast U.S. continental shelf. *Journal of Geophysical Research*, 114(G4), G04003. Retrieved 2023-03-23, from <http://doi.wiley.com/10.1029/2008JG000881> doi: 10.1029/2008JG000881
- Puglini, M., Brovkin, V., Regnier, P., & Arndt, S. (2020, June). Assessing the potential for non-turbulent methane escape from the East Siberian Arctic Shelf. *Biogeosciences*, 17(12), 3247–3275. Retrieved 2023-02-27, from <https://bg.copernicus.org/articles/17/3247/2020/> doi: 10.5194/bg-17-3247-2020
- Reeburgh, W. S. (2007, February). Oceanic Methane Biogeochemistry. *Chemical Reviews*, 107(2), 486–513. Retrieved 2023-03-27, from <https://pubs.acs.org/doi/10.1021/cr050362v> doi: 10.1021/cr050362v
- Rees, A. P., Bange, H. W., Arévalo-Martínez, D. L., Artioli, Y., Ashby, D. M., Brown, I., ... Turley, C. (2022, February). Nitrous oxide and methane in a changing Arctic Ocean. *Ambio*, 51(2), 398–410. Retrieved 2023-03-22, from <https://www.ncbi.nlm.nih.gov/pmc/articles/PMC8692636/> doi: 10.1007/s13280-021-01633-8
- Regnier, P., Friedlingstein, P., Ciais, P., Mackenzie, F. T., Gruber, N., Janssens, I. A., ... Thullner, M. (2013, June). Anthropogenic perturbation of the carbon fluxes from land to ocean. *Nature Geoscience*, 6(8), 597–607. Retrieved 2015-06-25, from <http://www.nature.com/doifinder/10.1038/ngeo1830> doi: 10.1038/ngeo1830
- Regnier, P., Resplandy, L., Najjar, R. G., & Ciais, P. (2022, March). The land-to-ocean loops of the global carbon cycle. *Nature*, 603(7901), 401–410. Retrieved 2022-04-18, from <https://www.nature.com/articles/s41586-021-04339-9> doi: 10.1038/s41586-021-04339-9
- Rehder, G., Keir, R. S., Suess, E., & Pohlmann, T. (1998, September). The Multiple Sources and Patterns of Methane in North Sea Waters. *Aquatic Geochemistry*, 4(3), 403–427. Retrieved 2023-02-14, from <https://doi.org/10.1023/A:1009644600833> doi: 10.1023/A:1009644600833
- Reichl, B. G., & Deike, L. (2020). Contribution of Sea-State Dependent Bubbles to Air-Sea Carbon Dioxide Fluxes. *Geophysical Research Letters*, 47(9), e2020GL087267. Retrieved 2021-10-08, from <https://onlinelibrary.wiley.com/doi/abs/10.1029/2020GL087267> (_eprint: <https://onlinelibrary.wiley.com/doi/pdf/10.1029/2020GL087267>) doi: 10.1029/2020GL087267
- Reimer, J. J., Wang, H., Vargas, R., & Cai, W. (2017, December). Multidecadal f CO₂ Increase Along the United States Southeast Coastal Margin. *Journal of Geophysical Research: Oceans*, 122(12), 10061–10072. Retrieved 2023-03-23, from <https://onlinelibrary.wiley.com/doi/10.1002/2017JC013170> doi: 10.1002/2017JC013170
- Repeta, D. J., Ferrón, S., Sosa, O. A., Johnson, C. G., Repeta, L. D., Acker, M., ... Karl, D. M. (2016, December). Marine methane paradox explained by bacterial degradation of dissolved organic matter. *Nature Geoscience*, 9(12), 884–887. Retrieved 2023-03-27, from <http://www.nature.com/articles/ngeo2837> doi: 10.1038/ngeo2837
- Resplandy, L., Keeling, R. F., Rödenbeck, C., Stephens, B. B., Khatiwala, S., Rodgers, K. B., ... Tans, P. P. (2018). Revision of global carbon fluxes based on a reassessment of oceanic and riverine carbon transport. *Nature Geoscience*, 11, 504–509. Retrieved 2018-06-11, from <https://www.nature.com/articles/s41561-018-0151-3> doi: 10.1038/s41561-018-0151-3
- Reynolds, R. W., Smith, T. M., Liu, C., Chelton, D. B., Casey, K. S., & Schlax,

- M. G. (2007, November). Daily High-Resolution-Blended Analyses for Sea Surface Temperature. *Journal of Climate*, 20(22), 5473–5496. Retrieved 2023-02-15, from <http://journals.ametsoc.org/doi/10.1175/2007JCLI1824.1> doi: 10.1175/2007JCLI1824.1
- Roobaert, A., Laruelle, G. G., Landschützer, P., Gruber, N., Chou, L., & Regnier, P. (2019). The Spatiotemporal Dynamics of the Sources and Sinks of CO₂ in the Global Coastal Ocean. *Global Biogeochemical Cycles*, 33(12), 1693–1714. Retrieved 2020-05-11, from <http://agupubs.onlinelibrary.wiley.com/doi/abs/10.1029/2019GB006239> (eprint: <https://onlinelibrary.wiley.com/doi/pdf/10.1029/2019GB006239>) doi: 10.1029/2019GB006239
- Roobaert, A., Laruelle, G. G., Landschützer, P., & Regnier, P. (2018, March). Uncertainty in the global oceanic CO₂ uptake induced by wind forcing: quantification and spatial analysis. *Biogeosciences*, 15(6), 1701–1720. Retrieved 2023-03-24, from <https://bg.copernicus.org/articles/15/1701/2018/> doi: 10.5194/bg-15-1701-2018
- Roobaert, A., Resplandy, L., Laruelle, G. G., Liao, E., & Regnier, P. (2022, January). A framework to evaluate and elucidate the driving mechanisms of coastal sea surface pCO₂ seasonality using an ocean general circulation model (MOM6-COBALT). *Ocean Science*, 18(1), 67–88. Retrieved 2022-03-17, from <https://os.copernicus.org/articles/18/67/2022/> doi: 10.5194/os-18-67-2022
- Rosentreter, J. A., Borges, A. V., Deemer, B. R., Holgerson, M. A., Liu, S., Song, C., ... Eyre, B. D. (2021, April). Half of global methane emissions come from highly variable aquatic ecosystem sources. *Nature Geoscience*, 14(4), 225–230. Retrieved 2023-02-14, from <http://www.nature.com/articles/s41561-021-00715-2> doi: 10.1038/s41561-021-00715-2
- Rosentreter, J. A., Laruelle, G. G., & et al. (2023). Coastal vegetation and estuaries are collectively a greenhouse gas sink Nature Climate Change, Accepted, 2023. *Accepted in Nature Climate Change*.
- Roth, F., Broman, E., Sun, X., Bonaglia, S., Nascimento, F., Prytherch, J., ... Norkko, A. (2023, January). Methane emissions offset atmospheric carbon dioxide uptake in coastal macroalgae, mixed vegetation and sediment ecosystems. *Nature Communications*, 14(1), 42. Retrieved 2023-02-20, from <https://www.nature.com/articles/s41467-022-35673-9> (Number: 1 Publisher: Nature Publishing Group) doi: 10.1038/s41467-022-35673-9
- Royer, S.-J., Ferrón, S., Wilson, S. T., & Karl, D. M. (2018, August). Production of methane and ethylene from plastic in the environment. *PLOS ONE*, 13(8), e0200574. Retrieved 2023-02-14, from <https://dx.plos.org/10.1371/journal.pone.0200574> doi: 10.1371/journal.pone.0200574
- Ruppel, C. D., & Kessler, J. D. (2017, March). The interaction of climate change and methane hydrates. *Reviews of Geophysics*, 55(1), 126–168. Retrieved 2023-03-27, from <https://onlinelibrary.wiley.com/doi/10.1002/2016RG000534> doi: 10.1002/2016RG000534
- Rutherford, K., & Fennel, K. (2018, October). Diagnosing transit times on the northwestern North Atlantic continental shelf. *Ocean Science*, 14(5), 1207–1221. Retrieved 2023-02-15, from <https://os.copernicus.org/articles/14/1207/2018/> doi: 10.5194/os-14-1207-2018
- Rutherford, K., & Fennel, K. (2022, March). Elucidating Coastal Ocean Carbon Transport Processes: A Novel Approach Applied to the Northwest North Atlantic Shelf. *Geophysical Research Letters*, 49(6). Retrieved 2022-09-13, from <https://onlinelibrary.wiley.com/doi/10.1029/2021GL097614> doi: 10.1029/2021GL097614
- Rutherford, K., Fennel, K., Atamanchuk, D., Wallace, D., & Thomas, H. (2021, December). A modelling study of temporal and spatial pCO₂ variability on the

- biologically active and temperature-dominated Scotian Shelf. *Biogeosciences*, 18(23), 6271–6286. Retrieved 2023-02-15, from <https://bg.copernicus.org/articles/18/6271/2021/> (Publisher: Copernicus GmbH) doi: 10.5194/bg-18-6271-2021
- Rödenbeck, C., DeVries, T., Hauck, J., Le Quéré, C., & Keeling, R. F. (2022, May). Data-based estimates of interannual sea–air CO₂ flux variations 1957–2020 and their relation to environmental drivers. *Biogeosciences*, 19(10), 2627–2652. Retrieved 2023-03-24, from <https://bg.copernicus.org/articles/19/2627/2022/> (Publisher: Copernicus GmbH) doi: 10.5194/bg-19-2627-2022
- Salisbury, J. E., & Jönsson, B. F. (2018, December). Rapid warming and salinity changes in the Gulf of Maine alter surface ocean carbonate parameters and hide ocean acidification. *Biogeochemistry*, 141(3), 401–418. Retrieved 2023-03-27, from <http://link.springer.com/10.1007/s10533-018-0505-3> doi: 10.1007/s10533-018-0505-3
- Saunio, M., Stavert, A. R., Poulter, B., Bousquet, P., Canadell, J. G., Jackson, R. B., ... Zhuang, Q. (2020, July). The Global Methane Budget 2000–2017. *Earth System Science Data*, 12(3), 1561–1623. Retrieved 2023-02-14, from <https://essd.copernicus.org/articles/12/1561/2020/> doi: 10.5194/essd-12-1561-2020
- Schmale, O., Wäge, J., Mohrholz, V., Wasmund, N., Gräwe, U., Rehder, G., ... Loick-Wilde, N. (2018, January). The contribution of zooplankton to methane supersaturation in the oxygenated upper waters of the central Baltic Sea: Methane supersaturation in the Baltic Sea. *Limnology and Oceanography*, 63(1), 412–430. Retrieved 2023-02-20, from <https://onlinelibrary.wiley.com/doi/10.1002/lno.10640> doi: 10.1002/lno.10640
- Schneider, B., & Müller, J. D. (2018). *Biogeochemical Transformations in the Baltic Sea*. Cham: Springer International Publishing. Retrieved 2023-02-14, from <http://link.springer.com/10.1007/978-3-319-61699-5> doi: 10.1007/978-3-319-61699-5
- Seitzinger, S. P., & Kroeze, C. (1998). Global distribution of nitrous oxide production and N inputs in freshwater and coastal marine ecosystems. *Global Biogeochemical Cycles*, 12(1), 93–113. Retrieved 2023-02-14, from <https://onlinelibrary.wiley.com/doi/abs/10.1029/97GB03657> (_eprint: <https://onlinelibrary.wiley.com/doi/pdf/10.1029/97GB03657>) doi: 10.1029/97GB03657
- Siegel, D. A., Doney, S. C., & Yoder, J. A. (2002, April). The North Atlantic Spring Phytoplankton Bloom and Sverdrup’s Critical Depth Hypothesis. *Science*, 296(5568), 730–733. Retrieved 2023-02-14, from <https://www.science.org/doi/10.1126/science.1069174> doi: 10.1126/science.1069174
- Signorini, S. R., Mannino, A., Najjar, R. G., Friedrichs, M. A. M., Cai, W.-J., Salisbury, J., ... Shadwick, E. (2013, October). Surface ocean *p* CO₂ seasonality and sea-air CO₂ flux estimates for the North American east coast: NORTH AMERICAN EAST COAST SEA-AIR CO₂ FLUXES. *Journal of Geophysical Research: Oceans*, 118(10), 5439–5460. Retrieved 2023-02-14, from <http://doi.wiley.com/10.1002/jgrc.20369> doi: 10.1002/jgrc.20369
- Stell, A. C., Bertolacci, M., Zammit-Mangion, A., Rigby, M., Fraser, P. J., Harth, C. M., ... Ganesan, A. L. (2022, October). Modelling the growth of atmospheric nitrous oxide using a global hierarchical inversion. *Atmospheric Chemistry and Physics*, 22(19), 12945–12960. Retrieved 2022-12-02, from <https://acp.copernicus.org/articles/22/12945/2022/> doi: 10.5194/acp-22-12945-2022
- Su, X., Yang, L., Yang, K., Tang, Y., Wen, T., Wang, Y., ... Zhu, Y.-g. (2022, July). Estuarine plastisphere as an overlooked source of N₂O production. *Nature Communications*, 13(1), 3884. Retrieved 2023-02-14, from

- 1889 <https://www.nature.com/articles/s41467-022-31584-x> (Number: 1
 1890 Publisher: Nature Publishing Group) doi: 10.1038/s41467-022-31584-x
- 1891 Séférian, R., Nabat, P., Michou, M., Saint-Martin, D., Voldoire, A., Colin,
 1892 J., ... Madec, G. (2019). Evaluation of CNRM Earth System
 1893 Model, CNRM-ESM2-1: Role of Earth System Processes in Present-
 1894 Day and Future Climate. *Journal of Advances in Modeling Earth*
 1895 *Systems*, 11(12), 4182–4227. Retrieved 2023-03-01, from [https://](https://onlinelibrary.wiley.com/doi/abs/10.1029/2019MS001791)
 1896 onlinelibrary.wiley.com/doi/abs/10.1029/2019MS001791 (eprint:
 1897 <https://onlinelibrary.wiley.com/doi/pdf/10.1029/2019MS001791>) doi:
 1898 10.1029/2019MS001791
- 1899 Terhaar, J., Lauerwald, R., Regnier, P., Gruber, N., & Bopp, L. (2021, January).
 1900 Around one third of current Arctic Ocean primary production sustained
 1901 by rivers and coastal erosion. *Nature Communications*, 12(1), 169. doi:
 1902 10.1038/s41467-020-20470-z
- 1903 Thomas, H., Bozec, Y., Elkalay, K., & de Baar, H. J. W. (2004, May). Enhanced
 1904 open ocean storage of CO₂ from shelf sea pumping. *Science (New York, N.Y.)*,
 1905 304(5673), 1005–1008. doi: 10.1126/science.1095491
- 1906 Tian, H., Xu, R., Canadell, J. G., Thompson, R. L., Winiwarter, W., Sunthar-
 1907 alingam, P., ... Yao, Y. (2020, October). A comprehensive quantification of
 1908 global nitrous oxide sources and sinks. *Nature*, 586(7828), 248–256. Retrieved
 1909 2023-02-14, from <https://www.nature.com/articles/s41586-020-2780-0>
 1910 doi: 10.1038/s41586-020-2780-0
- 1911 Tjiputra, J. F., Schwinger, J., Bentsen, M., Morée, A. L., Gao, S., Bethke, I., ...
 1912 Schulz, M. (2020, May). Ocean biogeochemistry in the Norwegian Earth Sys-
 1913 tem Model version 2 (NorESM2). *Geoscientific Model Development*, 13(5),
 1914 2393–2431. Retrieved 2023-02-15, from [https://gmd.copernicus.org/](https://gmd.copernicus.org/articles/13/2393/2020/)
 1915 [articles/13/2393/2020/](https://gmd.copernicus.org/articles/13/2393/2020/) (Publisher: Copernicus GmbH) doi: 10.5194/
 1916 gmd-13-2393-2020
- 1917 Tu, Z., Le, C., Bai, Y., Jiang, Z., Wu, Y., Ouyang, Z., ... Qi, D. (2021, August).
 1918 Increase in CO₂ Uptake Capacity in the Arctic Chukchi Sea During Sum-
 1919 mer Revealed by Satellite-Based Estimation. *Geophysical Research Letters*,
 1920 48(15). Retrieved 2023-03-27, from [https://onlinelibrary.wiley.com/doi/](https://onlinelibrary.wiley.com/doi/10.1029/2021GL093844)
 1921 [10.1029/2021GL093844](https://onlinelibrary.wiley.com/doi/10.1029/2021GL093844) doi: 10.1029/2021GL093844
- 1922 Turi, G., Lachkar, Z., & Gruber, N. (2014, February). Spatiotemporal variability
 1923 and drivers of pCO₂ and air–sea CO₂ fluxes in the California Current System:
 1924 an eddy-resolving modeling study. *Biogeosciences*, 11(3), 671–690. Retrieved
 1925 2019-04-02, from <https://www.biogeosciences.net/11/671/2014/> doi:
 1926 10.5194/bg-11-671-2014
- 1927 Wan, X. S., Lin, H., Ward, B. B., Kao, S.-J., & Dai, M. (2022). Sig-
 1928 nificant Seasonal N₂O Dynamics Revealed by Multi-Year Observa-
 1929 tions in the Northern South China Sea. *Global Biogeochemical Cy-*
 1930 *cles*, 36(10), e2022GB007333. Retrieved 2023-02-14, from [https://](https://onlinelibrary.wiley.com/doi/abs/10.1029/2022GB007333)
 1931 onlinelibrary.wiley.com/doi/abs/10.1029/2022GB007333 (eprint:
 1932 <https://onlinelibrary.wiley.com/doi/pdf/10.1029/2022GB007333>) doi:
 1933 10.1029/2022GB007333
- 1934 Wang, H., Hu, X., Cai, W.-J., & Sterba-Boatwright, B. (2017). Decadal fCO₂ trends
 1935 in global ocean margins and adjacent boundary current-influenced areas. *Geo-*
 1936 *physical Research Letters*, 44(17), 8962–8970. Retrieved 2022-04-15, from
 1937 <https://onlinelibrary.wiley.com/doi/abs/10.1002/2017GL074724> doi:
 1938 10.1002/2017GL074724
- 1939 Wanninkhof, R. (1992, May). Relationship between wind speed and gas exchange
 1940 over the ocean. *Journal of Geophysical Research: Oceans*, 97(C5), 7373–7382.
 1941 Retrieved 2015-06-22, from [http://onlinelibrary.wiley.com/doi/10.1029/](http://onlinelibrary.wiley.com/doi/10.1029/92JC00188/abstract)
 1942 [92JC00188/abstract](http://onlinelibrary.wiley.com/doi/10.1029/92JC00188/abstract) doi: 10.1029/92JC00188
- 1943 Wanninkhof, R. (2014, June). Relationship between wind speed and gas exchange

- over the ocean revisited. *Limnology and Oceanography: Methods*, 12(6), 351–362. Retrieved 2015-06-22, from <http://onlinelibrary.wiley.com/doi/10.4319/lom.2014.12.351/abstract> doi: 10.4319/lom.2014.12.351
- Ward, N. D., Megonigal, J. P., Bond-Lamberty, B., Bailey, V. L., Butman, D., Canuel, E. A., ... Windham-Myers, L. (2020, May). Representing the function and sensitivity of coastal interfaces in Earth system models. *Nature Communications*, 11(1), 2458. Retrieved 2023-02-14, from <https://www.nature.com/articles/s41467-020-16236-2> (Number: 1 Publisher: Nature Publishing Group) doi: 10.1038/s41467-020-16236-2
- Weber, T., Wiseman, N. A., & Kock, A. (2019, October). Global ocean methane emissions dominated by shallow coastal waters. *Nature Communications*, 10(1), 4584. Retrieved 2020-10-21, from <https://www.nature.com/articles/s41467-019-12541-7> (Number: 1 Publisher: Nature Publishing Group) doi: 10.1038/s41467-019-12541-7
- Woolf, D., Shutler, J., Goddijn-Murphy, L., Watson, A., Chapron, B., Nightingale, P., ... Paul, F. (2019, December). Key Uncertainties in the Recent Air-Sea Flux of CO₂. *Global Biogeochemical Cycles*, 33(12), 1548–1563. Retrieved 2023-04-03, from <https://onlinelibrary.wiley.com/doi/abs/10.1029/2018GB006041> doi: 10.1029/2018GB006041
- Wright, R. M., Le Quéré, C., Buitenhuis, E., Pitois, S., & Gibbons, M. J. (2021, February). Role of jellyfish in the plankton ecosystem revealed using a global ocean biogeochemical model. *Biogeosciences*, 18(4), 1291–1320. Retrieved 2023-03-27, from <https://bg.copernicus.org/articles/18/1291/2021/> (Publisher: Copernicus GmbH) doi: 10.5194/bg-18-1291-2021
- Xu, Y., Cai, W., Wanninkhof, R., Salisbury, J., Reimer, J., & Chen, B. (2020, July). Long-Term Changes of Carbonate Chemistry Variables Along the North American East Coast. *Journal of Geophysical Research: Oceans*, 125(7). Retrieved 2023-02-14, from <https://onlinelibrary.wiley.com/doi/abs/10.1029/2019JC015982> doi: 10.1029/2019JC015982
- Xue, Z., He, R., Fennel, K., Cai, W.-J., Lohrenz, S., Huang, W.-J., ... Zang, Z. (2016, August). Modeling $p\text{CO}_2$ variability in the Gulf of Mexico. *Biogeosciences*, 13(15), 4359–4377. Retrieved 2023-02-14, from <https://bg.copernicus.org/articles/13/4359/2016/> doi: 10.5194/bg-13-4359-2016
- Yang, S., Chang, B. X., Warner, M. J., Weber, T. S., Bourbonnais, A. M., Santoro, A. E., ... Bianchi, D. (2020, June). Global reconstruction reduces the uncertainty of oceanic nitrous oxide emissions and reveals a vigorous seasonal cycle. *Proceedings of the National Academy of Sciences*, 117(22), 11954–11960. Retrieved 2022-05-12, from <https://www.pnas.org/doi/10.1073/pnas.1921914117> (Publisher: Proceedings of the National Academy of Sciences) doi: 10.1073/pnas.1921914117
- Yukimoto, S., Kawai, H., Koshiro, T., Oshima, N., Yoshida, K., Urakawa, S., ... Ishii, M. (2019). The Meteorological Research Institute Earth System Model Version 2.0, MRI-ESM2.0: Description and Basic Evaluation of the Physical Component. *Journal of the Meteorological Society of Japan. Ser. II*, 97(5), 931–965. Retrieved 2023-02-15, from https://www.jstage.jst.go.jp/article/jmsj/97/5/97_2019-051/_article doi: 10.2151/jmsj.2019-051
- Zhou, J., Zheng, Y., Hou, L., An, Z., Chen, F., Liu, B., ... Liu, M. (2023, March). Effects of acidification on nitrification and associated nitrous oxide emission in estuarine and coastal waters. *Nature Communications*, 14(1), 1380. Retrieved 2023-03-22, from <https://www.nature.com/articles/s41467-023-37104-9> doi: 10.1038/s41467-023-37104-9

Supporting Information for ‘A Synthesis of Global Coastal Ocean Greenhouse Gas Air-sea Fluxes’

L. Resplandy¹, A. Hogikyan², H. W. Bange³, D. Bianchi⁴, T. Weber⁵, Wei-Jun Cai⁶, S.C. Doney⁷, K. Fennel⁸, M. Gehlen⁹, J. Hauck¹⁰, F. Lacroix¹¹, P. Landschützer^{12,13}, C. Le Quéré¹⁴, J. D. Müller¹⁵, R. G. Najjar¹⁶, A. Roobaert¹⁷, J. Schwinger¹⁸, S. Berthet¹⁹, L. Bopp²⁰, T.T.T. Chau⁹, M. Dai²¹, N. Gruber¹⁵, T. Ilyina¹³, A. Kock^{3*}, M. Manizza²², Z. Lachkar²³, G. G. Laruelle¹⁷, E. Liao^{1†}, I.D. Lima²⁴, C. Nissen^{10,25}, C. Rödenbeck²⁶, R. Séférian¹⁹, K. Toyama²⁷, H. Tsujino²⁷, P. Regnier¹⁷

¹Department of Geosciences and High Meadows Environmental Institute, Princeton University, Princeton, NJ, USA

²Atmospheric and Oceanic Sciences Program, Princeton University, Princeton, NJ, USA

³GEOMAR Helmholtz Centre for Ocean Research Kiel, Kiel, Germany

⁴Department of Atmospheric and Oceanic Sciences, University of California Los Angeles, Los Angeles, CA, USA

⁵Department of Earth and Environmental Science, University of Rochester, NY, USA

⁶School of Marine Science and Policy, University of Delaware, Newark, Delaware, 19716, USA

⁷Department of Environmental Sciences, University of Virginia, Charlottesville, VA, USA

⁸Department of Oceanography, Dalhousie University, Halifax, Canada

⁹Laboratoire des Sciences du Climat et de l'Environnement, LSCE/IPSL, CEA-CNRS-UVSQ, Université Paris-Saclay, F-91191 Gif-sur-Yvette, France

¹⁰Alfred-Wegener-Institut, Helmholtz-Zentrum für Polar und Meeresforschung, Germany

¹¹Climate and Environmental Physics / Oeschger Centre for Climate Change Research (OCCR), University of Bern, Switzerland

¹²Flanders Marine Institute (VLIZ), Ostend Belgium

¹³Max Planck Institute for Meteorology, Hamburg, Germany

¹⁴School of Environmental Sciences, University of East Anglia, Norwich Research Park, NR4 7TJ, Norwich, UK

¹⁵Environmental Physics, Institute of Biogeochemistry and Pollutant Dynamics, ETH Zurich, Zürich, Switzerland

¹⁶Department of Meteorology and Atmospheric Science, The Pennsylvania State University, University Park, Pennsylvania, USA

¹⁷Dept. Geoscience, Environment and Society - BGEOSSYS, Université Libre de Bruxelles, Brussels, Belgium

¹⁸NORCE Climate & Environment, Bjerknes Centre for Climate Research, Bergen, Norway

¹⁹CNRM, Université de Toulouse, Météo France, CNRS, Toulouse, France

²⁰LMD/IPSL, ENS, Université PSL, École Polytechnique, Institut Polytechnique de Paris, Sorbonne Université, CNRS, Paris, France

²¹State Key Lab of Marine Environmental Science and College of Ocean and Earth Sciences, Xiamen University, Xiamen 361102, China

²²Geosciences Research Division, Scripps Institution of Oceanography, University of California - San Diego, La Jolla, USA

²³Arabian Center for Climate and Environmental Sciences, New York University Abu Dhabi, Abu Dhabi, United Arab Emirates

²⁴Department of Marine Chemistry and Geochemistry, Woods Hole Oceanographic Institution, Woods Hole, MA, USA

²⁵Department of Atmospheric and Oceanic Sciences and Institute of Arctic and Alpine Research, University of Colorado, Boulder, Colorado, USA

²⁶MPI Biogeochemistry, Jena, Germany

²⁷JMA Meteorological Research Institute, Tsukuba, Ibaraki, Japan

Contents of this file

1. Text S1
2. Figures S1 to S12
3. Tables S1 to S3 (Table S3 provided as separate excel file per AGU requirements)

* now at State Office for the Environment of the State of Schleswig-Holstein, Flintbek, Germany

† now at School of Oceanography, Shanghai Jiao Tong University, Shanghai, 200030, China

Text S1. Observation-based products and models description

S1.a pCO₂-products

CMEMS-LSCE-FFNN (CMEMS)

The CMEMS-LSCE-FFNN product (Chau et al., 2022) referred to here as CMEMS provides estimates of monthly pCO₂ and air-sea CO₂ fluxes over the global coastal ocean at a spatial resolution of 1×1 degree from 1985 to 2018. Main characteristics setting CMEMS-LSCE-FFNN apart from similar approaches are (1) model design, (2) ensemble-based estimates of pCO₂ and air-sea CO₂ fluxes and uncertainty, and (3) consistency of the coastal-ocean reconstruction and the open-ocean reconstruction (Chau et al., 2022). Coastal estimates were evaluated thoroughly from a global scale to ocean basins and at time-series stations. The coastal estimates are part of a global reconstruction of pCO₂ fields based on monthly gridded SOCATv2020 data of CO₂ fugacity covering both the open ocean and the coastal zone (Bakker et al., 2016) (see Figure S1). The reconstruction is based on an ensemble of 100 feed-forward neural networks (FFNN), with two-thirds of SOCAT data used for model training and one third kept for validation of reconstructed pCO₂. The ensemble approach provides space-time varying uncertainty field (ensemble spread) associated with the best pCO₂ and air-sea fluxes' estimates (ensemble mean). These ensemble statistics permit the evaluation of reconstruction uncertainty over coastal regions with sparse data coverage. The seamless reconstruction of pCO₂ and air-sea fluxes over the global coastal and open ocean allows the assessment of gradients and horizontal variability of pCO₂ and air-sea CO₂ fluxes over the continental shelf and to the open ocean. The gas transfer velocity was calculated with 10-m ERA5 wind speed data (Hersbach et al., 2020) following the parameterization by Wanninkhof (2014). A scaling factor is applied such that the global average of kw equals to 16.5 cm h⁻¹ (Naegler, 2009). Air-sea CO₂ fluxes are also scaled proportional to CMEMS-OSTIA sea ice fraction over polar and subpolar regions (S. Good et al., 2020).

Coastal-SOM-FFN

The coastal air-sea CO₂ product (referred here as coastal-SOM-FFN) is based on the continuous coastal pCO₂ product of Laruelle et al. (2017) that used the Self-Organizing Map Feed Forward method developed by Landschützer et al. (2013) but adapted for the coastal ocean to fill region without data. The method in a first step clusters coastal ocean regions into dynamic biogeochemical provinces. In a second step, a non-linear regression step links physical, biological and chemical proxy data with existing CO₂ measurements. The coastal ocean is thereby explicitly reconstructed with coastal-only observations from the SOCATv4 database. The established regression relationship is then used to fill areas where no observations exist (a more detailed description can be found in Landschützer et al. (2013) and Laruelle et al. (2017). The coastal domain defined by Laruelle et al. (2017) excludes estuaries and inland water bodies with an outer limit defined as 300 km away from the shoreline (total surface area of 77 million km²). This pCO₂-product is available as monthly 0.25-degree maps for the 1998-2015 period. The SST, SSS, wind product and sea-ice used to calculate the air-sea CO₂ exchange derived from the daily NOAA OI SST V2 (Reynolds et al., 2007), the daily Hadley center EN4 SSS (S. A. Good et al., 2013), the monthly second moment of the 6-hour 0.25° global atmospheric reanalysis ERA-interim wind product (Dee et al., 2011) and the monthly mean of the daily 0.25° sea-ice dataset of Reynolds et al. (2007), respectively. We use the equation developed by (Ho et al., 2011) to calculate the gas exchange transfer velocity.

Merged-SOM-FFN

The air-sea CO₂ flux product based on Landschützer et al. (2020) (referred here as Merged-SOM-FFN) is built on the combination of the open ocean CO₂ product by Landschützer et al. (2014) using SOCATv5 and the coastal ocean product by Laruelle et al. (2017) using SOCATv4 (referred here as Coastal-SOM-FFN), both created using the Self-Organizing Map Feed Forward Network (SOM-FFN) method developed by Landschützer et al. (2013). Open ocean regions in the original product are broadly defined as all waters 1 degree off shore, whereas the coastal ocean in Laruelle et al. (2017) includes all ocean areas within 300 km offshore following the SOCAT definition (Bakker et al., 2016), whereas the overlap area is merged by simple error statistics (Landschützer et al., 2020). The merged climatology, presented in Landschützer et al. (2020), is available globally on a 0.25x0.25 degree grid to better resolve fine coastal characteristics and covers coastal ocean regions, shelf seas, as well as marginal seas. The dataset used to calculate the air-sea CO₂ flux (i.e., SST, SSS, wind) is the same as described for the coastal-SOM-FFN product.

Carboscope-1

The Carboscope pCO₂ interpolation is normally run at a resolution of 2 x 2.5 degree (version oc.v2021, update of Rödenbeck et al. (2013)) but we use here a higher-resolution version of 1 x 1 degree (CarboScope RunID oc.1x1.v2021) to better resolve spatial details. As a secondary change for computational feasibility, the calculation period has been shortened, now starting in 1988, with the valid period starting in 1992. We note that the Bayesian a-priori uncertainty is set according to a global normalization condition, even though the pCO₂ constraint is a local one; thus the effective local regularization strength in the 1 x 1 version might be somewhat different compared to that in the regular 2.5 x 2 version. This version uses SOCAT version 2021, sea ice coverage is based on HadISST 2.2.0.0 (Titchner & Rayner, 2014). Wind speed are from JRA55-do v1.5.0 (Tsujino et al., 2018) used quadratically as in (Wanninkhof, 1992), and global mean piston velocity are scaled to 16.5 cm h⁻¹ but the normalization of the gas transfer velocity to a global long-term average of 16.5 cm h⁻¹ might lead to slight differences in the local transfer velocities.

S1.b N₂O and CH₄ observation-based products

MARCATS-N₂O and MARCATS-CH₄

MARCATS-N₂O and MARCATS-CH₄ are based on the collection of in-situ concentration data of N₂O and CH₄ from the MEMENTO (Marine Methane and Nitrous Oxide) data base (Kock & Bange, 2015) and were computed at the scale of the 45 MARGins and CATCHments Segmentation (MARCATS) regions (Laruelle et al., 2013) (Figure S2). For each MARCATS region, N₂O and CH₄ surface (1 - 10 m) concentration data were extracted from MEMENTO. Individual DN₂O and DCH₄ values (D = measured in-situ concentration - equilibrium concentration at the time of sampling) were calculated in two ways (i) using in-situ measurements of atmospheric N₂O or CH₄ mole fractions when archived together with the dissolved concentration data in MEMENTO or (ii) using zonally averaged atmospheric N₂O and CH₄ mole fractions computed with the data from the World Data Centre for Greenhouse Gases (WDCGG, <https://gaw.kishou.go.jp/>) for the respective sampling month. N₂O and CH₄ flux densities were calculated by multiplying DN₂O and DCH₄ with the air-sea transfer coefficient (kw) which was estimated with the wind speed parameterization for kw from (Nightingale et al., 2000). Wind speeds for the respective sampling

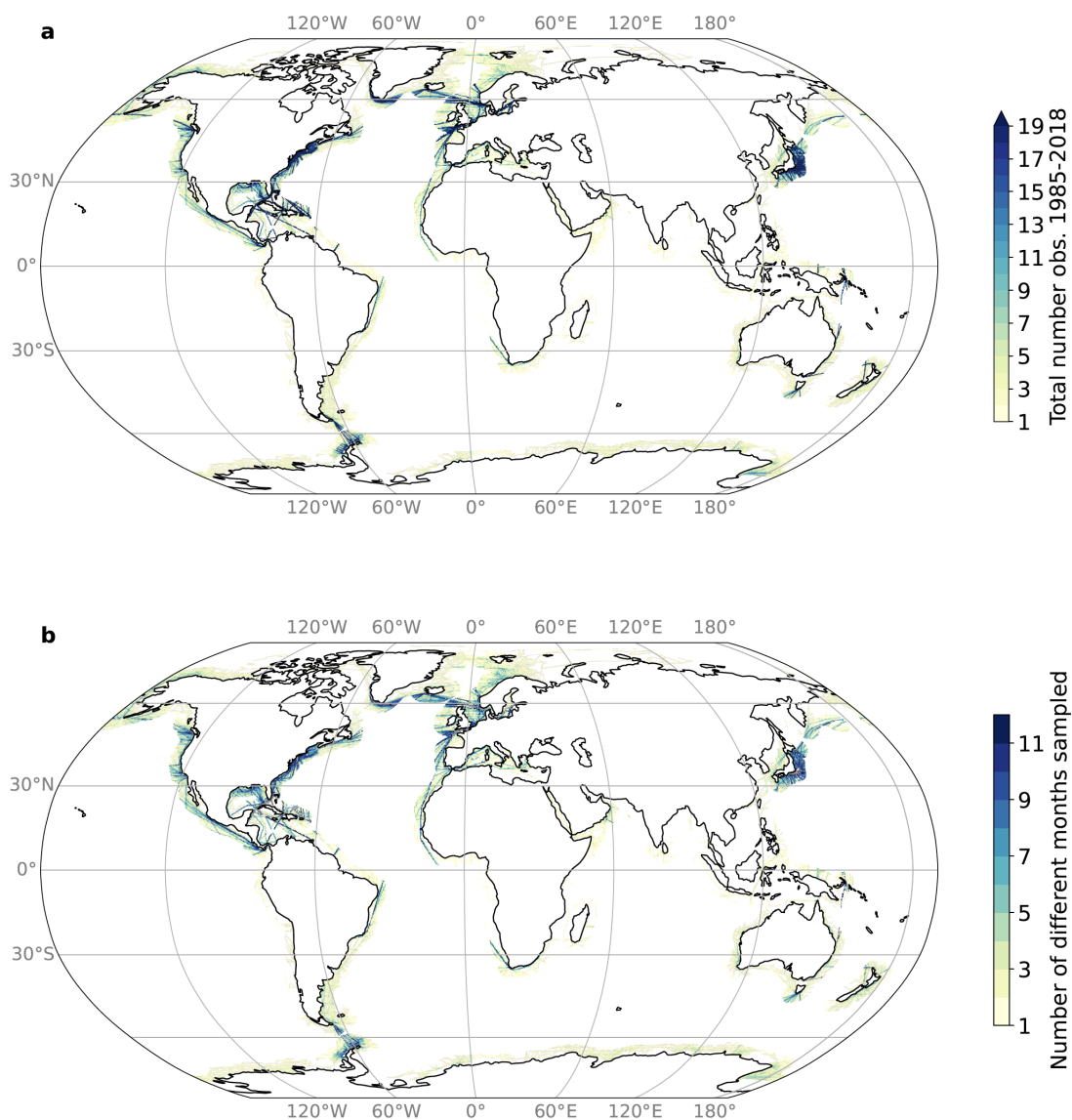


Figure S1. (a) areal coverage in 0.25 x 0.25 degree grid cells of SOCATv2.0 database calculated as the spatial density of the total number of observations 1985-2018 and (b) the number of distinct months sampled by SOCATv2.0 during this period. White areas represent where there are no observations (0 observations). See Methods and Laruelle et al. (2017) for definition of wide coastal ocean.

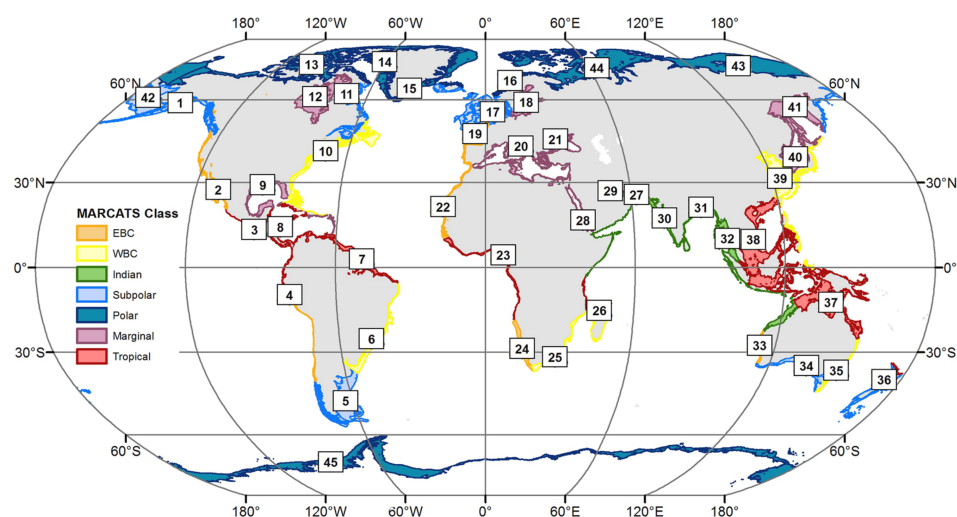


Figure S2. Locations of the 45 MARgins and CATchments Segmentation (MARCATS) regions (Laruelle et al., 2013) used to calculate the N_2O and CH_4 fluxes in MARCATS- N_2O and MARCATS- CH_4 .

<https://psl.noaa.gov>) (Kanamitsu et al., 2002). Finally, the individual N_2O and CH_4 flux densities were averaged and extrapolated to the area of each MARCATS region to obtain an emission estimate for the individual MARCATS regions. The number of observations used in each MARCATS to derive the CH_4 and N_2O fluxes is listed in Table S2. MARCATS- N_2O product has no observations in 6 MARCATS for the wide and 10 MARCATS for the narrow coastal oceans. Similarly, the MARCATS- CH_4 has no observations in 8 MARCATS for the wide and 14 MARCATS for the narrow coastal oceans.

Yang- N_2O

The N_2O air-sea flux reconstruction by Yang et al. (2020) is based on a synthesis of over 158,000 observations of N_2O mixing ratio, partial pressure, and concentration in the surface ocean from the MEMENTO database (Kock & Bange, 2015) and additional cruises (Yang et al., 2020). N_2O measurements are converted to surface N_2O mixing ratio anomalies using observations from the NOAA atmospheric flask dataset and extrapolated to a 0.25-degree resolution global monthly climatology using an ensemble of 100 random forest realizations. The random forest algorithm predicts N_2O mixing ratio anomalies based on their relationship to oceanographic predictors that include hydrographic variables, nutrients, oxygen, chlorophyll, net primary production, and seafloor depth. Reconstructed mixing ratio climatologies are used to estimate air-sea fluxes by applying a commonly used gas exchange parameterization (Wanninkhof, 2014). Two formulations of piston velocity are adopted: one based on a quadratic dependence on wind speed (Wanninkhof, 2014), and one that explicitly accounts for bubble-mediated fluxes (Liang et al., 2013). Sea ice cover, surface temperature, salinity and atmospheric pressure are taken from ERA5 reanalysis (Hersbach et al., 2020). Calculations are performed with two high-resolution wind products (ERA5 and Remote sensing Cross-Calibrated Multi-Platform version 2.0) that are available at 0.25, 6-hourly resolution for the period from 1988 to 2017, yielding four permutations of the piston velocity. The resulting ensemble of 400 global N_2O air-sea flux estimates is averaged in time to obtain monthly mean climatologies. A description of the dataset and methods is presented in (Yang et al., 2020). The compilation of N_2O measurements, the reconstructed global N_2O climatology and air-sea flux are available on the Biological and Chemical Oceanography Data Management Office (BCO-DMO) portal (DOI: 10.26008/1912/bco-dmo.810032.1). The code used to produce these datasets is archived on a public GitHub repository at <https://github.com/yangsi7/mapping-ocean-n2o> (DOI: 10.5281/zenodo.3757194).

Weber- CH_4

The diffusive sea-air CH_4 flux reconstruction by (Weber et al., 2019) is based on a compilation of 120,000 individual concentration and partial pressure measurements from the MEMENTO database (Kock & Bange, 2015) and additional cruise datasets (Weber et al., 2019). These measurements were converted to CH_4 disequilibrium using atmospheric partial pressure from the NOAA Global Monitoring Division archive, which has collected flask samples from a global network of monitoring stations since 1980 (www.esrl.noaa.gov/gmd/ccgg/) and extrapolated to a 0.25-degree monthly climatology using 10,000 artificial neural network and random regression forest models, each trained with 70% of the data. Air-sea fluxes were computed by combining each climatology with one of four piston velocity relationships (Wanninkhof, 1992, 2014; Nightingale et al., 2000; Liss & Merlivat, 1986), and one of four global wind products (ERA5, CCMP, NCEP, reanalysis products, and a blended WindSat/QuickSCAT satellite product). Flux calculations were conducted at daily resolution then integrated into an annual climatology representing the mean

1999-2016 flux. Ebullitive CH_4 emissions to the atmosphere were estimated using literature ranges for the global ebullition rate from continental shelf sediments (Hornafius et al., 1999; Hovland et al., 1993) and a bubble transfer model to estimate the fraction of CH_4 reaching the surface (McGinnis et al., 2006). Full methodology is described in Weber et al., 2019 and the product is available at https://figshare.com/articles/dataset/ocean_ch4.nc/9034451.

S1.c Global ocean biogeochemical models

CCSM-WHOI

The Community Earth System Model (CESM) is the global ocean component of a coupled climate/earth system model. The ocean component, the Biogeochemical Elemental Cycle (BEC) model, consists of an upper-ocean ecological module and a full-depth ocean biogeochemistry module both embedded in a three-dimensional (3-D) global physical ocean general circulation model. The physical model is the Parallel Ocean Program (POP) z-level, hydrostatic, primitive equation model. The specific CESM-LR version used here has coarse, non-eddy resolution and is described in detail in Doney et al. (2009). The ocean model is integrated in an uncoupled model forced with physical climate forcing from NCEP atmospheric reanalysis and satellite data products. The ecosystem module builds on traditional phytoplankton-zooplankton-detritus-nutrient food-web models and incorporates multi-nutrient limitation (N, P, Si, Fe) on phytoplankton growth and specific phytoplankton functional groups. The biogeochemical module includes full carbonate system thermodynamics and air-sea CO_2 and O_2 fluxes, nitrogen fixation, denitrification and a dynamic iron cycle with atmospheric dust deposition, water-column scavenging and a continental sediment source. There are 14 main compartments: pico/nano-plankton, diatoms, and diazotrophs; zooplankton; suspended and sinking particulate detritus; and dissolved nitrate, ammonia, phosphorus, iron, silicate, oxygen, dissolved inorganic carbon, and alkalinity. The model was forced with the NCEP reanalysis and did not include nutrients or carbon inputs by rivers.

CNRM-LR and CNRM-HR

CNRM-LR and CNRM-HR are the Earth System Models of second generation developed by CNRM-CERFACS for the sixth phase of the Coupled Model Intercomparison Project (CMIP6). Their ocean component uses the Nucleus for European Models of the Ocean (NEMO) Version 3.6 (Madec et al., 2017) coupled to both the Global Experimental Leads and ice for ATmosphere and Ocean (GELATO) sea ice model (Salas Méria, 2002) Version 6 and the marine biogeochemical model Pelagic Interaction Scheme for Carbon and Ecosystem Studies version 2-gas (PISCESv2-gas) (Aumont et al., 2015). In CNRM-LR, NEMOv3.6 operates on the eORCA1L75 grid, which offers a nominal resolution of 1 degree to which a latitudinal grid refinement of 1/3 degree is added in the tropics, while in CNRM-HR, NEMO is run on the eORCA025 grid having a 0.25 degree of horizontal resolution. Whatever the horizontal resolution, the ocean is described with 75 vertical layers using a vertical z^* coordinate with partial step bathymetry formulation (Bernard et al., 2006). The ocean layers are distributed unevenly as a function of depth with a resolution of 1 m at ocean surface to 200 m below 4000 m. Key differences between both configurations are detailed in Berthet et al. (2019). The simulations were forced at the surface by the atmospheric state of JRA55-do v1.5.0 (Tsujino et al., 2018). Atmospheric CO_2 concentration is given as annual means as specified by CMIP6 protocols and is linearly interpolated in time. Riverine inputs of dissolved inorganic carbon and alkalinity (Ludwig et al., 1996) as well as nutrients (Mayorga

Table S1. Number of observations and density [in observations per 10^6 km^2] from MEMENTO database used in each MARCATS to calculate the MARCATS-N₂O and MARCATS-CH₄ observational products in the wide and narrow coastals. See map in Figure S2 for MARCATS locations.

MARCATS	N ₂ O wide		N ₂ O narrow		CH ₄ wide		CH ₄ narrow	
	observations	density	observations	density	observations	density	observations	density
1	71	9	20	7	38	5	9	3
2	159	21	28	10	124	17	5	1
3	229	31	8	2	12	1	0	0
4	1301	179	551	204	20	2	13	4
5	248	34	129	47	26	3	15	5
6	539	74	148	54	4	0	1	0
7	375	51	250	92	4	0	0	0
8	136	18	0	0	0	0	0	0
9	0	0	0	0	1	0	0	0
10	575	79	411	152	0	0	0	0
11	259	35	0	0	2	0	0	0
12	0	0	0	0	0	0	0	0
13	130	17	130	48	117	16	102	37
14	28	3	7	2	13	1	7	2
15	472	65	70	25	28	3	0	0
16	519	71	330	122	28	3	3827	1420
17	1294	178	917	340	1013	139	1014	376
18	250	34	91	33	3312	457	15	5
19	457	63	481	178	629	86	648	240
20	102	14	39	14	111	15	52	19
21	3	0	4	1	32	4	24	8
22	1286	177	430	159	474	65	148	54
23	396	54	17	6	5	0	1	0
24	185	25	69	25	5	0	5	1
25	514	70	54	20	0	0	0	0
26	173	23	0	0	0	0	0	0
27	1306	180	6	2	557	76	1	0
28	0	0	0	0	0	0	0	0
29	0	0	0	0	0	0	0	0
30	243	33	47	17	16	2	1	0
31	289	39	22	8	55	7	62	23
32	321	44	21	7	20	2	24	8
33	476	65	76	28	7	0	0	0
34	88	12	20	7	53	7	12	4
35	276	38	206	76	113	15	144	53
36	144	19	16	5	43	5	10	3
37	37	5	37	13	7	0	3	1
38	182	25	129	47	89	12	46	17
39	253	34	111	41	72	9	48	17
40	0	0	0	0	0	0	0	0
41	0	0	0	0	22	3	3	1
42	62	8	48	17	17	2	13	4
43	33	4	17	6	659	90	655	243
44	48	6	0	0	85	11	36	13
45	1703	235	959	356	85	11	47	17

et al., 2010) are prescribed with a repeated seasonal cycle scaled on freshwater riverine inputs. Burial of carbon at the bottom of the ocean is emulated with a meta-model based on POC export (Aumont et al., 2015). Originally implemented by Martinez-Rey et al. (2015), the marine N₂O parameterization has benefited from a recoding and an improved calibration presented in Berthet et al. (2022). A comprehensive description of the configuration of the marine biogeochemical component is presented in Séférian et al. (2019).

FESOM-LR and FESOM-HR

We use the ocean circulation model FESOM1.4 (C. Wang et al., 2014) coupled to the ocean biogeochemical model REcoM2 (Hauck et al., 2020, 2013; Schourup-Kristensen et al., 2014). FESOM is an unstructured mesh model used in a low-resolution configuration (FESOM-LR) and a high-resolution configuration (FESOM-HR, see resolution meshes in Figure S3). The Regulated Ecosystem Model (REcoM) simulates the coupled cycles of carbon, nitrogen, silicic acid, iron and oxygen. In this version, it simulates two phytoplankton groups (small phytoplankton and diatoms) and one zooplankton group. It allows for variable stoichiometry in phytoplankton (C:N:Chl:CaCO₃ for small

phytoplankton and C:N:Chl:SI for diatoms), zooplankton (C:N) and detritus (C:N:Si). There are no inputs of carbon or nutrients by rivers and runoff. The FESOM-LR configuration is based on a coarse mesh with a global nominal resolution of 1 degree, which is increased to about 25 km north of 50°N and to about 1/3° in the equatorial belt, and is also moderately refined along the coasts (Sein et al., 2018). The model is started from initial conditions (World Ocean Atlas for nutrient fields (Garcia et al., 2014), Glodap for alkalinity and preindustrial dissolved inorganic carbon (Lauvset et al., 2016)). It is spun up from 1850-1957 years using repeated year atmospheric forcing from the year 1961. The atmospheric forcing fields for the spin-up and for the simulation period 1958 to 2018 are taken from the Japanese 55-year Reanalysis Version 1.4.0 (Tsujino et al., 2018). Further, spin-up and simulation period are forced with observed atmospheric CO₂ as provided by the Global Carbon Budget (Friedlingstein et al., 2020). Carbonate chemistry and air-sea CO₂ exchange are calculated with the mocsy routines (Orr et al., 2015) that apply a quadratic gas-exchange parameterization (Wanninkhof, 2014). This is the same model version as used in the Global Carbon Budget 2020

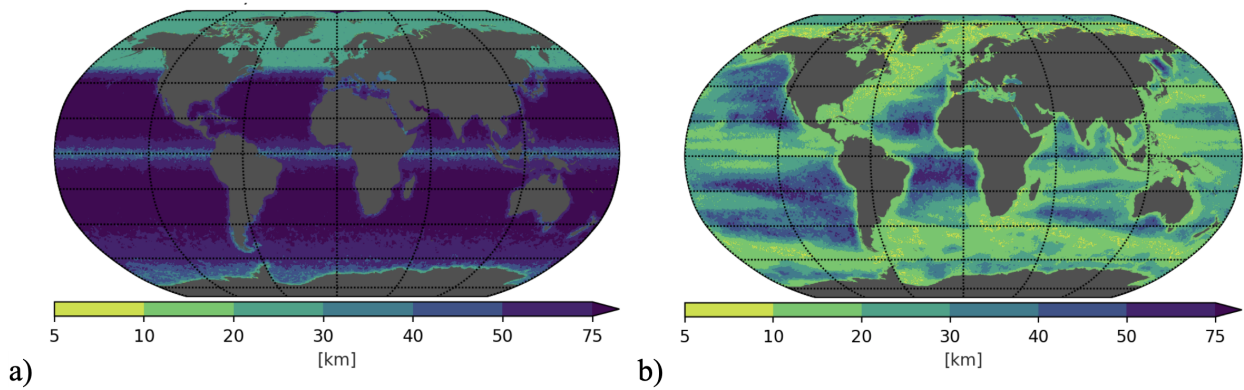


Figure S3. Horizontal resolution of the a) FESOM-LR and b) FESOM-HR models.

(Friedlingstein et al., 2020). The FESOM-HR configuration has a locally eddy-resolving mesh with the horizontal resolution varying according to the observed sea surface height (SSH) variability. The coarsest resolution is 60 km, and the finest is 8-10 km (Sein et al., 2018). This is equivalent to a $1/10^\circ - 1/4^\circ$ resolution. In particular, the high resolution is located along the pathways of the main currents, including the Gulf Stream. We performed a high-resolution physical ocean model spin-up run under JRA55 forcing. The spin-up spanned one full cycle from 1958-2017, and a second cycle 1958-1980 using FESOM-HR. We initialized our model from an existing simulation driven by CORE-II forcing (Large & Yeager, 2009). We branched off our simulations with coupled physics and biogeochemistry at the end of 1980 and ran the simulation from 1981 to 2019 using the HR mesh with an increasing atmospheric CO_2 concentration and interannual varying atmospheric forcing. The initial biogeochemical model fields for the year 1980 are taken from the FESOM-LR simulation and are interpolated to the FESOM-HR mesh.

IPSL

The IPSL ocean model uses the Nucleus for European Models of the Ocean (NEMO) Version 3.6 which includes three components, ocean physics from NEMO-OPA (Madec et al., 2017), the sea ice dynamics and thermodynamics from NEMO-LIM3 (Rousset et al., 2015), and the ocean biogeochemistry from NEMO-PISCES-v2 (Aumont et al., 2015). The global configuration used here is eORCA1L75, including a horizontal nominal resolution of 1° (with a latitudinal grid refinement of up to 0.3° in the equatorial region) and 75 levels on the vertical (with the partial step formulation of Barnier et al. (2006) and layer thicknesses increasing from 1m at the surface to 200m at the bottom). The simulation is forced at the surface by the atmospheric reanalysis product of JRA55-do-v1.4 (Tsujiro et al., 2018) and global and annual mean values of atmospheric CO_2 as specified in the Global Carbon Budget protocol (Friedlingstein et al., 2022). Riverine inputs of carbon, alkalinity and nutrients are based on (Ludwig et al., 1996) and (Mayorga et al., 2010), and prescribed with a repeated seasonal cycle. Sediment burial of carbon, alkalinity and nutrients is simulated using the formulation of (Dunne et al., 2007) and (Middelburg et al., 1996).

MOM6-Princeton

The MOM6-Princeton model uses the Modular Ocean Model version 6 (MOM6), the Sea Ice Simulator version 2 (SIS2), and the Carbon Ocean Biogeochemistry and Lower Trophics version 2 (COBALT v2) developed by the NOAA Geophysical Fluid Dynamics Laboratory (GFDL). The specific version used here is available on Github (Git commit: 48536b downloaded in October 2018) and was used

in Liao et al. (2020) and the global carbon budget 2020 (Friedlingstein et al., 2020). The physical and biogeochemical ocean configurations follow GFDL earth system model version 4 (ESM4) (Dunne et al., 2020)). The horizontal resolution is 0.5° in longitude and $0.25-0.5^\circ$ in latitude. On the vertical, it includes 75 hybrid isopycnal z^* coordinate, including a z^* coordinate near the surface (about 2 m thick layers in the upper 20 m in the tropical Pacific Ocean) and a modified potential density coordinate below (Adcroft et al., 2019). COBALT2 includes 33 state variables, including nutrients (nitrate, phosphate, and iron), silicate, three phytoplankton groups, three zooplankton groups, three dissolved organic carbon pools, one particulate detritus pool, oxygen, and the carbonate system (Stock et al., 2020). The model was spun up from rest for 81 years by repeating the year 1959 of the JRA55-do v1.3 forcing. Temperature, salinity, nutrients (nitrate, phosphate, and silicate), and oxygen were initialized from World Ocean Atlas version 2013 (Garcia et al., 2014; Locarnini et al., 2014; Zweng et al., 2014). Initial dissolved inorganic carbon (DIC) and alkalinity (Alk) are from GLODAP v2 (Olsen et al., 2016). The initial DIC is corrected for the accumulation of anthropogenic carbon to match the level expected in 1959 using the data-based estimate of ocean anthropogenic carbon content (Khatriwala et al., 2013). Other COBALT tracer initial conditions (e.g., ammonium, calcium carbonate) are from a preindustrial GFDL-ESM2M-COBALT simulation (Stock et al., 2014). The simulation includes riverine nutrients from the Global-NEWS2 model (Mayorga et al., 2010) and riverine carbon inputs designed to roughly balance carbon burial in the model (here input of 0.11 of DIC and 0.07 of DOC). At the end of the 81-year spin-up, the model has reached a near-equilibrium between atmospheric pCO_2 and surface ocean pCO_2 , with a drift in global air-sea CO_2 flux $\pm 0.004 \text{ PgC/yr}$ over the last 10 years of spin-up. The simulation was then performed from 1959 to 2018 using interannual forcing. In this version, the gas transfer coefficient was calculated using the parameterization of (Wanninkhof, 1992) but with the updated Schmidt number from (Wanninkhof, 2014).

MPIOM-HAMOCC

The Hamburg Ocean Carbon Cycle (HAMOCC) (Ilyina et al., 2013; Paulsen et al., 2017) model is a global ocean biogeochemical model embedded in the Max Planck Institute Ocean Model (MPIOM) (Jungclauss et al., 2013). The version used here is the same as used in the Global Carbon Budget 2021 (Friedlingstein et al., 2022). The nominal resolution here is 1.5° degree with 40 vertical levels.

The biogeochemical cycles of carbon, nutrients (nitrate, phosphate, iron), oxygen, silicate, phytoplankton (bulk and cyanobacteria), zooplankton, detritus, and organic matter in HAMOCC are computed in the water column and in the upper sediment. Biogeochemical tracers are transported with the ocean flow in the same way as temperature and salinity in MPIOM. The composition of organic matter follows a constant Redfield ratio of carbon (C:N:P:O₂ = 122:16:1:172). The sinking of organic matter follows the Martin curve, i.e. linearly increasing with depth. River inputs of carbon and nutrients are included (Lacroix et al., 2021). NCEP 6 hourly cyclic forcing (10 years starting from 1948) is used for the spin-up, transient NCEP forcing has been used during 1948–2021. The air-sea gas exchange parameterization follows the OMIP protocol (Orr et al., 2017).

MRI-ESM2-1

MRI-ESM2-1 is a modified version for the ocean component of Meteorological Research Institute Earth System Model version 2 (MRI-ESM2) (Yukimoto et al., 2019). The source code is taken from Meteorological Research Institute Community Ocean Model version 4 (MRI.COMv4) (Tsujino et al., 2017), which is formulated on general orthogonal curvilinear coordinate in the horizontal and z^* coordinate in the vertical directions and is discretized on Arakawa B-grid frame. The horizontal resolution is 1.0° in the zonal and $0.3\text{--}0.5^\circ$ in the meridional directions. There are 60 vertical levels with enhancement in the upper layer and an additional bottom boundary layer at the seafloor in the deep and bottom water formation regions such as the northern North Atlantic and in the Southern Ocean around Antarctica. The configuration and performance of this model in terms of physical fields are fully described and presented by Urakawa et al. (2020). The biogeochemical processes consist of a carbon cycle model with the carbonate chemistry and the surface gas exchange parameterization that follow the protocols of OMIP-BGC (Orr et al., 2017) and a simple NPZD (nutrient, phytoplankton, zooplankton, detritus) type ocean ecosystem model as used by (Nakano et al., 2011). Relative to the version used for CMIP6 (MRI-ESM2-0), the sinking velocity of detritus is changed from 7.0 m day⁻¹ to 2.0 m day⁻¹. Advection scheme for biogeochemical tracers is changed from MPDATA (Multi-dimensional Positive Definite Advection Tracer Algorithm) to PPM (Piecewise Parabolic Method). The simulation was forced at the surface by the atmospheric state of JRA55-do v1.5.0 (Tsujino et al., 2018). Atmospheric CO₂ concentration is given as the spatially uniform, annual mean as specified by CMIP6 protocols and is linearly interpolated in time. No riverine inputs of nutrients or carbon and no burial are included. Instead, surface DIC and Alkalinity fluxes are added in proportion to surface salinity flux due to a restoring of the model sea surface salinity to that of World Ocean Atlas 2013 version 2 (WOA13v2).

NEMO-PlankTOM

The NEMO-PlankTOM model is based on the ORCA2 version of the NEMO physical model, which calculates vertical diffusion explicitly and includes a dynamic-thermodynamic sea-ice model. PlankTOM is the biogeochemical module that represents full cycles of carbon, oxygen, phosphorus, silica, calcite, and a simplified cycle for iron and nitrogen. PlankTOM12, used here for its estimate of CO₂ fluxes, represents twelve Plankton Functional Types, six phytoplankton, five zooplankton and archaea. The version used here is based on the work of (Wright et al., 2021) and integrates pteropods and the aragonite cycle from (Buitenhuis et al., 2019). This is the same version published in the Global Carbon Budget 2022 (Friedlingstein et al., 2022). The model is initialized in 1750 and run forward with constant atmospheric forcing up to 1948, then forced with daily weather conditions using the NCEP reanalysis

data, and constant input of nutrient (N, P and Fe) and organic and inorganic carbon from rivers (see also Friedlingstein et al. 2022). NCEP winds are also used to calculate the gas exchange velocity using (Wanninkhof, 1992) formulation. PlankTOM5 is used to estimate N₂O fluxes. PlankTOM5 uses a simplified ecosystem composition with three phytoplankton and two zooplankton, and a full representation of N₂O production and loss processes (Buitenhuis et al., 2018).

NorESM-OC2.0

NorESM-OC2.0 is the ocean carbon-cycle stand-alone configuration of the Norwegian Earth System Model version 2 (NorESM2, (Seland et al., 2020; Tjiputra et al., 2020)). The physical ocean component of NorESM2, the Bergen Layered Ocean Model (BLOM), is configured on a tripolar grid with a nominal resolution of 1° horizontally and 51 isopycnal layers in the vertical with 2 additional layers representing a bulk mixed layer on top. Ocean biogeochemistry is represented by the iHAMOCC model, which is derived from HAMOCC5 (Ilyina et al., 2013) and includes a 12-layer sediment scheme. The iHAMOCC model includes a NPZD ecosystem parameterization (Six & Maier-Reimer, 1996) and carbon chemistry follows the OCMIP protocols (Orr et al., 2015). The influx of carbon and nutrients from rivers to the coastal oceans has been implemented based on the Global-NEWS2 model (Mayorga et al., 2010) and work by (Hartmann et al., 2009) for DIC and alkalinity fluxes. Riverine fluxes are distributed as a function of river mouth distance (with an e-folding length scale of 1000 km and cutoff of 300 km) to the ocean grid and are assumed to be constant over time at year 2000 levels. The NorESM-OC2.0 simulation used here follows the CMIP6 omip2 protocol, which employs the JRA-55 atmospheric forcing data set. The gas exchange coefficient formulation is from (Wanninkhof, 2014).

ECCO2-Darwin and ECCO-Darwin

Global air-sea fluxes of N₂O were evaluated from two versions of the ECCO family: the ECCO2-Darwin and ECCO-Darwin models which include the same biogeochemical component Darwin but are embedded in two different ocean physical settings. ECCO2-Darwin model, is a global physical-biogeochemical ocean model with nominal horizontal grid of $1/6$ of degree therefore eddy-permitting at lower latitudes. It is forced with ECMWF winds over the 2006–2008 period and JRA-55 winds over the 2009–2013 period, optimized with adjoint technique in order to realistically represent the observed physical ocean climate variability. ECCO-Darwin, a global physical-biogeochemical ocean model with nominal horizontal grid resolution of $1/3$ of degree, and is forced with ERA-Interim winds (Carroll et al., 2020). Both models have 50 vertical levels and in the top 100 m the model is vertically resolved with 10-meter grid boxes. An extensive description of this model run of ECCO2-Darwin including the optimized atmospheric forcing spanning from 2004 to 2013 can be found in (Manizza et al., 2019) while for ECCO-Darwin a more detailed model description can be found in Carroll et al. (2020). The Darwin biogeochemical/ecological model used for this study explicitly represents the cycle of carbon, oxygen, phosphorus, silica, and iron in the global ocean. It also has an ecosystem component representing five groups of phytoplankton and two groups of zooplankton (Manizza et al., 2019; Carroll et al., 2020). For this particular version of the model we implemented a parameterization of the oceanic cycle of (Manizza et al., 2012) using the scheme of (Nevison et al., 2003) based on the oceanic oxygen cycle previously represented in ECCO2-Darwin model (Ganesan et al., 2020). The air-sea gas flux of N₂O was parameterized according to Wanninkhof (1992). In addition, a thermal-only N₂O

tracer (a tracer in which biogeochemical sources and sinks are suppressed but with the same solubility as N_2O) was also added to the model to isolate the process of ocean ventilation affecting the N_2O concentration in the ocean at seasonal time scales as done in (Manizza et al., 2012). The ventilation component of the air-sea N_2O fluxes is obtained by subtracting the solubility-only N_2O air-sea flux from the total N_2O air-sea flux. In the ECCO2-Darwin simulation the 2004-2005 period was discarded and we used the 2006-2013 period only for our analysis. However, the ECCO-Darwin numerical simulation was run for the 1992-2014 period but we discarded the inclusion of the output relative to the 1992-1996 period in our analysis due to the model adjustment in this initial part of our numerical simulation.

S1.d Regional ocean biogeochemical models

ACM-NWAtl

The model is based on the Rutgers version of the Regional Ocean Modelling System (ROMS) (Haidvogel et al., 2008), has 30 vertical levels and approximately 10 km horizontal resolution (240×120 horizontal grid cells). The model uses atmospheric surface forcing from the European Centre for Medium-Range Weather Forecasts (ECMWF) global atmospheric reanalysis (ERA-Interim) (Dee et al., 2011), and CO_2 fluxes are calculated following the Ho et al. (2006) parameterization. Within the ocean, it uses the GLS vertical mixing scheme (Umlauf & Burchard, 2003; Warner et al., 2005), and the “high-order spatial interpolation at the middle temporal level” (HSIMT) advection scheme for tracers (Wu & Zhu, 2010). Physical initial and boundary conditions are defined using the regional physical ocean model of the northwest North Atlantic by Urrego-Blanco and Sheng (2012). Climatological river discharge is imposed for 12 major rivers and uses observed long-term monthly means from the Water Survey of Canada. Full details on the physical model setup and its validation can be found in Brennan et al. (2016) and Rutherford and Fennel (2018). These studies have shown that the model simulates the vertical structure and seasonal variations of temperature and salinity on the shelf well. The model captures mesoscale features and coastal upwelling events and simulates the volume transport throughout the region in agreement with observation-based estimates.

The biogeochemical model is based on the nitrogen-cycle model with the inorganic carbon component of (Fennel et al., 2006) and Fennel and Wilkin (2009) but was recently expanded to include two phytoplankton and two zooplankton functional groups (Laurent et al., 2021). For a detailed description and validation of the biological model and the model’s carbonate system parameters, we refer to Laurent et al. (2021) and Rutherford et al. (2021) respectively. Laurent et al. (2021) compared the model output with glider transects of temperature, salinity, and chlorophyll and in situ measurements of chlorophyll and nitrate. Rutherford et al. (2021) compared models results against a high-resolution pCO_2 time series and frequent cross-shelf transects of pCO_2 to ensure it faithfully represents both the seasonal cycle and cross-shelf gradients. Atmospheric pCO_2 is set to the seasonal cycle and secular trend derived from Sable Island monitoring data contributed by Environment Canada’s Greenhouse Gas Measurement Program (Environment and Climate Change Canada: Canadian Greenhouse Gas Measurement Program). The long-term linear trend in the atmospheric pCO_2 is $\sim 2 \text{ uatm yr}^{-1}$. Further details of the biogeochemical model, including the carbonate chemistry equations, can be found in the supplementary information of (Laurent et al., 2017). Nitrate concentrations in rivers are prescribed from Global NEWS model output (Seitzinger et al., 2005). DIC and total alkalinity (TA) in rivers were calculated by fitting a linear relationship with

salinity from Gulf of St. Lawrence bottle data and extrapolating to river water salinity.

ROMS-ETHZ-Atl and ROMS-ETHZ-Pac

The two regional models ETHZ-ROMS-Pac and ETHZ-ROMS-Atl rely on the coupling of the Regional Oceanic Modeling System (ROMS) (Shchepetkin & McWilliams, 2005) with the biogeochemical/ecological model BEC (Moore et al., 2013). Both setups rely on a telescopic grid that permits the model to resolve the mesoscale coastal processes in the region of interest, while covering at the same time nearly the entire ocean basin. In the ETHZ-ROMS-Pac setup, the telescopic grid is centered on the US West coast (resolution 4km), while in the ETHZ-ROMS-Atl setup, the telescopic grid has two poles, one centered in the Amazon outflow region (resolution 4km), and one on Western Africa. BEC simulates the cycling of carbon and 4 nutrients (N, P, Si, Fe) which govern, along with light and temperature, the growth of three phytoplankton types (Small Phytoplankton, Diatoms and Trichodesmium). The ETHZ-ROMS-Atl setup includes a fourth phytoplankton type representing a symbiosis between a diatom and a N_2 -fixer, i.e., Diatom-Diazotroph-Assemblages that have been shown to be regionally important for the cycling of carbon (Louchard et al., 2021). All phytoplankton are grazed by one zooplankton class. Particulate organic matter (POM) is produced as a result of non-grazing mortality, aggregation or grazing processes. POM is then exported and remineralized in an explicit manner (Frischknecht, 2018) in ETHZ-ROMS-Pac and following an implicit scheme in ETHZ-ROMS-Atl (Armstrong et al., 2001). The atmospheric forcing of surface short and long-wave radiations, wind stress, and surface freshwater fluxes is derived from the hourly ERA5 re-gridded product from 1979 to 2019 (Copernicus Climate Change Service [C3S], 2017; (Hersbach et al., 2020)). Additionally, the atmospheric forcing includes monthly varying atmospheric pCO_2 provided by (Landschützer et al., 2020), considering the dry air mixing ratio for the marine boundary layer from GLOBALVIEW-CO2 (2014), the atmospheric pressure and the water vapor contribution from Dickson et al. (2007). Also included in the atmospheric forcing are the input of iron from dust and nitrogen deposition, and only in the ETHZ-ROMS-Atl setup, phosphorus deposition, all derived from (Mahowald et al., 2009). The initial conditions and the boundary conditions are based on World Ocean Atlas for the main nutrients (Garcia et al., 2014). For DIC and Alkalinity, GLODAP gridded products (Global Ocean Data Analysis Project version 2, (Lauvset et al., 2016)) are used as a climatology (centered on 2002) in ETHZ-ROMS-Atl and to create transiently evolving conditions in ETHZ-ROMS-Pac, following the procedures described by (Franco et al., 2018). Major rivers in the domain are represented as a surface flux of freshwater and nutrients (N,P) as described in (Frischknecht, 2018). One exception in the ETHZ-ROMS-Atl setup is the Amazon River that is represented by an inflow across an open lateral boundary condition and is delivering the whole suite of dissolved inorganic/organic nutrients and dissolved organic/inorganic carbon (estimates based on (Araujo et al., 2014)).

ROMS-NYUAD-Indian

The circulation model is based on the Regional Ocean Modeling System (ROMS) (Shchepetkin & McWilliams, 2005). Vertical mixing is represented using the non-local K-profile parameterization (KPP) scheme (Large et al., 1994). The model domain covers the Indian Ocean from 31.5S to 31N and 30E to 120E with a $1/10$ degree horizontal resolution and 32 sigma-coordinate vertical layers with refined resolution near the surface. Coupled to the hydrodynamic model is a nitrogen-based nutrient, phytoplankton zooplankton, detritus (NPZD) model with two components for nutrients, nitrate and ammonium, one phytoplankton, one zooplankton, and two detrital classes (Gruber

et al., 2006). The model has a module describing the cycling of oxygen as well as a parameterization of water column and benthic denitrification (Lachkar et al., 2016, 2021). The model also includes a carbon module with three state variables: DIC, Total Alkalinity, and calcium carbonate (Gruber et al., 2012; Lachkar & Gruber, 2013; de Verneil et al., 2022). Organic carbon is linked to organic nitrogen through the Redfield ratio 106:16. Surface fluxes of DIC and Total Alkalinity driven by changes in sea surface salinity are included as virtual fluxes proportional to the sea surface salinity forcing. Carbonate chemistry is calculated using routines from the Ocean Carbon-Cycle Model Intercomparison Project (OCMIP) (Orr et al., 2005). The formulation of air-sea gas transfer uses a quadratic wind speed dependence following Wanninkhof (1992). Further details of the biogeochemical model are provided in (Lachkar et al., 2021; de Verneil et al., 2022). The hindcast simulation is forced with ECMWF ERA-Interim 6-hourly heat fluxes, air temperature, pressure, humidity, precipitation and winds over the period from January 1980 to December 2018. Initial and lateral boundary conditions for temperature, salinity, currents and sea surface height are based on the ECMWF Ocean Reanalysis System 5 (ORAS5). The initial and lateral boundary conditions for nitrate and oxygen are extracted from the World Ocean Atlas 2018. The initial and lateral boundary conditions for DIC and alkalinity are based on GLODAP. Atmospheric CO₂ concentrations are prescribed from monthly Mona Loa data (Keeling et al., 2005). Riverine inputs include nutrients (Krishna et al., 2016; Ramesh et al., 1995) but no carbon or alkalinity. To account for the accumulation of anthropogenic carbon at the lateral boundaries during the simulation period, we used decadal-varying DIC based on available estimates of anthropogenic CO₂ (Key et al., 2004; Gruber et al., 2019; Olsen et al., 2019) regressed to atmospheric CO₂ concentrations. Initial and boundary conditions for DIC and alkalinity are processed following de Verneil et al. (2022) to include a seasonal cycle in the upper ocean. The model is spun up for 30 years with a repeated normal year (1984) forcing. During the spin-up phase (1950-1979), time-varying atmospheric CO₂ concentrations and DIC are prescribed at the atmospheric and lateral boundaries, respectively. Atmospheric CO₂ data prior to 1958 is based on (Joos & Spahni, 2008).

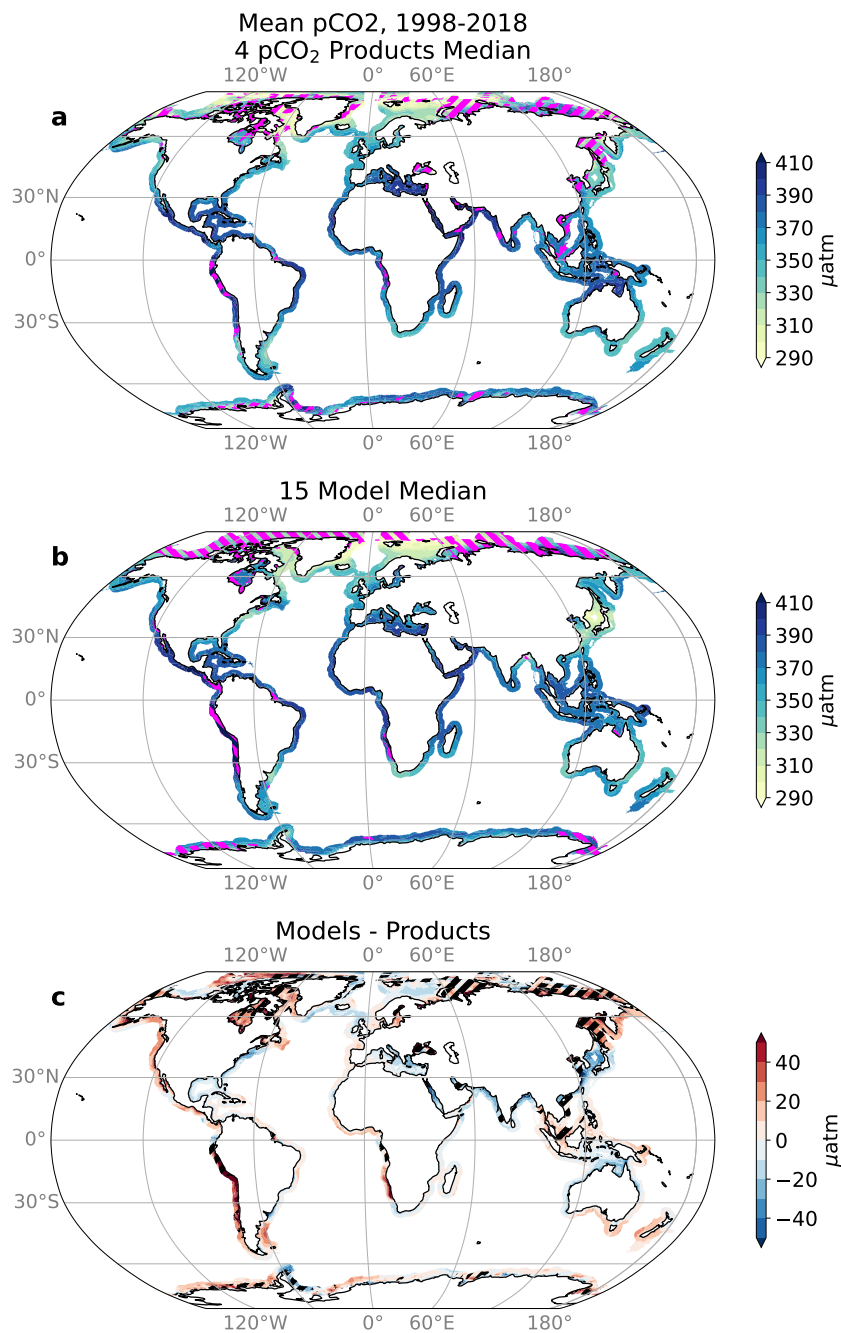


Figure S4. Annual mean coastal pCO₂ (in wide shelf waters) for a) the 4-product median, b) the 15-model median, and c) the difference between model and product medians. The model median in each point is calculated using the 11 global models and the 4 regional models. All are for 1998-2018 except coastal-SOM-FFN and merged-SOM-FFN pCO₂ products available for 1998-2015 only. Hatching indicates the coastal area with RMSD greater than 25 uatm across pCO₂ products (panels a and c) or 33 uatm across models (panel b) (20% of coastal area with highest RMSD in each case). Here pCO₂ is masked where sea ice on average covers 50% of the grid cell, to improve visual comparison with the flux.

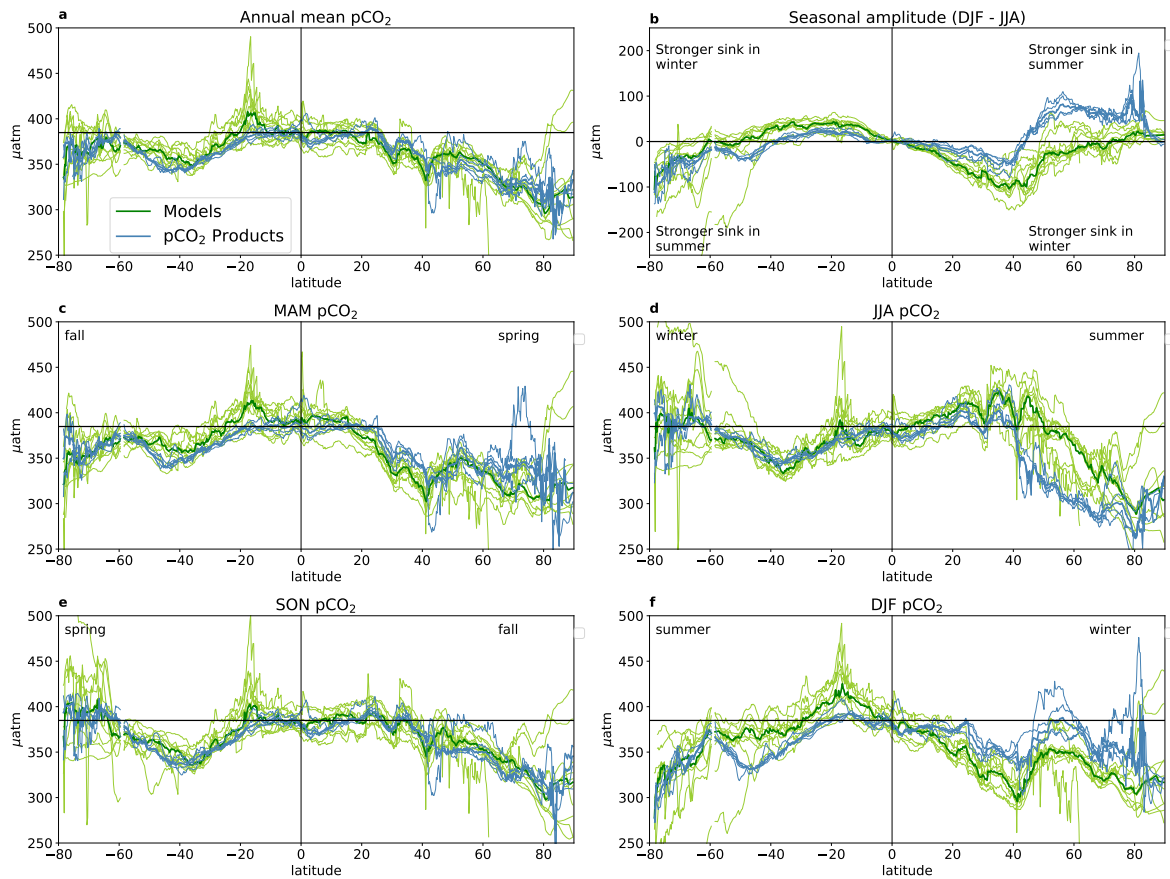


Figure S5. Latitudinal distribution of coastal ocean (wide shelf) a) annual mean $p\text{CO}_2$, b) $p\text{CO}_2$ seasonal amplitude computed as December-February minus June-August, c) March-May $p\text{CO}_2$, d) June-August $p\text{CO}_2$, e) September-November $p\text{CO}_2$, and f) December-February $p\text{CO}_2$ for the product and model medians (thick lines). Thin lines indicate the mean $p\text{CO}_2$ in each of 11 global models (green) and the 4 products (blue).

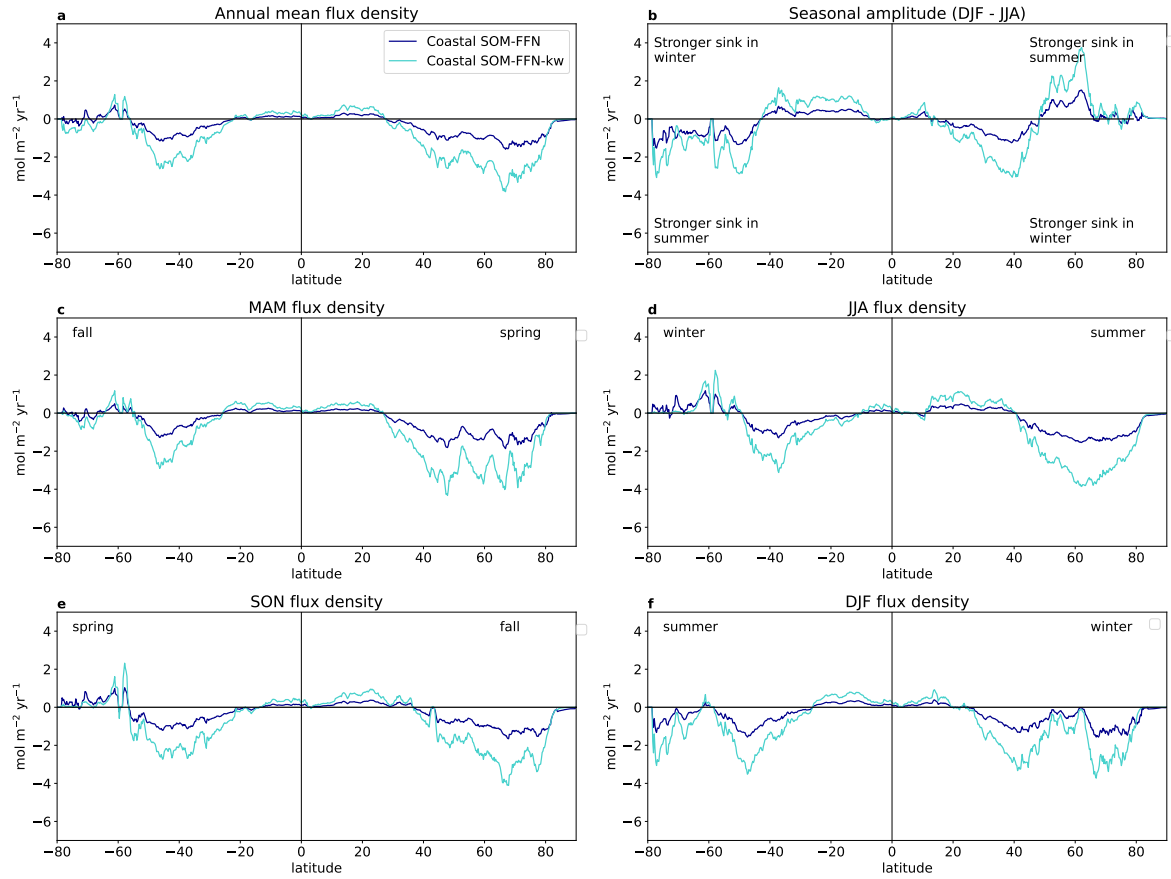


Figure S6. Influence of wind speed and gas exchange coefficient. Latitudinal distribution of coastal ocean (wide shelf) a) annual mean CO₂ flux, b) CO₂ flux seasonal amplitude computed as December-February minus June-August, c) March-May CO₂ flux, d) June-August CO₂ flux, e) September-November CO₂ flux, and f) December-February CO₂ flux in Coastal-SOM-FFN and Coastal SOM-FFN-kw (different wind product and gas exchange coefficient formulation, see Methods).

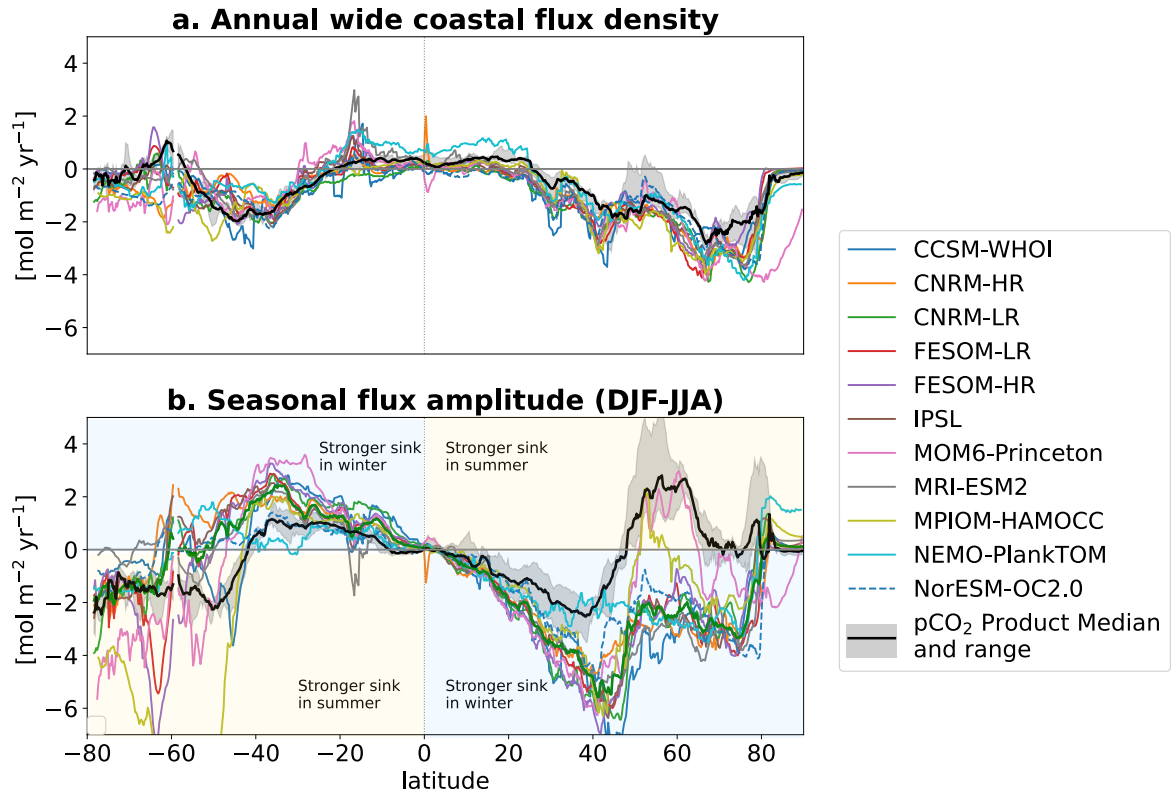


Figure S7. Latitudinal distribution of coastal ocean (wide shelf) a) annual mean CO₂ flux densities, b) CO₂ flux densities seasonal amplitude computed as December-February minus June-August, for the pCO₂-product median and range (black line and grey shading) and each individual models (colored lines).

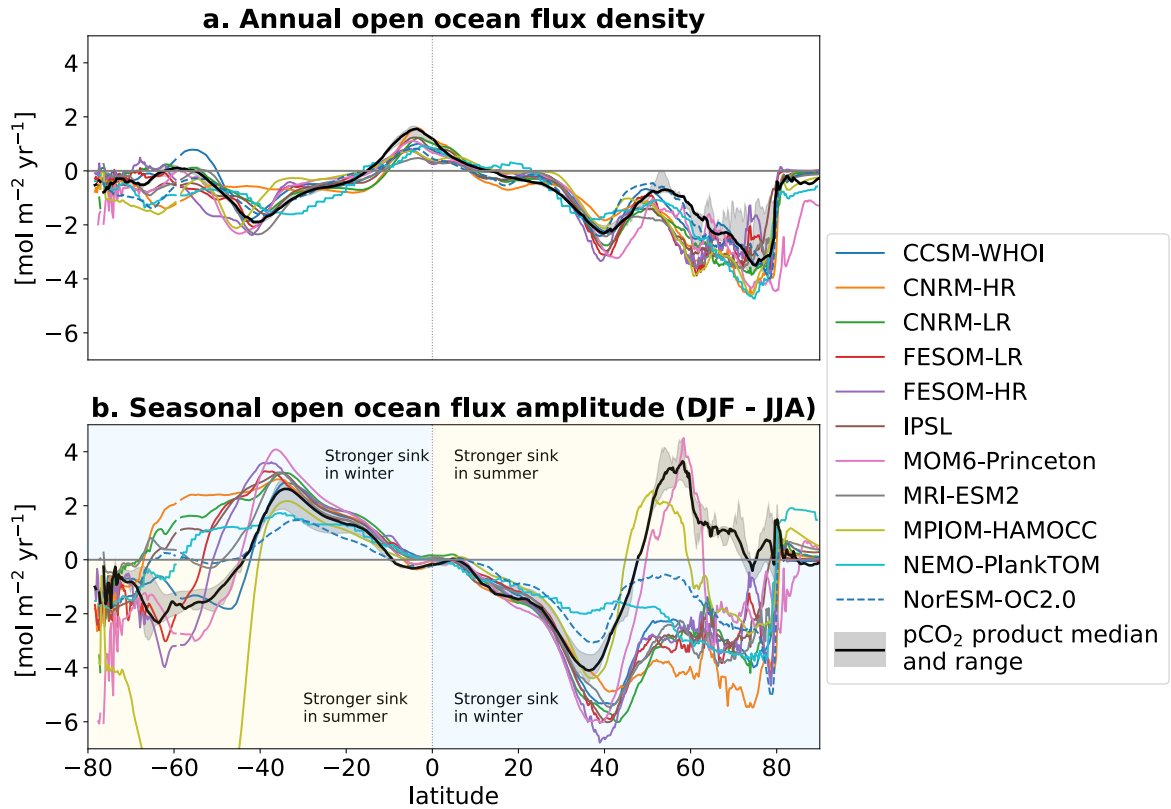


Figure S8. Latitudinal distribution of open ocean a) annual mean CO₂ flux densities, b) CO₂ flux densities seasonal amplitude computed as December-February minus June-August, for the pCO₂-product median (black line) and each individual models (colored lines). Note that the product median only includes the 3 (out of 4) products with open ocean values (CMEMS*, Carboscope-1 and Merged-SOM-FFN).

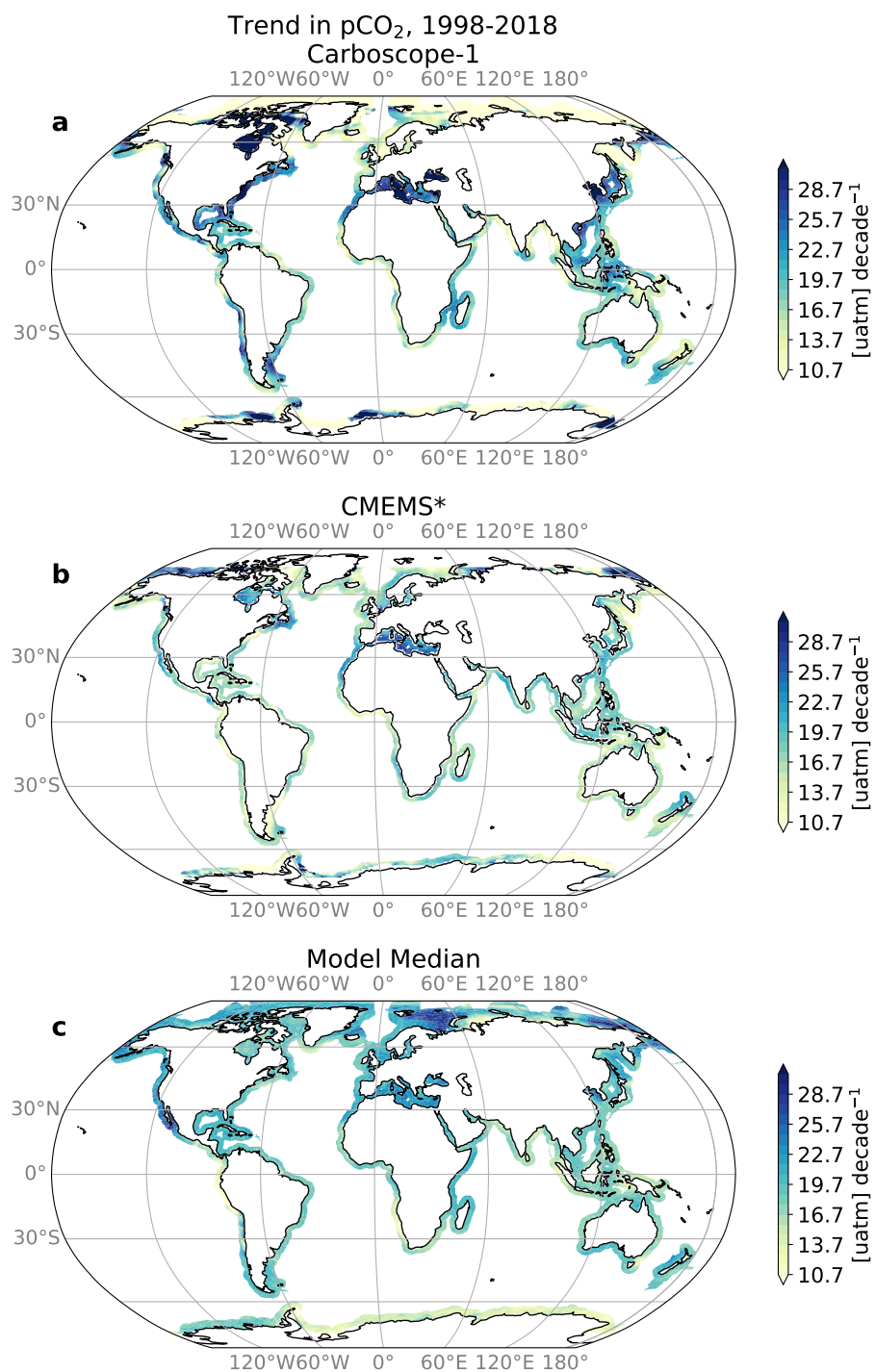


Figure S9. 1998-2018 trend in surface ocean pCO₂ in a) Carboscope-1 ; b) CMEMS* (area north of 75°N removed) c) multi-model median (global and regional models).

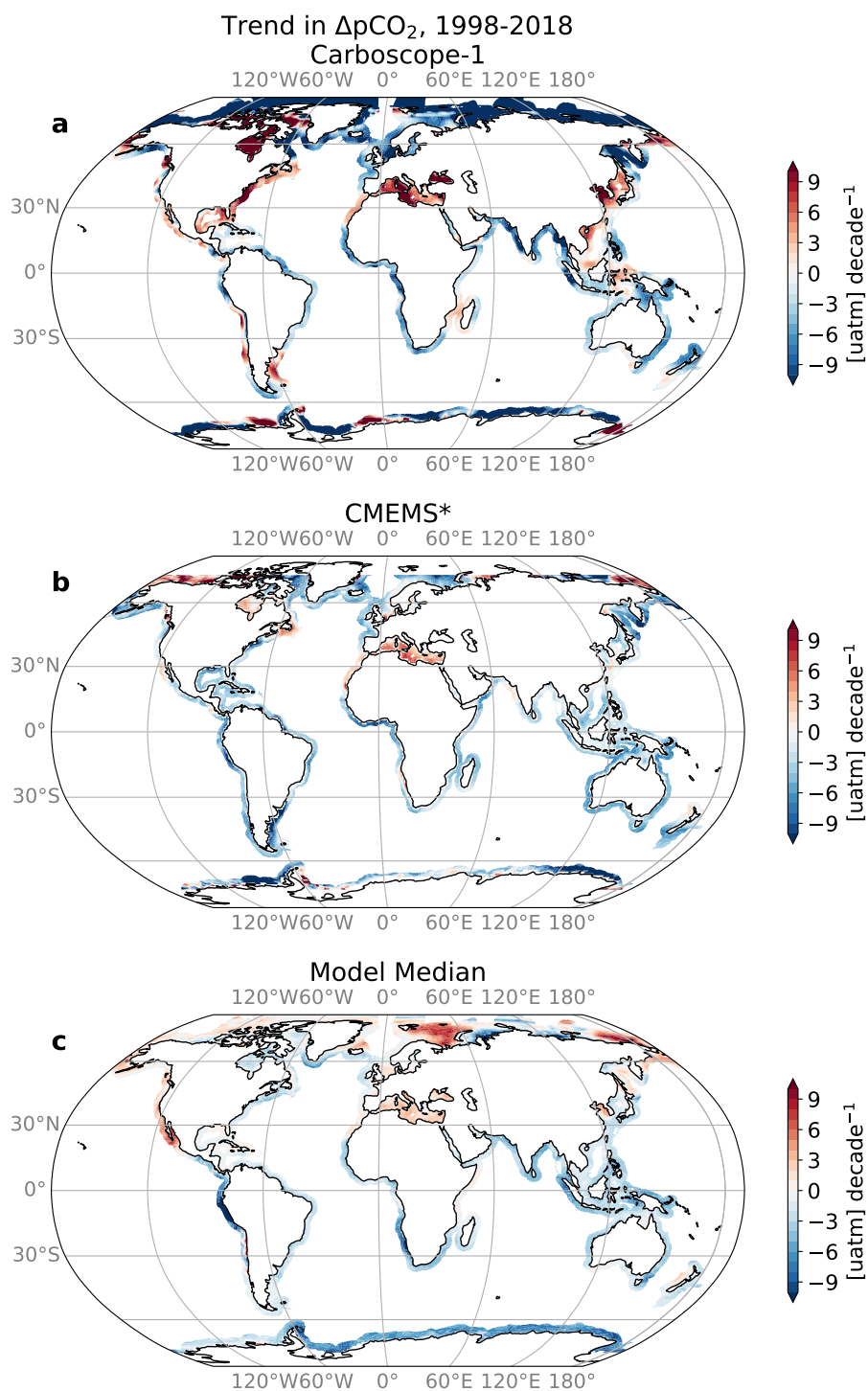


Figure S10. 1998-2018 trend in $\Delta p\text{CO}_2$ (difference between coastal ocean surface ocean $p\text{CO}_2$ and atmospheric) for a) Carboscope-1; b) CMEMS* (area north of 75°N removed) c) multi-model median (global and regional models). Negative $\Delta p\text{CO}_2$ trend values indicate that ocean $p\text{CO}_2$ increases at a lower rate than atmospheric and would therefore favor ocean uptake assuming constant wind and sea-ice coverage.

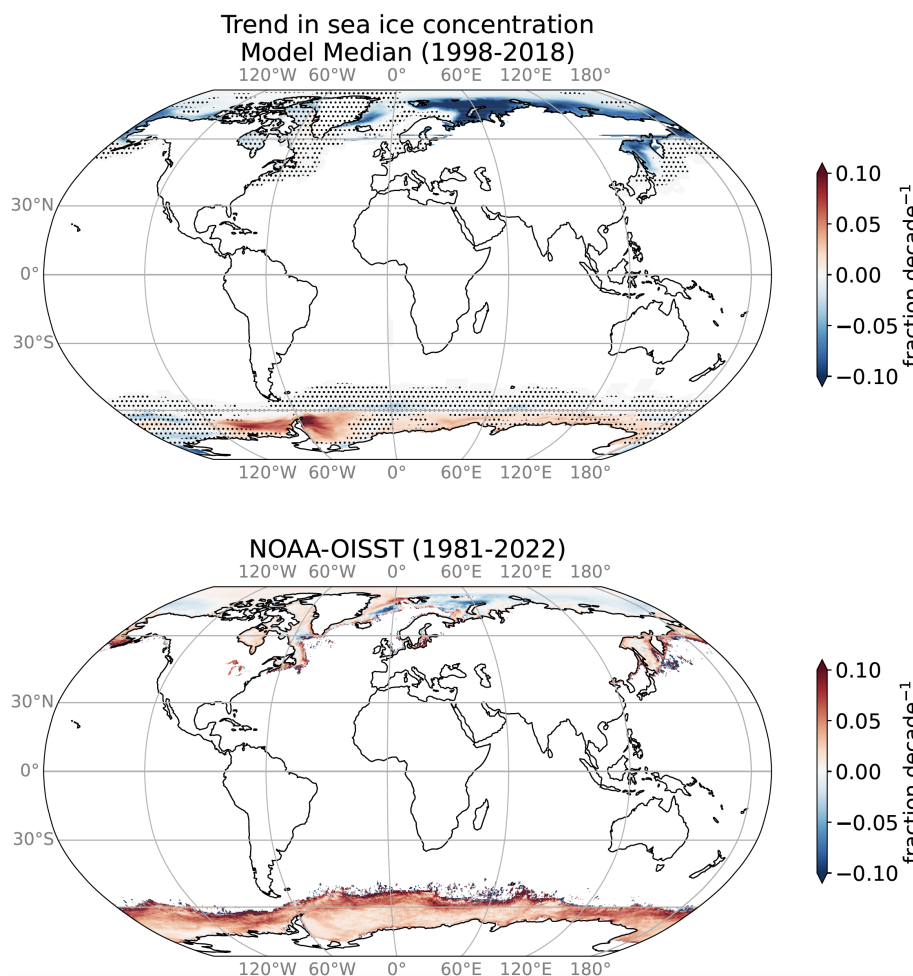


Figure S11. Linear trends in sea ice fraction from all 15 models median (top) and observation-based reference product NOAA-OISST (bottom). Stippling indicates where less than 6 out of the 11 global models agree on the sign of change.

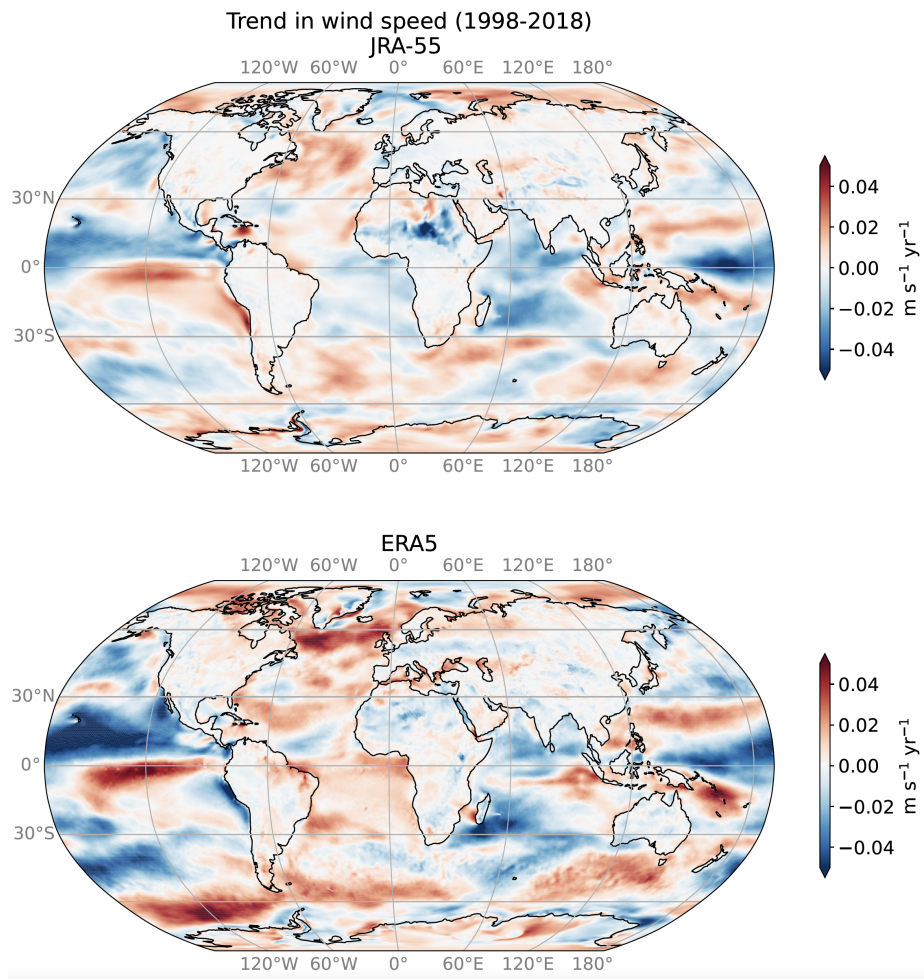


Figure S12. Linear trends in 10-meter wind speed from Japanese reanalysis JRA-55 (top) and ECMWF Reanalysis ERA-5 (bottom).

Table S2. Estimates of mean coastal ocean CO₂ flux densities, net CO₂ uptake and pCO₂ trends published since RECCAP-1 (Chen et al., 2013) and used in figures in the main text. Most prior estimates are given for coastal ocean areas similar to the area of the narrow coastal ocean used in this study (i.e. 28 million km²).

Study	Mean coastal CO ₂ flux density [mol m ⁻² yr ⁻¹]	Net coastal CO ₂ uptake [PgC yr ⁻¹]	Coastal pCO ₂ trends [uatm/decade]	Coastal area [million km ²]
Chen et al. (2013)	-1.09±2.9	-0.25±0.05	NA	30
Bauer et al. (2013)	NA	-0.25	NA	26
Laruelle et al. (2013)	-0.7	NA	NA	NA
Regnier et al. (2013)	NA	-0.2	NA	31
Laruelle et al. (2014)	-0.56 (global shelf) -0.7 (ice-free shelf)	-0.19±0.5 (1990-2011)	NA	28 22
Bourgeois et al. (2016)	NA	-0.1 (1993-2012)	NA	27
H. Wang et al. (2017)	NA	NA	+19.3±15.9 (from 10-30yr intervals in 1957-2014)	NA
Laruelle et al. (2018)	NA	-0.26 winter only	+13 [-6 to +32] winter only 1995-2006	30 (only 14 covered by obs. used)
Lacroix et al. (2021)	NA	-0.15 (1998-2015)	NA	24.5
Dai et al. (2022)	-0.68±0.14	-0.25±0.05 (1998-2021)	NA	30.32
Regnier et al. (2022)	NA	-0.32±0.08 (1990-2020)	NA	28

References

- Adcroft, A., Anderson, W., Balaji, V., Blanton, C., Bushuk, M., Dufour, C. O., ... Zhang, R. (2019). The GFDL Global Ocean and Sea Ice Model OM4.0: Model Description and Simulation Features. *Journal of Advances in Modeling Earth Systems*, 11(10), 3167–3211. Retrieved 2020-10-02, from <https://agupubs.onlinelibrary.wiley.com/doi/abs/10.1029/2019MS001726> doi: 10.1029/2019MS001726
- Araujo, M., Noriega, C., & Lefevre, N. (2014, May). Nutrients and carbon fluxes in the estuaries of major rivers flowing into the tropical Atlantic. *Frontiers in Marine Science*, 1. Retrieved 2023-02-15, from <http://journal.frontiersin.org/article/10.3389/fmars.2014.00010/abstract> doi: 10.3389/fmars.2014.00010
- Armstrong, R. A., Lee, C., Hedges, J. I., Honjo, S., & Wakeham, S. G. (2001, January). A new, mechanistic model for organic carbon fluxes in the ocean based on the quantitative association of POC with ballast minerals. *Deep Sea Research Part II: Topical Studies in Oceanography*, 49(1-3), 219–236. Retrieved 2023-02-15, from <https://linkinghub.elsevier.com/retrieve/pii/S0967064501001011> doi: 10.1016/S0967-0645(01)00101-1
- Aumont, O., Ethé, C., Tagliabue, A., Bopp, L., & Gehlen, M. (2015, August). PISCES-v2: an ocean biogeochemical model for carbon and ecosystem studies. *Geoscientific Model Development*, 8(8), 2465–2513. Retrieved 2023-02-15, from <https://gmd.copernicus.org/articles/8/2465/2015/gmd-8-2465-2015.html> (Publisher: Copernicus GmbH) doi: 10.5194/gmd-8-2465-2015
- Bakker, D. C. E., Pfeil, B., Landa, C. S., Metzl, N., O'Brien, K. M., Olsen, A., ... Xu, S. (2016, September). A multi-decade record of high-quality *f*CO₂ data in version 3 of the Surface Ocean CO₂ Atlas (SOCAT). *Earth System Science Data*, 8(2), 383–413. Retrieved from <https://www.earth-syst-sci-data.net/8/383/2016/> doi: <https://doi.org/10.5194/essd-8-383-2016>
- Barnier, B., Madec, G., Penduff, T., Molines, J., Treguier, A.-M., Le Sommer, J., ... de Cuevas, B. (2006, December). Impact of partial steps and momentum advection schemes in a global ocean circulation model at eddy-permitting resolution. *Ocean Dynamics*, 56(5-6), 543–567. Retrieved 2023-02-15, from <https://archimer.ifremer.fr/doc/00000/3514/> (Publisher: Springer) doi: 10.1007/s10236-006-0082-1
- Bauer, J. E., Cai, W.-J., Raymond, P. A., Bianchi, T. S., Hopkinson, C. S., & Regnier, P. A. G. (2013, December). The changing carbon cycle of the coastal ocean. *Nature*, 504(7478), 61–70. Retrieved 2016-01-12, from <http://www.nature.com/nature/journal/v504/n7478/abs/nature12857.html> doi: 10.1038/nature12857
- Bernard, B., Madec, G., Penduff, T., Molines, J.-M., Treguier, A.-M., Le Sommer, J., ... De Cuevas, B. (2006, December). Impact of partial steps and momentum advection schemes in a global ocean circulation model at eddy-permitting resolution. *Ocean Dynamics*, 56(5), 543–567. Retrieved 2023-02-15, from <https://doi.org/10.1007/s10236-006-0082-1> doi: 10.1007/s10236-006-0082-1
- Berthet, S., Jouanno, J., Séférian, R., Gehlen, M., & Llovel, W. (2022, August). How does the phytoplankton-light feedback affect marine N₂O inventory? *Earth Syst. Dynam. Discuss.* Retrieved 2023-03-01, from <https://esd.copernicus.org/preprints/>

- esd-2022-28/ doi: 10.5194/esd-2022-28
- Berthet, S., Séférian, R., Bricaud, C., Chevallier, M., Voldoire, A., & Ethé, C. (2019, June). Evaluation of an Online Grid-Coarsening Algorithm in a Global Eddy-Admitting Ocean Biogeochemical Model. *Journal of Advances in Modeling Earth Systems*, 11(6), 1759–1783. Retrieved 2023-03-01, from <https://onlinelibrary.wiley.com/doi/abs/10.1029/2019MS001644> doi: 10.1029/2019MS001644
- Bourgeois, T., Orr, J. C., Resplandy, L., Terhaar, J., Ethé, C., Gehlen, M., & Bopp, L. (2016, July). Coastal-ocean uptake of anthropogenic carbon. *Biogeosciences*, 13(14), 4167–4185. Retrieved 2016-09-23, from <http://www.biogeosciences.net/13/4167/2016/> doi: 10.5194/bg-13-4167-2016
- Brennan, C. E., Bianucci, L., & Fennel, K. (2016, May). Sensitivity of Northwest North Atlantic Shelf Circulation to Surface and Boundary Forcing: A Regional Model Assessment. *Atmosphere-Ocean*, 54(3), 230–247. Retrieved 2023-02-15, from <https://www.tandfonline.com/doi/full/10.1080/07055900.2016.1147416> doi: 10.1080/07055900.2016.1147416
- Buitenhuis, E. T., Le Quéré, C., Bednaršek, N., & Schiebel, R. (2019, March). Large Contribution of Pteropods to Shallow CaCO_3 Export. *Global Biogeochemical Cycles*, 33(3), 458–468. Retrieved 2023-02-15, from <https://onlinelibrary.wiley.com/doi/abs/10.1029/2018GB006110> doi: 10.1029/2018GB006110
- Buitenhuis, E. T., Suntharalingam, P., & Le Quéré, C. (2018, April). Constraints on global oceanic emissions of N_2O from observations and models. *Biogeosciences*, 15(7), 2161–2175. Retrieved 2023-02-07, from <https://bg.copernicus.org/articles/15/2161/2018/> (Publisher: Copernicus GmbH) doi: 10.5194/bg-15-2161-2018
- Carroll, D., Menemenlis, D., Adkins, J. F., Bowman, K. W., Brix, H., Dutkiewicz, S., ... Zhang, H. (2020, October). The ECCO-Darwin Data-Assimilative Global Ocean Biogeochemistry Model: Estimates of Seasonal to Multidecadal Surface Ocean $p\text{CO}_2$ and Air-Sea CO_2 Flux. *Journal of Advances in Modeling Earth Systems*, 12(10). Retrieved 2023-02-15, from <https://onlinelibrary.wiley.com/doi/10.1029/2019MS001888> doi: 10.1029/2019MS001888
- Chau, T. T. T., Gehlen, M., & Chevallier, F. (2022, February). A seamless ensemble-based reconstruction of surface ocean $p\text{CO}_2$ and air-sea CO_2 fluxes over the global coastal and open oceans. *Biogeosciences*, 19(4), 1087–1109. Retrieved 2023-02-15, from <https://bg.copernicus.org/articles/19/1087/2022/> doi: 10.5194/bg-19-1087-2022
- Chen, C.-T. A., Huang, T.-H., Chen, Y.-C., Bai, Y., He, X., & Kang, Y. (2013, October). Air-sea exchanges of CO_2 in the world's coastal seas. *Biogeosciences*, 10(10), 6509–6544. Retrieved 2021-09-03, from <https://bg.copernicus.org/articles/10/6509/2013/> doi: 10.5194/bg-10-6509-2013
- Dai, M., Su, J., Zhao, Y., Hofmann, E. E., Cao, Z., Cai, W.-J., ... Wang, Z. (2022). Carbon Fluxes in the Coastal Ocean: Synthesis, Boundary Processes, and Future Trends. *Annual Review of Earth and Planetary Sciences*, 50(1), 593–626. Retrieved 2022-09-26, from <https://doi.org/10.1146/annurev-earth-032320-090746> (eprint: <https://doi.org/10.1146/annurev-earth-032320-090746>) doi: 10.1146/annurev-earth-032320-090746
- Dee, D. P., Uppala, S. M., Simmons, A. J., Berrisford, P., Poli, P., Kobayashi, S., ... Vitart, F. (2011, April). The ERA-Interim reanalysis: configuration and performance of the data assimilation system. *Quarterly Journal of the Royal Meteorological Society*, 137(656), 553–597. Retrieved 2023-02-15, from <https://onlinelibrary.wiley.com/doi/10.1002/qj.828> doi: 10.1002/qj.828
- de Verneil, A., Lachkar, Z., Smith, S., & Lévy, M. (2022, February). Evaluating the Arabian Sea as a regional source of atmospheric CO_2 : seasonal variability and drivers. *Biogeosciences*, 19(3), 907–929. Retrieved 2023-02-15, from <https://bg.copernicus.org/articles/19/907/2022/> doi: 10.5194/bg-19-907-2022
- Dickson, A. G., Sabine, C. L., Christian, J. R., Barger, C. P., & Organization, N. P. M. S. (Eds.). (2007). *Guide to best practices for ocean CO_2 measurements* (No. no. 3). Sidney, BC: North Pacific Marine Science Organization.
- Doney, S. C., Lima, I., Feely, R. A., Glover, D. M., Lindsay, K., Mahowald, N., ... Wanninkhof, R. (2009, April). Mechanisms governing interannual variability in upper-ocean inorganic carbon system and air-sea CO_2 fluxes: Physical climate and atmospheric dust. *Deep Sea Research Part II: Topical Studies in Oceanography*, 56(8-10), 640–655. Retrieved 2018-09-13, from <http://linkinghub.elsevier.com/retrieve/pii/S096706450800427X> doi: 10.1016/j.dsr2.2008.12.006
- Dunne, J. P., Horowitz, L. W., Adcroft, A. J., Ginoux, P., Held, I. M., John, J. G., ... Zhao, M. (2020). The GFDL Earth System Model Version 4.1 (GFDL-ESM 4.1): Overall Coupled Model De-

- scription and Simulation Characteristics. *Journal of Advances in Modeling Earth Systems*, 12(11), e2019MS002015. Retrieved 2021-10-11, from <https://onlinelibrary.wiley.com/doi/abs/10.1029/2019MS002015> doi: 10.1029/2019MS002015
- Dunne, J. P., Sarmiento, J. L., & Gnanadesikan, A. (2007, December). A synthesis of global particle export from the surface ocean and cycling through the ocean interior and on the seafloor. *Global Biogeochemical Cycles*, 21(4), GB4006. Retrieved 2016-02-08, from <http://onlinelibrary.wiley.com/doi/10.1029/2006GB002907/abstract> doi: 10.1029/2006GB002907
- Fennel, K., & Wilkin, J. (2009, September). Quantifying biological carbon export for the northwest North Atlantic continental shelves. *Geophysical Research Letters*, 36(18), L18605. Retrieved 2023-02-15, from <http://doi.wiley.com/10.1029/2009GL039818> doi: 10.1029/2009GL039818
- Fennel, K., Wilkin, J., Levin, J., Moisan, J., O'Reilly, J., & Haidvogel, D. (2006, September). Nitrogen cycling in the Middle Atlantic Bight: Results from a three-dimensional model and implications for the North Atlantic nitrogen budget: NITROGEN CYCLING IN THE MIDDLE ATLANTIC. *Global Biogeochemical Cycles*, 20(3), n/a–n/a. Retrieved 2023-02-15, from <http://doi.wiley.com/10.1029/2005GB002456> doi: 10.1029/2005GB002456
- Franco, A. C., Gruber, N., Frölicher, T. L., & Kropuenske Artman, L. (2018, March). Contrasting Impact of Future CO₂ Emission Scenarios on the Extent of CaCO₃ Mineral Undersaturation in the Humboldt Current System. *Journal of Geophysical Research: Oceans*, 123(3), 2018–2036. Retrieved 2023-02-15, from <http://doi.wiley.com/10.1002/2018JC013857> doi: 10.1002/2018JC013857
- Friedlingstein, P., O'Sullivan, M., Jones, M. W., Andrew, R. M., Gregor, L., Hauck, J., ... Zheng, B. (2022). Global Carbon Budget 2022. *Earth System Science Data*, 14(11), 4811–4900. Retrieved from <https://essd.copernicus.org/articles/14/4811/2022/> doi: 10.5194/essd-14-4811-2022
- Friedlingstein, P., O'Sullivan, M., Jones, M. W., Andrew, R. M., Hauck, J., Olsen, A., ... Zaehle, S. (2020, December). Global Carbon Budget 2020. *Earth System Science Data*, 12(4), 3269–3340. Retrieved 2021-08-31, from <https://essd.copernicus.org/articles/12/3269/2020/> doi: 10.5194/essd-12-3269-2020
- Frischknecht, M. (2018). *New Perspectives on the Three-Dimensional Cycling of Carbon and Nutrients in the California Current System and its Response to ENSO* (Doctoral dissertation, ETH Zurich). (Artwork Size: 254 p. Medium: application/pdf Pages: 254 p.) doi: 10.3929/ETHZ-B-000283522
- Ganesan, A. L., Manizza, M., Morgan, E. J., Harth, C. M., Kozlova, E., Lueker, T., ... Rigby, M. (2020, July). Marine Nitrous Oxide Emissions From Three Eastern Boundary Upwelling Systems Inferred From Atmospheric Observations. *Geophysical Research Letters*, 47(14). Retrieved 2023-02-15, from <https://onlinelibrary.wiley.com/doi/10.1029/2020GL087822> doi: 10.1029/2020GL087822
- Garcia, H. E., Locarnini, R. A., Boyer, T. P., Baranova, O. K., Zweng, M. M., Reagan, J. R., & Johnson, D. R. (2014). *World Ocean Atlas 2013, Volume 3: Dissolved Oxygen, Apparent Oxygen Utilization, and Oxygen Saturation*. (Tech. Rep.). S. Levitus, Ed., A. Mishonov Technical Ed.; NOAA Atlas NESDIS 75, 27 pp.
- Good, S., Fiedler, E., Mao, C., Martin, M. J., Maycock, A., Reid, R., ... Worsfold, M. (2020, February). The Current Configuration of the OSTIA System for Operational Production of Foundation Sea Surface Temperature and Ice Concentration Analyses. *Remote Sensing*, 12(4), 720. Retrieved 2023-02-14, from <https://www.mdpi.com/2072-4292/12/4/720> doi: 10.3390/rs12040720
- Good, S. A., Martin, M. J., & Rayner, N. A. (2013, December). EN4: Quality controlled ocean temperature and salinity profiles and monthly objective analyses with uncertainty estimates: THE EN4 DATA SET. *Journal of Geophysical Research: Oceans*, 118(12), 6704–6716. Retrieved 2023-02-15, from <http://doi.wiley.com/10.1002/2013JC009067> doi: 10.1002/2013JC009067
- Gruber, N., Clement, D., Carter, B. R., Feely, R. A., Heuven, S. v., Hoppema, M., ... Wanninkhof, R. (2019, March). The oceanic sink for anthropogenic CO₂ from 1994 to 2007. *Science*, 363(6432), 1193–1199. Retrieved 2019-03-19, from <http://science.sciencemag.org.ezproxy.princeton.edu/content/363/6432/1193> doi: 10.1126/science.aau5153
- Gruber, N., Frenzel, H., Doney, S. C., Marchesiello, P., McWilliams, J. C., Moisan, J. R., ... Stolzenbach, K. D. (2006, September). Eddy-resolving simulation of plankton ecosystem dynamics in the California Current System. *Deep Sea Research Part I: Oceanographic Research Papers*, 53(9), 1483–1516. Retrieved 2023-02-15, from <https://www.sciencedirect.com/science/article/pii/S0967063706001713>

- doi: 10.1016/j.dsr.2006.06.005
- Gruber, N., Hauri, C., Lachkar, Z., Loher, D., Frölicher, T. L., & Plattner, G.-K. (2012, July). Rapid Progression of Ocean Acidification in the California Current System. *Science*, 337(6091), 220–223. Retrieved 2023-02-15, from <https://www.science.org/doi/10.1126/science.1216773> doi: 10.1126/science.1216773
- Haidvogel, D., Arango, H., Budgell, W., Cornuelle, B., Curchitser, E., Di Lorenzo, E., ... Wilkin, J. (2008, March). Ocean forecasting in terrain-following coordinates: Formulation and skill assessment of the Regional Ocean Modeling System. *Journal of Computational Physics*, 227(7), 3595–3624. Retrieved 2023-02-15, from <https://linkinghub.elsevier.com/retrieve/pii/S0021999107002549> doi: 10.1016/j.jcp.2007.06.016
- Hartmann, J., Jansen, N., Dürr, H. H., Kempe, S., & Köhler, P. (2009, December). Global CO₂-consumption by chemical weathering: What is the contribution of highly active weathering regions? *Global and Planetary Change*, 69(4), 185–194. Retrieved 2020-01-30, from <https://linkinghub.elsevier.com/retrieve/pii/S0921818109001349> doi: 10.1016/j.gloplacha.2009.07.007
- Hauck, J., Völker, C., Wang, T., Hoppema, M., Losch, M., & Wolf-Gladrow, D. A. (2013, December). Seasonally different carbon flux changes in the Southern Ocean in response to the southern annular mode. *Global Biogeochemical Cycles*, 27(4), 1236–1245. Retrieved 2023-02-15, from <https://onlinelibrary.wiley.com/doi/10.1002/2013GB004600> doi: 10.1002/2013GB004600
- Hauck, J., Zeising, M., Le Quéré, C., Gruber, N., Bakker, D. C. E., Bopp, L., ... Séférian, R. (2020). Consistency and Challenges in the Ocean Carbon Sink Estimate for the Global Carbon Budget. *Frontiers in Marine Science*, 7. Retrieved 2020-12-18, from <https://www.frontiersin.org/articles/10.3389/fmars.2020.571720/full> (Publisher: Frontiers) doi: 10.3389/fmars.2020.571720
- Hersbach, H., Bell, B., Berrisford, P., Hirahara, S., Horányi, A., Muñoz-Sabater, J., ... Thépaut, J.-N. (2020). The ERA5 global reanalysis. *Quarterly Journal of the Royal Meteorological Society*, 146(730), 1999–2049. Retrieved 2023-02-14, from <https://onlinelibrary.wiley.com/doi/abs/10.1002/qj.3803> doi: 10.1002/qj.3803
- Ho, D. T., Law, C. S., Smith, M. J., Schlosser, P., Harvey, M., & Hill, P. (2006). Measurements of air-sea gas exchange at high wind speeds in the Southern Ocean: Implications for global parameterizations. *Geophysical Research Letters*, 33(16). Retrieved 2019-06-25, from <https://agupubs.onlinelibrary.wiley.com/doi/abs/10.1029/2006GL026817> doi: 10.1029/2006GL026817
- Ho, D. T., Wanninkhof, R., Schlosser, P., Ullman, D. S., Hebert, D., & Sullivan, K. F. (2011, July). Toward a universal relationship between wind speed and gas exchange: Gas transfer velocities measured with ³He/SF₆ during the Southern Ocean Gas Exchange Experiment. *Journal of Geophysical Research*, 116, C00F04. Retrieved 2023-02-15, from <http://doi.wiley.com/10.1029/2010JC006854> doi: 10.1029/2010JC006854
- Hornafius, J. S., Quigley, D., & Luyendyk, B. P. (1999, September). The world's most spectacular marine hydrocarbon seeps (Coal Oil Point, Santa Barbara Channel, California): Quantification of emissions. *Journal of Geophysical Research: Oceans*, 104(C9), 20703–20711. Retrieved 2023-02-23, from <http://doi.wiley.com/10.1029/1999JC900148> doi: 10.1029/1999JC900148
- Hovland, M., Judd, A., & Burke, R. (1993, January). The global flux of methane from shallow submarine sediments. *Chemosphere*, 26(1-4), 559–578. Retrieved 2023-02-23, from <https://linkinghub.elsevier.com/retrieve/pii/0045653593904428> doi: 10.1016/0045-6535(93)90442-8
- Ilyina, T., Six, K. D., Segschneider, J., Maier-Reimer, E., Li, H., & Núñez-Riboni, I. (2013, June). Global ocean biogeochemistry model HAMOCC: Model architecture and performance as component of the MPI-Earth system model in different CMIP5 experimental realizations. *Journal of Advances in Modeling Earth Systems*, 5(2), 287–315. Retrieved 2023-02-15, from <https://onlinelibrary.wiley.com/doi/10.1029/2012MS000178> doi: 10.1029/2012MS000178
- Joos, F., & Spahni, R. (2008, February). Rates of change in natural and anthropogenic radiative forcing over the past 20,000 years. *Proceedings of the National Academy of Sciences*, 105(5), 1425–1430. Retrieved 2019-06-18, from <https://www.pnas.org/content/105/5/1425> doi: 10.1073/pnas.0707386105
- Jungclaus, J. H., Fischer, N., Haak, H., Lohmann, K., Marotzke, J., Matei, D., ... Storch, J. S. (2013, June). Characteristics of the ocean simulations in the Max Planck Institute Ocean Model (MPIOM) the ocean component of the MPI-Earth system model. *Journal of Advances in Modeling Earth Systems*, 5(2), 422–446. Retrieved 2023-02-20, from <https://onlinelibrary.wiley.com/doi/>

- 10.1002/jame.20023 doi: 10.1002/jame.20023
- Kanamitsu, M., Ebisuzaki, W., Woollen, J., Yang, S.-K., Hnilo, J. J., Fiorino, M., & Potter, G. L. (2002, November). NCEP–DOE AMIP-II Reanalysis (R-2). *Bulletin of the American Meteorological Society*, 83(11), 1631–1644. Retrieved 2023-02-15, from <https://journals.ametsoc.org/view/journals/bams/83/11/bams-83-11-1631.xml> (Publisher: American Meteorological Society Section: Bulletin of the American Meteorological Society) doi: 10.1175/BAMS-83-11-1631
- Keeling, C. D., Piper, S. C., Bacastow, R. B., Wahlen, M., Whorf, T. P., Heimann, M., & Meijer, H. A. (2005). Atmospheric CO₂ and 13CO₂ Exchange with the Terrestrial Biosphere and Oceans from 1978 to 2000: Observations and Carbon Cycle Implications. In I. T. Baldwin et al. (Eds.), *A History of Atmospheric CO₂ and Its Effects on Plants, Animals, and Ecosystems* (pp. 83–113). Springer New York. Retrieved 2016-09-16, from http://link.springer.com/chapter/10.1007/0-387-27048-5_5 doi: 10.1007/0-387-27048-5_5
- Key, R. M., Kozyr, A., Sabine, C. L., Lee, K., Wanninkhof, R., Bullister, J. L., ... Peng, T.-H. (2004, December). A global ocean carbon climatology: Results from Global Data Analysis Project (GLODAP): GLOBAL OCEAN CARBON CLIMATOLOGY. *Global Biogeochemical Cycles*, 18(4), n/a–n/a. Retrieved 2023-02-15, from <http://doi.wiley.com/10.1029/2004GB002247> doi: 10.1029/2004GB002247
- Khatiwala, S., Tanhua, T., Mikaloff Fletcher, S., Gerber, M., Doney, S. C., Graven, H. D., ... Sabine, C. L. (2013, April). Global ocean storage of anthropogenic carbon. *Biogeosciences*, 10(4), 2169–2191. Retrieved 2016-01-19, from <http://www.biogeosciences.net/10/2169/2013/> doi: 10.5194/bg-10-2169-2013
- Kock, A., & Bange, H. (2015, February). Counting the Ocean's Greenhouse Gas Emissions. *Eos*, 96. Retrieved 2023-02-14, from <https://eos.org/project-updates/counting-oceans-greenhouse-gas-emissions> doi: 10.1029/2015EO023665
- Krishna, M., Prasad, M., Rao, D., Viswanadham, R., Sarma, V., & Reddy, N. (2016, January). Export of dissolved inorganic nutrients to the northern Indian Ocean from the Indian monsoonal rivers during discharge period. *Geochimica et Cosmochimica Acta*, 172, 430–443. Retrieved 2023-02-23, from <https://linkinghub.elsevier.com/retrieve/pii/S0016703715005955> doi: 10.1016/j.gca.2015.10.013
- Lachkar, Z., & Gruber, N. (2013, January). Response of biological production and air–sea CO₂ fluxes to upwelling intensification in the California and Canary Current Systems. *Journal of Marine Systems*, 109–110, 149–160. Retrieved 2023-02-15, from <https://www.sciencedirect.com/science/article/pii/S092479631200108X> doi: 10.1016/j.jmarsys.2012.04.003
- Lachkar, Z., Mehari, M., Al Azhar, M., Lévy, M., & Smith, S. (2021, October). Fast local warming is the main driver of recent deoxygenation in the northern Arabian Sea. *Biogeosciences*, 18(20), 5831–5849. Retrieved 2023-02-15, from <https://bg.copernicus.org/articles/18/5831/2021/> doi: 10.5194/bg-18-5831-2021
- Lachkar, Z., Smith, S., Lévy, M., & Pauluis, O. (2016, September). Eddies reduce denitrification and compress habitats in the Arabian Sea. *Geophysical Research Letters*, 43(17), 9148–9156. Retrieved 2018-01-16, from <http://onlinelibrary.wiley.com/doi/10.1002/2016GL069876/full> doi: 10.1002/2016GL069876
- Lacroix, F., Ilyina, T., Laruelle, G. G., & Regnier, P. (2021). Reconstructing the Preindustrial Coastal Carbon Cycle Through a Global Ocean Circulation Model: Was the Global Continental Shelf Already Both Autotrophic and a CO₂ Sink? *Global Biogeochemical Cycles*, 35(2), e2020GB006603. Retrieved 2021-09-03, from <https://agupubs.onlinelibrary.wiley.com/doi/abs/10.1029/2020GB006603> doi: 10.1029/2020GB006603
- Landschützer, P., Gruber, N., Bakker, D. C. E., & Schuster, U. (2014, September). Recent variability of the global ocean carbon sink. *Global Biogeochemical Cycles*, 28(9), 927–949. Retrieved 2015-08-11, from <http://onlinelibrary.wiley.com/doi/10.1002/2014GB004853/abstract> doi: 10.1002/2014GB004853
- Landschützer, P., Gruber, N., Bakker, D. C. E., Schuster, U., Nakaoka, S., Payne, M. R., ... Zeng, J. (2013, November). A neural network-based estimate of the seasonal to inter-annual variability of the Atlantic Ocean carbon sink. *Biogeosciences*, 10(11), 7793–7815. Retrieved 2023-02-15, from <https://bg.copernicus.org/articles/10/7793/2013/> doi: 10.5194/bg-10-7793-2013
- Landschützer, P., Laruelle, G. G., Roobaert, A., & Regnier, P. (2020, October). A uniform pCO₂ climatology combining open and coastal oceans. *Earth System Science Data*, 12(4), 2537–2553. Retrieved 2023-02-14, from <https://essd.copernicus.org/articles/12/2537/2020/> doi: 10.5194/essd-12

- 2537-2020
- Large, W. G., McWilliams, J. C., & Doney, S. C. (1994). Oceanic vertical mixing: A review and a model with a nonlocal boundary layer parameterization. *Reviews of Geophysics*, 32(4), 363–403. Retrieved 2023-02-15, from <https://onlinelibrary.wiley.com/doi/abs/10.1029/94RG01872> doi: 10.1029/94RG01872
- Large, W. G., & Yeager, S. G. (2009, August). The global climatology of an interannually varying air–sea flux data set. *Climate Dynamics*, 33(2-3), 341–364. Retrieved 2015-04-02, from <http://link.springer.com/10.1007/s00382-008-0441-3> doi: 10.1007/s00382-008-0441-3
- Laruelle, G. G., Cai, W.-J., Hu, X., Gruber, N., Mackenzie, F. T., & Regnier, P. (2018, January). Continental shelves as a variable but increasing global sink for atmospheric carbon dioxide. *Nature Communications*, 9, 454. Retrieved 2021-09-03, from <https://www.ncbi.nlm.nih.gov/pmc/articles/PMC5792465/> doi: 10.1038/s41467-017-02738-z
- Laruelle, G. G., Dürr, H. H., Lauerwald, R., Hartmann, J., Slomp, C. P., Goossens, N., & Regnier, P. A. G. (2013, May). Global multi-scale segmentation of continental and coastal waters from the watersheds to the continental margins. *Hydrology and Earth System Sciences*, 17(5), 2029–2051. Retrieved 2020-03-27, from <https://www.hydrology-earth-syst-sci.net/17/2029/2013/> doi: 10.5194/hess-17-2029-2013
- Laruelle, G. G., Landschützer, P., Gruber, N., Tison, J.-L., Delille, B., & Regnier, P. (2017, October). Global high-resolution monthly pCO₂ climatology for the coastal ocean derived from neural network interpolation. *Biogeosciences*, 14(19), 4545–4561. Retrieved 2019-08-29, from <https://www.biogeosciences.net/14/4545/2017/> doi: 10.5194/bg-14-4545-2017
- Laruelle, G. G., Lauerwald, R., Pfeil, B., & Regnier, P. (2014). Regionalized global budget of the CO₂ exchange at the air–water interface in continental shelf seas. *Global Biogeochemical Cycles*, 28(11), 1199–1214. Retrieved 2021-09-03, from <https://agupubs.onlinelibrary.wiley.com/doi/abs/10.1002/2014GB004832> doi: 10.1002/2014GB004832
- Laurent, A., Fennel, K., Cai, W., Huang, W., Barbero, L., & Wanninkhof, R. (2017, January). Eutrophication-induced acidification of coastal waters in the northern Gulf of Mexico: Insights into origin and processes from a coupled physical–biogeochemical model. *Geophysical Research Letters*, 44(2), 946–956. Retrieved 2023-02-15, from <https://onlinelibrary.wiley.com/doi/abs/10.1002/2016GL071881> doi: 10.1002/2016GL071881
- Laurent, A., Fennel, K., & Kuhn, A. (2021, March). An observation-based evaluation and ranking of historical Earth system model simulations in the northwest North Atlantic Ocean. *Biogeosciences*, 18(5), 1803–1822. Retrieved 2023-02-15, from <https://bg.copernicus.org/articles/18/1803/2021/> doi: 10.5194/bg-18-1803-2021
- Lauvset, S. K., Key, R. M., Olsen, A., Heuven, S. v., Velo, A., Lin, X., ... Watelet, S. (2016, August). A new global interior ocean mapped climatology: the 1° × 1° GLODAP version 2. *Earth System Science Data*, 8(2), 325–340. Retrieved 2016-11-07, from <http://www.earth-syst-sci-data.net/8/325/2016/> doi: 10.5194/essd-8-325-2016
- Liang, J.-H., Deutsch, C., McWilliams, J. C., Baschek, B., Sullivan, P. P., & Chiba, D. (2013). Parameterizing bubble-mediated air–sea gas exchange and its effect on ocean ventilation. *Global Biogeochemical Cycles*, 27(3), 894–905. Retrieved 2023-02-14, from <https://onlinelibrary.wiley.com/doi/abs/10.1002/gbc.20080> doi: 10.1002/gbc.20080
- Liao, E., Resplandy, L., Liu, J., & Bowman, K. W. (2020). Amplification of the Ocean Carbon Sink During El Niños: Role of Poleward Ekman Transport and Influence on Atmospheric CO₂. *Global Biogeochemical Cycles*, 34(9), e2020GB006574. Retrieved 2020-10-15, from <http://agupubs.onlinelibrary.wiley.com/doi/abs/10.1029/2020GB006574> doi: 10.1029/2020GB006574
- Liss, P. S., & Merlivat, L. (1986). Air–Sea Gas Exchange Rates: Introduction and Synthesis. In P. Buat-Ménard (Ed.), *The Role of Air–Sea Exchange in Geochemical Cycling* (pp. 113–127). Dordrecht: Springer Netherlands. Retrieved 2023-02-23, from https://doi.org/10.1007/978-94-009-4738-2_5 doi: 10.1007/978-94-009-4738-2_5
- Locarnini, R. A., Mishonov, A. V., Antonov, J. I., Boyer, T. P., Garcia, H. E., Baranova, O. K., ... Seidov, D. (2014). *World Ocean Atlas 2013, Volume 1: Temperature*. (Tech. Rep.). S. Levitus, Ed., A. Mishonov Technical Ed.; NOAA Atlas NESDIS 73, 40 pp.
- Louchard, D., Gruber, N., & Münnich, M. (2021). The Impact of the Amazon on the Biological Pump and the Air–Sea CO₂ Balance of the Western Tropical Atlantic. *Global Biogeochemical Cycles*, 35(6), e2020GB006818. Retrieved 2021-09-22, from <https://onlinelibrary.wiley.com/doi/abs/10.1029/2020GB006818> doi: 10.1029/2020GB006818

- 2020GB006818
- Ludwig, W., Amiotte Suchet, P., & Probst, J.-L. (1996). River discharges of carbon to the world's oceans: determining local inputs of alkalinity and of dissolved and particulate organic carbon. *Sciences de la terre et des planètes (Comptes rendus de l'Académie des sciences)*, *t. 323*, 1007–1014. Retrieved 2023-02-15, from <https://oatao.univ-toulouse.fr/3498/> (Publisher: Gauthier-Villars)
- Madec, G., Bourdallé-Badie, R., Bouttier, P.-A., Bricaud, C., Bruciaferri, D., Calvert, D., ... Vancoppenolle, M. (2017). NEMO ocean engine. Retrieved 2023-02-15, from <https://zenodo.org/record/1472492> doi: 10.5281/ZENODO.1472492
- Mahowald, N. M., Engelstaedter, S., Luo, C., Sealy, A., Artaxo, P., Benitez-Nelson, C., ... Siefert, R. L. (2009). Atmospheric Iron Deposition: Global Distribution, Variability, and Human Perturbations. *Annual Review of Marine Science*, *1*(1), 245–278. Retrieved 2023-02-21, from <https://doi.org/10.1146/annurev.marine.010908.163727> doi: 10.1146/annurev.marine.010908.163727
- Manizza, M., Keeling, R. F., & Nevison, C. D. (2012, January). On the processes controlling the seasonal cycles of the air-sea fluxes of O₂ and N₂O: A modelling study. *Tellus B: Chemical and Physical Meteorology*, *64*(1), 18429. Retrieved 2023-02-15, from <https://b.tellusjournals.se/article/10.3402/tellusb.v64i0.18429/> doi: 10.3402/tellusb.v64i0.18429
- Manizza, M., Menemenlis, D., Zhang, H., & Miller, C. E. (2019). Modeling the Recent Changes in the Arctic Ocean CO₂ Sink (2006–2013). *Global Biogeochemical Cycles*, *33*(3), 420–438. Retrieved 2023-02-15, from <https://onlinelibrary.wiley.com/doi/abs/10.1029/2018GB006070> doi: 10.1029/2018GB006070
- Martinez-Rey, J., Bopp, L., Gehlen, M., Tagliabue, A., & Gruber, N. (2015, July). Projections of oceanic N₂O emissions in the 21st century using the IPSL Earth system model. *Biogeosciences*, *12*(13), 4133–4148. Retrieved 2016-06-07, from <http://www.biogeosciences.net/12/4133/2015/> doi: 10.5194/bg-12-4133-2015
- Mayorga, E., Seitzinger, S. P., Harrison, J. A., Dumont, E., Beusen, A. H., Bouwman, A., ... Van Drecht, G. (2010, July). Global Nutrient Export from WaterSheds 2 (NEWS 2): Model development and implementation. *Environmental Modelling & Software*, *25*(7), 837–853. Retrieved 2023-02-23, from <https://linkinghub.elsevier.com/retrieve/pii/S1364815210000186> doi: 10.1016/j.envsoft.2010.01.007
- McGinnis, D. F., Greinert, J., Artemov, Y., Beaubien, S. E., & Wüest, A. (2006). Fate of rising methane bubbles in stratified waters: How much methane reaches the atmosphere? *Journal of Geophysical Research*, *111*(C9), C09007. Retrieved 2023-02-23, from <http://doi.wiley.com/10.1029/2005JC003183> doi: 10.1029/2005JC003183
- Middelburg, J. J., Soetaert, K., Herman, P. M. J., & Heip, C. H. R. (1996, December). Denitrification in marine sediments: A model study. *Global Biogeochemical Cycles*, *10*(4), 661–673. Retrieved 2023-02-15, from <http://doi.wiley.com/10.1029/96GB02562> doi: 10.1029/96GB02562
- Moore, J. K., Lindsay, K., Doney, S. C., Long, M. C., & Misumi, K. (2013, August). Marine Ecosystem Dynamics and Biogeochemical Cycling in the Community Earth System Model [CESM1(BGC)]: Comparison of the 1990s with the 2090s under the RCP4.5 and RCP8.5 Scenarios. *Journal of Climate*, *26*(23), 9291–9312. Retrieved 2016-06-16, from <http://journals.ametsoc.org/doi/abs/10.1175/JCLI-D-12-00566.1> doi: 10.1175/JCLI-D-12-00566.1
- Naegler, T. (2009, January). Reconciliation of excess 14C-constrained global CO₂ piston velocity estimates. *Tellus B: Chemical and Physical Meteorology*, *61*(2), 372–384. Retrieved 2023-02-15, from <https://doi.org/10.1111/j.1600-0889.2008.00408.x> (Publisher: Taylor & Francis eprint: <https://doi.org/10.1111/j.1600-0889.2008.00408.x>) doi: 10.1111/j.1600-0889.2008.00408.x
- Nakano, H., Tsujino, H., Hirabara, M., Yasuda, T., Motoi, T., Ishii, M., & Yamanaka, G. (2011, December). Uptake mechanism of anthropogenic CO₂ in the Kuroshio Extension region in an ocean general circulation model. *Journal of Oceanography*, *67*(6), 765–783. Retrieved 2019-09-25, from <https://doi.org/10.1007/s10872-011-0075-7> doi: 10.1007/s10872-011-0075-7
- Nevison, C., Butler, J. H., & Elkins, J. W. (2003, December). Global distribution of N₂O and the N₂O-AOU yield in the subsurface ocean. *Global Biogeochemical Cycles*, *17*(4), n/a–n/a. Retrieved 2023-02-15, from <http://doi.wiley.com/10.1029/2003GB002068> doi: 10.1029/2003GB002068
- Nightingale, P. D., Malin, G., Law, C. S., Watson, A. J., Liss, P. S., Liddicoat, M. I., ... Upstill-Goddard, R. C. (2000, March). In situ evaluation of air-sea gas exchange parameterizations using novel conservative and volatile tracers. *Global Biogeochemical Cycles*, *14*(1), 373–387. Retrieved 2023-02-15, from <http://>

- doi.wiley.com/10.1029/1999GB900091 doi: 10.1029/1999GB900091
- Olsen, A., Key, R. M., van Heuven, S., Lauvset, S. K., Velo, A., Lin, X., ... Suzuki, T. (2016, August). The Global Ocean Data Analysis Project version 2 (GLODAPv2) – an internally consistent data product for the world ocean. *Earth System Science Data*, 8(2), 297–323. Retrieved 2023-02-15, from <https://essd.copernicus.org/articles/8/297/2016/> (Publisher: Copernicus GmbH) doi: 10.5194/essd-8-297-2016
- Olsen, A., Lange, N., Key, R. M., Tanhua, T., Álvarez, M., Becker, S., ... Wanninkhof, R. (2019, September). GLODAPv2.2019 – an update of GLODAPv2. *Earth System Science Data*, 11(3), 1437–1461. Retrieved 2023-02-16, from <https://essd.copernicus.org/articles/11/1437/2019/> (Publisher: Copernicus GmbH) doi: 10.5194/essd-11-1437-2019
- Orr, J. C., Epitalon, J.-M., & Gattuso, J.-P. (2015, March). Comparison of ten packages that compute ocean carbonate chemistry. *Biogeosciences*, 12(5), 1483–1510. Retrieved 2023-02-15, from <https://bg.copernicus.org/articles/12/1483/2015/> (Publisher: Copernicus GmbH) doi: 10.5194/bg-12-1483-2015
- Orr, J. C., Fabry, V. J., Aumont, O., Bopp, L., Doney, S. C., Feely, R. A., ... Yool, A. (2005, September). Anthropogenic ocean acidification over the twenty-first century and its impact on calcifying organisms. *Nature*, 437(7059), 681–686. Retrieved 2023-02-15, from <https://www.nature.com/articles/nature04095> (Number: 7059 Publisher: Nature Publishing Group) doi: 10.1038/nature04095
- Orr, J. C., Najjar, R. G., Aumont, O., Bopp, L., Bullister, J. L., Danabasoglu, G., ... Yool, A. (2017, June). Biogeochemical protocols and diagnostics for the CMIP6 Ocean Model Intercomparison Project (OMIP). *Geoscientific Model Development*, 10(6), 2169–2199. Retrieved 2020-02-20, from <https://www.geosci-model-dev.net/10/2169/2017/> doi: <https://doi.org/10.5194/gmd-10-2169-2017>
- Paulsen, H., Ilyina, T., Six, K. D., & Stemmeler, I. (2017, March). Incorporating a prognostic representation of marine nitrogen fixers into the global ocean biogeochemical model HAMOCC: PROGNOSTIC NITROGEN FIXERS IN HAMOCC. *Journal of Advances in Modeling Earth Systems*, 9(1), 438–464. Retrieved 2023-02-20, from <http://doi.wiley.com/10.1002/2016MS000737> doi: 10.1002/2016MS000737
- Ramesh, R., Purvaja, G. R., & Subramanian, V. (1995). Carbon and Phosphorus Transport by the Major Indian Rivers. *Journal of Biogeography*, 22(2/3), 409–415. Retrieved 2023-02-23, from <https://www.jstor.org/stable/2845937> (Publisher: Wiley) doi: 10.2307/2845937
- Regnier, P., Friedlingstein, P., Ciais, P., Mackenzie, F. T., Gruber, N., Janssens, I. A., ... Thullner, M. (2013, June). Anthropogenic perturbation of the carbon fluxes from land to ocean. *Nature Geoscience*, 6(8), 597–607. Retrieved 2015-06-25, from <http://www.nature.com/doifinder/10.1038/ngeo1830> doi: 10.1038/ngeo1830
- Regnier, P., Resplandy, L., Najjar, R. G., & Ciais, P. (2022, March). The land-to-ocean loops of the global carbon cycle. *Nature*, 603(7901), 401–410. Retrieved 2022-04-18, from <https://www.nature.com/articles/s41586-021-04339-9> doi: 10.1038/s41586-021-04339-9
- Reynolds, R. W., Smith, T. M., Liu, C., Chelton, D. B., Casey, K. S., & Schlax, M. G. (2007, November). Daily High-Resolution-Blended Analyses for Sea Surface Temperature. *Journal of Climate*, 20(22), 5473–5496. Retrieved 2023-02-15, from <http://journals.ametsoc.org/doi/10.1175/2007JCLI1824.1> doi: 10.1175/2007JCLI1824.1
- Rousset, C., Vancoppenolle, M., Madec, G., Fichefet, T., Flavoni, S., Barthélemy, A., ... Vivier, F. (2015, October). The Louvain-La-Neuve sea ice model LIM3.6: global and regional capabilities. *Geoscientific Model Development*, 8(10), 2991–3005. Retrieved 2023-02-15, from <https://gmd.copernicus.org/articles/8/2991/2015/> (Publisher: Copernicus GmbH) doi: 10.5194/gmd-8-2991-2015
- Rutherford, K., & Fennel, K. (2018, October). Diagnosing transit times on the northwestern North Atlantic continental shelf. *Ocean Science*, 14(5), 1207–1221. Retrieved 2023-02-15, from <https://os.copernicus.org/articles/14/1207/2018/> doi: 10.5194/os-14-1207-2018
- Rutherford, K., Fennel, K., Atamanchuk, D., Wallace, D., & Thomas, H. (2021, December). A modelling study of temporal and spatial $p\text{CO}_2$ variability on the biologically active and temperature-dominated Scotian Shelf. *Biogeosciences*, 18(23), 6271–6286. Retrieved 2023-02-15, from <https://bg.copernicus.org/articles/18/6271/2021/> (Publisher: Copernicus GmbH) doi: 10.5194/bg-18-6271-2021
- Rödenbeck, C., Keeling, R. F., Bakker, D. C. E., Metzl, N., Olsen, A., Sabine, C., & Heimann, M. (2013, March). Global surface-ocean $p\text{CO}_2$ and sea-air CO_2 flux variability from an observation-driven ocean mixed-layer scheme. *Ocean Science*, 9(2), 193–216. Retrieved 2015-05-12, from <http://www.ocean-sci.net/9/193/2013/> doi: 10.5194/os-9-193-2013
- Schourup-Kristensen, V., Sidorenko, D., Wolf-

- Gladrow, D. A., & Völker, C. (2014, November). A skill assessment of the biogeochemical model REcoM2 coupled to the Finite Element Sea Ice–Ocean Model (FESOM 1.3). *Geoscientific Model Development*, 7(6), 2769–2802. Retrieved 2023-02-15, from <https://gmd.copernicus.org/articles/7/2769/2014/> doi: 10.5194/gmd-7-2769-2014
- Sein, D. V., Koldunov, N. V., Danilov, S., Sidorenko, D., Wekerle, C., Cabos, W., ... Jung, T. (2018, August). The Relative Influence of Atmospheric and Oceanic Model Resolution on the Circulation of the North Atlantic Ocean in a Coupled Climate Model. *Journal of Advances in Modeling Earth Systems*, 10(8), 2026–2041. Retrieved 2023-02-15, from <http://doi.wiley.com/10.1029/2018MS001327> doi: 10.1029/2018MS001327
- Seitzinger, S. P., Harrison, J. A., Dumont, E., Beusen, A. H. W., & Bouwman, A. F. (2005, December). Sources and delivery of carbon, nitrogen, and phosphorus to the coastal zone: An overview of Global Nutrient Export from Watersheds (NEWS) models and their application: GLOBAL EXPORT OF C, N, AND P TO COASTAL SYSTEMS. *Global Biogeochemical Cycles*, 19(4), n/a–n/a. Retrieved 2023-02-15, from <http://doi.wiley.com/10.1029/2005GB002606> doi: 10.1029/2005GB002606
- Seland, O., Bentsen, M., Olivié, D., Toniazzo, T., Gjermundsen, A., Graff, L. S., ... Schulz, M. (2020, December). Overview of the Norwegian Earth System Model (NorESM2) and key climate response of CMIP6 DECK, historical, and scenario simulations. *Geoscientific Model Development*, 13(12), 6165–6200. Retrieved 2023-02-15, from <https://gmd.copernicus.org/articles/13/6165/2020/> doi: 10.5194/gmd-13-6165-2020
- Shchepetkin, A. F., & McWilliams, J. C. (2005, January). The regional oceanic modeling system (ROMS): a split-explicit, free-surface, topography-following-coordinate oceanic model. *Ocean Modelling*, 9(4), 347–404. Retrieved 2023-02-15, from <https://www.sciencedirect.com/science/article/pii/S1463500304000484> doi: 10.1016/j.ocemod.2004.08.002
- Six, K. D., & Maier-Reimer, E. (1996). Effects of plankton dynamics on seasonal carbon fluxes in an ocean general circulation model. *Global Biogeochemical Cycles*, 10(4), 559–583. Retrieved 2023-02-15, from <https://onlinelibrary.wiley.com/doi/abs/10.1029/96GB02561> doi: 10.1029/96GB02561
- Stock, C. A., Dunne, J. P., Fan, S., Ginoux, P., John, J., Krasting, J. P., ... Zadeh, N. (2020). Ocean Biogeochemistry in GFDL’s Earth System Model 4.1 and Its Response to Increasing Atmospheric CO₂. *Journal of Advances in Modeling Earth Systems*, 12(10), e2019MS002043. Retrieved 2021-10-11, from <https://onlinelibrary.wiley.com/doi/abs/10.1029/2019MS002043> doi: 10.1029/2019MS002043
- Stock, C. A., Dunne, J. P., & John, J. G. (2014, January). Global-scale carbon and energy flows through the marine planktonic food web: An analysis with a coupled physical–biological model. *Progress in Oceanography*, 120, 1–28. Retrieved 2016-02-22, from <http://www.sciencedirect.com/science/article/pii/S0079661113001079> doi: 10.1016/j.pocean.2013.07.001
- Séférian, R., Nabat, P., Michou, M., Saint-Martin, D., Voldoire, A., Colin, J., ... Madec, G. (2019). Evaluation of CNRM Earth System Model, CNRM-ESM2-1: Role of Earth System Processes in Present-Day and Future Climate. *Journal of Advances in Modeling Earth Systems*, 11(12), 4182–4227. Retrieved 2023-03-01, from <https://onlinelibrary.wiley.com/doi/abs/10.1029/2019MS001791> (eprint: <https://onlinelibrary.wiley.com/doi/pdf/10.1029/2019MS001791> doi: 10.1029/2019MS001791
- Titchner, H. A., & Rayner, N. A. (2014, March). The Met Office Hadley Centre sea ice and sea surface temperature data set, version 2: 1. Sea ice concentrations: HADISST.2.1.0.0 SEA ICE CONCENTRATIONS. *Journal of Geophysical Research: Atmospheres*, 119(6), 2864–2889. Retrieved 2023-02-17, from <http://doi.wiley.com/10.1002/2013JD020316> doi: 10.1002/2013JD020316
- Tjiputra, J. F., Schwinger, J., Bentsen, M., Morée, A. L., Gao, S., Bethke, I., ... Schulz, M. (2020, May). Ocean biogeochemistry in the Norwegian Earth System Model version 2 (NorESM2). *Geoscientific Model Development*, 13(5), 2393–2431. Retrieved 2023-02-15, from <https://gmd.copernicus.org/articles/13/2393/2020/> (Publisher: Copernicus GmbH) doi: 10.5194/gmd-13-2393-2020
- Tsujino, H., Nakano, H., Sakamoto, K., Urakawa, S., Hirabara, M., Ishizaki, H., & Yamanaka, G. (2017). Reference Manual for the Meteorological Research Institute Community Ocean Model version 4(MRI.COMv4). *Technical Reports of the Meteorological Research Institute No. 80*. (10.11483/mritechrepo.80) doi: 10.11483/mritechrepo.80
- Tsujino, H., Urakawa, S., Nakano, H., Small, R. J., Kim, W. M., Yeager, S. G., ... Yamazaki, D. (2018, October). JRA-55 based surface dataset for driving ocean–sea ice models (JRA55-do). *Ocean Mod-*

- elling, 130, 79–139. Retrieved 2023-02-15, from <https://linkinghub.elsevier.com/retrieve/pii/S146350031830235X> doi: 10.1016/j.ocemod.2018.07.002
- Umlauf, L., & Burchard, H. (2003, March). A generic length-scale equation for geophysical turbulence models. *Journal of Marine Research*, 61(2), 235–265. Retrieved 2023-02-15, from <http://www.ingentaselect.com/rpsv/cgi-bin/cgi?ini=xref&body=linker&reqdoi=10.1357/002224003322005087> doi: 10.1357/002224003322005087
- Urakawa, L. S., Tsujino, H., Nakano, H., Sakamoto, K., Yamanaka, G., & Toyoda, T. (2020, October). The sensitivity of a depth-coordinate model to diapycnal mixing induced by practical implementations of the isopycnal tracer diffusion scheme. *Ocean Modelling*, 154, 101693. Retrieved 2023-02-15, from <https://linkinghub.elsevier.com/retrieve/pii/S1463500320301955> doi: 10.1016/j.ocemod.2020.101693
- Urrego-Blanco, J., & Sheng, J. (2012, September). Interannual Variability of the Circulation over the Eastern Canadian Shelf. *Atmosphere-Ocean*, 50(3), 277–300. Retrieved 2023-02-15, from <http://www.tandfonline.com/doi/abs/10.1080/07055900.2012.680430> doi: 10.1080/07055900.2012.680430
- Wang, C., Zhang, L., Lee, S.-K., Wu, L., & Mechoso, C. R. (2014, March). A global perspective on CMIP5 climate model biases. *Nature Climate Change*, 4(3), 201–205. Retrieved 2015-09-23, from <http://www.nature.com/nclimate/journal/v4/n3/full/nclimate2118.html> doi: 10.1038/nclimate2118
- Wang, H., Hu, X., Cai, W.-J., & Sterba-Boatwright, B. (2017). Decadal fCO₂ trends in global ocean margins and adjacent boundary current-influenced areas. *Geophysical Research Letters*, 44(17), 8962–8970. Retrieved 2022-04-15, from <https://onlinelibrary.wiley.com/doi/abs/10.1002/2017GL074724> doi: 10.1002/2017GL074724
- Wanninkhof, R. (1992, May). Relationship between wind speed and gas exchange over the ocean. *Journal of Geophysical Research: Oceans*, 97(C5), 7373–7382. Retrieved 2015-06-22, from <http://onlinelibrary.wiley.com/doi/10.1029/92JC00188/abstract> doi: 10.1029/92JC00188
- Wanninkhof, R. (2014, June). Relationship between wind speed and gas exchange over the ocean revisited. *Limnology and Oceanography: Methods*, 12(6), 351–362. Retrieved 2015-06-22, from <http://onlinelibrary.wiley.com/doi/10.4319/lom.2014.12.351/abstract> doi: 10.4319/lom.2014.12.351
- Warner, J. C., Sherwood, C. R., Arango, H. G., & Signell, R. P. (2005, January). Performance of four turbulence closure models implemented using a generic length scale method. *Ocean Modelling*, 8(1-2), 81–113. Retrieved 2023-02-15, from <https://linkinghub.elsevier.com/retrieve/pii/S1463500303000702> doi: 10.1016/j.ocemod.2003.12.003
- Weber, T., Wiseman, N. A., & Kock, A. (2019, October). Global ocean methane emissions dominated by shallow coastal waters. *Nature Communications*, 10(1), 4584. Retrieved 2020-10-21, from <https://www.nature.com/articles/s41467-019-12541-7> (Number: 1 Publisher: Nature Publishing Group) doi: 10.1038/s41467-019-12541-7
- Wright, R. M., Le Quéré, C., Buitenhuis, E., Pitois, S., & Gibbons, M. J. (2021, February). Role of jellyfish in the plankton ecosystem revealed using a global ocean biogeochemical model. *Biogeosciences*, 18(4), 1291–1320. Retrieved 2023-03-27, from <https://bg.copernicus.org/articles/18/1291/2021/> (Publisher: Copernicus GmbH) doi: 10.5194/bg-18-1291-2021
- Wu, H., & Zhu, J. (2010, January). Advection scheme with 3rd high-order spatial interpolation at the middle temporal level and its application to salt-water intrusion in the Changjiang Estuary. *Ocean Modelling*, 33(1-2), 33–51. Retrieved 2023-02-15, from <https://linkinghub.elsevier.com/retrieve/pii/S1463500309002121> doi: 10.1016/j.ocemod.2009.12.001
- Yang, S., Chang, B. X., Warner, M. J., Weber, T. S., Bourbonnais, A. M., Santoro, A. E., ... Bianchi, D. (2020, June). Global reconstruction reduces the uncertainty of oceanic nitrous oxide emissions and reveals a vigorous seasonal cycle. *Proceedings of the National Academy of Sciences*, 117(22), 11954–11960. Retrieved 2022-05-12, from <https://www.pnas.org/doi/10.1073/pnas.1921914117> (Publisher: Proceedings of the National Academy of Sciences) doi: 10.1073/pnas.1921914117
- Yukimoto, S., Kawai, H., Koshiro, T., Oshima, N., Yoshida, K., Urakawa, S., ... Ishii, M. (2019). The Meteorological Research Institute Earth System Model Version 2.0, MRI-ESM2.0: Description and Basic Evaluation of the Physical Component. *Journal of the Meteorological Society of Japan. Ser. II*, 97(5), 931–965. Retrieved 2023-02-15, from https://www.jstage.jst.go.jp/article/jmsj/97/5/97_2019-051/_article doi: 10.2151/jmsj.2019-051
- Zweng, M. M., Reagan, J. R., Antonov, J. I., Locarnini, R. A., Mishonov, A. V., Boyer, T. P., ... Biddle, M. (2014). *World Ocean Atlas 2013, Vol-*

Volume 2: *Salinity*. (Tech. Rep.). S. Levitus, Ed., A. Mishonov Technical Ed.; NOAA Atlas NESDIS

74, 39 pp.